Triennial Scientific Report 2007 -2009

KNMI Research

Contents

Preface *4*

Introduction *5*

Highlights
- Sea ice extent from satellite microwave sensors *9*
- Observing the surface energy budget at Cabauw: A status report *15*
- Recent developments in KNMI's surface observing methods *21*
- High resolution observations for climate change monitoring of extremes *28*
- Regional differences in the extreme rainfall climatology in the Netherlands *34*
- Linking changes in hourly precipitation extremes to the Clausius-Clapeyron relation *39*
- Extreme rainfall climatology from weather radar *44*
- Monitoring bird migration by weather radar *50*
- Infrasound and seismology in the Low Frequency Array LOFAR *56*
- TROPOMI: Sensing the Troposphere from Space *62*
- The central role of the tropics in the methane life cycle *68*
- The statistical mechanics of turbulent flows *73*
- Technological developments in scientific data exchange:
  recently developed portals, services and networks at KNMI *79*
- A Monitoring and Forecasting System for Atmospheric Composition: The GEMS Project *85*
- Air quality monitoring and forecasting in China *90*
- The prediction and occurrence of aircraft lightning encounters at Amsterdam-Schiphol Airport *96*
- Improved and tailored low visibility forecasts for Amsterdam Airport Schiphol *101*
- EC-EARTH: goals, developments and scientific perspectives *106*
- High-end climate change scenarios for flood protection of the Netherlands *112*

Appendices
- Organisation chart *119*
- Publications per division *120*
  - Weather Research and Development *120*
  - Climate Observations *128*
  - Global Climate *134*
  - Regional Climate *139*
  - Chemistry and Climate *145*
  - Climate Services *149*
  - Seismology *153*
  - R&D Information and Observation Technology *155*

Acronyms *156*

Preface

The Royal Netherlands Meteorological Institute (KNMI) is known mainly for its weather forecasts and warnings, but in its capacity as the national knowledge and data centre for weather, climate and seismology, it performs also many research activities on these subjects.

In fact, the Law on KNMI that has been accepted in Parliament in 2002, explicitly states that it is a task of KNMI to perform research.

These research activities are of both applied and fundamental nature, and are focused on observations, modeling, and understanding weather and climate. They lead to scientific publications in peer-reviewed journals, about 100 per year, and to various development activities and services for external and internal users, such as the development of numerical weather and climate models, the performance of remote sensing and in-situ observations, and the construction of climate scenario's for the Netherlands.

This report aims to give a representative overview of this quite extensive range of research activities as carried out in the years 2006, 2007 and 2008, written in a style that should be accessible also for the interested layman.

This Triennial Report has been preceded by six Biennial Reports. We have changed the length of the reporting period from two to three years, as in this way the timing of the scientific reports becomes the same as that of the scientific evaluations of KNMI's research. Our research is evaluated externally once every six years, and every three years a self-evaluation is produced. The latest self-evaluation covers the period 2007-2009, and in the autumn of 2010 an external evaluation will be carried out for the period 2004-2009.

In this respect I want to thank the members of the KNMI-Board ('KNMI-Raad'), which is a committee with external members with whom I discuss a few times per year general aspects of the organization of KNMI's research and its quality.

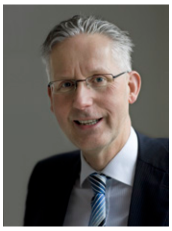

When you have read this report, I hope you can understand why I am so proud of KNMI's research! I wish you a pleasant reading.

September 2010

Dr. Ir. Frits J.J. Brouwer
Director General KNMI

Introduction

In this Triennial Scientific Report an overview is presented of the research activities carried out by KNMI in the period 2007-2009. KNMI's research is focused on the subjects of weather, climate, and seismology, and on the information and observation technology that is related to these subjects. This report covers a broad range of subjects, covering the chain from observation to modeling, analysis, understanding and advice.

KNMI's research aims to maximize its benefits for society. KNMI provides advanced scientific knowledge, observations and advice on the global climate system, substantiating the efforts of the Dutch government to protect the Netherlands to the impacts of severe weather and climate change. In this capacity, KNMI provided extensive information on climate change and sea level rise to the Delta Committee that was appointed by the government to formulate a vision on the long-term protection of the Dutch coast and its hinterland. KNMI also contributed to the Nationaal Waterplan, in which the Dutch water policy for the period until 2015 is formulated.

KNMI assures the high quality of its activities by participating in the national and international climate research efforts. KNMI's climate activities are carried out for an important part through international cooperation, on an appropriate high-level, to ensure the availability of state-of-the-art, high-quality results and to maintain the international stature and visibility of the Netherlands. Many of KNMI's research results are included or referred to in the reports of the Intergovernmental Panel on Climate Change (IPCC), and several KNMI-researchers are author or reviewer of the IPCC reports. The Nobel Peace Prize 2007 for IPCC is for KNMI a welcome encouragement for its participation in the activities of IPCC.

KNMI aims to be a stimulating working place. The cover of this report shows a photo of a major part of KNMI's research staff. In 2009 the total research staff, including supporting staff, was 200 FTE's. The fraction of the total staff that is formed by temporary positions has increased during the last years, for two reasons. Firstly, KNMI has been quite successful in attracting external project funding, which has lead to an increase of the temporary staff. Secondly, there has been a decrease of the permanent staff as a result of budget cuts by the government. The mentioned 200 FTE's research staff is the sum of about 120 permanent and 80 temporary FTE's.

The organization of KNMI is such (see appendix on page 119) that there are three business areas (weather, climate, and seismology), organized in two departments. Next to those there is a third department which supports the business areas with ICT and observation technology. These departments have a varying number of divisions, fully or partly devoted to research.

In de following 19 chapters we present a representative selection of our research activities in the years 2007, 2008 and 2009, followed by a list of publications per research division. The chapters are ordered with respect to three types of research, starting with observational work, followed by more theoretical and technical studies, and ending with modeling activities on weather and climate prediction. The publications are ordered with respect to peer-reviewed publications and other publications. Several publications appeared in high-impact journals such as Nature Geoscience.

For more information on our research we refer you to our website www.knmi.nl.

Dr. Hein W. Haak
Director
Climate and Seismology Department

Dr. Remco den Besten
Director
Weather Service Department

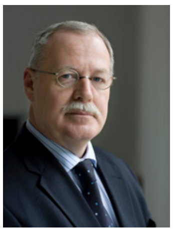

Ir. Wouter Nieuwenhuizen
Director
Information and Observation Services and Technology Department

Highlights

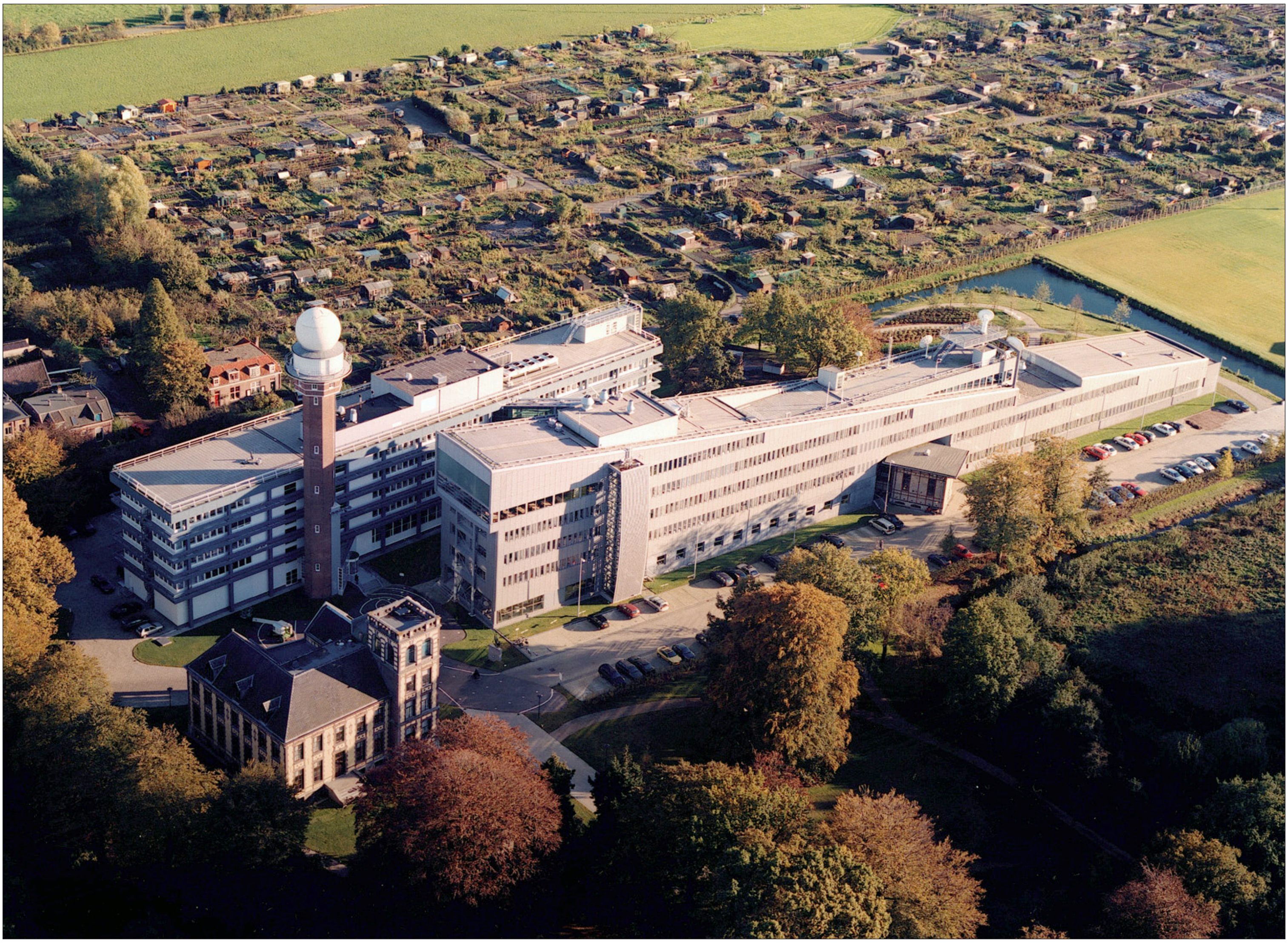

Sea ice extent from satellite microwave sensors

Maria Belmonte Rivas

Introduction

In 2007, the summer extent of Arctic sea ice observed by the Special Sensor Microwave Imager (SSM/I) reached its lowest value on record since 1979. Satellite sensors provide a convenient way to monitor the vast expanses of sea ice in the Polar Regions and this is done primarily using microwave techniques, which contrary to optical instruments, can operate at night and in all-weather conditions. The determination of sea ice extents from satellite platforms can be exploited as a marker for climate change, a navigation tool and a reference for coupled ocean-ice-atmosphere models. Sea ice detection is routinely performed by two families of microwave instruments: radiometers, which observe the natural emission from the surface in the range of microwave frequencies, and scatterometers, which observe the energy reflected from a transmitted pulse. Earlier work has shown reasonable agreement between scatterometer and radiometer sea ice extents, albeit with systematic discrepancies characterized by defective scatterometer extents during the sea ice growth season[1] and deficient radiometer extents during the summer melt[2]. In this highlight, we revisit the determination of sea ice extents using satellite microwave sensors, propose an improved approach to sea ice detection for the SeaWinds scatterometer based on a Bayesian methodology, and compare its performance against other existing active and passive microwave algorithms throughout a full annual freeze/melt cycle. The improved Bayesian algorithm has been developed for inclusion in the EUMETSAT-KNMI SeaWinds Data Processor and is currently undergoing pre-opera-tional testing.

The determination of sea ice extents from satellite platforms can be exploited as a marker for climate change, a navigation tool and a reference for coupled ocean-ice-atmosphere models

Sea ice detection with the SeaWinds scatterometer

Scatterometers are active microwave sensors whose primary mission consists in the determination of near-surface winds over the oceans. Similarly to a radar detector, scatterometers radiate energy pulses and collect the backscattered returns from a variety of incidence and azimuth angles, providing a diversity of views that allows for the detection of the wind signature over the ocean (Figure 1).
The dielectric permittivity of seawater at microwave frequencies is many times larger than that of sea ice. The wind induced ocean returns arise from the reflective sea-water surface, while returns from the semi-transparent sea ice arise from volume interactions deeper in the ice slab. This results in distinct polarization, intensity and directional scattering properties that allow their effective separation. In particular, while ocean scattering is characterized by steep backscatter derivatives relative to the incidence angle, a remarkable azimuthal anisotropy and substantial polarization, volume scattering from sea ice results in smaller backscatter derivatives, azimuthal isotropy and nearly total depolarization. The first sea ice detection algorithms relied on hard threshold tests that capitalized on these properties. They evolved in time into

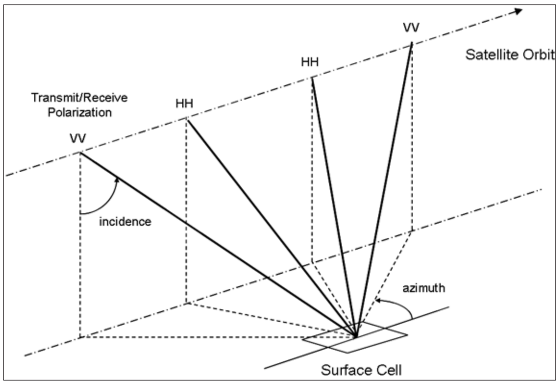

Figure 1. Incidence, azimuth and polarization diversity for the SeaWinds scatterometer (HH and VV refer to horizontal and vertical Transmit/Receive polarization).

maximum likelihood methods with separate point-wise class clusters for mean backscatter, polarization and anisotropy combinations[3].

The novel sea ice detection approach proposed here takes advantage of improved knowledge about the distribution of backscatter points in the scatterometer measurement space to replace the former point-wise class clusters by extended geophysical model functions (GMFs) for ocean wind and sea ice[4]. For the SeaWinds case, the GMF for ocean winds is the one applied operationally to retrieve wind vectors over ocean surfaces. The empirical GMF for sea ice is drawn from the observed distribution of pure winter ice backscatter, which groups along an extended line in the SeaWinds dB measurement space $\{\sigma_{HH,fore}, \sigma_{VV,fore}, \sigma_{VV,aft}, \sigma_{HH,aft}\}$. The advantage of this approach relative to previous algorithms is that the spread of measurements about extended class model functions is smaller than that about point-wise class clusters, allowing class covariances to decrease to instrumental noise levels thus enhancing their discrimination power. Our Bayesian algorithm computes the normalized square distances (or maximum likelihood estimators, MLE) to the ocean wind and sea ice model functions as:

$$MLE_{wind} = \sum_{i=1,\dots,N} (\sigma^o_i - \sigma^o_{wind,i})^2 / var[\sigma^o_{wind,i}]$$

$$MLE_{ice} = \sum_{i=1,\dots,N} (\sigma^o_i - \sigma^o_{ice,i})^2 / var[\sigma^o_{wind,i}]$$

where σ^o are backscatter measurements, σ^o_{class} are the class model functions and the normalization factors $var[\sigma^o_{class}]$ guarantee that the variance of square distances about each class model is unity. The Bayesian posterior sea ice probability is then calculated as:

$$p(ice\,|\,\sigma^o) = \frac{p(\sigma^o\,|ice)\,p_0(ice)}{p(\sigma^o\,|ice)\,p_0(ice) + p(\sigma^o|wind)\,p_0(wind)}$$

where p_o(ice) and p_o(wind) are a priori sea ice and ocean wind probabilities, and the conditional probabilities $p(\sigma^o|ice)$ and $p(\sigma^o|wind)$ reflect the actual location of a measurement relative to the expected backscatter distributions about the ice and wind model functions, expressed in terms of the MLEs defined above. The Bayesian sea ice detection algorithm implemented for SeaWinds at KNMI generates daily sea ice masks using a std$[\sigma^o_{ice}]$ = 1.5 dB and a 50% threshold to posterior sea ice probabilities. The masks are filled with backscatter strength values, which are indicative of ice type or thickness by proxy and archived for dissemination (see Figures 2 and 3).

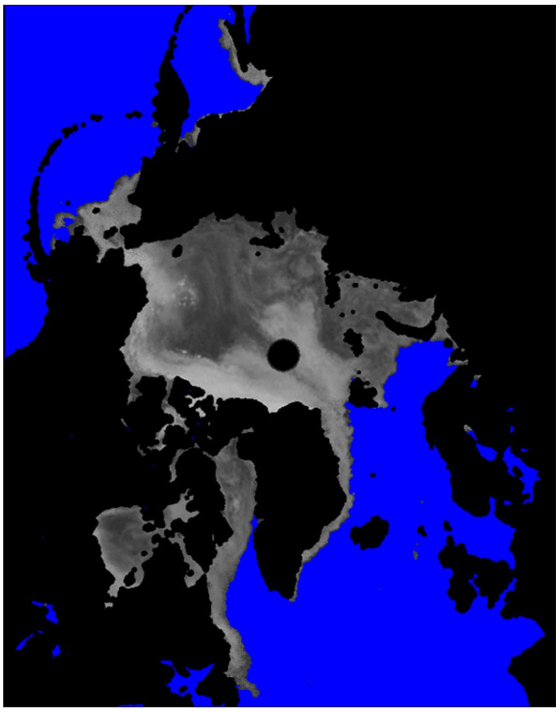

Figure 2. NH sea ice mask with backscatter values from SeaWinds (8th May 2009).

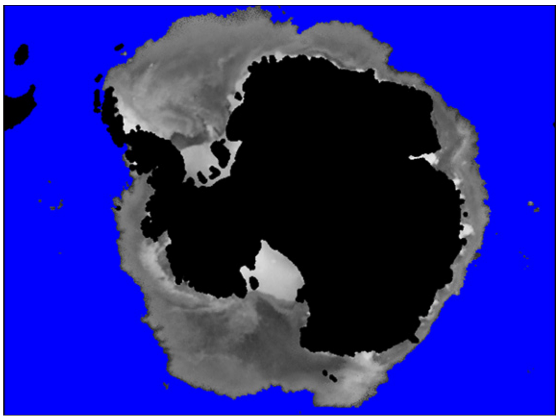

Figure 3. NH sea ice mask with backscatter values from SeaWinds (8th May 2009).

Scatterometer versus radiometer sea ice extents

We would like to compare the sea ice masks observed from passive and active microwave instruments. The radiometer masks (from AMSR, the Advanced Microwave Scanning Radiometer) are calculated using the Enhanced NASA Team algorithm (NT2)[5)], while the scatterometer masks (from SeaWinds on QuikSCAT) are estimated using both the cluster method[3)] and the Bayesian GMF algorithm developed at KNMI. It has been proven that passive microwave masks lie within 10 km of the ice edge observed by optical (and synthetic aperture radar) sensors in the wintertime[6)], although accuracy becomes worse during the summer months, as these masks become affected by weather effects, unresolved thin/low concentration ice types and surface melt effects[5)].

Figure 4 compares the daily sea ice extents calculated from satellite active and passive microwaves during the freeze/melt cycle running from September 2006 to September 2007, to show that all the selected methods are found in excellent agreement during the hemispherical fall and winter months, but show discrepancies as the melt season sets in, with passive microwaves biased negatively relative to active microwaves in terms of summer sea ice extents. It should be noted that the old scatterometer cluster method is also biased negatively relative to the new Bayesian GMF method developed at KNMI, and that the former is affected by a substantial amount of misclassification noise along the ice edge, which manifests in Figure 4 as an appreciable dispersion in daily areas, particularly during the stormy fall season in the Arctic.

Having determined the overall convergence of daily sea ice extent estimates from satellite active and passive microwave algorithms during the fall and winter seasons, we are left to evaluate the nature of the observed discrepancies. For this purpose, we make use of higher resolution MODIS and Envisat ASAR imagery. While the extensive and frequent cloud cover in the Polar Regions is a factor against the use of optical techniques for the monitoring of sea ice conditions, the contrast between sea ice and open water is not always well-defined for the cloud penetrating ASAR. The combined use of optical and high resolution microwave datasets allows for more imagery to be used for an in-depth validation study. In general, the combined MODIS and ASAR records helps us confirm that during the winter months, under conditions such that the open ocean is terminated by a compact boundary of consolidated ice, all three algorithms come to agree to within 2 grid pixels or 25 km in their determination of the sea ice edge. Figures 5 to 8 illustrate typical discrepancies found between active and passive microwave sea ice detection algorithms, generally involving mixed ice/ocean scenarios due to thin, water saturated and low concentration sea ice conditions. During the growth season, thick and consolidated sea ice slowly progresses behind a rapidly advancing band of thin ice. The accurate determination of the ice edge in areas of active formation is difficult because the representativity of daily maps degrades rapidly, but also because new ice is so thin and saline that it resembles a smooth ocean surface. Figure 5 shows

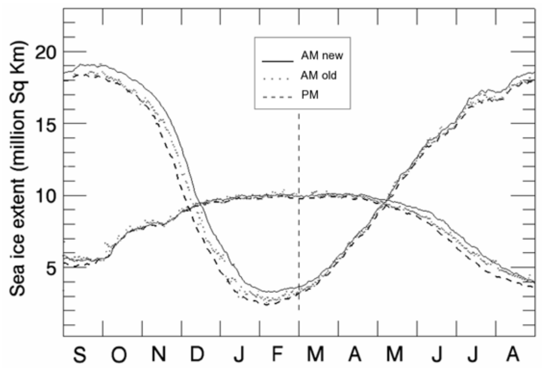

Figure 4. Arctic and Antarctic sea ice extents for Sep'06 to Sep'07 from passive microwaves (PM, dashed line) and active microwaves (AM, the dotted line represents the old cluster method, the continuous line the new Bayesian GMF method developed at KNMI).

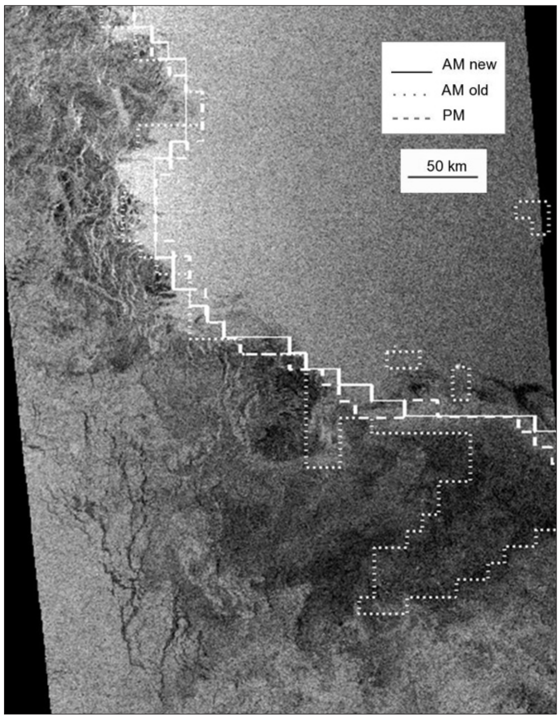

Figure 5. Sea ice detection discrepancies during the growth season (ASAR truth)

one such instance taken in the East Siberian Sea, where the old cluster scatterometer algorithm has difficulties to resolve a tongue of new ice with dark smooth appearance in the ASAR image, which is nevertheless detected by the passive microwave and the improved KNMI SeaWinds algorithms. The capability of passive microwave algorithms to detect partly translucent thin ice is indisputable, mostly because they can rely on higher frequency channels (up to 89 GHz) than scatterometers (SeaWinds operates at 13 GHz) to probe into thinner skin depths. However, the ability of the improved KNMI algorithm to detect thin ice is here comparable to that of passive microwaves, giving proof that the problem with scatterometer growth season biases has been overcome to great extent.

During the melt season, the sea ice margin includes lower concentrations of decaying floes with water saturated ice among them, along with sea ice bands of varying concentration, which are all examples of diffuse ice conditions most likely to pass undetected by passive microwave algorithms[7]. Figure 6 provides an example of passive microwave summer biases in an area located in the northern edge of the Beaufort Sea, featuring a large expanse of melting and water soaked sea ice. This figure clearly indicates how surface melt effects lead to significant errors in passive microwave estimates. The ability of the improved KNMI Bayesian algorithm to capture diffuse ice conditions at the edge remains unmatched.

Figure 7 provides another instance of passive microwave summer biases, this time focusing on the development of large sea ice bands in the Southern Ocean, which are entirely missed by the passive microwave algorithm. Once more, scatterometer algorithms appear to be more robust in terms of detection of summer ice, partly due to the sensitivity of sea ice microwave emissions to surface

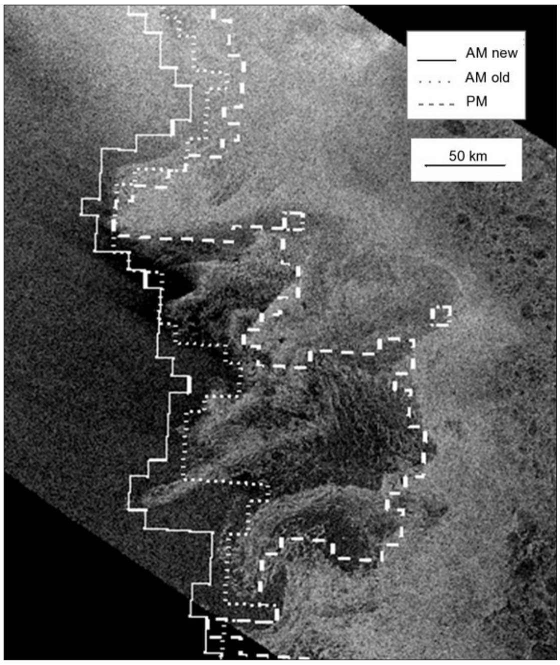

__Figure 7.__ Sea ice detection discrepancies during the melt season (ASAR truth, Antarctic).

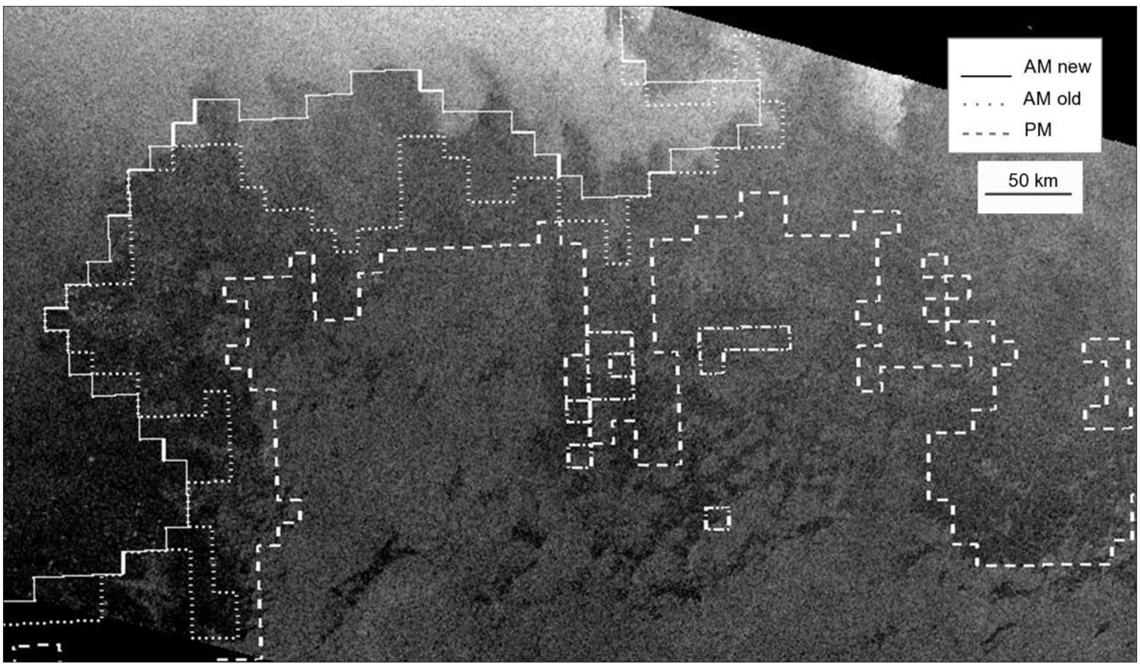

__Figure 6.__ Sea ice detection discrepancies during the melt season (ASAR truth, Arctic).

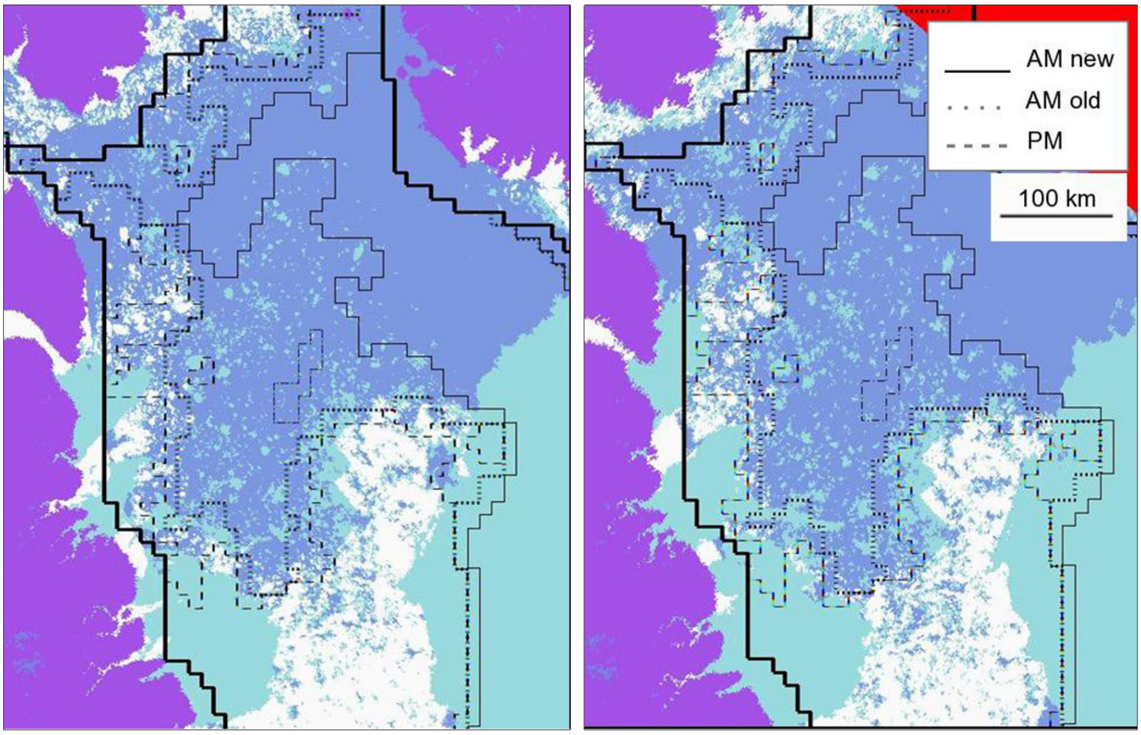

Figure 8. Sea ice detection discrepancies during the melt season (sequential MODIS overpasses 1.5 hours apart. White = ice, blue = ocean, magenta = land and cyan = cloud).

melt effects. One last example is shown in Figure 8, taken from two sequential orbital passes of the MODIS sensor over the Baffin Bay and featuring a large but sparse ice floe field that is mistakenly labelled as a cloud field by the optical algorithm.

The sparse floe field is detected by neither the passive microwave nor the old cluster based scatterometer algorithms. However, the improved KNMI Bayesian sea ice detection algorithm sets out to provide a most inclusive and conservative definition of sea ice edge to date, one that is more in line with that provided by ship observations and well-suited for applications that require reliable indication of sea ice presence all year round, such as satellite-based retrievals of ocean wind and sea surface temperatures.

The improved KNMI Bayesian sea ice detection algorithm sets out to provide a most inclusive and conservative definition of sea ice edge to date

Conclusions

KNMI has developed an improved Bayesian sea ice detection algorithm for the SeaWinds satellite scatterometer and has validated its performance against state-of-the-art passive microwave and scatterometer methods throughout a full sea ice growth/melt cycle. It is shown that, although all the methods under study agree very well during the winter months, the new Bayesian approach improves on the misclassification scores that affect earlier scatterometer and passive microwave algorithms and remains sensitive to the summer sea ice species that populate the Arctic edge during the melt season and the Antarctic margin all year round. The improved determination of the sea ice edge provides an all-inclusive daily sea ice mask recommended for use in ground processors that require an effective filtering of sea ice contaminated pixels. The Bayesian scheme has been successfully applied to SeaWinds and is currently under development for the MetOp ASCAT scatterometer. A reprocessing of the entire SeaWinds data record up to 1999 is also foreseen.

References

1) Abreu, R.D., K. Wilson, M. Arkett and D. Langloi, 2002. *Evaluating the use of QuikSCAT data for operational sea ice monitoring.* IEEE IGARSS, **5**, 3032-3033.
2) Markus, T. and S. Dokken, 2002. *Evaluation of late summer passive microwave Arctic sea ice retrievals.* IEEE Transactions on Geoscience and Remote Sensing, **40**, No.2, 348-356.
3) Remund, Q.P. and D.G. Long, 1999. *Sea ice extent mapping using Ku-band scatterometer data.* J. Geophys. Res., **104**, No.C5, 11,515-11,527.
4) Stoffelen, A.C.M., 1998. *Scatterometry*. PhD-Thesis, Utrecht University, 187pp.
5) Markus, T. and D. Cavalieri, 2000. *An enhancement of the NASA Team sea ice algorithm.* IEEE Transactions on Geoscience and Remote Sensing, **38**, 1387-1398.
6) Heinrichs, J.F., D.J. Cavalieri and T. Markus, 2006. *Assessment of the AMSR sea ice concentration product at the ice edge using RADARSAT-1 and MODIS imagery.* IEEE Transactions on Geoscience and Remote Sensing, **44**, No.11, 3070-3080.
7) Worby, A.P. and J.C. Comiso, 2004. *Studies of the Antarctic sea ice edge and ice extent from satellite and ship observations.* Remote Sens. Environ., **92**, 98-111.

Observing the surface energy budget at Cabauw: A status report

Fred Bosveld

Introduction

Closing the surface energy budget (SEB) is one of the longest outstanding problems in micro-meteorology. At the earth's surface the net radiation (Q_N), consisting of the budget of shortwave incoming ($K^{\downarrow}$), shortwave outgoing ($K^{\uparrow}$), longwave incoming ($L^{\downarrow}$) and longwave outgoing radiation ($L^{\uparrow}$), should be balanced by the transport of heat into the soil (G) and to the atmosphere in the form of sensible (H) and latent heat (LE):

$$K - K^{\uparrow} + L^{\downarrow} - L^{\uparrow} = Q_N = H + LE + G$$

Here the radiation components are defined all positive and the heat fluxes are defined positive when directed away from the surface. The sum of the three heat fluxes is called the total heat flux. Many field studies[1] report a significant imbalance in the SEB with almost always more net radiation than total heat flux. Here we define the imbalance as the net radiation minus the total heat flux and the fractional imbalance as the imbalance divided by net radiation. Over the years observational techniques have improved and nowadays the conclusion is widely accepted that in general the observed imbalance is significantly larger then the estimated measurement error, which points to a fundamental problem in our understanding of surface fluxes and how to measure them.

There exist a few studies that show good closure of the SEB. For example Heusinkveld et al.[2] show closure for a desert site where latent heat flux is almost absent. Bosveld et al.[3] show closure of 5%, well within the measurement error, for a forest site with high aerodynamic roughness. Other studies show imbalances of typical 10-20% of the net radiation during daytime and up to 50% or more during night time.

At the Cabauw Experimental Site for Atmospheric Research (CESAR)[4] a long-term meteorological measurement programme over grassland is performed. The programme includes all surface radiation components, soil heat flux, profiles of temperature, humidity, wind and CO_2 along the 200 m tower and the fluxes of sensible heat, latent heat, momentum and CO_2 at 3, 60, 100 and 180 m. A windprofiler/RASS (Radio Acoustic Sounding System) is operated that gives boundary layer height estimates and wind profiles up to several kilometres height. A scintillometer is operated at 60 m height over a 10 km path from the Cabauw tower to the IJsselstein TV-tower.

At CESAR the same SEB imbalance is found as at many other sites over the world. Figure 1 shows a typical example. Kroon[5] analysed 2 years of observations. Figure 2 shows the averaged diurnal variation in fractional imbalance. Around sunrise and sunset fractional imbalance is uncertain and therefore excluded. During night time higher values are found then during day time and during daytime the magnitude

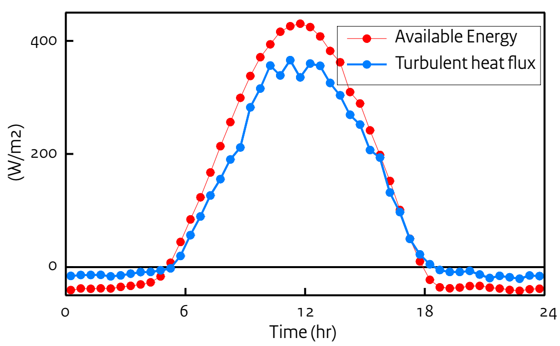

***Figure 1.** A clear-sky day at Cabauw, showing that the turbulent heat flux is smaller in magnitude than the available energy.*

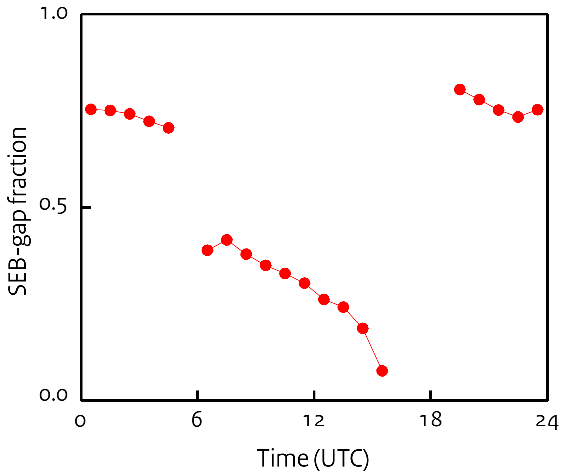

***Figure 2**. Mean fractional imbalance as a function of local time at Cabauw 1995-1996.*

of the imbalance decreases during the day. During night time a clear influence of wind speed was found with a reasonable closure at high wind speeds as shown in Figure 3. Here we will discuss observational issues of the various components of the SEB and in the final section show the relation with other research performed at CESAR.

Radiation

Net radiation observations have improved over the years. In the past specific net-radiation instruments were used. The drawback of these instruments is that they have to compromise on conflicting design specifications for longwave and shortwave radiation. Nowadays separate dedicated instruments for shortwave and longwave radiation are used. Main improvements in these separate instruments are a smaller sensitivity of shortwave instruments for longwave radiation and a more accurate measurement of longwave downward radiation under clear-sky conditions. Calibration of radiation observations is well established. For shortwave radiation there exist calibration standards (World Radiation Centre, Davos, Switzerland). For longwave radiation there is not a true standard but a reasonable one. Independent radiation transport models confirm the adequate accuracy of current state-of-the-art instruments as they are nowadays employed at the sites of the Baseline Surface Radiation Network of which Cabauw is one[6)].

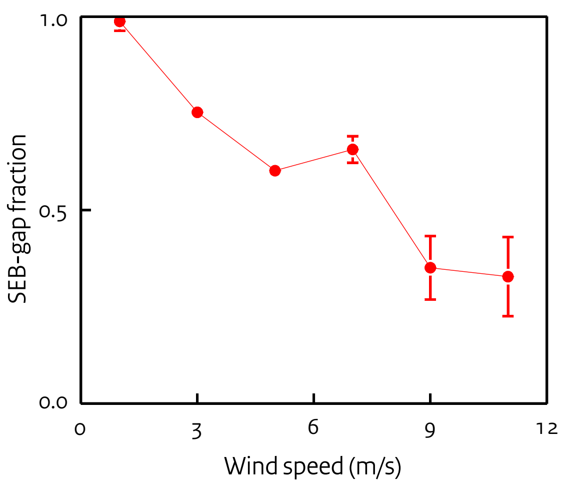

***Figure 3.** Mean night-time fractional imbalance for clear nights as a function of wind speed at Cabauw 1995-1996.*

Surface soil heat flux

Soil heat flux is measured with soil heat flux plates. They are positioned typically at 5-10 cm depth. Special attention is needed with regard to horizontal representativeness and with regard to the large vertical gradients in flux in the top soil layer. An ingenious combination of soil heat flux plates at two depths and temperature sensors in the top soil tackles this issue[7)]. Part of the inhomogeneity problem is treated by measuring at three locations at the vertices of a 2 m wide triangle. Corrections are still needed for the disturbance of the soil heat flux by the soil heat flux plates. Further uncertainty arises from the heat transport associated with water vapour transport in the soil.

If the soil heat flux at Cabauw for some reason would be underestimated by a factor of two, a large part of the SEB problem would disappear. Underestimation of the soil heat flux would also explain the night time wind speed dependence of the imbalance. At high wind speeds the diurnal amplitude of the surface soil heat flux is much smaller than at low wind speeds. However, occasional observations with a snow cover at Cabauw reveal that the same problem in SEB-closure remains (Figure 4). This despite the very small soil heat fluxes and thus very small absolute errors in soil heat flux during snow cover. This shows that problems in soil heat flux observations alone cannot explain the observed SEB-imbalance. By using a soil heat transfer model and an assimilation system Ronda and Bosveld8) were able to show that the observed soil heat fluxes were consistent with the observed thermal properties of the soil.

Atmospheric fluxes

The most direct way of measuring atmospheric transport of heat is by means of the eddy-correlation (EC) technique. This method assumes that turbulence is the

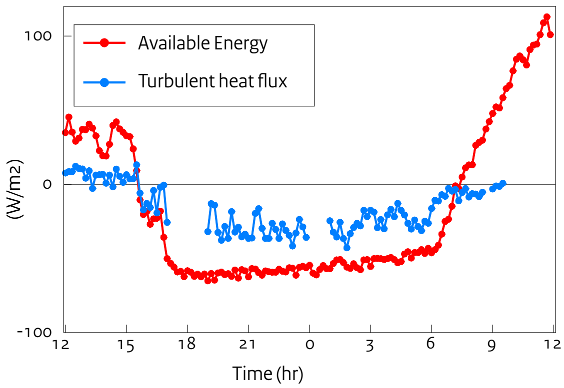

Figure 4. A night with a snow cover, showing that the turbulent heat flux is smaller in magnitude than the available energy.

dominating mechanism of transport. With well-established techniques (sonical anemometer/thermometers and open path optical hygrometers) the fluctuations of wind, temperature and humidity can be measured over a broad range of timescales. Many error sources are recognized, most of them related to the instrumental limits both on the small and on the long time scales. Reasonable estimates of these errors can be made as a function of atmospheric conditions and instrumental properties. Most of these error sources have already been known for a longer time in micro-meteorology. Recently a renewed interest is found in the field of greenhouse gas flux observations[9)].

When combining the observations of radiation, soil heat flux and atmospheric fluxes to make up the SEB there is the issue of different footprints of the instruments. The instruments should all see a surface with the same properties with respect to the energy fluxes. At Cabauw the surface consists of reasonable homogeneous grassland on clay soil. Inhomogeneities on the local scale exist due to different maintenance regimes for the grass and the presence of ditches covering circa 10% of the surface.

Questioning the eddy-correlation technique

Here we will put forward arguments that at least the eddy correlation technique does not represent atmospheric transport properly. To judge the performance of this technique we need independent estimates of the atmospheric fluxes. Traditionally various profile estimates are used to estimate sensible and latent heat fluxes. For an overview of the applied methods at Cabauw see Beljaars and Bosveld[10)]. The Energy balance Bowen ratio technique uses an estimate of the available energy from net radiation and soil heat flux observations. The available energy flux is then partitioned over latent – and sensible heat flux by measuring the ratio of differences in the vertical profile of temperature and humidity. This technique is inadequate for our purpose since it assumes SEB closure. The aerodynamic method uses vertical differences of temperature and humidity in the lowest meters of the atmosphere and a model for the turbulent mixing efficiency of the atmosphere. The latter is a function of wind speed and static stability of the atmosphere. This method has been tuned on eddy-correlation measurements and is therefore not completely independent. Moreover this technique suffers from serious problems under non-uniform surface conditions in the upwind direction. It has been hypothesized that at very stable conditions the eddy-correlation instruments are not capable of measuring the small-scale fluctuations dominating the transport. This has been tested at Cabauw by comparing vertical wind speed observations of a sonic anemometer with a laser Doppler anemometer which is able to measure turbulence down to the smallest scales. No significant deviation was found from theoretical correction procedures for high-frequency loss by Kroon et al.[11)]. Here we discuss comparisons between eddy-correlation observations and some other independent estimates of atmospheric fluxes.

Night time CO2 respiration flux

At night no assimilation of CO_2 takes place by the grass. Night time CO_2 fluxes are a result of respiration in the soil. The magnitude of the respiration flux is mainly determined by soil temperature related to bacterial processes in the soil. We tuned a respiration model[12)] on night time eddy-correlation CO_2 flux observations under high wind speed situations and found a clear response to soil temperature. Then we applied this model with tuned soil temperature response to low wind speed cases. In Figure 5 the ratio of observed and modelled respiration flux is plotted in bins of friction velocity (u*). Friction velocity is a measure for turbulent intensity and is linearly related to wind speed and further depends on atmospheric stability. A clear decrease of observed flux is seen for friction velocities smaller than 0.1 m/s. This shows a similar behaviour as Figure 3 for total heat flux, where observations are plotted as function of wind speed. Assuming that the bacterial process that drives respiration is not dependent on the weather conditions above the soil, except for the indirect influence on the soil temperature, we must conclude that the eddy-correlation method underestimates CO_2 flux under night time low wind speed conditions.

Night time dew formation

The long-term observations of temperature and humidity along the 200 m tower enable an independent estimate

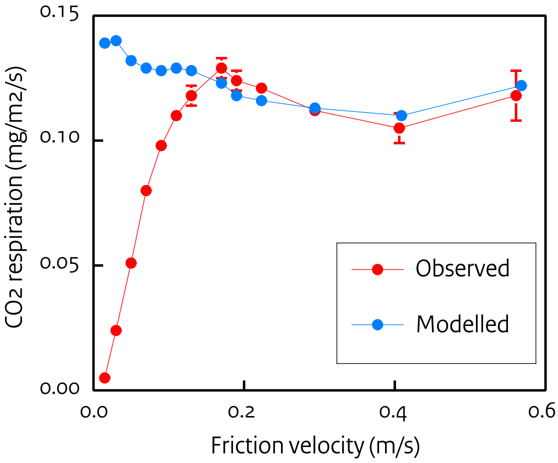

Figure 5. *Mean ratio of observed and modelled night time respiration flux as a function of friction velocity.*

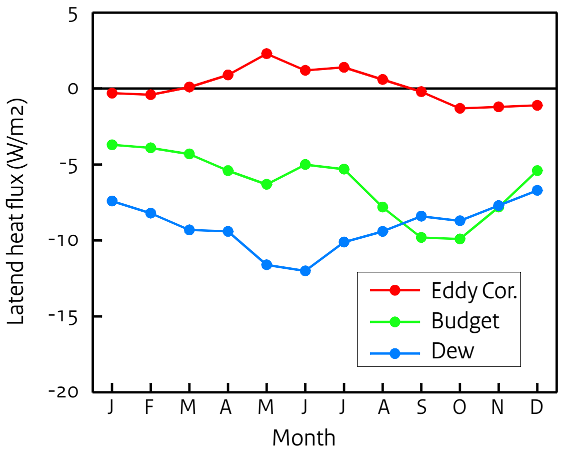

Figure 6*. Night time latent heat flux from eddy-correlation, atmospheric budget and dewfall estimates classified per month for the period 2001-2008 at Cabauw.*

of night time sensible and latent heat flux by making up the atmospheric budget in the lowest 200 m. Estimating surface fluxes from atmospheric budgets are problematic due to the influence of horizontal differential advection. Roode et al.[13)] analyzed many nights from the long observational record and found a systematic decrease of heat and water vapour content in the 200 m column, which most likely is due to a downward surface sensible and latent heat flux. Comparing with eddy-correlation measurements they found a reasonable correspondence for sensible heat but a significant underestimation of EC-based downward latent heat flux. Figure 6 shows the mean diurnal cycle of the budget method and of the eddy-correlation method for latent heat flux. Jacobs et al.[14)] performed direct measurements of dew formation in Wageningen, the Netherlands. The typical values they found correspond reasonably to the mean values obtained at Cabauw from the atmospheric budget technique as is also shown in Figure 6.

Daytime

From observations and in Large Eddy Simulation (LES) studies[15)] it is shown that considerable transport takes place at large scales in the convective boundary layer. These so-called Turbulent Organized Structures (TOS) are most apparent in the middle of the convective boundary layer. In the atmospheric surface layer the contributions of these structures to the total flux decreases linearly with height, because there is no space for a considerable spatial extended vertical wind structure close to the surface. A specific experiment has been performed by Kohsiek (unpublished) at Cabauw in 2003 with the hypothesis that the SEB-imbalance is caused by this TOS. The aim was to measure the difference in turbulent flux between 1.25 and 5 m. Despite precautions taken to avoid differences in spectral loss between the two sets of instruments the results were inconclusive.

Relation with other research at Cabauw

Although the TOS cannot explain the surface SEB problem it is of interest for the interpretation of flux observations higher up in the atmospheric boundary layer as are done at Cabauw. This elevated flux observations can also be used to study the SEB by incorporating the storage of heat and water vapour below the observation level and select on periods that advection is negligible. As a preparation for this kind of studies it is crucial to have a good understanding of the interaction between transport on the large spatial scales and time windows used in deriving eddy-correlation fluxes. In cooperation with the Delft University of Technology two studies have been performed. One[16)] looks at the behaviour of vertical wind speed at the long time scales and finds that at elevated levels mean vertical wind speeds persist at considerably longer time scales than expected from surface layer similarity theory. The other study[17)] quantifies the long time scales contribution to the vertical flux at different levels and shows that this contribution can reasonably be described with surface layer theory. These findings are then confirmed by analysis of LES results. This paves the way to correct elevated fluxes for low-frequency loss. The results of this study are of direct significance for a study in cooperation with the Wageningen University[18)] into the interpretation of scintillometer observations at 60 m height over a 10 km path between Cabauw and the IJsselstein TV-tower and for a study on atmospheric budgets of CO_2 [19)].

Conclusion

SEB-imbalance is a fundamental problem in micrometeorology. We have presented evidence that radiation observations are well-established and an order of magnitude more accurate then the magnitude of the SEB-imbalance. Soil heat flux observations remain problematic, but it is shown that uncertainties in soil heat flux alone cannot explain the SEB-imbalance. For night time conditions it is shown that serious inconsistencies exist between eddy-correlation measurements and independent estimates of surface fluxes of heat and CO_2. For daytime it is shown that at higher levels in the boundary layer large-scale structures are not well captured by the EC-method. It is, however, unlikely that these structures play a significant role close tot the surface. Unclear at this stage is the role of ditches which cover approximately 10% of the surface at Cabauw and which always will give significant temperature contrasts at the surface. The problematic conclusion is that as long as we cannot pin-down which part of the observed SEB is erroneous we must prescribe an error of 10-20% of the net-radiation to all the components of the surface energy budget. This seriously hampers progress when for example comparing observations with models or with satellite products. One route that will be pursued is exploiting the eddy-correlation observations at higher levels in the tower. It will be interesting to learn whether energy balance closure can be obtained from these levels.

References

1) Foken, T., 2008. *The energy balance closure problem: an overview.* Ecological Applications, **18**, 6, 1351-1367.
2) Heusinkveld, B., A.F.G. Jacobs, A.A.M. Holtslag and S.M. Berkowicz, 2004. *Surface energy balance closure in an arid region: role of soil heat flux.* Agric. and Forest Met., **122**, 21-37.
3) Bosveld, F.C. and W. Bouten, 2001. *Evaluation of transpiration models with observations over a Douglas fir forest.* Agric. and Forest Met., **108**, 4, 247-264.
4) http://www.cesar-observatorium.nl
5) Kroon P.S., 2004. *De sluiting van de oppervlakte energiebalans in Cabauw gedurende TEBEX (1995-1996).* KNMI Technical Report TR-261, 63pp.
6) Wang, P., W.H. Knap, P. Kuipers Munneke and P. Stammes, 2009. *Clear-sky shortwave radiative closure for the Cabauw Baseline Surface Radiation Network site, the Netherlands.* J. Geophys. Res., **114**, D14206, doi:10.1029/2009JD011978
7) Holtslag, A.A.M. and H.A.R. de Bruin, 1988. *Applied modelling of the night time surface energy balance over land.* J. Appl. Meteor., **27**, 6, 689-704.
8) Ronda, R.J. and F.C. Bosveld, 2009. *Deriving the surface soil heat flux from observed soil temperature and soil heat flux profiles using a variational data-assimilation approach.* J. Appl. Meteor., **48**, 3, 644-656.
9) Kroon, P., A. Hensen, H. Jonker, H. Ouwersloot, A. Vermeulen and F.C. Bosveld, 2010. *Uncertainties in eddy co-variance flux measurements assessed from CH_4 and N_2O observations.* Agric. and Forest Met., **150**, 6, 806-816.
10) Beljaars, A.C.M. and F.C. Bosveld, 1997. *Cabauw data for the validation of land surface parameterization schemes.* J. Climate, **10**, 1172-1193.
11) Kroon, P., A. Schuitmaker, H. Jonker, M. Tummers, A. Hensen and F.C. Bosveld, 2010. *An evaluation by laser Doppler anemometry of the correction algorithm based on Kaimal co-spectra for high frequency losses of EC flux measurements of CH_4 and N_2O.* Agric. and Forest Met., **150**, 6, 794-805.
12) Jacobs, C.M.J., A.F.G. Jacobs, F.C. Bosveld, D.M.D. Hendriks, A. Hensen, P.S. Kroon, E.J. Moors, L. Nol, A. Schrier-Uijl and E.M. Veenendaal, 2007. *Variability of annual CO_2 Exchange from Dutch Grasslands.* Biogeosciences, **4**, 803-816.
13) Roode, S.R., F.C. Bosveld and P.S. Kroon, 2010. *Dew formation, eddy-correlation latent heat fluxes, and the surface energy imbalance at Cabauw during stable conditions.* Bound.-Layer Meteorol., **135**, 369–383.
14) Jacobs, A.F.G., B.G. Heusinkveld, R.J.W. Kruit and S.M. Berkowicz, 2006. *Contribution of dew to the water budget of a grassland area in the Netherlands.* Water Resour. Res., **42**, WO3415, doi:10.1029/2005WR004055
15) Kanda, M., A. Inagaki, M. Letzel, S. Raasch and T. Watanabe, 2003. *LES study of the energy imbalance problem with Eddy Covariance fluxes.* Bound.-Layer Meteorol., **110**, 381–404.
16) Ouwersloot H., 2009. *The behaviour and consequences of Flux Imbalances in the Convective Boundary Layer.* Master-Thesis, Delft University of Technology, 87pp.
17) Schalkwijk, J., F.C. Bosveld and A.P. Siebesma, 2010. *Timescales and Structures in Vertical Transport in the Atmospheric Boundary Layer.* KNMI Scientific Report WR 2010-02, 69pp.
18) Braam, M., 2008. *Determination of the surface sensible heat flux from the structure parameter of temperature at 60 m height during day-time.* KNMI Technical Report TR-303, 40pp.
19) Casso-Torralba, P., J. Vilà-Guerau de Arellano, F.C. Bosveld, M.R. Soler, A. Vermeulen, C. Werner and E. Moors, 2008. *Diurnal and vertical variability of the sensible heat and carbon dioxide budgets in the atmospheric surface layer.* J. Geophys. Res., **113**, D12 doi:10.1029/2007JD009583

Recent developments in KNMI's surface observing methods

Marijn de Haij and Wiel Wauben

Introduction

Meteorological measurements are essential in meteorology and climatology and are core task of KNMI. The R&D Information and Observation Technology Division (I-RD) works continually on improvements of KNMI's observation infrastructure. Concerning surface observations ongoing activities are related to: (i) selecting, introducing and accepting sensor replacements for sensors that are at the end of their life cycle; (ii) selection and evaluation of sensors that use measurement techniques with economical or quality advantages; (iii) investigate sensor behaviour and data processing in order to solve known shortcomings; (iv) exploration and evaluation of new sensors that are a potential source of additional information. Below three highlights of ongoing activities are given that illustrate the introduction of a new measurement technique (sonic wind sensor), the investigation for improvement of precipitation detection and discrimination of precipitation type (TeNSor), and the evaluation of a new sensor system (NubiScope) for cloud measurements.

Introduction of a new measurement technique: sonic wind sensors

Introduction

Sonic wind sensors measure the time a sound pulse takes to travel between two transducers. When the travel times forward and back over a known distance are known, the wind speed component along that path can be derived together with the speed of sound in air. The latter is dependent on ambient temperature and to lesser degree also on relative humidity. A two dimensional (2D) sonic wind sensor with two transducer pairs gives the horizontal wind speed and direction as well as the so-called virtual temperature.

Meteorological measurements are essential in meteorology and climatology and are a core task of KNMI

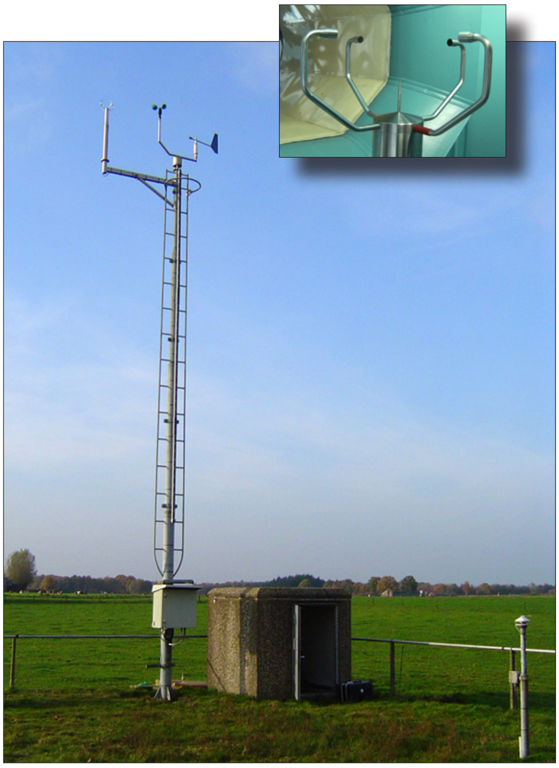

Figure 1. *The wind mast at Hupsel equipped with a sonic wind sensor and the operational KNMI cup anemometer and wind vane. The inset shows the Thies 2D sonic.*

In 2002-2003 three commercial 2D sonic wind sensors have been evaluated by KNMI[1]. The results were promising although the sensors did not meet all the requirements of KNMI. Newer versions of the 2D sonics, that meet the criteria, have recently come on the market. Hence KNMI selected a 2D sonic and started a project to introduce the sonics in the measurement network and get operational experience under various conditions. Although the reason for the replacement of conventional cup anemometers and wind vanes by sonic wind sensors is economical - sonics have no moving parts and require much less maintenance - the project is not only an INFRA Department affair. Users of the Climate and Weather Departments are involved in order to evaluate the results and to study the small differences with conventional cup anemometers and wind vanes that can be expected due to the different dynamical properties of the wind sensors.

Wind tunnel tests

Wind tunnel tests have been performed in the Low Speed Tunnel (LST) of the Dutch National Aerospace Laboratory (NLR) and in the TNO (Netherlands Organisation for Applied Scientific Research) wind tunnel. The LST wind tunnel tests are used for the verification of the absolute calibration of the horizontal wind whereas the TNO wind tunnel has been used for performing tests with inclined sonic wind sensors. All sensors have also been tested in the KNMI wind tunnel. Since the measurement volume of the KNMI tunnel is too small it cannot be used for the absolute calibration. However, it proved to be useful for testing the reproducibility of the sonic wind measurements.

Figure 2 (lower panel) shows the deviations of the azimuth averaged wind speed of two 2D sonics and three cup anemometers versus the LST wind tunnel reference up to 75 m/s. The results of the KNMI cup anemometers show an underestimation of the wind speed at low values (due to friction) and at high values (due to turbulence), but the results are well within the WMO accuracy limit of ±10%. The sonic wind sensors are close (<1%) to the reference wind speed over the full wind speed range. Note that the deviations in sonic wind speed and direction depend on the wind direction (upper panel). These errors are largest (3%) when the wind is parallel to a transducer pair because then the wind field along the measurement path is disturbed.

Field test

The sonics have been installed at 10 locations throughout the Netherlands which have been selected to give a wide variety of conditions. The location include e.g.: climatological stations Vlissingen and De Bilt with long

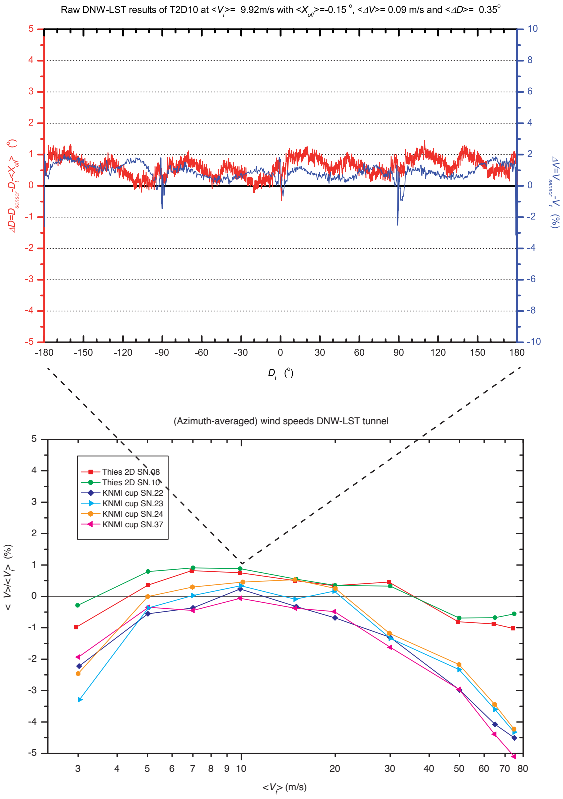

Figure 2. *The errors in wind speed (blue) and direction (red) depending on the azimuth of the sonic at 10 m/s (top) and the deviations of the azimuth averaged wind speed of two sonics and three cup anemometers from the DNW-LST wind tunnel reference for wind speeds between 3 and 75 m/s (bottom).*

historical records and high spatial variations in surface roughness around the locations; North Sea platform Lichteiland Goeree and the pier of IJmuiden where high wind speeds are observed in a saline environment; airports Schiphol (runway 18R) and Volkel where noise and vortices by aviation can be expected; the Cabauw research site of KNMI with optimal measurement conditions; Vlieland with the wind sensor on a sandy plain. At all locations the sonic wind sensor is installed in parallel to the existing cup anemometer wind vane combination (see Figure 1). The distance between the sonic and cup anemometer is 1 m and the sensors are aligned perpendicular to the prevailing South West wind direction. Figure 3 shows an example of the measurements obtained at 20 m altitude in De Bilt.

Conclusion

The wind tunnel tests showed that the 2D sonic wind sensors and cup anemometers meet the accuracy requirements for wind speed and direction over the full wind speed range, the results of the sonics generally being better. The field test shows that the wind speed and

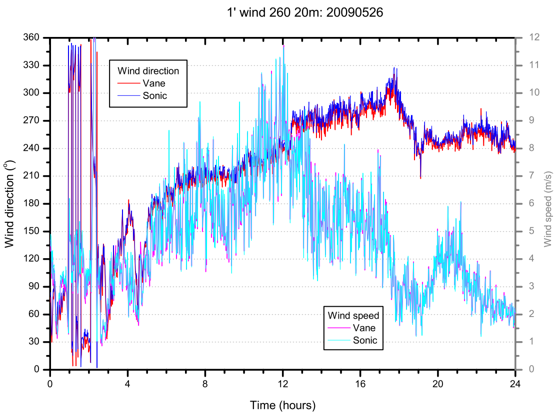

Figure 3. The 1-minute averaged wind direction and wind speed at De Bilt on May 26th, 2009 reported by cup/vane and sonic. The differences in wind direction show an alignment error of 4° and have a standard error of 3°. The daily averaged difference in wind speed is 0.03m/s with a standard error of 0.11m/s.

direction reported by the sonic are generally in very good agreement with those reported by the KNMI cup anemometer and wind vane, respectively. Some larger deviations and even data outages have been observed at De Bilt that are related to solid precipitation events and birds disturbing or even blocking the measurement path. The manufacturer provided a sensor with an improved heating and equipped with bird refuses, which is currently installed at De Bilt. The sonics have been made available in the measurement network in order to facilitate the user evaluation.

Exploration of new sensors for the observation of precipitation type

Introduction

KNMI operates the Vaisala FD12P present weather sensor for observations of visibility, precipitation type and duration in the national meteorological observation network. The sensor uses the principle of forward scattering of infrared light in a small volume of air.
Precipitation type is derived internally by analysing the signals from the optical receiver and a capacitive rain detector, together with temperature. However, some shortcomings of this observation have been recognized since its introduction[2,3,4)], particularly with precipitation type discrimination around zero degree Celsius, hail detection and the detection of very light precipitation events. Correction algorithms for the precipitation type did not give sufficient improvement. Therefore, it was decided to investigate the performance of new sensors for the observation of precipitation type in the TeNSor project, and investigate their added value over the FD12P.

Four sensors were selected and purchased for this test in the beginning of 2008. The optical disdrometers Thies Laser Precipitation Monitor (LPM) and Ott Parsivel measure the extinction in a horizontal sheet of light to estimate the diameter and fall velocity of each individual particle. The precipitation type is determined from the particle property statistics compared to empirical relationships. The Lufft R2S sensor, a small 24 GHz Doppler radar system, is also included, as well as the Vaisala WXT520 weather transmitter. The latter sensor is an all-in-one compact weather station with a piezoelectric precipitation sensor on top that is able to distinguish between rain and hail particles.

Field test and evaluation

The sensors are installed on the test field in De Bilt since September 12th, 2008 (see Figure 4). Data messages are acquired every minute and averaged to 10-minute and hourly weather codes, which are evaluated on a routine basis by data validation specialists and meteorologists. They can enter their level of agreement with the sensors in a web-based form. The sensors on the test field are co-located within 30 m of the FD12P and the other meteorological sensors, which offers the opportunity to analyse the relation with other parameters (e.g. precipitation amount, wind) as well.

A winter situation where the Thies LPM and Ott Parsivel significantly deviate from the FD12P is presented in Figure 5 (left panels). Both optical disdrometers start to report mixed and solid precipitation from 16UT, which is in better agreement with the evaluation of the meteorologist than the rain reported by the FD12P. The reported large amount of hail reports by the Parsivel, which is a common feature for this sensor, has however not been confirmed. Note furthermore that the LPM seems more sensitive for very light precipitation, reporting a

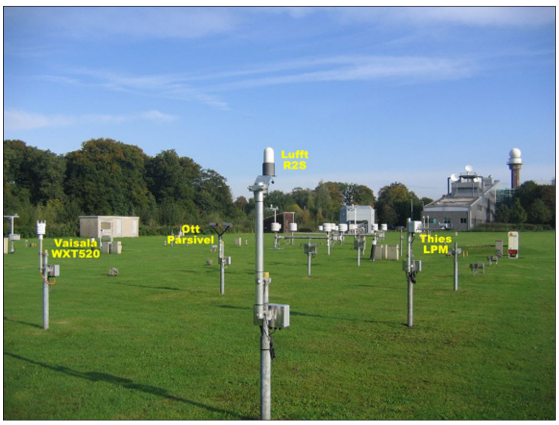

Figure 4. The test field in De Bilt, with the four precipitation type sensors under test indicated in the foreground.

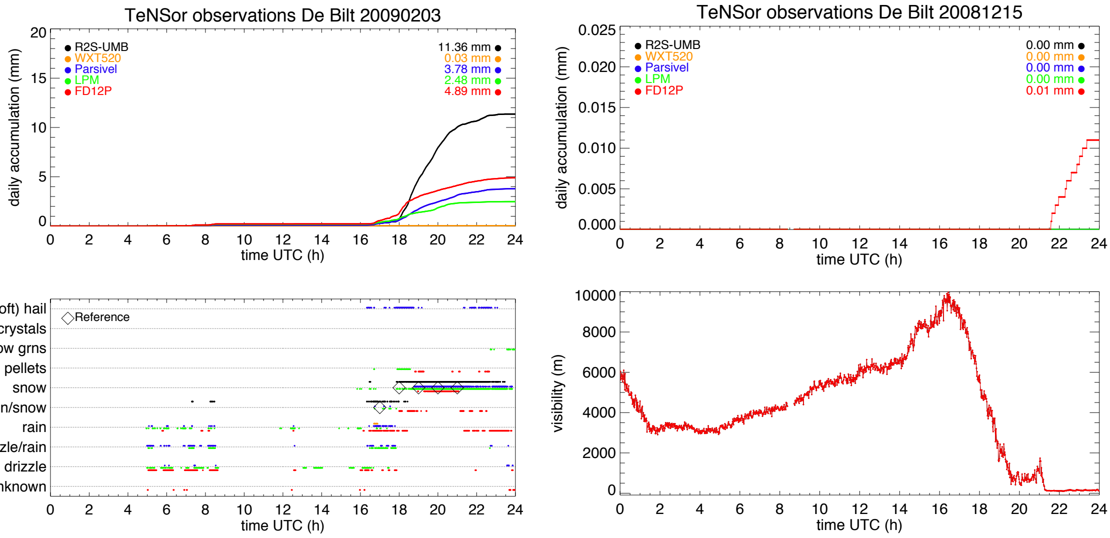

Figure 5. Overview of the precipitation accumulation for two days in the field test: a) wintry precipitation on February 3rd, 2009 (left), and faulty detections of precipitation by the FD12P sensor due to dense fog on December 15th, 2008 (right). For the first case, the reported precipitation types are shown in the lower left panel, with the observation of the meteorologist ('Reference') indicated by black diamonds. For the second case, the visibility presented in the lower right panel is the Meteorological Optical Range (MOR).

significant number of drizzle events between 13 and 14 UT. The detection and precipitation type capabilities of the Lufft R2S and Vaisala WXT520 seem inadequate.

Another case, where the FD12P falsely detects precipitation during dense fog, is illustrated in Figure 5 (right panels). Visibility values drop below 200 m shortly after 21 UT, leading to successive reports of snow and snow grains with intensities up to 0.03 mm/h. Improvement can be achieved on this point as well, as the other sensors in the test clearly suffer less from this problem.

Conclusion

Based on the evaluation in the first winter of the test, the Thies disdrometer is the most promising sensor for improving the observation of the precipitation type in the maerurement network of KNMI. More specifically, it seems to give added value on hail discrimination and demonstrates good results during transitions between liquid and solid precipitation and the detection of very light precipitation. It should however be mentioned that the Thies disdrometer also has its shortcomings, i.e. it suffers from false detections due to insects and spider webs and shows a significant wind direction dependency of the measured precipitation amount. The latter was confirmed in an analysis of DWD data from three LPM sensors with different orientations.

Wintry precipitation events in one season are sparse and the evaluation by meteorologists has its limitations because they scarcely have the opportunity to perform a detailed evaluation during solid precipitation events. Therefore the test was extended to the end of the winter season 2009-2010. Furthermore a second field test with the Thies LPM at the airports Schiphol and Rotterdam airport is being prepared since the human observer can play an important role in the evaluation. In addition,

Figure 6. The NubiScope at the Baseline Surface Radiation Network (BSRN) site of Cabauw.

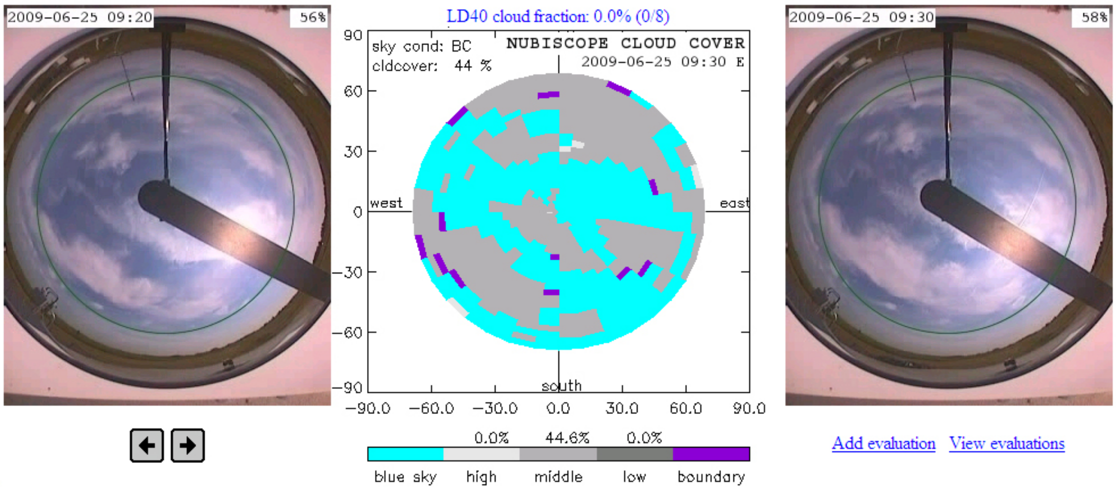

Figure 7. The NubiScope evaluation screen showing: a daily overview of the total cloud cover of NubiScope (gray), LD40 (green) and TSI (red) on June 25th, 2009 and the differences LD40-NubiScope (blue) (bottom); the video images of the TSI at the start and end of the NubiScope scan and the NubiScope cloud mask at 9:30UT (top).

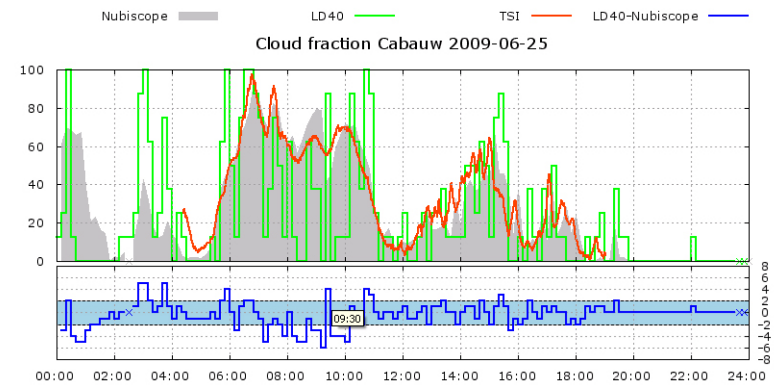

the combination of the results of the rain gauge, the FD12P and the disdrometer in order to obtain an optimal precipitation detection and type discrimination needs to be investigated in more detail.

Evaluation of a new sensor system for cloud observations: NubiScope

Introduction

Since November 2002 all synoptic cloud observations at KNMI are performed automatically and more recently the aeronautical cloud observations in the aviation routine weather reports (METAR) are automated for some regional and military airports. For that purpose the cloud base detections of a ceilometer (Vaisala LD40) of the previous half hour (10 minutes for AUTOMETAR) are processed with an algorithm that combines the individual cloud hits into up to 3 cloud layers each with base and cloud amount. Experience indicated that although the results of manual and automated cloud observations show good overall agreement, large differences do occur in certain situations when the measurements of the ceilometer are not representative for the full hemispheric cloud cover as reported by an observer. In 2006 KNMI evaluated a scanning Infrared (IR) sensor, the so-called NubiScope (Figure 6), which can determine the cloudiness over the full hemisphere during day- and night-time[5]. In 2008 such a sensor was purchased by the Regional Climate Division in order to improve the cloud observation at Cabauw and also to provide temperature information of the cloud base and the ground surface. An evaluation of the NubiScope is performed jointly by the Regional Climate, Infra R&D and Weather Production Divisions.

NubiScope measurements

Since April 2008 the NubiScope is installed at the Baseline Surface Radiation Network (BSRN) site of Cabauw. The NubiScope consists of a pyrometer which is sensitive in the thermal infrared (10-14 µm) with a field of view of 3° mounted on a pan-and-tilt unit. The NubiScope works fully automatic and performs a scan of the overhead hemisphere (36 azimuth and 30 zenith angles) and two surface temperature measurements every 10 minutes. The observed temperatures are processed in order to

NubiScope okta →

↓ okta LD40 (AUTOMETAR)	NA	0	1	2	3	4	5	6	7	8	Sum
NA	2164	134	103	28	26	15	26	21	193	326	3036
0	3379	2654	2609	371	162	116	97	71	307	141	9907
1	1195	1100	1105	348	180	127	81	73	276	128	4613
2	380	235	298	193	129	71	61	35	173	76	1651
3	333	129	203	136	141	88	55	38	196	67	1386
4	439	101	172	146	171	126	92	73	239	81	1640
5	383	58	109	95	135	129	117	99	311	91	1527
6	472	41	67	54	85	129	131	126	389	156	1650
7	1388	25	85	75	116	183	309	438	1736	1042	5397
8	5343	22	89	50	46	95	173	402	5498	10035	21753
Sum	15476	4499	4840	1496	1191	1079	1142	1376	9318	12143	52560

Δn±0 = 45% Δn±1 = 80% Δn±2 = 88% <Δn> = 0,04 |Δn|> = 1,07

Table 1. *The contingency table of the total cloud cover reported by the NubiScope and LD40 for the period May 2008 – May 2009 in Cabauw. The green diagonal contains 45% of the data where LD40 and NubiScope give identical total cloud cover. The yellow and orange bands contain 80% and 88% of the data that is within ±1 and ±2 okta, respectively. The averaged difference in total cloud cover is 0.04 okta and mean absolute deviation is 1.1 okta. Although the agreement between LD40 and NubiScope is generally good, situations where one reports overcast (8 okta) whereas the other reports clear sky (0 okta) do occur.*

derive the obscuration type (fog, precipitation, clouds) and cloud characteristics (cloud cover, layering and altitude). The NubiScope determines the presence of clouds from the deviation of the measured sky temperature from a clear sky value. The cloud height follows from the temperature by assuming a standard temperature profile. A product of the NubiScope is a cloud mask that shows the spatial distribution of low, middle and high cloud (see Figure 7).

NubiScope evaluation

The total cloud results of the NubiScope are being evaluated by comparing the results with those obtained by the LD40 ceilometer and other sensors available at Cabauw, such as the cloud radar and Total Sky Imager. The differences between the NubiScope and the LD40 are similar to the differences observed between the manual observer and the LD40. The differences in total cloud cover are in 88% of the cases ±2 okta or less (see Table 1). As a result of scanning the NubiScope is able to detect clouds in almost clear sky situations or gaps in overcast situations. This is illustrated by the reduced number of occurrences of 0 and 8 okta and increased occurrences of 1 and 7 okta of the NubiScope compared to the LD40. The evaluation by the Weather Department is performed by the observers at Rotterdam airport by analysing the 10-minute NubiScope, LD40 and TSI results. Their findings are entered in a web tool.

Conclusion

The evaluation showed that the total cloud cover reported by the NubiScope has a better spatial representativeness than the LD40 and its frequency distribution shows better agreement with reports by human observers. The sensitivity of the NubiScope for high clouds is still a bit unclear. Often it seems to be better than that of the LD40, but certainly not as good as that of the cloud radar. The results of the NubiScope might be affected by contamination of the lens and atmospheric moisture. This needs to be investigated in more detail. The Climate Division decided to keep the NubiScope as a permanent instrument at the Cabauw research site.

References

1) Wauben, W. M. F., 2007. *Wind Tunnel and Field Test of Three 2-D Sonic Anemometers.* KNMI Technical Report TR 296, KNMI, De Bilt, the Netherlands.
2) Wauben, W.M.F., 2002. *Automation of visual observations at KNMI; (I) Comparison of present weather.* Symposium on Observations, Data Assimilation and Probabilistic Prediction, Orlando, Florida, 13-17 January 2002, American Meteorological Society.
3) Meulen, J.P. van der, 2003. *Exploratory actions on automatic present weather observations.* Final report. EUMETNET PWS-SCI report, De Bilt, the Netherlands.
4) Haij, M.J. de, 2007. *Automated discrimination of precipitation type using the FD12P present weather sensor: evaluation and opportunities.* KNMI Technical Report TR 297, KNMI, De Bilt, the Netherlands.
5) Wauben, W.M.F., 2006. *Evaluation of the NubiScope.* KNMI Technical Report TR 291. De Bilt, the Netherlands.

High resolution observations for climate change monitoring of extremes

Albert Klein Tank

Introduction

A basic requirement for the monitoring of climate extremes is the availability of (and access to) high resolution observation data from meteorological stations. Availability of high resolution observation data is also required for delivering climate change information services in support of adaptation measures.

In Europe, the station network for near-surface climate observations is managed by a large number of predominantly National Meteorological and Hydrological Services (NMHSS). Although each of these NMHSS has its own data archive and its own data distribution policy, they are convinced that sharing their data is essential for assessing climate change in a European and worldwide context. KNMI has developed a framework which enables sharing and analyzing high resolution observation data. This highlight describes the approach, recent progress and future plans for this activity.

The activities under the umbrella of ECA&D provide vital ingredients for a successful monitoring of climate extremes in Europe

European Climate Assessment & Dataset (ECA&D)

The need for exchanging observation data with higher temporal and spatial resolution than available in existing international databases formed the motivation for the EUMETNET-European Climate Support Network (ECSN) to start the project "European Climate Assessment & Dataset (ECA&D)" in 1998. The goal was to realize a sustainable operational system for gathering, archiving, quality control, analysis and dissemination of high resolution data.

The data gathering aspect refers to the collection of long-term daily resolution climatic time series from meteorological stations throughout Europe and the Mediterranean. Currently, over 50 countries participate. The archiving aspect refers to the transformation of time series to standardized formats and subsequent storage in a centralized database system at KNMI. Quality control refers to the use of standard procedures to check the data and attach quality and homogeneity flags. Analysis refers to the calculation of derived indices for climate extremes, such as the number of frost days or the number of high precipitation events, according to internationally agreed procedures. Finally, dissemination refers to making available to users both the daily data (including quality flags and homogeneity information) and the derived indices. Most of the daily series and all derived indices information (including time series plots, trend maps, anomaly maps and climatology maps) are publicly available at http://eca.knmi.nl. Among the users is the European Environment Agency (EEA)[1].

The ECA&D database has seen important updates over the past few years, significantly extending the number of stations and variables[2]. To meet the changing requirements towards near real-time information, many of the scripts leading to the derived indices were made more computationally efficient in 2009. Data from synoptic messages distributed through the Global Telecommunication System (GTS) are now collected and merged as near real-time supplements to the climatic time series. The amount of metadata in the database has been increased and made accessible via the ECA&D webpage. This information is required for the correct interpretation of the observational series. The metadata now includes not only station location, but also such things as pictures of the observing site, surface coverage information, station relocations, and (changes in) observing practices where available.

The analysis of changes in the frequency and strength of extremes using derived indices in ECA&D continues to be aligned with worldwide indices activities[3)]. To illustrate the use of derived indices for analyzing observed changes in moderate extremes, Figure 1 shows the trends in the index "precipitation fraction due to very wet days (above the long term 95 percentile)". This index can be used to investigate whether there has been a relatively larger change in extreme precipitation events than in the total amount. At stations where the total annual amount increases, positive trends in this index indicate that extremes are disproportionately increasing more quickly than the total. At stations where the annual amount decreases, positive trends in this index indicate that very wet days are less affected by the trend in the total compared to the other wet days. Negative trends indicate a smaller than proportional contribution of very wet days to observed changes in total precipitation.

Figure 1a shows a positive trend in this index of 0.46 % per decade for De Bilt. The majority of the precipitation series in the Netherlands (Figure 1b) and Europe (Figure 1c) also show a positive trend in this index, indicating a disproportionately large change in the extremes relative to the total amounts. The Europe-average trend over the period 1946-2008 is 0.32% per decade (95% confidence interval: 0.14-0.51%). This supports the notion of a relatively larger change in extreme precipitation events compared to the annual

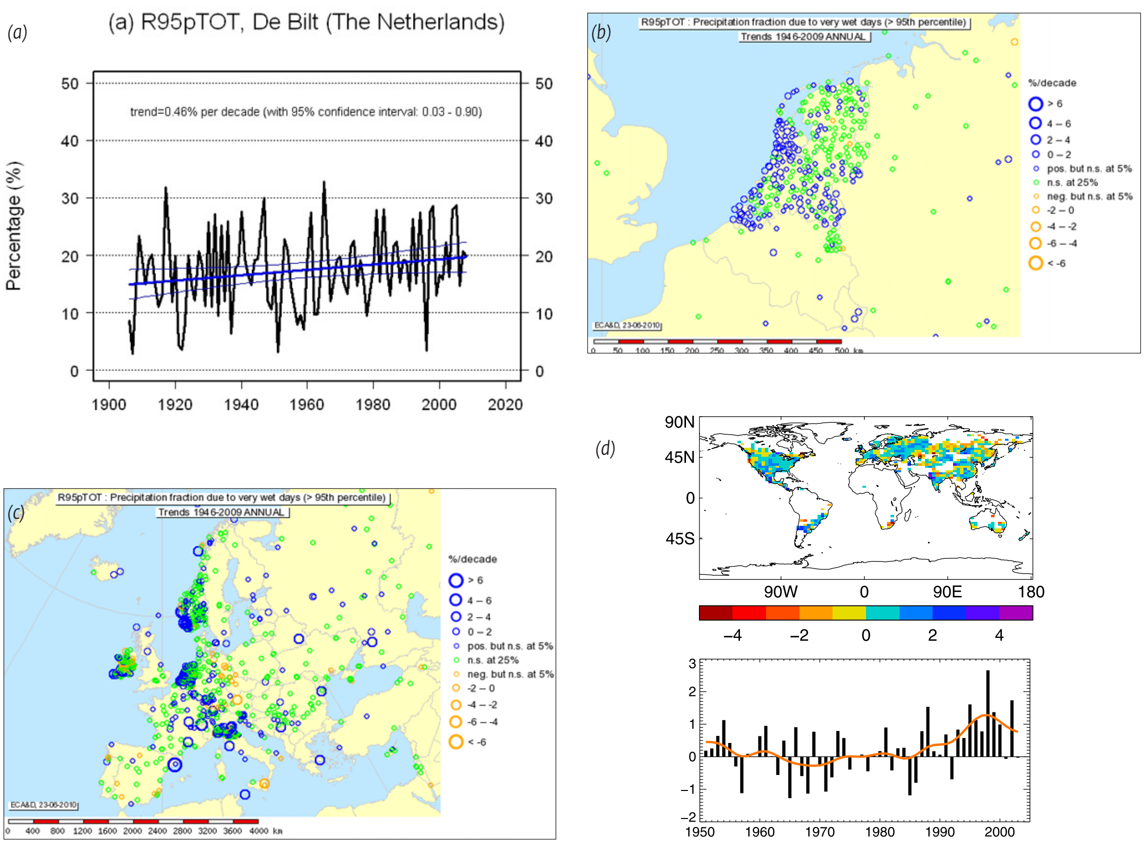

Figure 1. Observed trends in the extremes index "precipitation fraction due to very wet days" derived from daily ECA&D series: (a) the time evolution at station De Bilt (blue lines indicate the trend and its 95% confidence interval); (b) the trends over the period 1946 to 2009 at stations in the Netherlands; (c) the trends over the same period at stations in Europe; and (d) the worldwide trends between 1951 and 2003 and the anomalies averaged over grid cells with data. Source: http://eca.knmi.nl and 4). The analysis consists of the following steps: 1) identification of the very wet days in the daily precipitation series using a site specific threshold calculated as the 95th percentile of wet days in the 1961-90 period; 2) determination of the percentage of total precipitation in each year that is due to these very wet days; and 3) calculation of the trends in the time series of these yearly percentages. The maps show that positive trends dominate, but information is only available for roughly half of the global land area.

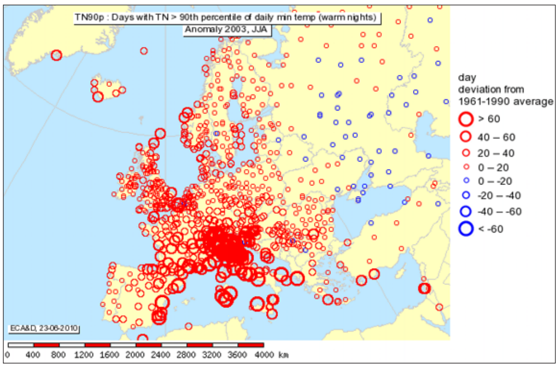

Figure 2. *Use of ECA&D station series to describe the heat wave summer of 2003 in Central and Western Europe with the extremes index "warm nights". For every station, the circle represents the number of nights with minimum temperature falling in the long-term 90th percentile range for the local climate. The size of the circle is proportional to the number of nights: blue indicates fewer "warm nights" than the climatological value and red indicates more "warm nights" than the climatological value. During summer 2003 in particular, the number of "warm nights" was much higher than usual in a large part of Central and Western Europe (red circles dominate the map). In areas with large red circles, there have been more than 40 additional "warm nights" compared to a normal summer season. This anomaly corresponded with mean summer temperatures that were more than 3°C higher than the long term average. (source: http://eca.knmi.nl).*

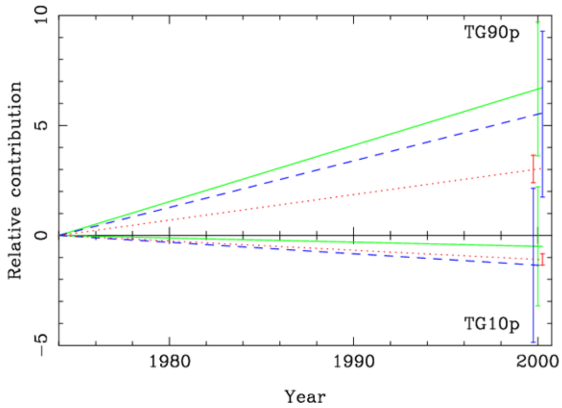

Figure 3. *Relative contributions of several factors to the trend in the extremes indices "cold days" (below the zero line) and "warm days" (above the zero line) observed at ECA&D stations averaged over Europe. The green, solid lines show the trends as observed in the index for "cold days" (TG10p) and "warm days" (TG90p). The red, dotted lines show the trend contribution due to global warming. The blue, dashed lines show the accumulated contributions of global warming and changes in the frequency of circulation types. The error bars (uncertainties) are shown for the year 2000 (slightly shifted for clarity). (source[5])*

totals. Together with similar results for other regions of the world (Figure 1d), this led IPCC[4] to conclude that heavy precipitation events increased over most areas during the second half of the 20th century, leading to a larger proportion of total yearly rainfall due to heavy falls.

Another example of the use of derived indices for analysing extremes is shown in Figure 2, in which the index "warm nights" is portrayed for the European heat wave summer of 2003. The results indicate that during this summer, the number of warm nights has been much higher than usual in a large part of Central and Western Europe. The anomalies in "warm nights" were generally larger than the anomalies in the number of "warm daytimes" (not shown).

Recent indices analysis has focussed on the influence of atmospheric circulation changes on the observed changes in the number of "warm days" and "cold days" in Europe[5]. In this study, the temperature series were first adjusted for global warming before determining the indices for cold and warm extremes. The results show a warming effect for both winter and summer. For the "warm day" index, this change is not accounted for by the frequency change of circulation types, nor is it accounted for by the global warming trend (Figure 3). A simple snow model shows that variations in the European snow cover extent are likely influencing the cold and warm day indices in winter, i.e., the decreasing trend of snow cover extent is associated with the increasing (decreasing) trend of the number of warm (cold) days for stations throughout Europe.

E-OBS gridded version

In recent years, the ECA&D station data have been used in several activities and projects. Within the EU-FP6 project ENSEMBLES[6], a new daily gridded observation dataset (E-OBS) has been developed on the basis of the ECA&D station data[7]. This new dataset enables, for the first time, evaluation of how well extremes are represented in Regional Climate Model simulations.

The E-OBS dataset is a European land-only, daily high-resolution dataset for precipitation and surface air temperature (minimum, mean and maximum) for the period 1950-now. This dataset improves on other products in its spatial resolution and extent, time period, number of contributing stations, and research into finding the most appropriate method for spatial interpolation of daily climate observations. Figure 4 shows the E-OBS dataset for the maximum temperature

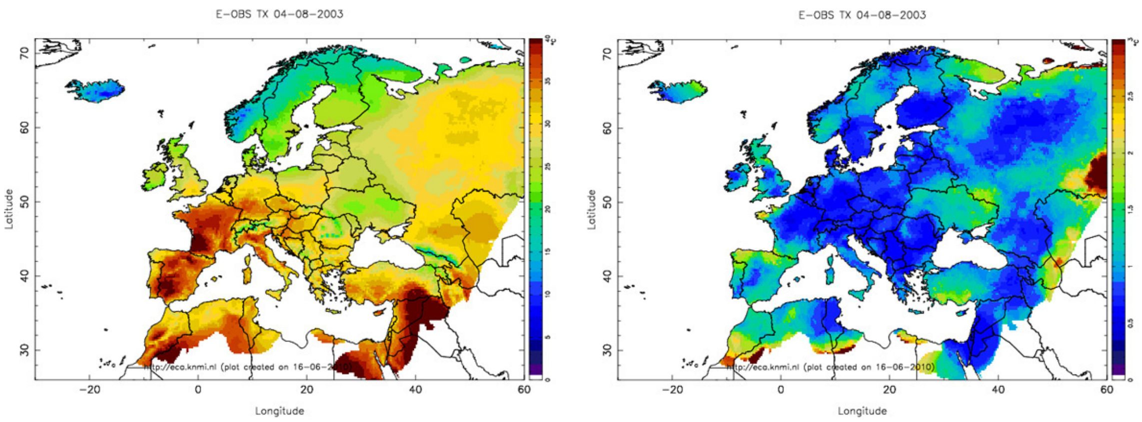

Figure 4. *Illustration of the E-OBS dataset (0.25 degree regular grid) showing the maximum temperature (left) plus standard error (right) on the hottest day in Europe since 1950: 29 July 2002. The maximum temperature averaged over Europe on this day was 30.3°C, compared to the 1961-1990 summer mean of 22.4°C. The box defines the geographical extent of the dataset and white land areas indicate that there is not enough station data for interpolation. (source: http://eca.knmi.nl/ensembles).*

on the hottest day in Europe since 1950, 29 July 2002. The E-OBS dataset is accessible by the public at http://eca.knmi.nl/ensembles. It will continue to be maintained and updated beyond the duration of the ENSEMBLES project, which ends in December 2009.

The new E-OBS daily gridded dataset for Europe enables, for the first time, evaluation of extremes in Regional Climate Model simulations

Statistical homogeneity tests performed routinely within ECA&D[8] and for ENSEMBLES[9] reveal that many of the underlying station series are subject to potential inhomogeneities due to, for instance, changes in observing practices. This affects, in particular, the understanding of extremes because changes in extremes are often more sensitive to inhomogeneous climate monitoring practices than changes in the mean. In addition, there are limitations in the ability of the interpolation method to estimate grid values from the underlying station network. In areas where relatively few stations have been used for the interpolation, both precipitation and temperature are 'over-smoothed'. This leads to reduced interpolated values relative to the 'true' area-averages, in particular for extremes[10]. This implies that future work on the E-OBS gridded dataset is necessary and care must be taken when using it. But E-OBS is the only daily gridded dataset currently available and quality control procedures have successfully filtered out the most severe data problems.

Outlook

After more than 10 years, ECA&D has entered a mature phase. From 2009 onwards, the system will continue to be maintained by KNMI as an operational activity, rather than as a research activity. Recently, the status of Regional Climate Centre (RCC) for high resolution observation data in WMO Region VI (Europe and the Middle East) has been obtained. This means that the activity is recognized by WMO as an important contribution to regional and global climate monitoring and service delivery. RCCs are Centres of Excellence that assist WMO members in a given region to deliver better climate services and products, and to strengthen their capacity to meet national climate information needs. ECA&D provides such RCC-services for daily station data and derived extremes indices data.

Starting in 2010, KNMI will develop new ECA&D functionalities and conduct scientific research with the observation data within the EU-FP7 funded project European Reanalysis and Observations for Monitoring (EURO4M), for which KNMI is the coordinator. The aim of EURO4M is to describe the evolution of the Earth system components by seamlessly combining two different but complementary approaches: regional observation datasets of Essential Climate Variables (ECVs) such as provided by ECA&D on the one hand, and newly developed state-of-the-art (model based) regional reanalysis on the other.

EURO4M will extend, in a cost-effective manner, European capacity to systematically monitor climate variability and change (including extremes) on a range of space and time scales. The project will reach out with innovative and integrated data products and climate change services to policy-makers, researchers, planners and citizens at European, national and local levels. This will directly address the needs of, for instance, the EEA for their environmental assessment reports, and even provide online reporting during emerging extreme events.

EURO4M is an important building block for Global Monitoring for Environment and Security (GMES). It has the potential to evolve into a future GMES service on climate change monitoring that is fully complementary and supportive to the existing operational services for land, marine, emergency, atmosphere, and security.

Conclusion

The activities under the umbrella of ECA&D provide vital ingredients for a successful monitoring of climate extremes in Europe. ECA&D also enables adequate climate change information services in support of adaptation measures on a European scale. The project is well on its way to become Europe's primary source of timely and reliable information about the state of the climate. This will help us better understand and predict climate change, extremes and weather related hazards, so that society can respond in the best possible way.

References

1) EEA-JRC-WHO, 2008. *Impacts of Europe's changing climate – 2008 indicator-based assessment.* EEA Report No 4/2008, JRC Reference Report NoJRC47756. doi:10.2800/48117
2) Klok, E.J. and A.M.G. Klein Tank, 2008. *Updated and extended European dataset of daily climate observations.* Int. J. Climatology. doi:10.1002/joc.1779
3) Klein Tank, A.M.G., F.W. Zwiers and X. Zhang, 2009. *Guidelines on Analysis of extremes in a changing climate in support of informed decisions for adaptation.* WMO-TD No. 1500, WMO, Geneva, Switzerland, 56pp.
4) IPCC, 2007. *Climate Change 2007: The Physical Science Basis. Contribution of Working Group I to the Fourth Assessment Report of the Intergovernmental Panel on Climate Change, Solomon, S., D. Qin, M. Manning, Z. Chen, M. Marquis, K.B. Averyt, M.Tignor and H.L. Miller (Eds.).* Cambridge University Press, Cambridge, United Kingdom and New York, NY, USA, 996pp.
5) Besselaar, E.J.M. van den, A.M.G. Klein Tank and G. van der Schrier, 2010. *Influence of circulation types on temperature extremes in Europe.* Theor. Appl. Climatol., 99, 431-439. doi:10.1007/s00704-009-0153-6
6) Van der Linden, P. and J.F.B. Mitchell (Eds.), 2009. *ENSEMBLES: Climate Change and its Impacts: Summary of research and results from the ENSEMBLES project.* Met Office Hadley Centre, FitzRoy Road, Exeter EX1 3PB, UK., 160pp.
7) Haylock, M.R., N. Hofstra, A.M.G. Klein Tank, E.J. Klok, P.D. Jones and M. New, 2008. *A European daily high-resolution gridded dataset of surface temperature and precipitation.* J. Geophys. Res, **113**, D20119. doi:10.1029/2008JD10201
8) ECA&D-group, 2009. *Algorithm Theoretical Basis Document (ATBD) for the European Climate Assessment & Dataset (ECA&D).* Available from: http://eca.knmi.nl/documents/ecad_atbd.pdf
9) Begert, M., E. Zenkusen, C. Haeberli, C. Appenzeller and L. Klok, 2008. *An automated homogenization procedure; performance assessment and application to a large European climate dataset.* Meteor. Z., **17**, 5, 663-672.
10) Hofstra, N., M. Haylock, M. New, P.D. Jones, 2009. *Testing E-OBS European high-resolution gridded dataset of daily precipitation and surface temperature.* J. Geophys. Res., **114**, D 21101, 16pp. doi:10.1029/2009JD011799

Regional differences in the extreme rainfall climatology in the Netherlands

Adri Buishand, Rudmer Jilderda and Janet Wijngaard

Introduction

The Netherlands is a small and flat country, and climatological differences are therefore small. Mean annual rainfall ranges from about 700 to 900 mm, see Figure 1. The small area in the extreme south-east corner of the Netherlands where mean annual rainfall slightly exceeds 900 mm coincides with the highest part of the country (up to 322 m).

Rainfall frequency analysis in the Netherlands has often been based on rainfall measurements at the KNMI observatory in De Bilt, in the middle of the country. The latest update was presented in 2004[1,2]. For this update hourly data for the period 1906-2003 were used. Apart from the hourly record of De Bilt, ten daily rainfall series from different locations were analysed. It was concluded that for the time being relative regional differences in mean annual rainfall could be used to account for regional differences in the quantiles of the distributions of extreme rainfall for durations of 24 h or longer. Further research using more rainfall data was recommended.

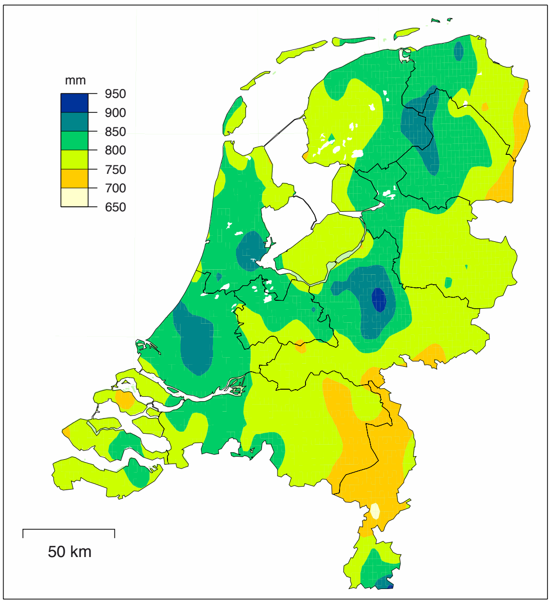

Figure 1. *Mean annual rainfall in the Netherlands for the period 1971-2000.*

Frequent flooding in coastal areas has led to discussions whether extreme rainfall might occur more often along the coast than is assumed in present-day hydrologic design practices. For extreme daily rainfall within the Delfland Water Authority area, situated to the west of Rotterdam, it was found that the adjustment of the quantiles of the extremes for De Bilt needs to be larger than what the ratio of the mean annual rainfall amounts of both places suggests[3]. In an other study seven hourly rainfall records were compared by calculating the extreme water levels for six different water systems[4].
The 5-year events obtained from the Rotterdam record turned out to be considerably higher than those from the De Bilt record. Relatively high water levels were also found for Valkenburg, near the west coast to the north of The Hague, but these were less high than for Rotterdam.

A detailed study on regional differences in extreme rainfall climatology in the Netherlands has been completed recently[5]. For this study the daily rainfall records from 141 rainfall stations for the 55-year period 1951-2005 were analysed. The stations were evenly distributed over the country. The selected records did not reveal serious artificial breaks regarding daily rainfall events of 10 mm or more. The analysis of extreme values and the application of the results are discussed below.

For this study the daily rainfall records from 141 rainfall stations for the 55-year period 1951-2005 were analysed

The analysis of extreme values

For each of the 55-year records the annual maximum rainfall amounts were abstracted for durations D of 1, 2, 4, 8 and 9 days. These durations are the same as those considered in the latest rainfall frequency analysis for De Bilt[1,2]. As in that previous work, the Generalized Extreme Value (GEV) distribution was used to describe the distribution of the annual maximum amounts for each duration. The quantile $x(T)$ that is exceeded on average once in T years (the 'T-year event') for a given duration D can then be represented as:

$$x(T) = \mu \left\{ 1 + \frac{\gamma}{\kappa} \left[1 - \left(- \ln \left(1 - \frac{1}{T} \right) \right)^{\kappa} \right] \right\}, \quad \kappa \neq 0$$

For $\kappa = 0$, the GEV distribution reduces to the Gumbel distribution, for which

$$x(T) = \mu \left\{ 1 - \gamma \ln \left[- \ln \left(1 - \frac{1}{T} \right) \right] \right\}$$

The GEV distribution has three parameters: a location parameter μ, a dispersion coefficient γ, and a shape parameter κ. Note that $x(T) = \mu$ if $T = 1/(1-1/e) \approx 1.58$ years, i.e., the location parameter corresponds to the value that is on average exceeded in 100/1.58 = 63% of the years. The dispersion coefficient γ is a measure of the year-to-year variability of the rainfall extremes (comparable to the coefficient of variation). The shape parameter κ is important if one is interested in very rare events ($T \geq 100$ years). For $\kappa < 0$ the GEV distribution has a heavier upper tail than the Gumbel distribution, implying that very rare events occur more frequently. The converse holds if $\kappa > 0$.

The three GEV parameters determine the magnitude of regional differences in extreme rainfall climatology. Regional variation in the shape parameter is discussed first, followed by the regional differences in the dispersion coefficient and the location parameter.

The shape parameter

Koutsoyiannis[6] analysed the 1-day annual maxima in long rainfall records from the USA, UK and Mediterranean and came to the remarkable conclusion that the shape parameter is the same in these geographical regions. Research in Belgium and the Netherlands has also not revealed any systematic differences between the values of the shape parameter for the two countries[7,8]. Based on this research, the following relationship between κ and the duration D (expressed in days) has been derived in the latest rainfall frequency analysis for De Bilt[1]:

$$\kappa = -0.090 + 0.0170D$$

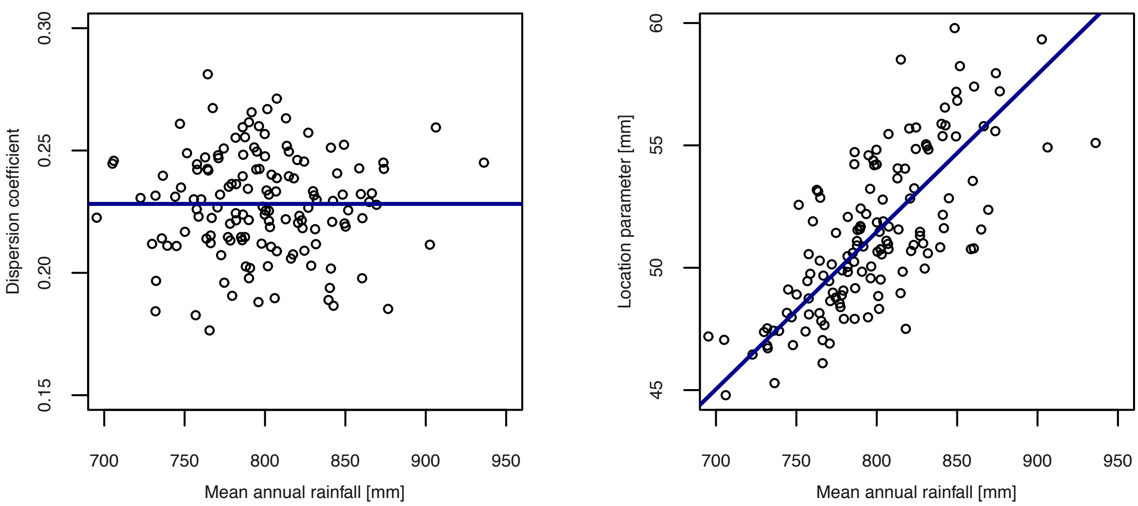

Figure 2. *Dispersion coefficient (left) and location parameter (right) of 4-day annual maximum rainfall versus mean annual rainfall. The horizontal line in the left panel depicts the average dispersion coefficient. The straight line in the right panel represents a proportional relationship between the location parameter and mean annual rainfall.*

Note that κ is negative for $D \leq 5$ days (heavy tailed distribution) and positive for $D \geq 6$ days. This relationship was needed because it is not possible to obtain a reliable estimate of κ from a single rainfall record. In line with that work, the same values of κ were employed in the research described here.

The dispersion coefficient

In Figure 2 (left panel) the estimated dispersion coefficients of the 4-day rainfall extremes for the 141 selected rainfall stations are plotted versus the mean annual rainfall. There seems to be no relationship between the two quantities. This was confirmed by a generalized least-squares regression. Generalized rather than ordinary least squares is necessary here because of the correlation between the estimated dispersion coefficients at neighbouring stations resulting from the spatial dependence of rainfall. This correlation decreases with increasing distance between stations (Figure 3). It further turned out that the difference between the dispersion coefficients for coastal and inland stations is statistically not significant. Similar results were obtained for the 1-day and 9-day rainfall extremes, so that we may assume that the dispersion coefficient is constant across the Netherlands for a given duration.

From the assumption of a constant κ and γ, it follows that $x(T)/\mu$ is also constant over the Netherlands for a given duration, or in other words the distribution of the extremes is everywhere the same after scaling with the location parameter. This corresponds with the index-

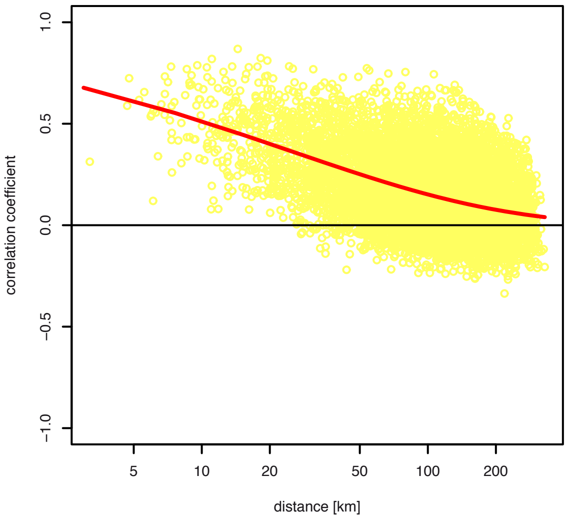

Figure 3. *Correlation between the estimated dispersion coefficients as a function of the distance between stations for the 4-day rainfall extremes. The estimates for the individual station pairs are printed in yellow. These estimates are based on a bootstrap technique. The red line represents a fitted curve that was used in the generalized least squares regressions.*

flood assumption in hydrology. The ratio of the T-year events at two locations A and B is then equal to the ratio of their location parameters:

$$\frac{x_A(T)}{x_B(T)} = \frac{\mu_A}{\mu_B}$$

for any T. This alone does not justify a scaling based on mean annual rainfall yet. It is also necessary that the location parameter is proportional to mean annual rainfall.

The location parameter

The right panel of Figure 2 shows that for the 4-day rainfall extremes the location parameter μ increases with mean annual rainfall. This relationship is statistically significant. However, it also turned out that a proportional relationship between the location parameter and mean annual rainfall performs poorly. From Figure 2 it can be seen that the estimated location parameter deviates up to 6 mm (more than 10%) from the value obtained from such a relationship. Therefore, the linkage with mean annual rainfall was abandoned. Instead, another simple rainfall attribute was chosen that summarises the values of the location parameter for the five considered durations:

$$\mu_{\mathrm{rel}} = \sum_D w_D \mu_D / \bar{\mu}_D$$

with μ_D the value of the location parameter for duration D, $\bar{\mu}_D$ the average of the μ_D's for the 141 selected rainfall stations, and w_D a weight ($w_D = 1/4$ for $D = 1$, 2 and 4 days and $w_D = 1/8$ for $D = 8$ and 9 days). This relative location parameter gives a better picture of the regional differences in the location parameter than mean annual rainfall (deviations from the estimated location parameter for the individual durations are reduced by a factor 2 to 3).

Adjusting for regional differences in extreme rainfall climatology

The parameter μ_{rel} varies from 0.90 to 1.18 on the 141 selected rainfall stations. The country average of μ_{rel} equals 1, which also happens to be the value for De Bilt. The rainfall frequency distributions for this station can therefore be regarded as average rainfall frequency distributions for the Netherlands. Consultation with representatives of regional water authorities has led to the recommendation to adjust the quantiles of extreme rainfall in areas where μ_{rel} deviates more than 5% from the value for De Bilt. These areas are indicated in Figure 4. The multiplying factors in this figure are equal to the average values of μ_{rel} for the respective areas. From the figure it is clear that the extreme rainfall climatology of De Bilt applies to the larger part of the country.

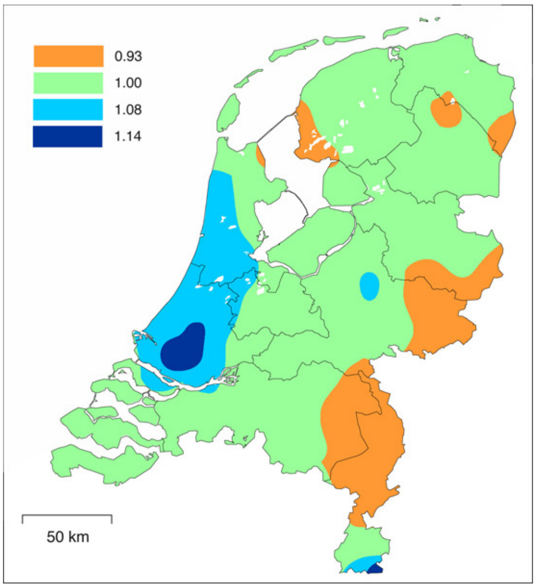

Figure 4. *Multiplying factors for converting the quantiles of extreme rainfall for De Bilt to other locations in the Netherlands.*

A number of areas were identified where the distributions of extreme rainfall for durations of 1 to 9 days significantly deviated from those in De Bilt

However, adjustments of +8% and +14% are advised for a region along the west coast. The higher adjustment in this region applies to the Rotterdam area. This adjustment is larger than an adjustment based on mean annual rainfall. A 14% adjustment is also recommended for the outermost south-east of the Netherlands. Areas with a negative adjustment are mainly found in the eastern part of the country.

The multiplying factors apply to extreme rainfall for durations of 1 to 9 days. Relatively large values of the location parameter are also found in a region along the west coast for the 24-h rainfall extremes in the radar data set, which is discussed in the highlight by Overeem et al. in this Triennial Report, but this region does not show up for the 60-min rainfall extremes. Distinct areas with relatively low values of the location parameters are also not found for the 60-min extremes. The use of the multiplying factors from Figure 4 is therefore discouraged for durations shorter than 1 day.

Conclusion

Regional differences in the extreme rainfall climatology in the Netherlands were explored using daily rainfall data from 141 rainfall stations. A number of areas were identified where the distributions of extreme rainfall for durations of 1 to 9 days significantly deviated from those in De Bilt. It appeared that a simple scaling of the quantiles of these distributions with the ratio of mean annual rainfall is insufficient to describe the regional differences accurately. Instead, another rainfall attribute (relative location parameter) is suggested to account for regional differences in the quantiles of the distributions of extreme rainfall.

Acknowledgements

The research was part of the project “From Rainfall to Damage”, which was coordinated by HKV Consultants, and partially funded by the Dutch knowledge impulse programme “Living with Water”, the Foundation of Applied Water Research (STOWA), the Province of South-Holland, and the Verbond voor Verzekeraars.

References

1) Smits, I., J.B. Wijngaard, R.P. Versteeg and M. Kok, 2004. *Statistiek van extreme neerslag in Nederland.* STOWA publication 2004-26. STOWA, Utrecht, the Netherlands, 95pp.
2) Wijngaard, J., M. Kok, A. Smits and M. Talsma, 2005. *Nieuwe statistiek voor extreme neerslag.* H2O, **38**, 6, 35-37.
3) Diermanse, F., H. Ogink, J. van Dansik and E. Goudemans, 2005. *Neerslagstatistiek, extreem gevoelig?* H2O, **38**, 17, 25-27.
4) Hoes, O., J. Biesma, K. Stoutjesdijk and F. van Kruiningen, 2005. *Invloed van de zee op de neerslagverdeling en de frequentie van wateroverlast.* H2O, **38**, 1, 32-34.
5) Buishand, T.A., R. Jilderda and J.B. Wijngaard, 2009. *Regionale verschillen in extreme neerslag.* KNMI Scientific Report WR 2009-01, 53pp.
6) Koutsoyiannis, D., 2004. *Statistics of extremes and estimation of extreme rainfall: II, Empirical Investigation of long rainfall records.* Hydrol. Sci. J., **49**, 4, 591-610.
7) Gellens, D., 2003. *Etude des précipitations extrêmes: Etablissement des fractiles et des périodes de retour d'événements pluviométriques.* Thèse de doctorat, Université Libre de Bruxelles, Belgique, 232pp.
8) Buishand, T.A., 1991. *Extreme rainfall estimation by combining data from several sites.* Hydrol. Sci. J., **36**, 4, 345-365.

Linking changes in hourly precipitation extremes to the Clausius-Clapeyron relation

Geert Lenderink and Erik van Meijgaard

Introduction

Events of extreme precipitation have a huge influence on society. They are associated with flooding, erosion, water damage, and may have impacts on transport and safety. It is commonly expected that precipitation extremes will increase as the climate warms. Changes in extreme precipitation are even often considered to be more predictable than changes in average precipitation[1,2]. For example, the KNMI'06 scenarios predict increases in extreme precipitation for all scenarios, but are not conclusive about the sign of the change in mean precipitation in summer[3].

The primary reason why precipitation extremes are expected to increase is that a warmer atmosphere has a larger saturation water vapour content. The relation between "moisture-holding capacity" of the atmosphere, temperature and pressure is expressed by the Clausius-Clapeyron relation, which is based on the atmospheric thermodynamics. From this relation follows an increase in the moisture-holding capacity of the atmosphere of approximately 7% per degree temperature rise. If the relative humidity in the future climate remains approximately the same as in the present-day climate – which is generally expected based on model results and also on physical understanding – the amount of water vapour in the atmosphere will increase also with 7% per degree temperature rise. Now, the commonly used argument is that in extreme showers all water vapour in the air (or a constant fraction of it) is converted into rain. Hence, extreme precipitation will scale with the Clausius-Clapeyron relation (see figure 1).

There is some model evidence from Global Climate Models (GCMs) that indeed precipitation extremes increase at the rate predicted by the Clausius-Clapeyron

The primary reason why precipitation extremes are expected to increase is that a warmer atmosphere has a larger saturation water vapour content

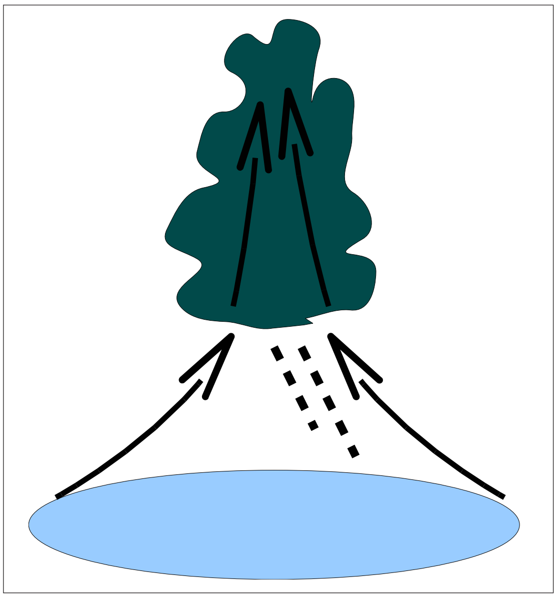

Figure 1. *Schematic diagram of a precipitating convective cloud. Water vapour from the sub-cloud area is drawn into the base of the cloud by the convective storm dynamics and low level convergence. In the cloud water vapour condenses into cloud droplets, and eventually converts into rain. During the cloud's lifecycle air from a certain area (in fact an air volume) visualised by the blue oval is within reach of the cloud, and a substantial amount of the moisture from this area is converted into rain.*

(hereafter CC) relation[2]. However, a CC scaling is not obtained in every model and there exists no observational evidence for such a scaling. Also, despite the conceptual understanding as outlined above, there is no reason why extremes should exactly follow the CC relation. For instance, changes in the dynamics of the atmosphere and the convective cloud, in the moist adiabatic temperature profile[4], and in the size of the convective cloud could cause deviations from the CC-scaling. In addition, it is not clear how robust such a scaling relation is across different time and spatial scales.

We have investigated whether a CC-scaling can be found in the observations. A relation between precipitation extremes and temperature has been derived from day-to-day variations in temperature and precipitation. We have done so for both daily and hourly extremes, but here we focus on hourly precipitation extremes since showers have a typical lifetime of one to a few hours. Finally, we examined the output from a regional climate model integration to see whether such a scaling also exists for the climate change signal. Most of the results presented here have been published in Nature Geoscience[5].

Observations

We used a long data set of hourly precipitation observed at De Bilt, starting in 1906. This data set has been homogenized and quality controlled. We divided the precipitation data based on the daily mean temperature into bins of 2 °C width. Daily mean temperatures are used, instead of hourly temperatures, because we are interested in a proxy representing the temperature of the air mass. The hourly temperatures are to a large extent controlled by boundary-layer processes and radiation. From the binned data we computed the 90th, 99th and 99.9th percentiles of the distribution of wet events (hours or days) in each bin. The 99th and 99.9th percentile are computed from a generalized Pareto distribution fitted to the upper 5% of the data, and uncertainty bands are computed using the bootstrap. Besides the data set of De Bilt, also data from Belgium (Ukkel) and Switzerland (Bern, Basel and Zürich) has been analysed.

Figure 2a shows results from the analysis of hourly precipitation extremes for De Bilt. For temperatures below 10 °C a dependency close to 7% per degree is found for the higher percentiles (90th percentile and higher). Thus for lower temperatures the behaviour of the extremes is close to the behaviour predicted by the Clausius-Clapeyron relation. For temperatures abov e 10 °C a transition is seen to a stronger temperature dependency close to 14% per degree: a super CC scaling. For the most extreme events this super CC scaling occurs at slightly lower temperatures than for the less extreme events. For moderate events, like the 75th percentile, no clear scaling is obtained[5] (not shown here).

Analysis of the other data sets confirms that the scaling relation found in the De Bilt data is robust. Data from Belgium and Switzerland reveal very similar behaviour for the most extreme events (Figures 2b,c). Differences, however, occur for the less extreme events (90th percentile and lower).

Daily precipitation extremes show less strong temperature dependencies than the hourly extremes, in general close to or below the CC relation. The scaling behaviour is also less clearly defined[5].

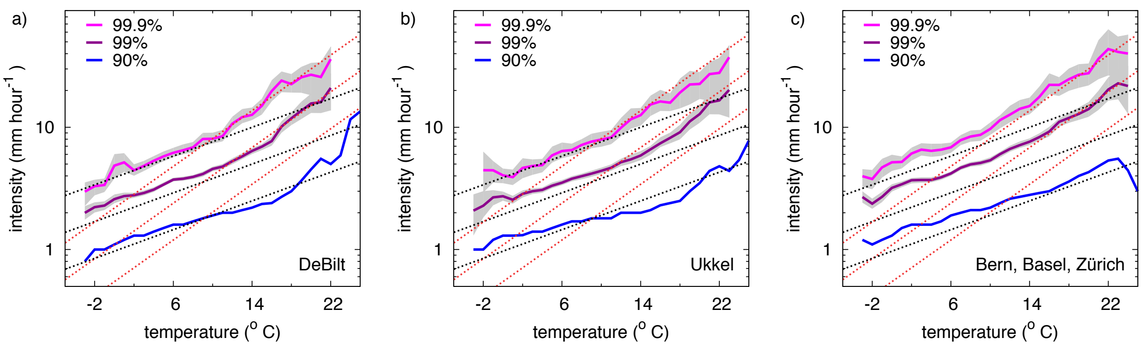

Figure 2. Scaling of observed hourly precipitation extremes with temperature for three different data sources (De Bilt: source KNMI; Ukkel: source RMI; Bern, Basel and Zürich: source MeteoSwiss). Shown are different percentiles of the distribution (90th to 99.9th percentiles) of hourly precipitation for each temperature bin. The grey shading plotted for the 99.9th and 99th percentiles denotes the 90% confidence intervals estimated by the bootstrap. Exponential relations given by a 7% increase per degree and 14% per degree are given by the black and red stippled lines, respectively. Note the logarithmic y-axis, due to which these exponential relations appear as straight lines.

Model results

Can the scaling between temperature and extreme precipitation inferred from present-day climate observations be used as a predictor of extreme precipitation we may be confronted with in a warmer climate? To investigate this, we analysed precipitation extremes from a climate integration with the KNMI regional climate model RACMO. This high resolution run, 25 km grid spacing on a domain covering the whole of Europe, has been done in the project ENSEMBLES[6] funded by the European Union. Boundaries for this climate scenario run are taken from a global simulation with the climate model ECHAM5.

Figure 3a shows that for large parts of central Europe the change in 1-hour extremes indeed exceeds the Clausius-Clapeyron prediction significantly. In large areas typical dependencies of 10-20 % per degree are found. The increase in daily extremes is less (Figure 3b).

The model results show that changes in hourly precipitation extremes in a warmer climate could be as large as 14% per degree temperature rise due to increases in atmospheric moisture with temperature. However, there are more factors that influence the change in the extremes, such as changes in the atmospheric circulation and soil moisture content. For example, due to severe soil drying the actual increase in water vapour in the atmosphere may not scale with temperature. In correspondence, the model results show that increases in southern Europe are much smaller, in general displaying a temperature dependency below the CC relation. Work is in progress to further clarify the relation between atmospheric circulation changes, soil drying and changes in precipitation extremes.

Cause of the super Clausius-Clapeyron scaling

There is some debate about the cause of the super CC scaling in the observations[7,8]. In our opinion, the explanation must be searched in the physics of deep convective clouds. For this type of precipitating clouds the strength of the upward motions in the atmosphere is (largely) determined by the latent heat release occurring in the cloud. More rainfall formation implies more latent heat release, which forces stronger updrafts and potentially a stronger rate of condensation and rainfall formation in the cloud. Thus, we argue that a positive feedback between water vapour and the dynamics of rainfall formation in a convective cloud causes the super CC scaling.

Alternatively, statistical effects potentially affect the scaling as well. Different temperature ranges are characterized by different atmospheric conditions, and these give rise to different precipitation regimes. Low temperatures mostly occur in the winter season, with the prevalence of synoptic large scale cyclones. In these large-scale systems rainfall intensities are generally low, but the rainfall duration is long (typically 4 to 6 hours). Conversely, the high temperature range is dominated by convective rainfall, with high intensities and short durations (typically 1 hour). Therefore, the change from low temperature to higher temperatures involves a change in the frequencies of both the large scale and the convective events, whereby on average less intense large

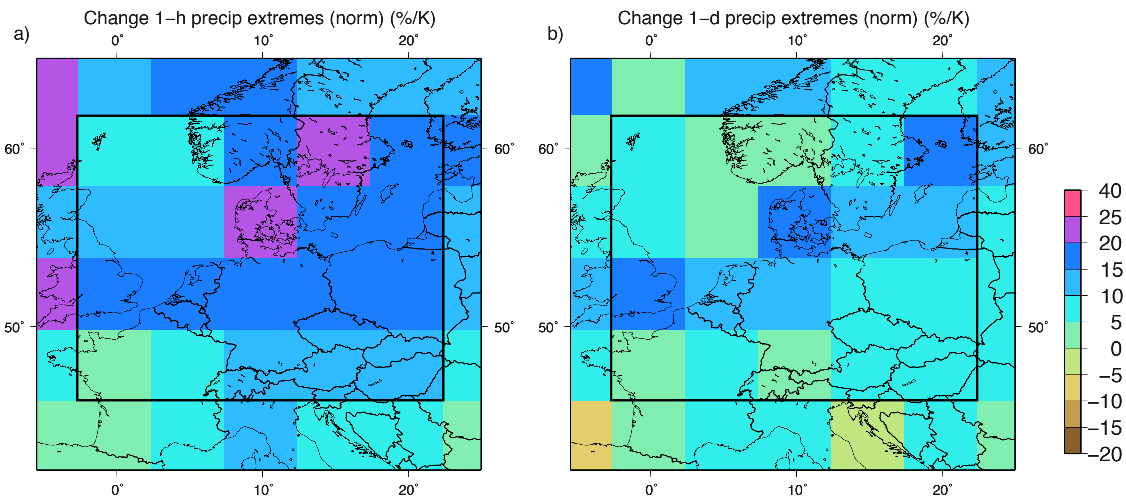

Figure 3. *The change in the 99.9th percentile of extreme precipitation on a grid scale (25x25 km²) normalized by the seasonal mean local temperature change. Changes are computed from the difference between the future period 2071-2100 and the reference period 1971-2000. The check board pattern is the result of the statistical postprocessing in which data from a larger area is analysed at the same time.*

scale events (with longer duration) are replaced by more intense convective events (with shorter duration). This statistical effect could give rise to an enhanced temperature dependency of hourly precipitation[7)].

The reason why it is important to establish the cause of the super CC scaling is that this has direct consequences for how this scaling will manifest itself in the climate change signal. It is not expected that the ratio between the frequencies of large-scale and convective precipitation events will change considerably due to climate change. Therefore, if the super CC scaling is due to the proposed statistical effect, changes in precipitation extremes would likely be not larger than predicted by the CC relation (that is, 7% per degree). However, if the super CC scaling is due to the physics of the convective precipitation process, than one would expect this scaling to hold under warmer future climate conditions. In that case, changes in precipitation extremes are likely to be larger than predicted by the CC relation.

Although the scaling relation could be influenced by the statistical effect mentioned above, we think that the primary cause of the super CC scaling is to be found in the physics of the convective events. One reason is that an almost identical scaling for higher temperatures is obtained when considering the summer season only, and rainfall in the summer season is dominated by small scale convective events. Also when taking only data that has been classified to be convective, a super CC scaling is obtained for this sub-selection of events. (This classification is based on the ww code in the SYNOP message, that contains a subjective description of the past hour weather as reported by the meteorological observer.) Another reason is that the regional model simulation indeed shows a response larger than predicted by the CC relation.

We obtained a temperature dependency of hourly precipitation extremes of approximately 14% per degree in observations at De Bilt

Conclusion

We obtained a temperature dependency of hourly precipitation extremes of approximately 14% per degree in observations at De Bilt. This relation exceeds the well known Clausius-Clapeyron relation, which is commonly used as a predictor of the increases in precipitation extremes, by a factor of two. Similar relations are obtained from time series from Belgium and Switzerland, and the results therefore appear to be a robust feature of hourly precipitation extremes in this part of Europe.

Our hypothesis is that the relation found in the present-day climate can be used as a predictor for the climate change signal. This hypothesis is confirmed by simulations with the KNMI regional climate model RACMO. However, we also note that a recent ensemble of model simulations, which is performed in the ENSEMBLES project[6)], shows a very large range of predicted changes in hourly precipitation extremes. New research will focus on understanding the range of model outcomes in order to reduce the uncertainty in predictions of future changes in precipitation extremes.

Ackowledgements.

Hourly precipitation data has been provided by the Swiss Federal Office of Meteorology and Climatology MeteoSwiss, and the Royal Meteorological Institute in Belgium. Financial support by the EU FP6 Integrated Project ENSEMBLES (Contract number 505539) and the Dutch programs Climate Changes Spatial Planning (CCSP) and Knowledge for Climate (KFC) is gratefully acknowledged.

References

1) Emori, S. and S. Brown, 2005. *Dynamic and thermodynamic change in mean and extreme precipitation under climate change*. Geophys. Res. Lett., **32**, L177061.
2) Pall, P., M. Allen and D. Stone, 2007. *Testing the Clausius-Capeyron constraint on changes in extreme precipitation under CO2 warming.* Clim. Dyn., **28**, 351-363.
3) Lenderink, G., A. van Ulden, B. van den Hurk and F. Keller, 2007. *A study on combining global and regional climate model results for generating climate scenarios of temperature and precipitation for the Netherlands.* Clim. Dyn., **29**, 157-176.
4) O'Gorman, P. A. and T. Schneider, 2009. *The physical basis for increases in precipitation extremes in simulations of 21st-century climate change.* Proc. Nat. Acad. Sciences, **106**, 14773-14777.
5) Lenderink, G. and E. van Meijgaard, 2008. *Increase in hourly precipitation extremes beyond expectations from temperature changes.* Nature Geosci., **1**, 511-514.
6) Hewitt, C. and D. Griggs, 2004. *Ensembles-Based Predictions of Climate Changes and Their Impacts* (ENSEMBLES). EOS-Transactions, **85**, 566.
7) Haerter, J. O. and P. Berg, 2009. *Unexpected rise in extreme precipitation caused by a shift in rain type?* Nature Geosci., **2**, 372-373.
8) Lenderink, G. and E. van Meijgaard, 2009. Reply to: *Unexpected rise in extreme precipitation caused by a shift in rain type?* Nature Geosci., **2**, 373.

Extreme rainfall climatology from weather radar

Aart Overeem, Iwan Holleman and Adri Buishand

Introduction

Extreme rainfall events have a large impact on society and can lead to loss of life and property. Weather radars give quantitative precipitation estimates over large areas with a high spatial and temporal resolution unmatched by conventional rain gauge networks. The current quality of quantitative precipitation estimation with radar and the length of the available time series make it feasible to derive a radar-based extreme rainfall climatology. KNMI has an archive of 11 years of radar rainfall depths for the entire land surface of the Netherlands. After adjustment using rain gauge data a high-quality rainfall climatology is obtained. Subsequently, a generalized extreme value (GEV) distribution is fitted to annual radar rainfall maxima and rainfall depth-duration-frequency (DDF) curves are derived, which describe the extreme rainfall depth as a function of duration for given return periods. It is shown that weather radar is suitable to derive the statistics of extreme rainfall, which can, for example, be used for design purposes in water management or the evaluation of the rarity of severe weather.

KNMI has an archive of 11 years of radar rainfall depths for the entire land surface of the Netherlands

Radar and rain gauge data

KNMI operates two C-band Doppler weather radars, from which rainfall intensities were obtained with a 2.4 km spatial resolution and a 5-min temporal resolution for the period 1998-2008 with a data availability of approximately 82%. The radars are located in the Netherlands in De Bilt and Den Helder, see Figure 1. From the rainfall intensities, accumulations were derived for durations of 15 min to 24 h. Accumulation images from both radars were combined into one composite covering the land surface of the Netherlands (35 500 km^2). Quantitative precipitation estimation with radar can become less accurate due to, for example, overshooting of precipitation by the radar beam, variability of the drop-size distribution and attenuation in the case of strong precipitation or a wet radome. Rain gauges are considered to produce accurate point measurements. Because of this, rain gauge networks (Figure 1) were utilized to adjust the radar-based accumulations: an automatic network with 1-h rainfall depths for each clock-hour (≈ 1 station per 1000 km^2) and a manual network with 24-h 08-08 UTC rainfall depths (≈ 1 station per 100 km^2). A daily spatial adjustment is applied to the 24-h 08 UTC rainfall depths using the manual gauge network. A mean-field bias (MFB) adjustment is applied to the 1-h unadjusted radar rainfall depths using the automatic gauge network. Both adjustment procedures were combined and are denoted by mean-field bias and spatial (MFBS) adjustment.

Verification

The radar data set of rainfall depths was verified using rain gauges for the period 1998-2007. The bias in unadjusted daily radar rainfall depths with respect to manual rain gauge depths is -0.88 mm, which is a considerable underestimation since the average daily manual rain gauge depth is 2.55 mm. The MFB and MFBS adjustment methods reduce the bias to respectively -0.15 and -0.03 mm. The residual standard deviation is reduced from 2.71 (unadjusted) to 2.14 mm (MFB) and 1.03 mm (MFBS). Rain gauges produce point measurements, whereas radar

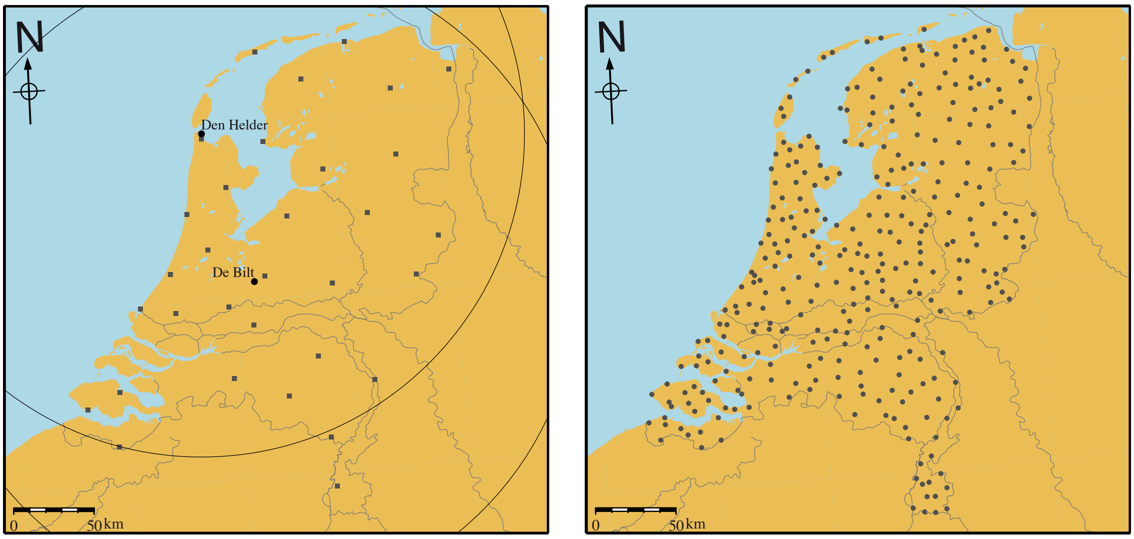

***Figure 1.** Maps of the Netherlands with left the locations of the weather radars in De Bilt and Den Helder, their 200-km range (circles), and the 33 automatic rain gauges (squares) and right the locations of the 326 manual rain gauges.*

samples a volume with a horizontal surface of 5.7 km^2. The standard deviation of the differences in daily rainfall depths between manual and automatic rain gauges within a 2.4-km radius is 1.06 mm. This indicates that an important part in the differences between radar and rain gauge accumulations is caused by sub-pixel variation.

To investigate the spatial quality of rainfall depths, biases in the mean daily rainfall and the residual standard deviation are calculated for each radar-gauge pair for the MFB and MFBS adjustments. In the MFB adjustment method a constant factor is applied to the entire radar image, so that regional differences in the biases are not taken into account. Figure 2 shows that such an adjustment results in quite negative biases near the borders of the Netherlands and quite positive ones in the middle of the country. A constant adjustment factor only partly corrects the large negative biases in winter due to partial overshooting of precipitation from shallow stratiform clouds, and turns the smaller negative biases at short ranges into an overestimation. The MFBS adjustment clearly removes range dependencies in radar rainfall depths.
The 1-h radar rainfall depths are also verified against the depths obtained from the automatic rain gauges. Both adjustment methods are successful in removing the bias in the mean hourly rainfall depth and in reducing the residual standard deviation. If only radar and/or rain gauge depths larger than 5 mm in 1 h are considered, the bias in the unadjusted radar rainfall depths is -3.81 mm. This is reduced to -0.82 mm for the MFB-adjusted data and -0.51 mm for the MFBS-adjusted data. For these extreme events, the residual standard deviation decreases from 4.60 mm (unadjusted) to 3.96 mm (MFB) and 3.80 mm (MFBS). This implies that a daily adjustment using a dense gauge network, which improves the spatial quality of the rainfall depths, has added value if applied to already MFB-adjusted 1-h rainfall depths.

Fitting a GEV distribution

Data sets are usually too short to accurately estimate extreme rainfall depths for design purposes in water management. Often extrapolation is needed. A well-established method is to abstract annual rainfall maxima from a rain gauge record for a given duration and model these extremes with a GEV distribution. The quantile function of this distribution can be used to estimate rainfall depths for given average return periods T, and is given by:

$$x(T) = \mu \left\{ 1 + \frac{\gamma}{\kappa} \left[1 - \left(-\ln\left(1 - \frac{1}{T}\right) \right)^{\kappa} \right] \right\} \quad \text{for} \quad \kappa \neq 0 \qquad (1)$$

$$x(T) = \mu \left\{ 1 - \gamma \ln\left[-\ln\left(1 - \frac{1}{T}\right) \right] \right\} \quad \text{for} \quad \kappa = 0$$

with μ the location and κ the shape parameter of the distribution; γ is the dispersion coefficient. The value of κ determines the type of distribution, if $\kappa = 0$ the Gumbel distribution is obtained.

Rainfall depth-duration-frequency curves

A novel approach is to estimate extreme rainfall depths based on weather radar data, which is particularly

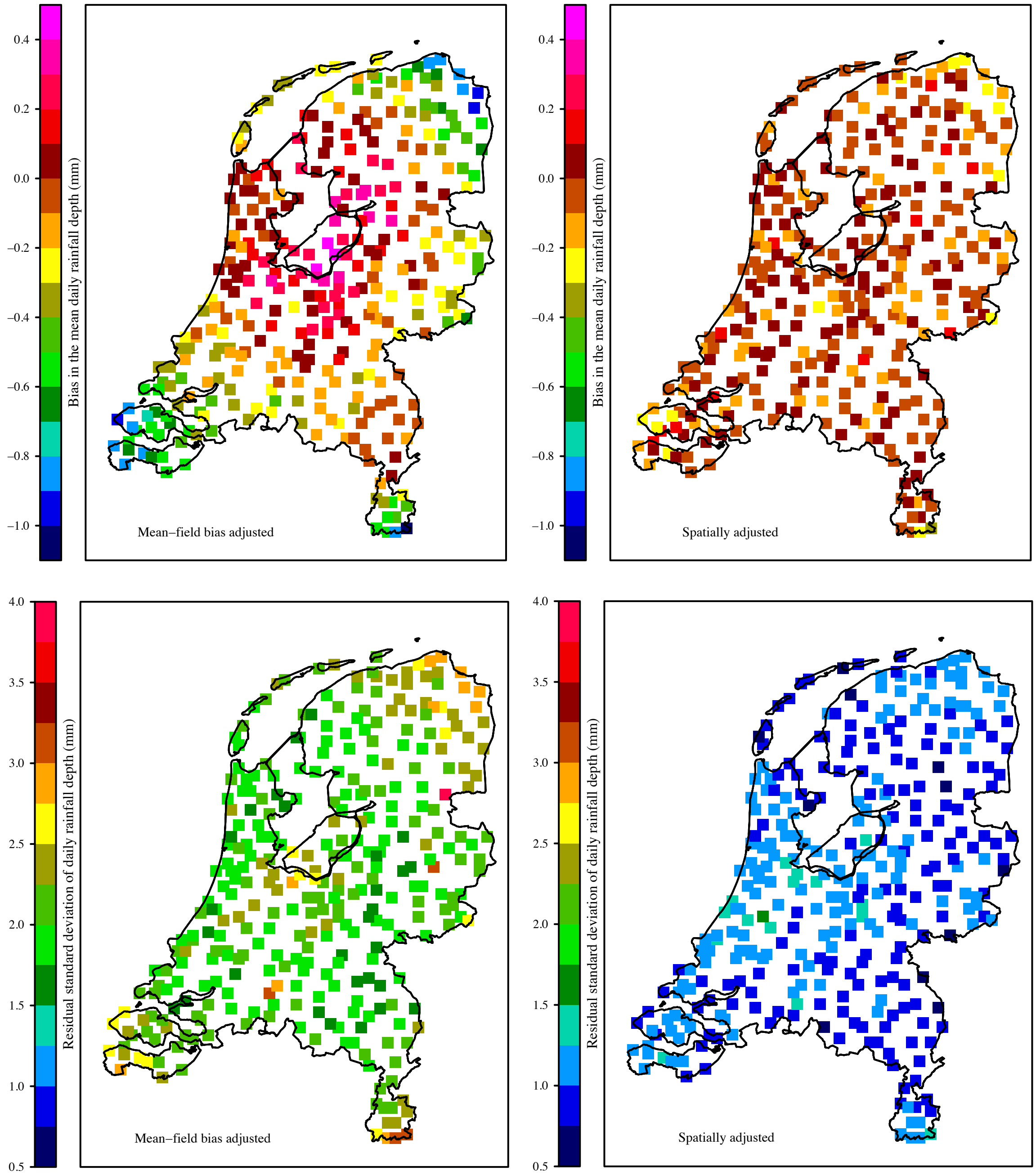

Figure 2. *Spatial verification of 24-hour 0800 UTC rainfall depths of radar composites against manual gauges for MFB- and MFBS-adjusted radar data: bias in the mean (upper panel) and residual standard deviation (lower panel).*

interesting for short durations for which few rain gauge data are available. For the 11-year period, each pixel contains 11 annual maxima, which are abstracted for durations *D* of 15 min to 24 h. For each individual duration, GEV distributions are fitted to the 6190 (pixels) × 11 (years) annual maxima assuming that the dispersion coefficient and shape parameter are constant over the Netherlands.

For longer durations the validity of this assumption is demonstrated by Buishand et al. in this Triennial Report. The location parameter is estimated for each radar pixel separately. In this paragraph, the estimated location parameters for the individual pixels are averaged to obtain one value of this parameter for each *D*. Relationships are found, which model the GEV parameters as function of *(in h)*:

$$\ln \mu = 2.559 + 0.318D \quad (2)$$
$$\gamma = 0.312 - 0.025D \quad (3)$$
$$\kappa = -0.163 \quad (4)$$

These relationships are similar to those found using rain gauge data[1)]. Substituting them in Eq. (1) gives a general expression for the rainfall depth quantile $x(T)$, which can be used to obtain rainfall DDFs. An example of such a rainfall DDF curve is given in Figure 3 for T = 50 years based on radar data from this study (solid line) and based on 514 annual maxima from 12 rain gauges[1)] (dashed line). Most rain gauge data refer to the period 1977-2005. For instance, for a return period of 50 years the 60-min radar extreme rainfall is 35 mm. The underestimation of rainfall depths with respect to rain gauges for short durations may be related to remaining errors in the radar data.

It is important to estimate the uncertainty in DDF curves and to take this uncertainty into account in the design of hydraulic structures. The bootstrap method is employed to assess the uncertainty in the estimation of the GEV parameters, i.e. sampling errors. In the bootstrap method new samples (bootstrap samples) are generated by sampling with replacement from the original sample. The 95%-confidence intervals for the rainfall depth quantiles are shown as a light gray-shaded area (radar) or a dark gray-shaded area (rain gauge). The overlap region of the rain gauge and radar-based confidence intervals is shown in gray. For the radar data uncertainties become rather large for the longest durations. For example, the 95%-confidence interval ranges from 72 to 92 mm for D = 24 h and T = 50 years, which is due to the relatively small size of the radar data set for calculating the statistics of extreme rainfall. Nevertheless, the uncertainties for the radar data are small for short durations. This is because of the low spatial correlation of short-duration rainfall. The large number of observations in space then compensates for the small number of observations in time. The effective length of the 11-year radar data set ranges from approximately 80 years for D = 24 h to a few hundred years for D = 15 min.

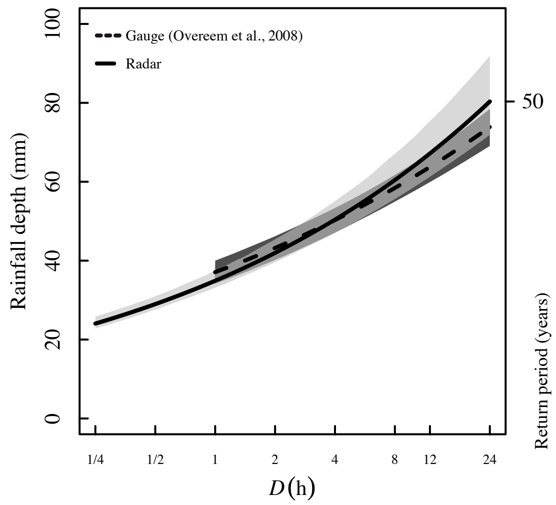

Figure 3. *Rainfall depth-duration-frequency curves for a return period of 50 years based on rain gauge data[1)] (dashed line) and based on radar data (solid line). Also shown are pointwise 95%-confidence intervals: dark gray for the rain gauge data, light gray for the radar data. The overlap region of these confidence intervals is shown as gray.*

Local rainfall depth-duration-frequency curves

Due to spatial variation of the value of the location parameter, the average DDF curve in Figure 3 cannot be used everywhere in the Netherlands. Figure 4 shows the location parameters for D = 60 min and 24 h and gives the rainfall depths for D = 24 h and T = 20 years. Most noticeable are the high values of the location parameter in the western part of the country, near the coast, for D = 24 h, which are considerably larger than those in the rest of the country. This is in correspondence with results presented by Buishand et al. in this Triennial Report, where annual daily rainfall maxima were obtained from 55-year records of 141 manual rain gauges. However, in radar-based data larger spatial differences in the location parameter are found, resulting in rainfall depths ranging from 48 to 94 mm for T = 20 years and D = 24 h. For D = 60 min, several isolated areas with high values of the location parameter can be distinguished, but no clear spatial pattern is revealed. Although regional variability in the GEV location parameter in the Netherlands is statistically significant for most durations, an important part of the differences can be attributed to randomness, which will be relatively large for an 11-year data set.

If DDF curves are derived for each radar pixel, the uncertainties in the estimated quantiles of rainfall depths become rather large. As a compromise, local DDF curves are derived for the areas indicated by the white boxes in Figure 4b. For 24 h, area A is one of the 'driest' areas and area B one of the 'wettest' areas in the Netherlands. Local DDF curves for 50 years are shown in Figure 5, together with their 95%-confidence bands. For durations longer than approximately 4 hours, the 95%-confidence bands for the DDF curves of areas A and B do not overlap implying these DDF curves differ significantly. In general, the 95%-confidence bands are wider than those for the average DDF curve for the Netherlands, shown in Figure 3, due to the larger uncertainty of the location parameter.

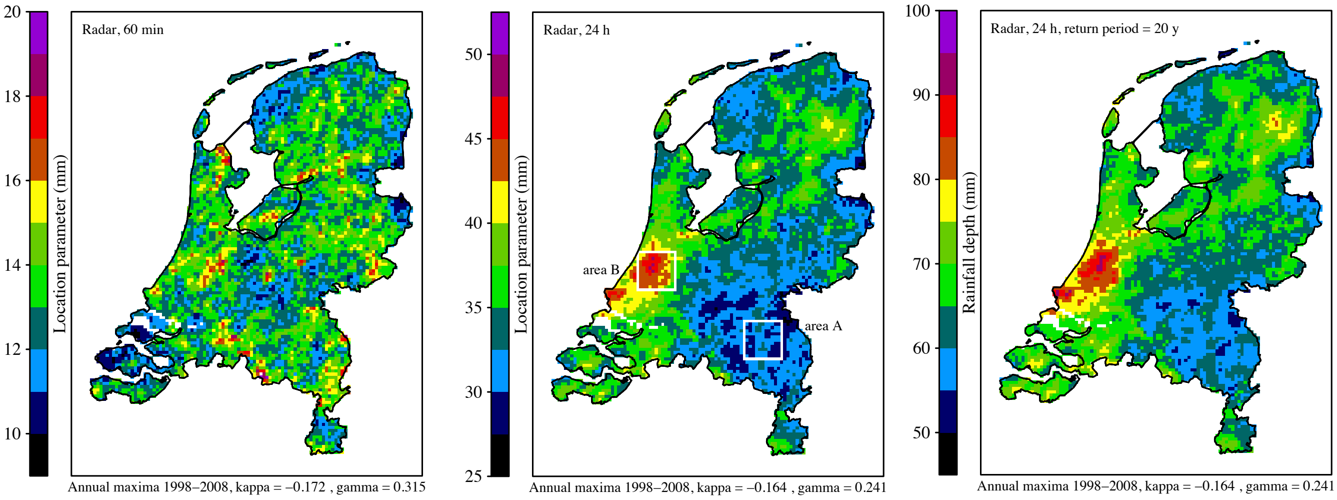

Figure 4. *The location parameter for 60 min (left) and 24 h (middle) and the 24-h rainfall depth for a return period of 20 years (right) for each pixel in the Netherlands.*

Weather radar is suitable to estimate extreme rainfall depths for chosen return periods

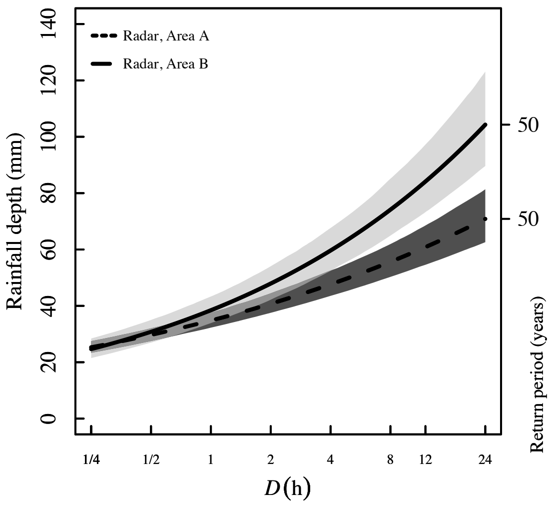

Figure 5. *Local rainfall depth-duration-frequency curves for the two areas indicated in Fig. 4b for a return period of 50 years based on radar data and their pointwise 95%-confidence bands.*

Conclusion

Using weather radar an 11-year rainfall climatology was constructed for the Netherlands for durations of 15 min to 24 h. The adjustment of radar rainfall depths employing rain gauges results in high-quality radar rainfall composites with a spatially homogeneous quality, which covers the land surface of the Netherlands. For an extensive description of the adjustment and verification, see [2,3]. It has been shown that weather radar is suitable to estimate extreme rainfall depths for chosen return periods[3]. The radar data set is potentially useful for rainfall parameterization in weather and climate models and for use in hydrological models. The climatological radar data set of 1-h rainfall depths for every clock-hour is available at the Climate Services division.

References

1) Overeem A., T.A. Buishand and I. Holleman, 2008. *Rainfall depth-duration-frequency curves and their uncertainties.* J. Hydrol., **348**, 124-134, doi:10.1016/j.jhydrol.2007.09.044
2) Overeem A., I. Holleman and A. Buishand, 2009. *Derivation of a 10-year radar-based climatology of rainfall.* J. Appl. Meteor. and Climatology, **48**, 1448-1463, doi:10.1175/2009JAMC1954.1
3) Overeem A., T.A. Buishand and I. Holleman, 2009.*Extreme rainfall analysis and estimation of depth-duration-frequency curves using weather radar.* Water Resour. Res., **45**, W10424, doi:10.1029/2009WR007869

Monitoring bird migration by weather radar

Adriaan Dokter and Iwan Holleman

Introduction

Weather and bird migration are intimately related. Evolution has shaped the migration strategies of birds such that they optimally respond to and make use of weather conditions during their long distance travels between breeding and wintering grounds. Both wind and precipitation strongly determine the day-to-day timing of migration and altitude use by birds.

Spatiotemporal information on bird migration is of invaluable use to scientists and society alike, but so far no sensor networks have been established that can monitor bird movement continuously over large areas. In aviation bird migration information is important for improving flight safety. Especially military low level flying has a high risk of en-route bird strikes and spatial bird migration information is essential for generating reliable flight warnings to pilots. Comprehensive monitoring of bird migration at continental scales can also provide insight into migration patterns and the impact on migratory flight of synoptic scale factors like weather and orography.

As part of an international project by the European Space Agency (ESA) aimed at reducing collisions between aircrafts and birds, we have explored the potential of operational Doppler weather radar as a bird migration sensor.

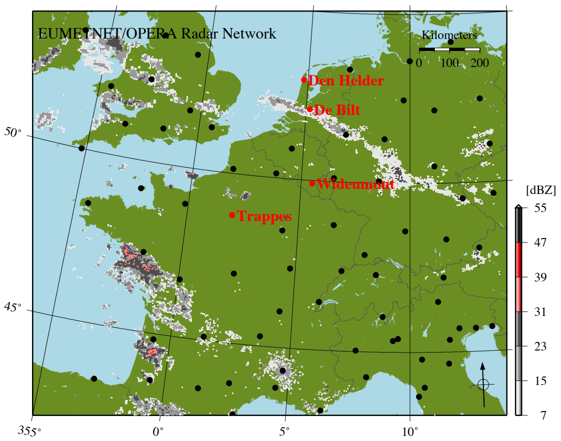

Figure 1. *Map of operational weather radars for part of Western Europe. Radar sites are indicated by bullets, the weather radars used in this study are labelled and coloured red. The OPERA reflectivit y composite is overlaid for 19 April 2008 19.30 UTC.*

Observing bird migration by Doppler weather radar

Operational weather radar networks exist in e.g. Europe and the United States for meteorological applications. These networks have a large spatial coverage as illustrated in Figure 1, showing part of the European network OPERA (Operational Programme for the Exchange of weather Radar information)[1]. Although weather radars are used primarily for precipitation monitoring, also biological scatterers can be observed by these systems. Boundary layer clear-air weather radar echoes are caused nearly exclusively by arthropods (mostly insects) and flying birds. Weather radars are therefore a promising sensor for providing bird migration information.

A bird migration quantification algorithm needs to automatically distinguish bird-scattered signals from all other echoes detected by weather radar. Bird echoes and other clear-air signals tend to be considerably weaker than meteorologically relevant signals from hydrometeors. Birds, insects and hydrometeors give rise to signals in an overlapping reflectivity regime, which makes it challenging to distinguish them.

Doppler weather radars provide information on the radial velocity of scatterers, which we use to select out echoes related to bird migration. Figure 2 shows weather radar images during intense bird migration (top row) and during a case with convective showers (bottom row). Bird migration gives rise to a characteristically high spatial variability of the radial velocity scan data, which is not observed for echoes from precipitation or insects. Unlike precipitation and insects, birds perform active flight which varies in speed and direction per individual, causing a higher variability in the Doppler velocity.

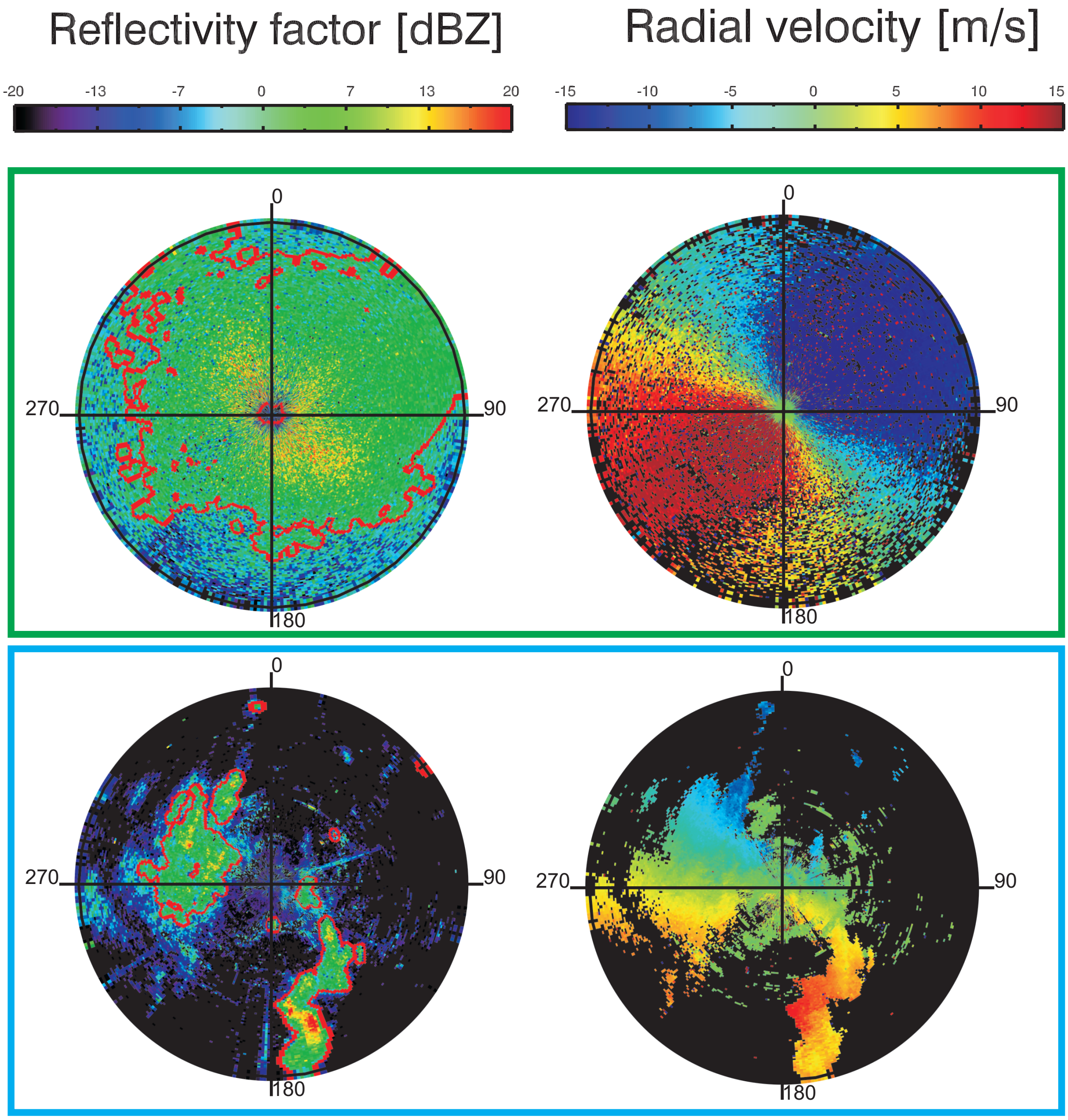

Figure 2. *Radar displays for reflectivity factor (left) and radial velocity (right) during a bird migration event (top rectangular box in green) and an event with weak convective showers (bottom rectangular box in blue). The displays show the 1.2 degree elevation scan for a circular area of 25 km radius around the weather radar in De Bilt. Contiguous areas of echoes identified by the algorithm are indicated within the reflectivity displays by red borders. For the precipitation case (bottom) these areas removed from the data based on a low spatial variance of the radial velocities, while for the bird migration case (top) these areas are retained based on a high spatial variance of radial velocities. After removing precipitation echoes average bird densities are calculated from the remaining reflectivity data.*

We developed a bird detection algorithm[3,4]) based on existing wind-profiling algorithms for Doppler weather radars, using the Volume Velocity Profiling (VVP) technique[5]). A target identification scheme was developed to filter out non-bird echoes from the radar volume data, based on an analysis of the local variance in radial velocity. The filtered reflectivity data is used to construct a bird density altitude profile, and an analysis of the radial velocity data yields the average bird speed and direction. Reflectivity was converted to bird density by assuming a constant bird radar cross section of 11 cm², which we found to be an adequate approximation during nocturnal migration over Western Europe, which is strongly dominated by passerines (small song-birds).

Figure 4. *Wingbeat pattern of a small songbird with regular phases of wingbeats (frequency around 15 Hz) and pauses as recorded by the Superfledermaus bird radar. The single wingbeats are clearly visible. The envelope of increasing and decreasing amplitude (vertical axis) of the signal along the time axis (horizontal axis) reflects the bird's flight entering the radar beam at one edge, flying through the centre and leaving at the other edge.*

Bird radar field campaigns for validation

In corporation with the Swiss Ornithological Institute we used a dedicated bird radar of the type "Superfledermaus" (see Figure 3) to validate the weather radar observations of bird migration. The dedicated radar is capable of detecting the wingbeat pattern for individual radar targets[6]) (see Figure 4). Based on these echo signatures, insects, birds and hydrometeors can be distinguished with a high selectivity. The mobile tracking radar is therefore a state-of-the-art reference for validating the weather radar bird observations[7]).

Three field campaigns were organized to validate the weather radar bird observations. The bird radar has been stationed within the measurement volume of the weather radar in De Bilt, the Netherlands from 19 Aug - 16 Sep 2007, in Wideumont, Belgium from 18 Sep - 22 Oct 2007 and in Trappes, France from 10 Mar - 9 May 2008, thus covering a full autumn and spring migration season.
In Figure 5 the bird densities altitude profiles detected by bird radar (top panel) and weather radar (middle panel) are displayed for the period of 11-16 October 2007, when the bird radar was stationed in Trappes. We find a remarkable correspondence in the detected bird densities by the two sensors during all field campaigns. The altitude distributions and absolute number of detected birds match quantitatively. Weather radar can thus be used as a reliable sensor for bird migration quantification.

Weather radar can be used as a reliable sensor for bird migration quantification

Figure 3. *The bird radar Superfledermaus equipped with a camera mounted parallel to the radar antenna.*

The effect of wind on bird migration

The effect of the environmental wind on flight altitudes becomes evident by comparing the weather radar bird density profile (Figure 5 middle panel) with the wind profiles calculated by the HIRLAM numerical weather prediction model (Figure 5 bottom panel). We find that birds adjust their flight altitude to make optimal use of tail winds along the predominant (south-westerly) migratory direction. For example, the HIRLAM wind profile (bottom panel Figure 5) shows that on October 4 wind conditions at high altitude were unfavourable, where strong westerly winds cause negative wind effects. Migration therefore does not extend above 1 km (see middle panel Figure 5). On the other hand, on October 6 tail winds are most favourable above 1 km and as a result a large fraction of migration takes place at high altitude.

Bird migration patterns observed at single sites can strongly depend on weather conditions elsewhere. This applies particularly to northern temperate climate, where frequent passages of high and low pressure s ystems cause a large spatial variability in weather. Using four weather radars (see Figure 1) we

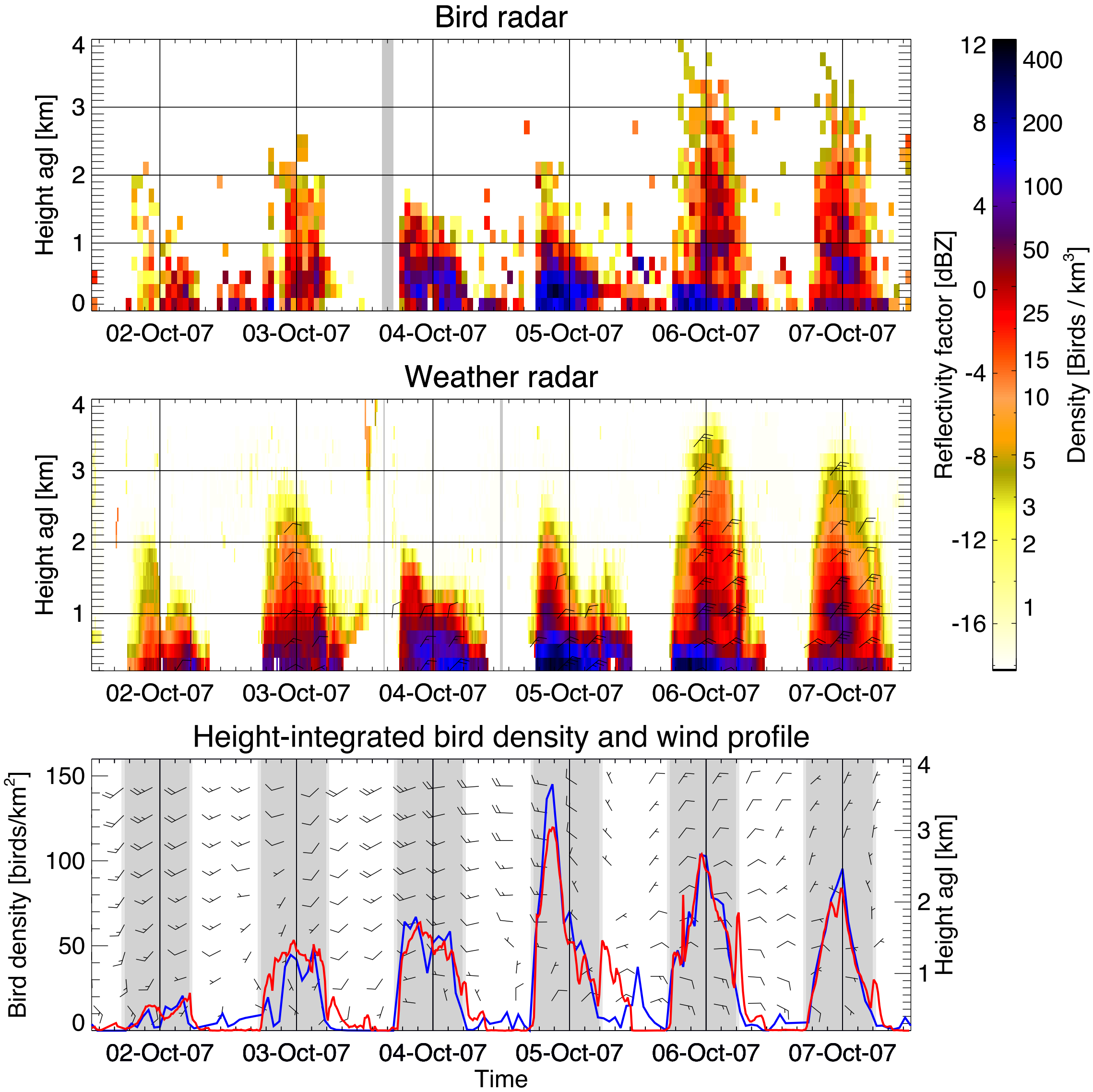

Figure 5. Comparison of the bird densities altitude profiles determined by bird radar (top panel) and weather radar (middle panel). Integrated bird densities over all height layers are displayed in the lower panel for both weather radar (red) and bird radar (blue) (left vertical axis). The period between sunset and sunrise is shaded in grey. Wind barbs in the lower panel show the wind profile from the HIRLAM numerical weather prediction model (right vertical axis). Wind barbs in the middle panel indicate the bird speed and direction as retrieved by the weather radar algorithm. Each half flag represents 10 km/h and each full flag 20 km/h.

monitored the bird migration flyway at several sites simultaneously.
Weather radar bird observations for the night of 19-20 April 2008 are depicted in Figure 6. For this night the OPERA reflectivity composite is overlaid on Figure 1 to give an impression of the large scale weather conditions.

At each site, the timing and altitude profile of bird migration is observed to be influenced by weather conditions at locations passed earlier during a migratory flight. As an example, migration at the most southern site (Trappes) is characterized by strong departure and ascent to high altitudes around 2.5 km, where birds experience favourable tail winds along the preferred migratory direction (NE in spring). Low altitude migration is avoided because of unfavourable easterly low level winds. At one radar site north-east of Wideumont, we observe the appearance of a migration layer centred around 2 km height after 22 UTC. This migration layer appears after 4 hours of flight time, which corresponds with a measured bird ground speed of 70 km/h to birds having travelled over a distance of about 280 km towards

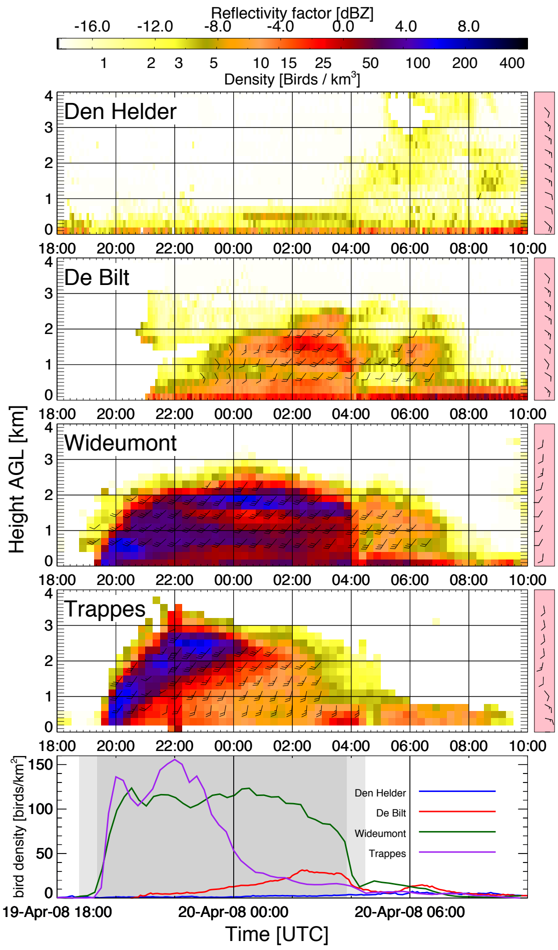

Figure 6. *Bird densities as a function of time and altitude at different weather radar sites (see Figure 1) for the night of 19 April 2008. The wind barbs represent the measured bird ground speed and direction. The lower panel shows the height integrated bird densities over 0.2-4 km altitude. The period between sunset and sunrise is shaded in grey and civil twilight is shaded in light grey. The pink boxed inset on the right hand side of each panel shows the HIRLAM wind profile at 00 UTC. Around 00 UTC a double layered bird density profile is observed in Wideumont. We attribute the top band to birds that departed in the vicinity of Trappes, while the lower band results from birds departed at closer distance.*

north-east. These birds must therefore have departed in the vicinity of Trappes in northern France, where birds chose a flight altitude of 2.5 km. Since Wideumont is located 500 m above mean sea level, the 2 km altitude band closely matches the cruising altitude after departure near Trappes. Birds have thus maintained a constant flight altitude during their migratory flight with respect to sea level. The altitude profile observed in Wideumont is clearly affected by the particular wind conditions at the more southern site of Trappes.

In De Bilt, north of Wideumont, no birds depart in the early night. This is explained by the weak occlusion front slightly south of De Bilt, which blocks most migration. With this front weakening in activity, migration conditions became more favourable over the course of the night, and after 00 UTC we do observe the passage and arrival of migrating birds. No migration is observed on the most northerly located weather radar in Den Helder. The extent to which birds are able to adapt their flight altitudes in response to changing meteorological conditions will be topic of future research.

Conclusion

We find that Doppler weather radar is highly successful in determining quantitative bird densities and average flight speeds and directions as a function of altitude. We find that weather radar reflectivity can be quantitatively correlated to the bird-densities determined independently by bird radar. The developed methods for bird detection and quantification can be easily extended to full operational weather radar networks. With the establishment of the OPERA data centre for radar data within the coming two years[1)] the establishment of a continent-wide bird migration sensor network in Europe is within reach. Such a network can enable important applications both in flight safety, health (avian disease spread) and environmental impact assessments.

The establishment of a continent-wide bird migration sensor network in Europe is within reach

References

1) Holleman I., L. Delobbe and A. Zgonc, 2008. *Update on the european weather radar network* (OPERA). Proc. Fifth European Conf. on Radar in Meteorology and Hydrology, June-July 2008, Helsinki, Finland, 5pp
2) Holleman, I., H. van Gasteren and W. Bouten, 2008. *Quality assessment of weather radar wind profiles during bird migration.* J. Atm. Oceanic Technol., **25**, 2188-2198, htpp://journals.ametsoc.org/doi/pdf/10.1175/2008JTECHA1067.1
3) Dokter, A.M., F. Liechti, H. Stark, L. Delobbe, P. Tabary and I. Holleman, 2010. *Bird migration flight altitudes studied by a network of operational weather radars.* J. R. Soc. Interface 7, doi:10-1098/rsif.2010.0116
4) Gasteren, H. van, I. Holleman, W. Bouten, E. van Loon, and J. Shamoun-Baranes, 2008. *Extracting bird migration information from C-band weather radars.* Ibis, **150**, 674-686.
5) Waldteufel, P. and H. Corbin, 1979. *On the analysis of single doppler radar data.* J. Appl. Meteor., **18**, 532-542.
6) Zaugg, S., G. Saporta, E. van Loon, H. Schmaljohann and F. Liechti, 2008. *Automatic identification of bird targets with radar via patterns produced by wing flapping.* J. Royal Soc. Interface, **5**, 1041-1053.
7) Schmaljohann, H., F. Liechti, E. Bächler, T. Steuri, and B. Bruderer, 2008. *Quantification of bird migration by radar - a detection probability problem.* Ibis, **150**, 342-355.

Infrasound and seismology in the Low Frequency Array LOFAR

Läslo G. Evers and Bernard Dost

Introduction

Infrasound was first discovered after the destructive eruption of the Krakatoa in Indonesia (1883). Low frequency acoustic waves, caused by this eruption, appeared to have travelled around the globe up to four times[1)]. These infrasonic waves were detected world-wide on traditional barographs as small air pressure fluctuations. Due to its low-frequency content, infra-sound hardly experiences attenuation in the atmosphere and travels to thermospheric altitudes of over 100 km. In addition to seismology, infrasound was used to measure the occurrence of atmospheric nuclear tests and to estimate their yield[2)]. It was also in this period that the possibility to use infrasound as passive atmospheric probe started to be recognized[3)]. This interest diminished after nuclear tests were confined to the subsurface under the Limited Test Ban Treaty (1963). Recently, the study of infrasound is experiencing a renaissance as it was chosen as a verification technique for the Comprehensive Nuclear-Test-Ban Treaty (CTBT), that opened for signing in 1996[4)]. Infrasound science currently concentrates on source identification and passive remote sensing of the upper atmosphere.

The construction of the largest radio-telescope in the world in the northern part of the Netherlands and neighbouring countries, the Low Frequency Array (LOFAR), opened the possibility to co-locate geophysical sensors and realize an efficient multi-sensor network. The KNMI, Delft University of Technology and TNO, all partners in LOFAR, make use of the advanced LOFAR infra-structure to build-up an infrasound and seismological research network. This network consists of a temporary 80 element high density array, a permanent 30 element microbarometer array with an aperture of 100 km and, at the same locations, a 20 to 30 element seismological component. Here, we present the scientific background, goals and first results.

Recently, the study of infrasound is experiencing a renaissance as it was chosen as a verification technique for the Comprehensive Nuclear-Test-Ban Treaty (CTBT), that opened for signing in 1996[4)]

The physical characteristics of infrasound

Sound waves below 20 Hz are inaudible for the human ear. These sound waves are called infrasound. The lower limit of infrasound is controlled by the thickness of the atmosphere or of an atmospheric layer. For the troposp-here, the acoustic cut-off period is roughly 5 minutes. For longer period waves gravity acts as restoring force, instead of the molecular relaxation for sound waves, and hence these are called gravity waves. These gravity waves propagate with typical wind speed velocities of 5 to 10 m/s. Infrasonic waves travel with the sound speed which is 340 m/s for air of 20 °C. The amplitudes of infrasonic waves are small with respect to the ambient pressure and vary between milli-pascals (Pa) to tens of Pa.

The propagation of infrasound is controlled by the effective sound speed, which is a function of the temperature and wind along the source-receiver trajectory[5)]. Infrasonic waves will be refracted if vertical gradients in the effective sound speed exist. Waves will be bended back towards the earth's surface in case these gradients are strong enough. There are three regions in the atmosphere where strong wind and/or temperature

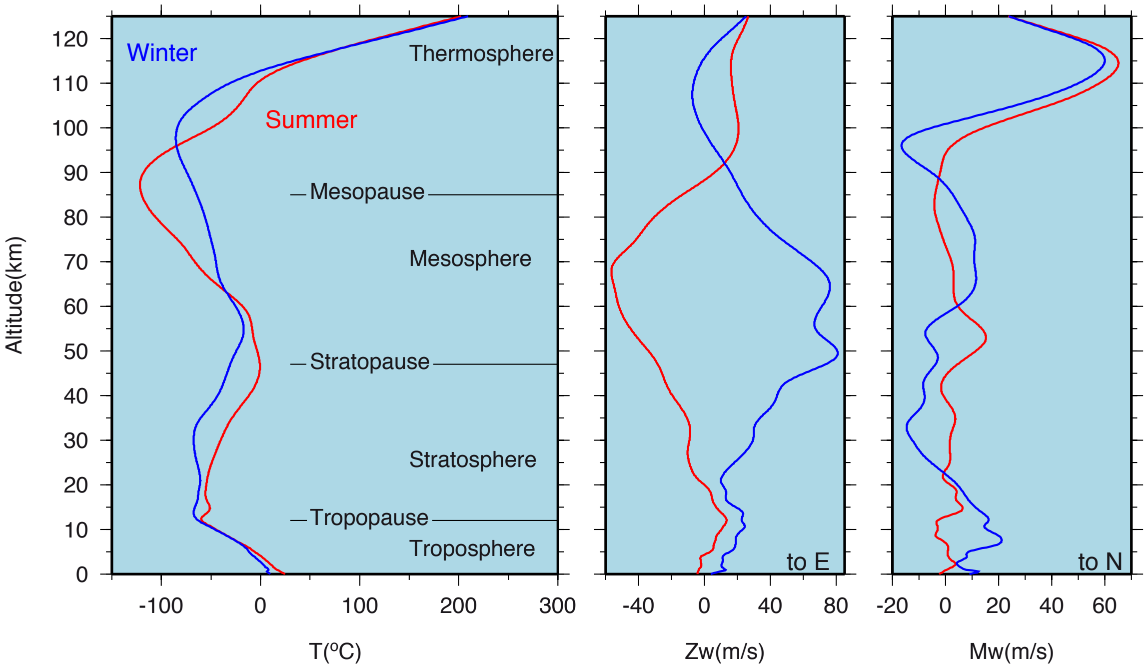

***Figure 1**. Typical summer (red, 2007-07-01) and winter (blue, 2007-12-01) temperature and wind models for De Bilt, the Netherlands. The wind is split in a zonal (Zw), west to east, and meridional (Mw) component, south to north.*

gradients (may) exist that lead to turning infrasonic waves. (1) In the troposphere, in case of a temperature inversion near the surface or a strong jet stream around the tropopause at 10 km altitude. (2) In the stratosphere, due to the combined effect of a temperature increase with increasing altitude due to presence of ozone and strong seasonal winds around the stratopause at 50 km altitude. (3) In the thermosphere, where from 100 km and upwards the temperature strongly increases with increasing altitude due to direct influence of solar radiation on the molecules. As an example, the temperature and wind for a winter and summer atmosphere in De Bilt (the Netherlands) are shown in Figure 1.

Figure 2 shows how infrasound refracts in the stratosphere and thermosphere in a raytracing approach through the summer profiles of Figure 1. Multiple returns are predicted from both the stratopause (labelled as *Is*) and thermosphere (*It*). The polar vortex in the stratosphere is directed westwards during the northern Hemisphere summer and eastwards during winter, making the refractivity of the medium seasonal dependent. In other words, the atmosphere is an anisotropic medium. This anisotropy is also reflected in Figure 3. *It* phases are to be observed in all directions from the source, while *Is* phases only occur to the west. This signature on the earth surface changes as function of time of the day and geographical location. Therefore, Figure 3 is illustrative for the challenge in source identification from a verification point of view. But it also shows the enormous amount of information on the state of the upper atmosphere concealed in the surface based microbarometer recordings.

The general scientific challenges

A large amount of infrasound is continuously being recorded from a variety of man-made and natural sources. Anthropogenic sources include: explosions, nuclear tests, mining, military activities and supersonic flights. The latter is the cause of frequent reports in the Netherlands of tremors felt in buildings, similar to the sensation of an earthquake. Natural sources comprise: avalanches, oceanic waves, severe weather, sprites (lightning from cloud top to ionosphere), earthquakes, meteors, lightning, volcanoes and aurora. The measurement of infrasound is affected by noise due to wind and turbulence in the boundary layer. Therefore, infrasound is measured with arrays to increase the signal-to-noise ratio (SNR) through signal summation. Arrays are also used to estimate the direction of arrival of a wave and its propagation velocity. Typical sizes, i.e., apertures, are in the order of 100 to 1000 meters. Additional noise reduction at each array element is achieved by a wind barrier, a porous hose or pipe array with discrete inlets[6]. The recorded signals are thus a function of the state of the boundary layer and the upper

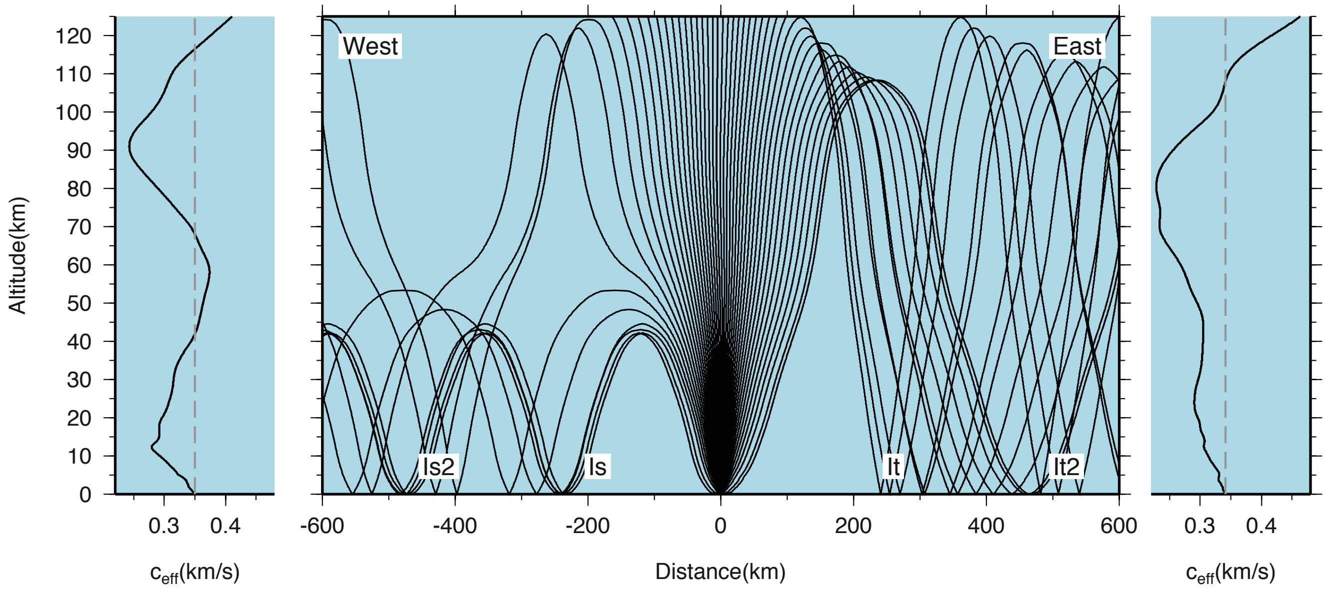

Figure 2. *Ray tracing through the summer profiles of Figure 1, towards the west and east. Refractions back to the earth's surface occur from the stratosphere (Is) and thermosphere (It). The polar vortex is directed to the west during the northern Hemisphere summer, therefore, Is phases are only predicted to the west. The effective sound speeds C_{eff} are given in the left and right hand frames and incorporate the effect of both wind and temperature. Refractions occur from regions where the effective sound speed becomes larger than its surface value, denoted by the dashed line.*

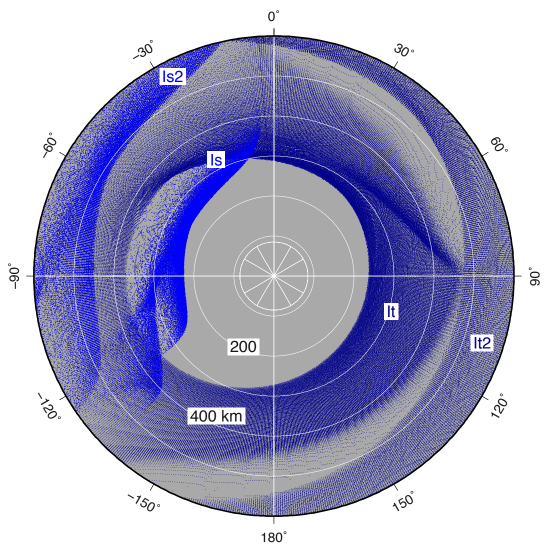

Figure 3. *Ray tracing through the summer profiles in all directions up to a distance of 600 km. The bounce points of the rays, in blue, on the earth, in gray, are plotted for a source located in the centre at an altitude of 0 km. Blue colours refer to stratospheric phases (Is) and dark blue is used for thermospheric arrivals (It). The impinging rays from Figure 2 are on a west (-90°) to east (90°) cross section.*

atmosphere, which changes with time and geographical location. To unravel this complex picture, is the major challenge in source identification[7)].

High frequency seismological arrays are similar in layout to those used in infrasound. The co-location of infrasound and seismic equipment is beneficial for both techniques. The processing techniques developed in infrasound and seismology can be interchanged. Such techniques are applied in data processing and signal detection. Furthermore, atmospheric waves can interact with the solid earth. The interaction between both media is a field of recent research interest.

The surface based microbarometers can also be used as a passive probe for the upper atmosphere (higher than 30 km) with the large amount of sources continuously present. Actual recordings of the basic properties, like wind and temperature, of the upper atmosphere are sparse. Meteorological balloons reach an altitude of roughly 35 km but lack spatial and temporal coverage. Rocket sondes can reach the upper atmosphere but also lack coverage. Satellites have global coverage but have a limited vertical resolution and are difficult to validate for stratospheric altitudes. Therefore, most information currently depends on numerical weather prediction model characteristics. Infrasound can validate such models, and even information on a finer temporal and spatial scale is expected to be retrieved. Such information is very welcome for future atmospheric research. The troposphere and stratosphere have long been considered two isolated layers, split by an impermeable tropopause. The influence of the stratosphere on our daily weather and climate has recently been firmly established, showing that processes in the upper atmosphere do couple to the troposphere[8)].

The microbarometers not only sense infrasound but also gravity waves. The amplitudes of tens of pascal associated with these internal waves fall within the dynamic range of the sensors. Gravity waves are not represented in climate models while they play an important role in many atmospheric processes and, therefore, this leads to uncertainties in climate predictions.

Technical details

The geophysical application within LOFAR, i.e., GEO-LOFAR, consists of seismological and infrasound equipment. The astronomical application will be realized on antenna fields where infrastructure, like power and high-speed Internet, is being established. GEO-LOFAR will make use of this infrastructure. The acquired data will be gathered at Groningen University from where they are distributed to the GEO-LOFAR partners, which are TU Delft, TNO and KNMI. The infrasound contribution consists of a High Density Infrasound Array (HDIA) and a Large Aperture Infrasound Array (LAIA).

A six element infrasound array (EXL) was realized at LOFAR's Initial Test Station near Exloo. EXL has an aperture of 250 meter and contributed to the discovery of exceptional fast infrasonic phases observed after the explosion of an oil-depot in the UK[10,11)] (see Figure 4). The array also showed its value in the detection of lightning, by combining infrasound and electro-magnetic measurements within LOFAR[12,13)].

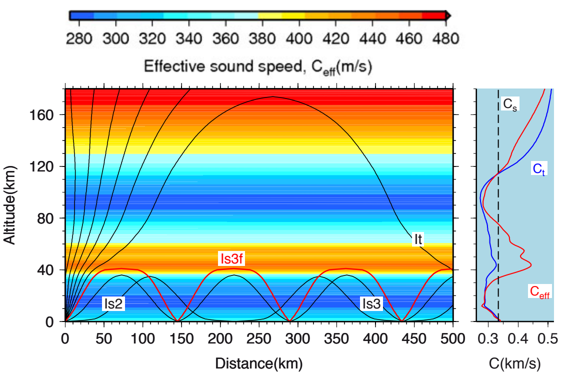

***Figure 4**. Regular (Is3) and exceptionally fast (Is3f) infrasonic phases, i.e., forerunners, observed over the Netherlands after the explosion of an oil-depot in the UK. The forerunners are caused by a very strong polar vortex wind, at 40 km altitude, reaching up to 180 m/s. This wind is reflected in the strong gradient in C_{eff} (see red line in right hand frame); shown also is C_t (in blue), which only accounts for the temperature.*

HDIA has been a temporary deployment of 80 acoustic pressure and vector sensors (of type Microflown) in an 80x80 meters array. The aim was to characterize the acoustic and noise field on a small spatial scale. HDIA's size was comparable to the size of an analog wind filter used at each array element in a conventional array (see Figure 5). Furthermore, the use of a vector sensor enables direction finding with a small instrument instead of a large array. A first analysis of the collected data looks promising[14)].

LAIA will consist of 30 microbarometers, mostly co-located with seismic sensors, in an array with an aperture of 100 km. Recordings from LAIA will provide excellent research opportunities through its unique layout. Only one comparable array has been operational, which was used to analyze the spatial coherence of short period acoustic-gravity waves, with period from 30 to 50 seconds. The Large Aperture Microbarograph Array (LAMA) functioned in the 1960's in the US to detect atmospheric waves from nuclear tests[15)].

In order to also sense gravity waves, the KNMI-microbarometer (KNMI-mb) has been adapted to periods of 1000 seconds, as lower cut-off. The earlier version of the KNMI-mb had a cut-off at 500 seconds and was specially designed to measure acoustic waves. The influence of temperature on the differential KNMI-mb is of main concern when lowering the frequency response. Temperature stability is ensured by properly insulating

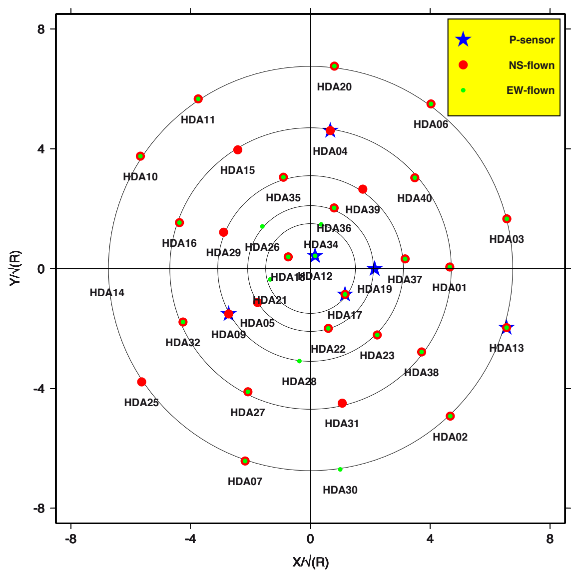

***Figure 5.** The array layout from the High Density Infrasound Array (HDIA). Acoustic pressure and vector sensors (Microflown) are used. The axes are scaled to show the inner rings of the array more clearly. The diameter of the outer ring is approximately 80 meters.*

the instrument's fault and by its subsurface mounting. A detailed study of the amplitude and frequency response has been carried out[16].
An experimental seismological array has been installed at the EXL location which recorded induced earthquakes that occurred in producing gas fields in the region. A test of real time event detection and processing, using e.g. techniques developed for infrasound processing, was carried out successfully[17]. The build-up of a larger array near Annerveen will allow real-time detection and possible identification of induced seismic events.

Conclusion

The high-quality infrastructure provided by LOFAR enables the deployment of large infrasound and seismic installations, in terms of spatial and temporal coverage. Infrasound measurements on such a scale are unique in the world. This uniqueness will provide excellent research opportunities on subjects like source identification and passive acoustic remote sensing of the upper atmosphere[18,19].

The high-quality infrastructure provided by LOFAR enables the deployment of large infrasound and seismic installations, in terms of spatial and temporal coverage. Infrasound measurements on such a scale are unique in the world

The combined measurement of elastic waves in the solid earth and acoustic waves in the atmosphere enables a so-called seismo-acoustic analysis. Specific sources, like explosions and oceanic waves, generate both seismic and infrasonic waves. The infrasonic signature of such a source highly depends on the state of the atmosphere. On the other hand, the seismic waveform is more or less similar throughout the seasons. A seismo-acoustic analysis may reveal the influence of the atmosphere on the detection and localization capability of infrasound as monitoring technique and will also allow for acoustic remote sensing.

Furthermore, infrasound not only travels through the atmosphere but also couples to the solid earth as air-coupled Rayleigh wave or ground-coupled air wave. In this case, the propagation velocity of Rayleigh waves approaches the sound speed. As seismic and infrasound observations are done at the same site, the atmospheric contribution to seismic noise can be quantified.

Future studies with the LOFAR data will be carried out and show the enormous potential of large scale sensor networks.

References

1) Symons, G.J., 1888. *The eruption of Krakatoa and subsequent phenomena.* Trübner & Co., London, UK, 487pp.
2) Posey, J.W. and A.D. Pierce, 1971. *Estimation of nuclear explosion energies from microbarograph records.* Nature, **232**, 253.
3) Donn, W.L. and D. Rind, 1971. *Natural infrasound as an atmospheric probe.* Geoph. J. R. Astr. Soc., **26**, 111-133.
4) Dahlman, O., S. Mykkeltveit and H. Haak, 2009. *Nuclear Test Ban.* Springer, Dordrecht, the Netherlands, 250pp.
5) Drob, D.P., J.M. Picone and M.A. Garcés, 2003. *The global morphology of infrasound propagation.* J. Geoph. Res., **108**, D21, 4680, doi:10.1029/2002JD003307
6) Hedlin, M.A.H., B. Alcoverro and G. D'Spain, 2003. *Evaluation of rosette infrasonic noise-reducing spatial filters.* J. Acoust. Soc. Am., **114**, 1807-1820.
7) Evers, L.G. and H.W. Haak, 2001. *Listening to sounds from an exploding meteor and oceanic waves.* Geoph. Res. Lett., **28**, 41-44.
8) Ineson, S. and A.A. Scaife, 2009. *The role of the stratosphere in the European climate response to El Niño.* Nature Geoscience, **2**, 32-36.
9) Gossard, E.E. and W.H. Hooke, 1975. *Waves in the atmosphere.* Elsevier, Amsterdam, the Netherlands, 456pp.
10) Evers, L.G. and H.W. Haak, 2007. *Infrasonic forerunners: Exceptionally fast acoustic phases.* Geoph. Res. Lett., **34**, L10806, doi:10.1029/2007GL029353
11) Ottemöller, L. and L.G. Evers, 2008. *Seismo-acoustic analysis of the Buncefield oil depot explosion in the UK.* Geoph. J. Int., **172**, 1123-1134.
12) Holleman, I, H. Beekhuis, S. Noteboom, L. Evers, H. Falcke and L. Bähren, 2006. *Validation of an operational lightning detection system.* 19th International Lightning Detection Conference, Tucson, USA, 12pp.
13) Assink, J.D, L.G. Evers, I. Holleman and H. Paulssen, 2008. *Characterization of infrasound from lightning.* Geoph. Res. Lett., **35**, L15802, doi:10.1029/2008GL034193
14) Van Zon, T., L.G. Evers, R. van Vossen and M. Ainslie, 2009. *Direction of arrival estimates with vector sensors: First results of an atmospheric infrasound array in the Netherlands.* Proc. 3d Int. Conf. on Underwater acoustic measurements: Technologies and results, Nafplion, Greece, 6pp.
15) Mack, H. and E. A. Flinn., 1971. *Analysis of the spatial coherence of short-period acoustic gravity waves in the atmosphere.* Geoph. J. R. Astr. Soc., **26**, 255-269.
16) Mentink, J. and L.G. Evers. *The response of the KNMI microbarometer.* J. Acoust. Soc. Am., in preperation.
17) Hazel, G.-J. van den, 2008. *Detection and processing 3C signals from a small scale seismic array,* MSc thesis, Utrecht University, 68pp.
18) Godin, O.A., 2006. *Recovering the acoustic Green's function from ambient noise cross correlation in an inhomogeneous moving medium.* Phys. Rev. Lett., **97**, doi:10.1103/PhysRevLett.97.054301
19) Wapenaar, K., 2006. *Nonreciprocal Green's function retrieval by cross correlation.* J. Acoust. Soc. Am., **120**, EL7-13.17.

TROPOMI: Sensing the Troposphere from Space

Pieternel Levelt and Pepijn Veefkind

Introduction

The growth of human population and the industrialisation in the 19^{th} and 20^{th} century have led to dramatic changes in the Earth system. The chemical composition of the lowest part of the atmosphere, the troposphere, is changing as a result of human activities. The Earth has entered the 'Anthropocene' epoch, where the activities of humans play a key role in air quality and climate change. The rapid development of megacities (see Figure 1) and the strong development in the Asian countries are clear examples of rapid changes that affected the atmosphere in the last decades and will continue to do so in the future.

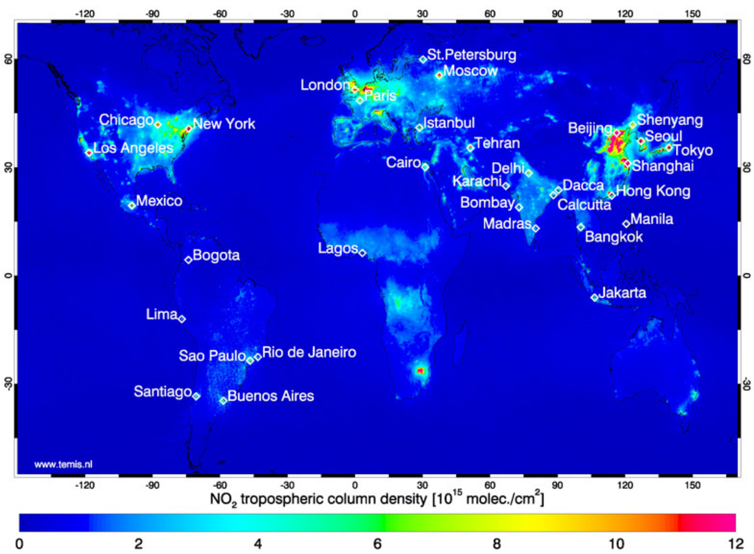

Figure 1. *Cities with over 5 millions inhabitants as reported by the UN for 1995, superimposed on measurements of tropospheric NO_2 from OMI on EOS-Aura averaged over 2006. The development of these megacities will have a major impact on future air quality.*

Global change in the chemical composition of the troposphere is one of the main drivers for changes in the climate and air quality. Especially the global inventory of emission sources plays a key role in understanding and modelling the troposphere in relation to climate change and air pollution. Also regional and long-range transport of pollution, as well as the rapid development of pollution levels during the day, are important for understanding air quality and climate change and their interaction.

Global atmospheric composition measurements from space started in the 70th's with US sensors SBUV[1)] and TOMS[2)], focussing on the ozone layer residing in the higher layers in the atmosphere. Sensing the lower atmosphere from space is a recent development in satellite remote sensing, where instruments like GOME-1[3)] (launched in 1995 on board ESA-ERS-2), SCIAMACHY[4)] (launched in 2002 on board ESAS ENVISAT), OMI[5)] (launched in 2004 on board NASA's EOS-Aura) and GOME-2[6)] (launched in 2006 on board EUMETSAT MetOp-A) play a leading role. Unprecedented measurements from space from OMI reveal tropospheric pollution maps on a daily basis with urban-scale resolution. Measurements from Thermal Infrared instruments also provide unique information on the troposphere, providing tropospheric profile information.
In the last 15 years satellite instruments and retrieval techniques have been improved, enabling tropospheric measurements from space with considerably improved accuracy (see Figure 2). Current satellite measurements uniquely obtain global coverage of the troposphere with consistent quality. The composition of the troposphere plays a major role in air quality and climate change. Tropospheric satellite measurements therefore provide essential information for the understanding of air quality and climate change. The Dutch initiative for the

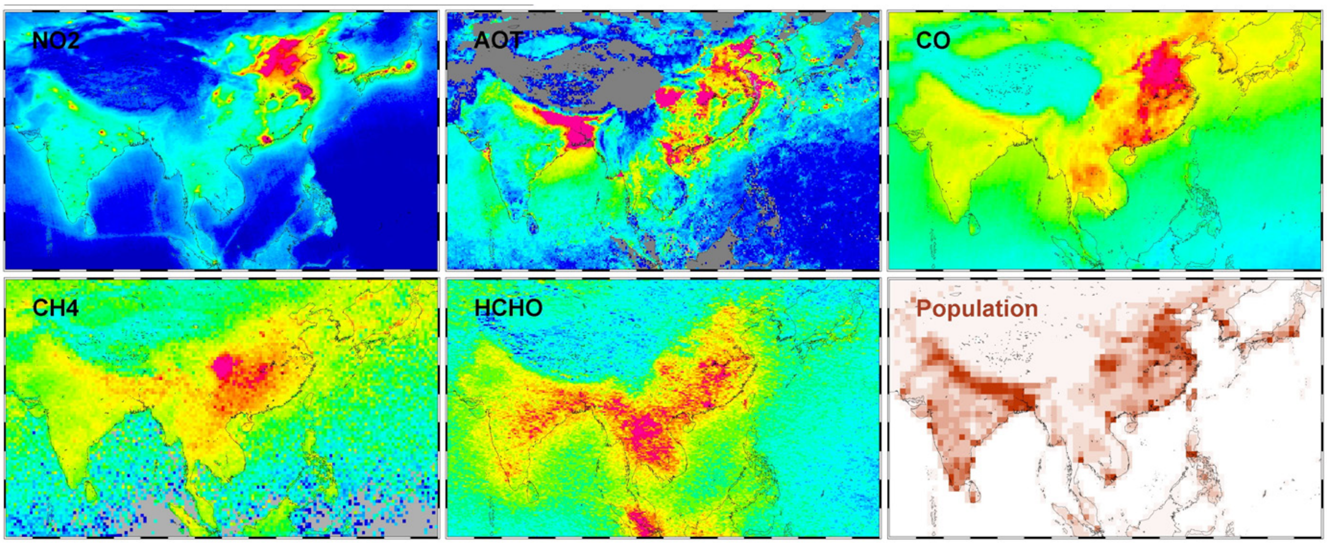

Figure 2. *Tropospheric concentrations of key species over Asia, originating from several instruments. Colour scale concentrations range from red, via yellow and green, to blue, which represent very high, high, medium and low values, respectively. For population (lower right) white represent small, and dark brown-red represent large population numbers. The NO_2 map presents OMI measurements averaged over 2007. Note that major shipping routes are clearly visible. The AOT map shows the Aerosol optical thickness, averaged over March 2005 to May 2008, derived from PARASOL fine mode measurements. The CO map shows MOPITT measurements averaged over 2000 till 2007. The CH_4 map is obtained from observations by SCIAMACHY, averaged over January 2003 till October 2007. The Formaldehyde (HCHO) map is also obtained from observations by SCIAMACHY, averaged over 2003 till 2007. The Center for International Earth Science Information Network (CIESIN), Columbia University and Centro Internacional de Agricultura Tropical, are acknowledged for the population number data, available at http://sedac.ciesin.columbia.edu/gpw.*

Global change in the chemical composition of the troposphere is one of the main drivers for changes in the climate and air quality

satellite instrument TROPOMI (Tropospheric Monitoring Instrument) is developed to improve the detection of the tropospheric composition in view of climate change and air pollution research and monitoring.

Tropospheric Monitoring Instrument TROPOMI

TROPOMI is a satellite instrument for remote sensing of the Earth's atmosphere. Its primary goal is to obtain measurements of the troposphere down to the boundary layer and the Earth's surface in order to quantify emissions and transport of anthropogenic and natural trace gases and aerosols, which impact air quality and climate. The Sentinel 5 precursor (S5p)/TROPOMI will allow continuing the 15 year satellite data sets started with GOME, OMI and SCIAMACHY and will form the bridge towards the ESA sentinel 4 and 5 missions. The S5p/TROPOMI mission was advised by EU and ESA expert groups[6,7].

To address the key user requirements, TROPOMI will measure the main tropospheric pollutants (O_3, NO_2, CO, formaldehyde (HCHO) and SO_2) and two major greenhouse gases (tropospheric O_3 and methane (CH_4)). In addition, it will measure important parameters of aerosols (aerosol scattering, absorption and type identification), which play a key role in climate change as well as in tropospheric pollution.

TROPOMI measures in the UV/VIS wavelength range (270 to 490 nm) like OMI, and in addition in two bands, one in the near infrared (710-790 nm) for dedicated cloud detection, and one in the short wave infrared (around 2300 nm) for CO and methane. The instrument targets 7×7 km^2 pixel size, with daily global coverage. TROPOMI will be launched on ESA's Sentinel 5 precursor in 2014 in an afternoon orbit in loose formation with the future (2013) NOAA Polar Orbiting Earth Operational Environmental Satellites.

TROPOMI is a Dutch initiative building upon the successes of SCIAMACHY and OMI. This new instrument combines all innovative aspects of the previous instruments and improves on most specifications. Notably improved are horizontal resolution and the accuracy of the tropospheric columns, due to improved cloud and surface albedo characterization capabilities. By flying in an afternoon orbit (overpass time is 13:30 local time), the TROPOMI measurements can be combined with the GOME-2 measurements flying in the morning (9:30 am) to obtain information on the diurnal cycle of several of the trace gases. It will be for the first time that the diurnal cycle will be measured from space on a daily basis.

The instrument is designed (see Figure 3 for an impression) by TNO and Dutch Space in the Netherlands, who were also involved to great extent in TROPOMI's predecessors OMI, SCIAMACHY, GOME-1 and -2. KNMI is the Principal Investigator (PI) Institute of TROPOMI, SRON fulfils the co-PI position. Within KNMI there are several Divisions that will cooperate and benefit from the TROPOMI mission. The Climate Observations Division hosts the PI and Chair of the S5p/TROPOMI Mission Advisory Group. The Chemistry and Climate Division supported the formulation of the scientific objectives of TROPOMI and will be a user of the data. The Information and Observation Services and Technology Department will help to design the ground segment. Use of the data by others within KNMI is envisaged.

Scientific themes of TROPOMI

TROPOMI aims at providing data for the scientific and operational community dealing with climate, an quality and weather. In order to fulfil the requirements of these groups, the following four TROPOMI scientific objectives have been identified:

To better constrain the strength, evolution, and spatiotemporal variability of the sources of trace gases and aerosols impacting air quality and climate

For a proper understanding of air quality and emissions of trace gases contributing to climate change it is needed to quantify the strength, distribution and variability of emissions of NO_2, CO, aerosols, SO_2, CH_4 and volatile organic compounds, and to identify the contribution of anthropogenic emissions, such as fossil fuel burning and agriculture, and natural emissions, such as lightning. Currently emission inventories are characterized by large error bars and incomplete estimates of inter-annual, seasonal and diurnal variability. TROPOMI will provide state-of-the art measurements of the above mentioned compounds to improve on the emission inventories.

To improve upon the attribution of climate forcing by a better understanding of the processes controlling the lifetime and distribution of methane, tropospheric ozone, and aerosols

Unlike CO_2 and other major well-mixed greenhouse gases including CH_4 and N_2O, aerosols and tropospheric ozone are inhomogeneously distributed climate forcing agents. Together, CH_4 and tropospheric O_3 contribute about 30% to the present-day total forcing due to anthropogenic greenhouse gases compared to the pre-industrial situation, while CO_2 accounts for 53%. Poorly quantified

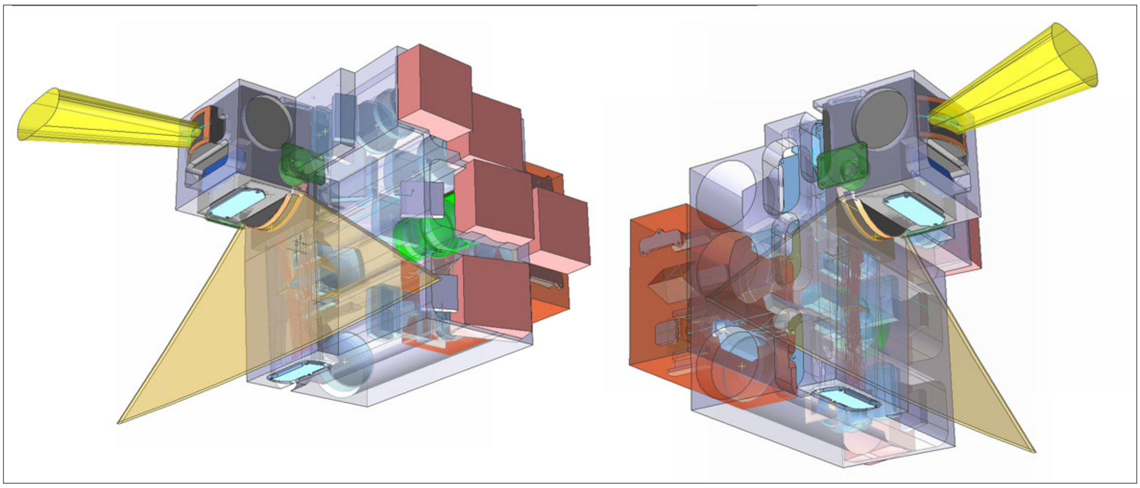

Figure 3. *Impression of the TROPOMI instrument, seen from different directions. The yellow beam enters the solar calibration port, while the orange beam represents the Earth measurements wide angle swatch providing daily global coverage. The blue/purple transparent box shows the UV-VIS-NIR module, which will measure O_3, NO_2, formaldehyde (HCHO), SO_2 tropospheric O_3 aerosol parameters (aerosol scattering, absorption and type identification) and detection of clouds. The orange box in the right hand image is the short wave infrared module (SWIR) for measuring CO and methane around 2300 nm. (source: Dutch Space / TNO Space).*

is the transformation of gaseous precursors (NO_X, SO_2, CO and VOCs) into radiatively active constituents, including CO_2, O_3 and secondary aerosols. TROPOMI will contribute to understanding the attribution of climate forcing by detecting aerosols and tropospheric ozone and methane, which have a direct radiative effect on climate. TROPOMI also measures precursors (especially NO_2, SO_2, CO and VOCs) of radiatively active constituents, including CO_2, O_3 and secondary aerosols[8], which will help to improve the understanding of the lifetime and distribution of methane, tropospheric ozone and aerosols.

A specific challenging research topic is the connection between air quality and climate. In a warmer climate, air pollution episodes will become more severe as a result of higher temperatures, promoting photochemical ozone formation. At the same time, air pollutants are often radiatively active (e.g. O_3), or a precursor for a radiatively active constituent (e.g. NO_2), and thus also have a direct impact on climate.

To better estimate long-term trends in the troposphere related to air quality and climate from the regional to the global scale

Long-term measurements are showing that human activities change the composition of the Earth's atmosphere. These changes resulted in the development of the ozone hole, the increase of greenhouse gases, smog episodes, acid rain, air pollution, brown clouds, intercontinental transport of pollutants, changes in atmospheric oxidation efficiency, etc. Long-term observational records are essential to quantify the impact of the atmospheric composition on climate. In order to understand changes in tropospheric composition, local and global data records are needed. Local air pollution is determined not only by local sources and sinks, but also by long-range transport of pollutants. Therefore, in order to have a full picture and an in-depth understanding of air pollution and tropospheric composition, both local and global observations are needed. Satellite measurements can quantify the (inter-)continental transport and dispersion of pollution plumes, by which important information on the non-local contribution to air pollution is obtained.

To develop and improve air quality model processes and data assimilation in support of operational services including air quality forecasting and protocol monitoring

Operational applications that will benefit from TROPOMI satellite data include air quality forecasts and environmental hazard warnings. At present mainly space-borne tropospheric NO_2 and aerosol measurements are used to improve air quality forecast applications. O_3 observations are used for UV warnings and the improvement of the operational weather forecast. CO, aerosols and tropospheric NO_2 measurements are being applied for operational monitoring of forest fires, and SO_2 observations are used for aviation control warnings and monitoring of volcanic eruptions. TROPOMI will be able to continue the near-real-time services already existing for OMI and SCIAMACHY and will provide important data for the GMES EU project Monitoring Atmospheric Composition and Climate (MACC), lead by ECMWF.

The main advantage of TROPOMI type satellite measurements for measuring the troposphere

There are basically two methods used to measure trace gases in the troposphere, both based on passive remote sensing techniques: the solar backscatter technique and the thermal infrared technique. In the solar backscatter technique the instrument measures the solar radiation that has been absorbed and scattered by the atmosphere. This so-called Earth radiance spectrum contains the specific absorption features of the molecules of interest. The Solar backscatter instruments usually provide tropospheric columns of the trace gases. This technique has the advantage to be sensitive to the surface, since the atmosphere is transparent in this visible wavelength range. Therefore, this method is best suited to determine emission sources, which is the main objective of the TROPOMI instrument. In the thermal infrared technique the thermal emission of the Earth-atmosphere system is measured, revealing the specific absorption features of the trace gases. With the thermal infrared technique some vertical information can be obtained, approxi-mately two layers in the troposphere, but the sensitivity to the surface is less, so that accurate total column amounts are considerable more difficult to obtain.

Challenges in measuring the troposphere from space

In order to address the scientific themes related to the troposphere, new instruments need to improve in horizontal and vertical resolution, diurnal information, amount of collocated measurements, and cloud and surface albedo detection capabilities. TROPOMI makes major steps forward on horizontal resolution, amount of collocated cloud-, and albedo measurements and, combined with the morning measurements of GOME-2, also on the diurnal cycle.

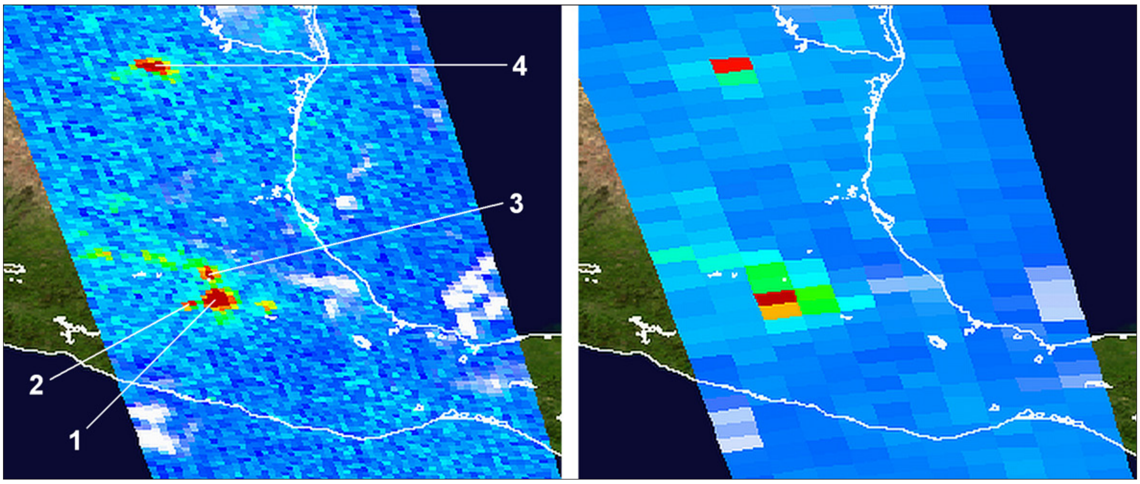

Figure 4. *Tropospheric NO_2 around Mexico City on 20 January 2005. The image on the left shows OMI measurements recorded in the so-called 'zoom-in mode', resulting in ground pixels of the order 12 × 13 km^2. De numbers refer to: 1 = Mexico City and suburbs; 2 = Toluca de Lerdo; 3 = industrial complex near Tula, Hidalgo (consisting of a large oil refinery and a power plant, amongst others); and 4 = Monterrey and suburbs. The image on the right shows the same measurements, but now re-gridded to the resolution of GOME-2 (72 × 39 km^2). Much detail is now lost.*

TROPOMI's measurements will lead to improved emission estimates which are of paramount importance for climate and air quality modelling

Conclusion

Information on the tropospheric composition is of fundamental importance for understanding climate change and air quality. In the last decade a rapid development took place in sensing the troposphere from space, enabling measurements of tropospheric columns and providing the first tropospheric profile retrievals. TROPOMI, to be launched in 2014 on ESA's Sentinel 5 precursor, will improve on current capabilities in terms of horizontal pixel size (see Figure 4), cloud and surface albedo detection and correction algorithms and will enable daily diurnal cycle measurements in combination with GOME-2. TROPOMI's measurements will lead to improved emission estimates which are of paramount importance for climate and air quality modelling.

References

1) Hilsenrath, E., R.P. Cebula, M.T. Deland, K. Laamann, S. Taylor, C. Wellemeyer and Bhartia, P.K., 1995. *Calibration of the NOAA-11 Solar Backscatter Ultraviolet (SBUV/2) Ozone Data Set from 1989 to 1993 using In-Flight Calibration Data and SBUV.* J. Geophys. Res., **100**, 1351-1366.
2) McPeters, R.D., P.K. Bhartia, A.J. Krueger, J.R. Herman, B.M. Schlesinger, C.G. Wellemeyer, C.J. Seftor, G. Jaross, S.L. Taylor, T. Swissler, O. Torres, G. Labow, W. Byerly, and R.P. Cebula, 1996. *Nimbus-7 Total Ozone Mapping Spectrometer (TOMS) Data Products User's Guide.* NASA Reference Publication 1384.
3) Burrows, J.P., M. Weber, M. Buchwitz, V.V. Rozanov, A. Ladstatter-Weissenmayer, A. Richter, R. de Beek, R. Hoogen, K. Bramstedt, K.W. Eichmann, M. Eisinger and D. Perner, 1999. *The Global Ozone Monitoring Experiment (GOME): Mission Concept and First Scientific Results.* J. Atmos. Sci., **56**, 151-175.
4) Bovensmann, H., J.P. Burrows, M. Buchwitz, J. Frerick, S. Noël, V.V. Rozanov, K.V. Chance and A.P.H. Goede, 1999. *SCIAMACHY - Mission objectives and measurement modes.* J. Atmos. Sci., **56**, 127-150.
5) Levelt, P.F., G.H.J. van den Oord, M.R. Dobber, A. Malkki, H. Visser, J. de Vries, P. Stammes, J. Lundell and H. Saari, 2006. *The Ozone Monitoring Instrument.* IEEE Transactions On Geoscience and Remote Sensing [Special Issue on the EOS-Aura mission], **44** (5), 1199-1208.
6) EU GAS (GMES Atmospheric Services)-IP (2007-2009), 2009. Final Report, 40, 43), April 2009. http://www.gmes.info/pages-principales/library/implementation-groups/gmes-atmosphere-core-service/
7) ESA CAPACITY (2003-2005), 2005. Final and Summary Report, Oktober 2005. http://www.knmi.nl/capacity
ESA CAMELOT (2007-2009), 2009. Final and Summary Report, December 2009.
http://www.knmi.nl/publications/fulltexts/rpcamknmi051_camelot_summary_report_i1.pdf and
http://www.knmi.nl/publications/fulltexts/rpcamknmi050_camelot_final_report_i1.pdf.
8) Shindell, D.T., G. Faluvegi, D.M. Koch, G.A. Schmidt, N. Unger, and S.E. Bauer, 2009. *Improved Attribution of Climate Forcing to Emissions.* Science, **326**, (5953), 716. doi:10.1126/science.1174760

The central role of the tropics in the methane life cycle

Highlights of the EU-project HYMN

Michiel van Weele, Lisa Neef and Peter van Velthoven

Introduction

Carbon dioxide (CO_2) concentrations in the atmosphere are increasing. Anthropogenic emissions due to the burning of fossil fuels are primary held responsible. However, also the concentrations of several other greenhouse gases, such as methane (CH_4) and nitrous oxide (N_2O), are increasing. For these gases expanding agricultural activities are the primary cause. Still a lot of questions remain with respect to the life cycles of these important non-CO_2 greenhouse gases.

In the European project HYMN (Hydrogen, Methane and Nitrous oxide) three atmospheric trace gases have been studied: CH_4, N_2O and hydrogen (H_2). The atmosphere-biosphere interactions of these three gases are tightly coupled. H_2 is not a greenhouse gas. The presently increasing interest in H_2 is related to the possible transition to a *hydrogen economy* that may occur within the coming decades. A switch to H_2 as alternative energy source – assuming that the H_2 is produced using renewable energies and would replace fossil fuels, could have benefits for both air quality and climate, but the possible environmental impacts need to be evaluated.

The three-year HYMN project started in 2006 and was executed by a multi-disciplinary consortium of 12 institutes and universities in Europe led by KNMI. In this highlight we focus on the life cycle of CH_4.

Anthropogenic CH_4 emissions are an important contribution to climate change

The importance of CH_4 emissions for climate change

In 2007 the global-mean CH_4 surface concentration was 1790 ppbv (parts per billion by volume), in 2008 it reached 1797 ppbv, and the preliminary data for 2009 show continued growth in CH_4. This increase came after a period of near-zero growth from about 1999 to 2006. Present-day CH_4 concentrations are more than a factor 2.5 larger than pre-industrial concentrations due to anthropogenic CH_4 emissions.

CH_4 emissions are contributing importantly to climate change. There are several arguments underlining this importance: The increase in anthropogenic CH_4 emissions since 1750 has resulted in a climate forcing of almost 1 Wm^{-2}, which can be compared to 1.6 Wm^{-2} for CO_2 emissions[1)]. CH_4 has a 100-year global warming potential (GWP) of 25 relative to CO_2, and therefore it is a more powerful greenhouse gas than CO_2. An important reason for the higher GWP of CH_4 is that the chemical breakdown of CH_4 in the atmosphere additionally causes increases of tropospheric ozone and stratospheric water vapour, which are taken into account in the GWP. In addition, CH_4 is more effective than CO_2 in warming the surface on a per molecule basis, also because, compared to the CO_2 forcing, a larger part of the CH_4 forcing occurs in the troposphere. On the other hand, perturbations of CH_4 have a much shorter lifetime (about 12 years) than those of CO_2 (of the order of centuries).

Improved knowledge on CH_4 emissions

The largest contribution to the CH_4 emissions of anthropogenic origin is the release of digestive gases by ruminants (cattle) which constitute about one third of all anthropogenic emissions. Other important anthropogenic sources are emissions related to fossil fuel use (coal mining, gas leakages) which constitute another third, and the treatment of waste (landfills). Rice cultivation and biomass burning are also anthropogenic sources of CH_4. Total present-day anthropogenic emissions exceed the natural total emissions by more than 50%. Natural CH_4 emissions are dominated by wetlands, i.e. saturated soils, peat lands, bogs, swamps, marshes, etc., and these emissions depend on the actual local climate conditions. Figure 1 shows the wetland CH_4 emission distribution for two months in 2004 calculated with a global dynamical vegetation model[2)]. The figure shows that tropical regions as well as the northern extra-tropics are important emission regions. The figure also shows that the exact location of the major emission regions varies with the season.

Within the HYMN project the retrieval of CH_4 from the SCIAMACHY satellite instrument has been significantly improved by implementing improved spectroscopic information[3,4)]. The satellite data are used together with surface observations of CH_4 to constrain the geographical distribution and temporal variations in the natural and anthropogenic CH_4 emissions. The left panel of Figure 2 shows the improved emission distribution for the year 2004. Important anthropogenic emission regions are, for example, the densely populated areas of Asia, North- and South-America and Europe, while natural emissions are large over Amazonia and some other large river basins such as those of the Orinoco, the Mississippi, and the Ganges. The right panel of Figure 2 shows the differences with the prior assumed CH_4 emissions, which are either taken from the vegetation model (Figure 1) or, for the anthropogenic ones, estimated from socio-economic statistics (e.g. the number of cows per country). Some care is needed in the interpretation of the patterns in the right panel as many factors contribute to the final result.

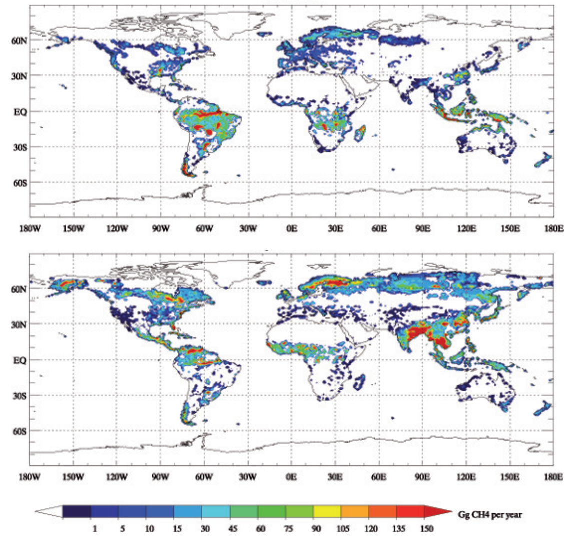

Figure 1. Modelled CH_4 wetland emissions for March (top) and September (bottom) of the year 2004. Units: Gg (10^9 g) per grid cell per year.

The picture over Asia is complex and mixed, including, e.g., a northward redistribution of emissions within India. Wetland CH_4 emissions are estimated high over certain regions (e.g. Scandinavia) and low over other regions (e.g. central Africa). Ruminant emissions over Brazil are larger than assumed a priori, conspicuously because Brazil has experienced a rapid increase in cattle number over the years. In 2006 the UN Food and Agriculture Organisation FAO noted that Brazil has become the largest meat (beef) exporter in the world.

Figure 2 shows that CH_4 emissions at tropical latitudes dominate over extra-tropical emissions even more than expected a priori. It has been suggested that large increases in northern CH_4 emissions might lead to a tipping

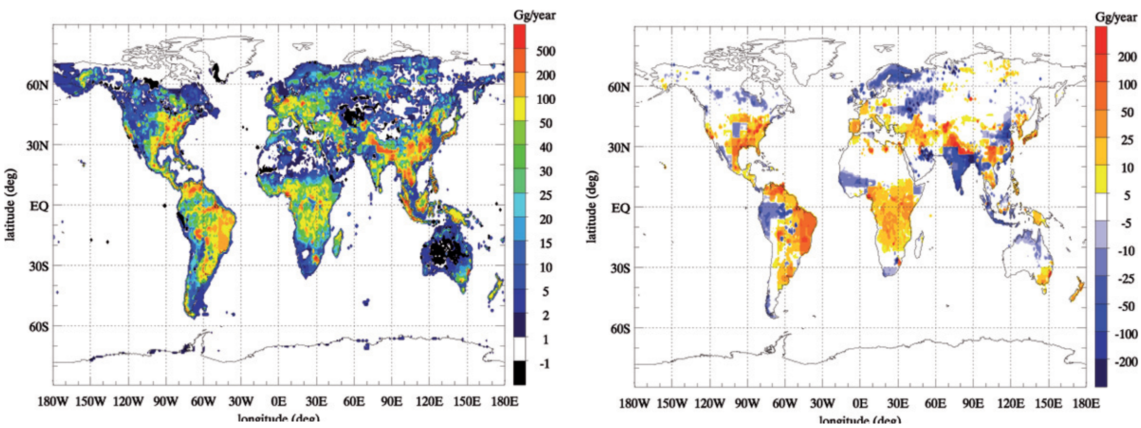

Figure 2. *(left panel) Observationally constrained global annual CH_4 emission distribution for the year 2004. (right panel) Differences between the observationally constrained emissions and prior knowledge on CH_4 emissions. Both natural and anthropogenic source categories are included. Units are Gg (10^9 g) per grid cell per year.*

point in climate[5]. However, even though the temperature-sensitivity of northern CH_4 emissions is well-established we found as yet no observational evidence for large increases in CH_4 emissions related to permafrost melting or destabilisation of hydrates in response to Arctic warming.

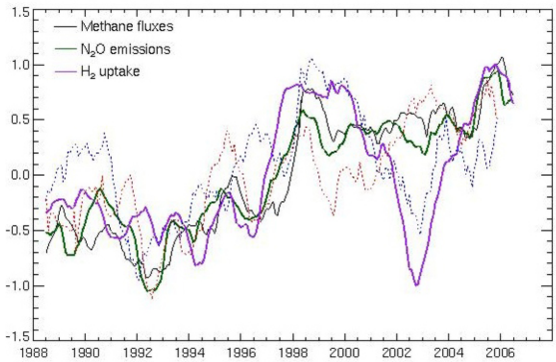

Figure 3. Inter-annual variability in the global annual CH_4 and N_2O surface exchange fluxes (natural emissions minus soil uptake), and H_2 soil uptake over the period 1988-2006. Dotted lines represent variations in global land surface temperature (red) and precipitation (blue). All variations are normalised against the global average and derived from 12-month running means.

Inter-annual variability

Inter-annual variability in global CH_4 concentrations is caused by variations in the natural CH_4 emissions and by variations in the chemical breakdown of CH_4 in the atmosphere. Figure 3 shows the variability in the natural net CH_4 surface fluxes (i.e. emissions minus soil uptake) over the period 1988-2006, as well as variations in surface temperature and precipitation. The figure shows that the CH_4 variability is largely driven by the variations in surface temperature and rainfall. Figure 3 also shows the natural net exchange fluxes of N_2O and H_2, which are highly correlated with the CH_4 fluxes, except for a strong decrease in H_2 uptake during 2002 when global precipitation levels dropped. The figure shows that trends and variations in the global natural surface fluxes of CH_4 probably have been limited over the considered time period. On the other hand, because a climatology for inundated areas has been used instead of actual inundation observations, the inter-annual variability is likely underestimated in the figure. Variations in temperature, humidity and incoming solar ultraviolet radiation in the tropical lower troposphere drive inter-annual variations in the chemical breakdown of CH_4. Chemistry model simulations have indicated that, over the last two decades, trends and inter-annual variations in the meteorologically driven loss rates are likely to have been limited[6].

Evidence is emerging that the current moderate growth in CH_4 is primarily caused by the wide-spread presence of (sub-)tropical air pollution and less by CH_4 emission mitigation

What is currently limiting the increase in the CH_4?

Even though the inter-annual variability in CH_4 loss rates has been small, a long-term trend in the chemical loss can not be ruled out. Over the last 15 years the annual growth rate in CH_4 has been consistently smaller than in the 1980s when growth rates regularly exceeded 10 ppb per year. Figure 4 shows the gradual increase in tropospheric CH_4 since 1995 observed at Jungfraujoch, Switzerland. These column observations are in line with the evolution seen by the global surface networks for CH4. A period of near-zero growth (1999–2006) has recently been followed by renewed moderate growth. It has been suggested that the lack of growth after 1999 was largely due to an episodic reduction in the tropical natural emissions related to sustained relatively dry conditions in the tropics, and it was predicted in 2006 that the CH_4 growth rate would probably recover soon in response to further increasing anthropogenic CH_4 emissions[7].

Per year the present-day anthropogenic emissions are growing faster than in the 1980s and most of the increase in the annual emissions since 1995 has occurred after the year 2000. These emission increases can not easily be reconciled with the moderate annual growth as shown

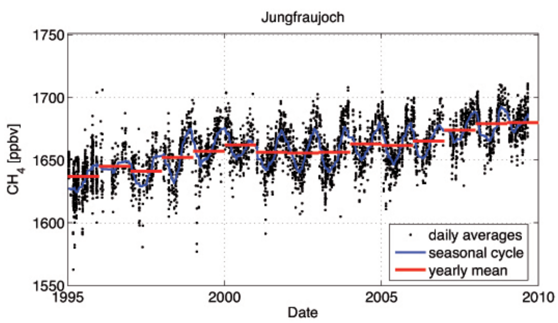

Figure 4. Atmospheric CH_4 since 1995 at Jungfraujoch, Switzerland. These are CH_4 column mixing ratios (in ppbv) made using Fourier Transform Infra Red (FTIR) spectroscopy.

in Figure 4 – unless the chemical lifetime of CH_4 would be significantly shorter now than in the 1980s. Note that there are no indications for large sustained reductions in natural CH_4 emissions (Figure 3).

In HYMN it has been found that the global CH_4 lifetime is sensitive to air pollution, and mostly to nitrogen oxides (NO_x) emitted under sunny, warm and humid conditions such as in the tropics. Rapid increases in low-latitude NO_x emissions have recently been observed by satellite NO_2 instruments such as OMI and SCIAMACHY. An estimated decrease of 3-5% [6)] in CH_4 lifetime due to increased (sub-)tropical NO_x pollution since about 1995 could compensate for 15 – 25 Mt of CH_4 emissions per year, which is a significant fraction of the emission increase. Therefore, evidence is emerging that the current moderate growth in CH_4 is primarily caused by the wide-spread presence of (sub-)tropical air pollution and less by CH_4 emission mitigation.

N_2O and H_2

The increase in N_2O in the atmosphere from a pre-industrial level of 270 ppb to about 322 ppb in 2008 is largely caused by expanding agricultural activities and has resulted in a radiative forcing of 0.16 Wm^{-2}. N_2O has a chemical lifetime of more than 100 years and is thus much longer lived than CH_4. The relatively large pre-industrial concentration of N_2O shows the relative importance of natural N_2O emissions, mainly from vegetated soils. Natural N_2O emissions are largest over tropical forests and savannas, and are estimated to sum globally up to 11 ± 3 TgN per year (including a minor ocean source), still exceeding anthropogenic N_2O emissions (7 ± 1 TgN per year).

Hydrogen has a chemical lifetime of only about 2 years. The present-day H_2 concentration of about 550 ppb is largely a product of atmospheric chemistry and the uptake by soils (Figure 3). Future air quality and climate scenarios will need to include hydrogen (H_2) emissions, such as e.g. from leakages, to assess the possible impacts on atmospheric composition and climate, most notably by increasing stratospheric water vapour. The transition to a hydrogen economy might mitigate climate change due to the potential CO_2 emission reduction. Clear advantages for future air quality are found because of the reduction in air pollution by fossil-fuel burning associated with a hydrogen economy.

Conclusion

By observations and model calculations the EU-funded project HYMN has provided improved insights in the life cycle of CH_4 and some other gases in the atmosphere. Key findings are that (sub-)tropical latitudes are dominant for CH_4 emissions and chemical breakdown and thus also for inter-annual variability in CH_4 and, secondly, that evidence is emerging that the atmospheric lifetime of CH_4 is being reduced by increasing (sub-)tropical air pollution. Continued observations of atmospheric composition are essential to get a better understanding of the chemistry-climate interactions and relations between climate change and other important environmental issues related to the trace gases CH_4, N_2O, and H_2, such as the recovery of the ozone layer in the 21st century and future changes in global air quality.

Acknowledgements

We are indebted to the participants in the HYMN project for providing materials and results. Figures 1 and 3 courtesy of Renato Spahni and Rita Wania (University of Bristol), and figure 4 courtesy of Emmanuel Mahieu and Pierre Duchatelet (University of Liège).

References

1) Shindell, D.T., G. Faluvegi, D.M. Koch, G.A. Schmidt, N. Unger and S.E. Bauer, 2009. *Improved attribution of climate forcing to emissions.* Science, **326**(5953), 716-718, doi:10.1126/science.1174760
2) Spahni, R., R. Wania, L. Neef, M. van Weele, I. Pison, P. Bousquet, C. Frankenberg, P. Foster, F. Joos, I. C. Prentice and P. van Velthoven, 2010. *Constraining global net emissions of natural methane sources and sinks from wet ecosystems.* Submitted to Biogeosciences, 2010.
3) Frankenberg, C., P. Bergamaschi, A. Butz, S. Houweling, J. F. Meirink, J. Notholt, A. K. Petersen, H. Schrijver, T. Warneke and I. Aben, 2008. *Tropical methane emissions: A revised view from SCIAMACHY onboard ENVISAT.* Geophys. Res. Lett., **35**, L15811, doi:10.1029/2008GL034300
4) Frankenberg, C., J. F. Meirink, M. van Weele, U. Platt and T. Wagner, 2005. *Assessing methane emissions from global space-borne observations.* Science, 308(5724), 1010-1014, doi:10.1126/science.1106644
5) Climate Change Science Program (CCSP), 2008. *Abrupt Climate Change. Report by the U.S. Climate Change Science Program and the Subcommittee on Global Change Research.* (Clark, P.U., A.J. Weaver (coordinating lead authors), E. Brook, E.R. Cook, T.L. Delworth and K. Steffen (chapter lead authors)). U.S. Geological Survey, Reston, VA, USA, 459pp.
6) Weele, M. van, and P.F.J. van Velthoven, 2010. *Multi-year analysis of recent changes in global atmospheric methane levels,* submitted to Journal of Integrative Environmental Sciences special issue to the Non-CO2 Greenhouse Gas5 (NCGG-5) Symposium 30 June – 3 July 2009, Wageningen, the Netherlands.
7) Bousquet P, P. Ciais, J.B. Miller, E.J. Dlugokencky, D.A. Hauglustaine, C. Prigent, G.R. van der Werf, P. Peylin, E.G. Brunke, C. Carouge, R.L. Langenfelds, J. Lathière, F. Papa, M. Ramonet, M. Schmidt, L.P. Steele, S.C. Tyler and J. White, 2006. *Contribution of anthropogenic and natural sources to atmospheric methane variability.* Nature, 443 (7110), 439–443, doi:10.1038/nature05132

The statistical mechanics of turbulent flows

Wim Verkley

Introduction

In a paper that appeared 70 years ago in the Journal of the Dutch Physical Society, Burgers[1] addressed the question whether the statistics of turbulent flows can be investigated by the methods of statistical mechanics.

In the past these methods had been very successfully applied to the microscopic motion of molecules. In extending their application to the realm of turbulent motion, one encounters the difficulty that the fluid dynamical equations are continuous. By using a representation of the flow fields in terms of Fourier components this problem can be solved to the extent that a phase space can still be defined although it is infinite dimensional. Another difficulty is that, in turbulent motion, energy is not conserved but flows through the system. Burgers therefore proposed that the statistics of a turbulent system is controlled by an average balance between input and output of energy and not, as is appropriate to assume in the realm of molecular motion, by the conservation of energy. Taking the dissipation to be quadratic, when expressed in terms of the Fourier coefficients, and constraining the statistics to respect an average balance between forcing and dissipation, he applied the techniques of statistical mechanics and concluded that the dissipation is equally partitioned among the Fourier components.

Our aim is to deduce the model's climate from its basic equations, as an alternative to averaging over long numerical time-integrations

This conclusion was both interesting and problematic. Equipartition of dissipation leads to an unphysical infinite total dissipation if the phase space of the system is infinite dimensional. Quantum mechanics does not come to the rescue here as it had done earlier when an analogous problem arose in the statistical mechanics of electromagnetic radiation. Despite a series of publications, many of which are reprinted in the memorial volume by Nieuwstadt and Steketee[2], a completely satisfying solution did not emerge and Burgers finally abandoned the subject. Several years later Onsager[3] took it up again but decided to pursue a course that is more in line with equilibrium statistical mechanics, as detailed in the review article by Eyink and Sreenivasan[4].

The work described below[5] can be considered as an attempt to revisit Burgers' approach. It will thus be investigated whether statistical mechanics can be used to deal with forced-dissipative turbulent systems, using as a basic assumption that the statistics is controlled by an average balance between forcing and dissipation.
The problem of the infinite dissipation is not resolved but moderated by limiting ourselves to finitely truncated spectral representations of fluid flows. We will phrase the theory in the language of probability theory and the principle of maximum entropy, as advocated by Jaynes[6].

The method will be applied to a simple one-layer model of the large-scale atmospheric circulation. In this context the model's statistics can be identified with the model's climate. From the perspective of this model our aim is to deduce the model's climate from its basic equations, as an alternative to averaging over long numerical time-integrations.

A model of the large-scale atmospheric circulation

The model to be considered describes the motion of a single layer of incompressible fluid on the surface of a rotating sphere. Orography is taken into account and the flow is assumed to be geostrophically balanced and thus approximately governed by the horizontal advection of quasigeostrophic potential vorticity. The equation that is used is a somewhat simplified version of an equation discussed recently by the author[7)]. The system is forced by relaxation towards a zonally symmetric circulation that consists of jet-streams in both hemispheres, and is damped by a term that has the same structure as the viscosity term in fluid dynamics. The two-dimensional streamfunction, in terms of which the horizontal velocity is expressed, is the basic field of the model and is represented by a finite set of spherical harmonics, indexed by the integers m and n, where n runs from 1 to $N = 42$ and m runs from $-n$ to $+n$. The variables of the model are expressed in units formed by appropriate combinations of the earth's radius and angular velocity of rotation.

The phase space of the model consists of the Fourier coefficients ψ_{mn} of the streamfunction. By projecting the advection equation of potential vorticity onto the finite set of spherical harmonics, one obtains a dynamical system of quadratically non-linear equations in the Fourier coefficients. When integrated numerically, this finite-dimensional dynamical system displays chaotic turbulent motion, not unlike what is seen in large-scale atmospheric flow. To demonstrate this, we show in Figure 1 two snapshots of the vorticity and the zonally averaged zonal velocity, separated by 10 days in time, at the end of an integration of 2000 days.

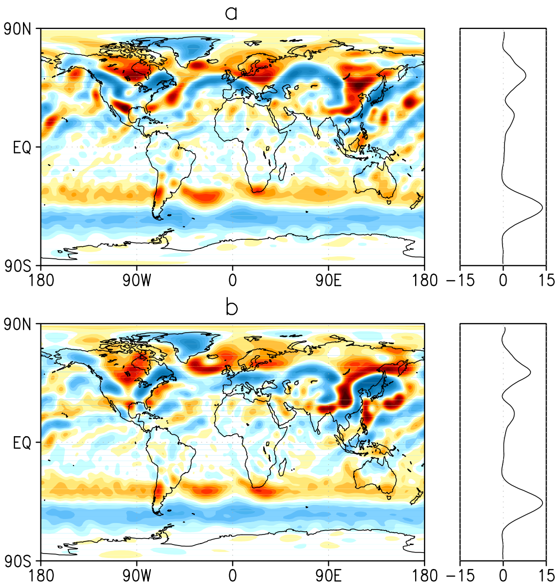

Figure 1. *The vorticity field at day 1990 and day 2000 (a and b, respectively) in a numerical integration of the spectral model of large-scale atmospheric flow. The values of the vorticity are expressed in units of the earth's angular velocity and are in the range (-0.50, 0.55) and (-0.57, 0.61), respectively, and are displayed with a contour interval of 0.04. The colour scale is from blue (low values) to red (high values). The profiles to the right of the vorticity fields are the zonally averaged zonal velocity in meters per second.*

Energy and enstrophy

The global state of the system can be characterized by the energy E and the enstrophy Z, given by

$$E = \Sigma_{mn} (1/2)\, \varepsilon_n \psi^2_{mn},$$
$$Z = \Sigma_{mn} (1/2)\, (\varepsilon_n \psi_{mn} - f_{mn})^2.$$

Here is ε_n a system parameter and f_{mn} is related to the Coriolis parameter and the orography. In the presence of forcing and dissipation, we have

$$dE/dt = F - D,$$
$$dZ/dt = G - H,$$

in which the energy forcing F, energy dissipation D, enstrophy forcing G and enstrophy dissipation H are given by

$$F = \Sigma_{mn} (-F_{mn} \psi_{mn}),$$
$$D = \Sigma_{mn} (d_n \psi^2_{mn}),$$
$$G = \Sigma_{mn} (-\varepsilon_n F_{mn} \psi_{mn} + f_{mn} F_{mn}),$$
$$H = \Sigma_{mn} (d_n \varepsilon_n \psi^2_{mn} - d_n f_{mn} \psi_{mn}).$$

In these expressions F_{mn} is the Fourier coefficient of the forcing and d_n is related to the form and the strength of the dissipation. It can be seen that, if the forcing coefficients F_{mn} and dissipation parameters d_n are zero, the energy E and the enstrophy Z are conserved. If these coefficients and parameters are not zero, this is no longer the case. However, for a statistically stationary state we have instead that dE/dt and dZ/dt, or $F - D$ and $G - H$, are zero on average.

Statistical mechanics and maximum entropy

The central concept in a statistical mechanical theory is the probability density function, denoted by P, which in our case gives the probability to find the system in a state with Fourier coefficients ψ_{mn}. According to Jaynes' principle of maximum entropy, the probability density function should have a maximum value of its information entropy S_1, defined by

$$S_I = -\int \ldots \int d\psi_{-N-N} \ldots d\psi_{NN} \times$$
$$P(\psi_{-N-N}, \ldots, \psi_{NN}) \log \frac{P(\psi_{-N-N}, \ldots, \psi_{NN})}{M(\psi_{-N-N}, \ldots, \psi_{NN})} .$$

The measure M, for which a product of constants is taken, incorporates any a-priori knowledge of the system such as its basic symmetries. All additional information on the system is used to constrain the maximization of S_I, like the normalization condition on P. The additional information consists of fixed averages of certain functions Q, with the average $\langle Q \rangle$ defined by

$$\langle Q \rangle = \int \ldots \int d\psi_{-N-N} \ldots d\psi_{NN} \times$$
$$P(\psi_{-N-N}, \ldots, \psi_{NN}) Q(\psi_{-N-N}, \ldots, \psi_{NN}).$$

Without these averages as constraints, the maximization of the information entropy S_I would result in $P = M$. Although the constant values that we take to define M turn out to influence the maximum value of the information entropy S_I, these values do not influence the probability density function P and thus do not influence the resulting statistics.

In the equilibrium statistical mechanical theory that emerged from Onsager's approach, the information entropy is maximized with fixed values of the average energy $\langle E \rangle$ and the average enstrophy $\langle Z \rangle$. This has been shown[5)] to work rather well if the statistics is controlled by conservation of energy and enstrophy, i.e., in the unforced-undamped case - which is not very realistic. If forcing and dissipation are present then, in line with Burgers' approach, it is more appropriate to maximize the information entropy with fixed (zero) values of $\langle F - D \rangle$ and $\langle G - H \rangle$. Fortunately, the mathematics is similar in both cases because all constraints are quadratic and lead to a probability density function that is a product of normal distributions. Once the probability density function is known, all relevant statistics can be calculated, such as spectra of energy and enstrophy and average vorticity fields.

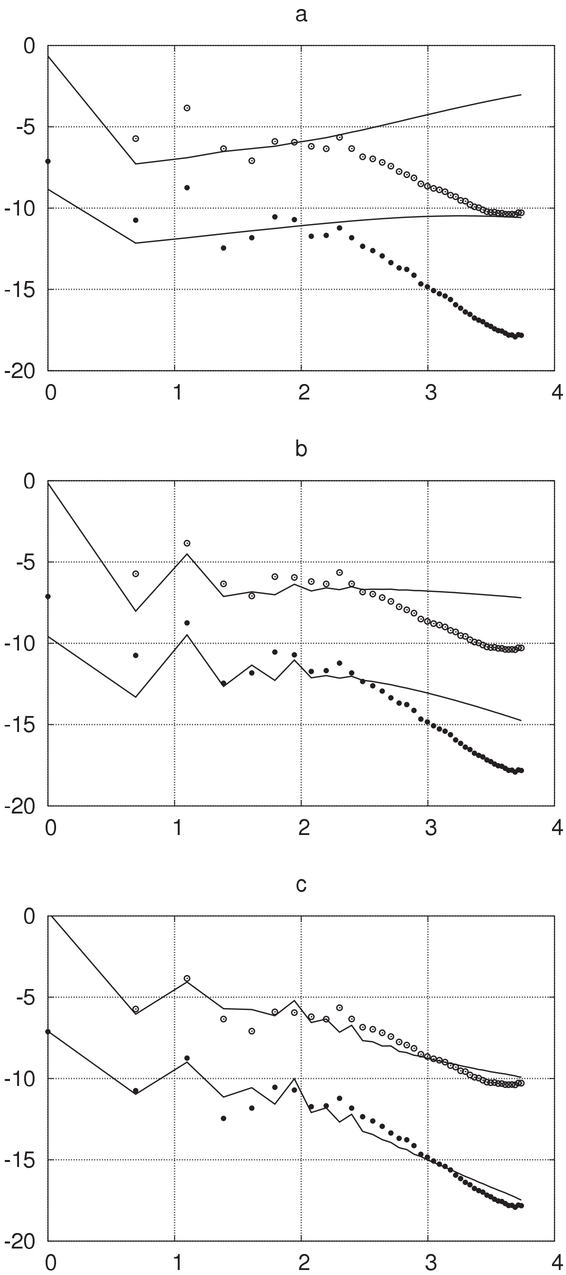

***Figure 2**. The values of log E_n (energy) and log Z_n (enstrophy) as a function of log n, averaged over the last 500 days of the numerical integration. The solid dots represent the spectra of energy, the open circles represent the spectra of enstrophy and the solid curves are the theoretical spectra, based on maximum entropy. In the upper panel (a) the constraints in the maximization of entropy are energy and enstrophy, in the middle panel (b) the constraints are the decay rates of energy and enstrophy (taken to be zero), and in the lower panel (c) both energy and enstrophy as well as their decay rates are used as constraints.*

Results

We will focus on the numerical integration of 2000 days of which two snapshots of vorticity have been shown in Figure 1. We use the last 500 days of the integration to calculate average spectra, vorticity and velocity fields in order to compare these with the theoretical results. To define the spectra of energy and enstrophy, we write the energy E and the entrophy Z as a sum over N functions E_n and Z_n, the latter containing the sums over m. The spectra of energy and enstrophy are thus E_n and Z_n as functions of n, where n runs from 1 to 42.

The solid dots and open circles in the three panels of Figure 2 are the numerically obtained values of log E_n and log Z_n, respectively, as a function of log n,

for $n = 1, \ldots, 42$. The solid curves in panel a are the spectra based on maximum entropy if the numerically obtained values of $\langle E \rangle$ and $\langle Z \rangle$ are used as constraints.
Whereas this has been shown to work quite well in the unforced-undamped case, in the forced-damped case that we consider here it does not work at all. The numerically obtained spectra are very different from the spectra that characterize the unforced-undamped case.

The solid lines in panel b of Figure 2 show the theoretical spectra if the entropy is maximized using as constraints that $\langle F - D \rangle$ and $\langle G - H \rangle$ are zero. This is the case that corresponds to Burgers' basic idea. In contrast to the case displayed in panel a of Figure 2, we do not need any information from the numerical run except for the fact that it has reached a state of statistical equilibrium. The resemblance between the theoretical and numerical spectra is nevertheless substantially better that in the case of panel a of Figure 2, in particular for the lower values of the wavenumber n.

In panel c of Figure 2 we show the theoretical spectra if the numerically obtained values of $\langle E \rangle$ and $\langle Z \rangle$ are used as constraints in addition to the constraints that $\langle F - D \rangle$ and $\langle G - H \rangle$ are zero. Whereas on their own the former constraints do not lead to proper spectra (as we have just seen), when combined with the constraints that $\langle F - D \rangle$ and $\langle G - H \rangle$ are zero, they lead to an improvement that is quite substantial. It shows that the values of $\langle E \rangle$ and $\langle Z \rangle$ contain useful extra information and that the theory is able to incorporate that extra information in a consistent way.
In panel a of Figure 3 we show the vorticity and zonally averaged zonal velocity obtained numerically, averaged over the last 500 days of the integration. In panel b the theoretical average is given, calculated on the basis of maximum entropy using the numerically obtained values of $\langle E \rangle$ and $\langle Z \rangle$ as constraints. In panel c the theoretical average is shown that results if zero values of $\langle F - D \rangle$ and $\langle G - H \rangle$ are used as constraints in the maximization of entropy. In panel d, finally, the result is shown if the numerically obtained values of $\langle E \rangle$ and $\langle Z \rangle$ are used as extra constraints in the maximization of entropy. The most striking difference is between panels b and c, the former showing no trace of the two jet-streams, the latter showing these jet-streams quite clearly. Panel d confirms that additional information in the form of given values of $\langle E \rangle$ and $\langle Z \rangle$ leads to theoretical results that are more in accord with the numerical simulations.

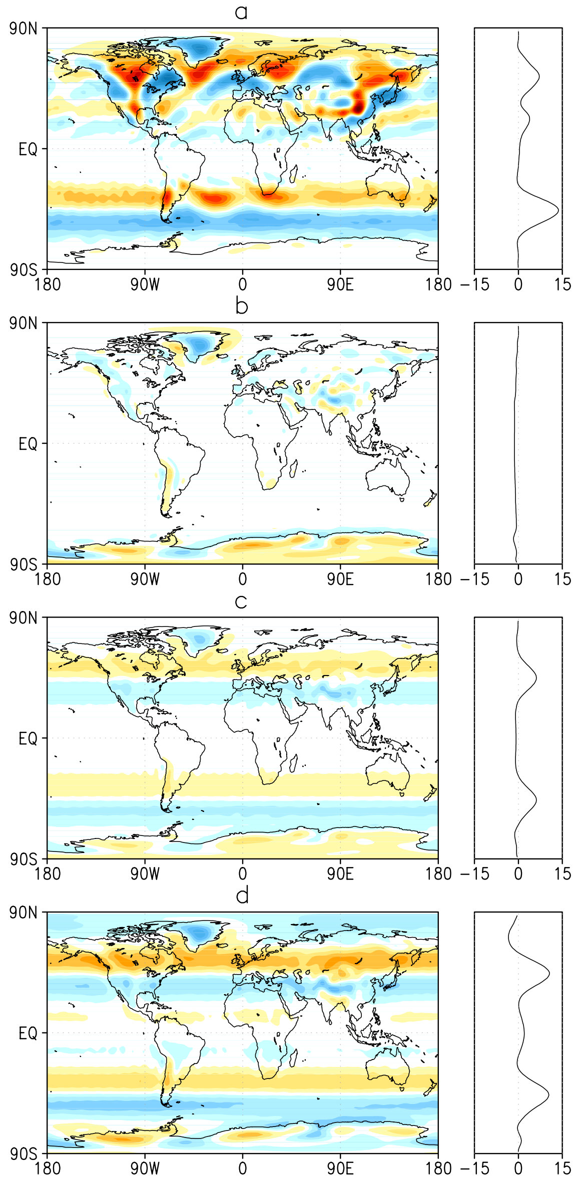

Figure 3. *Vorticity fields, expressed in units of the earth's angular velocity, displayed with a contour interval of 0.04, using the same colour scale as in Figure 1. Zonally averaged zonal velocity profiles in meters per second are displayed to the right of the vorticity fields. Panel a shows the results averaged over the last 500 days of the numerical integration. Panels b, c and d show the theoretical averages, based on maximization of entropy. The constraints in b are energy and enstrophy, in c the (zero) decay rates of energy and enstrophy and in d both energy and enstrophy and their zero decay rates. The vorticity fields in the consecutive panels vary between (-0.41, 0.46), (-0.21, 0.15), (-0.13, 0.09) and (-0.21, 0.17), respectively.*

Conclusion

We have shown that the formalism of statistical mechanics, expressed in the language of probability theory and the principle of maximum entropy, is able to produce statistics of forced-dissipative turbulent flows. The basic idea is that the statistics of a stationary turbulent system is controlled by the average balance between forcing and dissipation, an idea pursued earlier by Burgers. The theory was applied to a finitely truncated spectral model of large-scale atmospheric flow with the aim of deducing the climate of the model from its equations as an alternative to averaging over long numerical time-integrations.

The theory has shown its most predictive side if, in line with Burgers' idea, the average time derivative of energy and enstrophy are constrained to be zero in the maximization of entropy. In this case no information from the numerical run is needed except the fact that the system is in a statistically stationary state. The results compare favourably with the results obtained in the case that the energy and enstrophy, obtained from the numerical run, are used as constraints in the maximization of entropy. When all constraints are combined, the theoretical results compare best with their numerical counterparts. From the latter it may be concluded that, if the values of energy and enstrophy are available, the additional information that these values contain can be incorporated consistently by the principle of the maximum entropy.

A procedure that would avoid the use of average values of the energy and enstrophy, to be taken from the numerical run and therefore at the expense of the theory's predictive power, is to use as additional constraints the condition that the second- and higher-order time derivatives of energy and enstrophy are zero. This is justified in case the system is statistically stationary and, in view of the form of these constraints, is expected to lead to more structure in the resulting statistics such as correlations between the spectral coefficients. The price to be paid is a mathematically more complex analysis but, in view of the possibilities that it promises, would be worthwhile to pursue as a topic of further research.

References

1) Burgers, J.M., 1941. *Beschouwingen over de statistische theorie der turbulente stroming.* Nederlands Tijdschrift voor Natuurkunde, **8**, 5-18.
2) Nieuwstadt, F.T.M. and J.A. Steketee, Eds., 1995. *Selected Papers of J.M. Burgers.* Kluwer Academic, 650pp.
3) Onsager, L., 1949. *Statistical hydrodynamics.* Nuovo Cimento, **6**, 279-287.
4) Eyink, G.L. and K.R. Sreenivasan, 2006. *Onsager and the theory of hydrodynamic turbulence.* Rev. Mod. Phys., **78**, 87-135.
5) Verkley, W.T.M. and P. Lynch, 2009. *Energy and enstrophy spectra of geostrophic turbulent flows derived from a maximum entropy principle.* J. Atmos. Sci., **66**, 2216-2236. http://journals.ametsoc.org/doi/pdf/10.1175/2009JAS2889.1
6) Jaynes, E.T., 2003. *Probability Theory - The Logic of Science.* Cambridge University Press, 727pp.
7) Verkley, W.T.M., 2009. *A balanced approximation of the one-layer shallow-water equations on a sphere.* J. Atmos. Sci., **66**, 1735-1748. http://journals.ametsoc.org/doi/pdf/10.1175/2008JAS2837.1

Technological developments in scientific data exchange: recently developed portals, services and networks at KNMI

Wim Som de Cerff, Bert van den Oord, Alessandro Spinuso and Maarten Plieger

Introduction

During the last decade data is becoming both an increasingly important and a limiting factor in science[1,2]. Due to the continuously increasing demands for higher spatial and temporal resolution, data volumes from new generations of space instrumentation (e.g., Meteosat Third Generation and TROPOMI) and numerical models (e.g., Harmony and EC-Earth) grow faster than available storage, network and computing capacities. In order to provide scientists with tools to handle these data, new technologies for computationally intensive sciences (e-Science) are under development. The concept of distributed computing (clouds, Grid) and storage of datasets in (virtual) data centres requires that both the 'findability' and the data exchange mechanisms must be optimized and harmonized. The findability aspect is tackled by various initiatives to harmonize metadata while the exchange mechanism optimization and harmonization is tackled by defining requirements to promote the interoperability of web services. These developments are endorsed by both governmental (e.g. the WMO and the European Union through the INSPIRE framework) and non-governmental organizations (standardizing organisations like Open Grid Forum (OGF) for Grid computing and Open Geospatial Consortium (OGF) for geospatial services). These harmonization efforts will foster interdisciplinary research. For example, it will become possible to couple climate model results (almost) directly to climate effect models. With the increasing possibilities to access datasets (insight in) the quality of the data becomes increasingly important. Therefore, tools are being developed to annotate datasets with standardized metadata and other annotations.
Over the past years KNMI has been involved in both national and international consortia to help develop the above mentioned new technologies. This has resulted in various web services supporting the climate and seismology communities. Examples are the web services from the ADAGUC project; these provide access to various satellite data ranging from monthly averaged ozone to soil moisture maps. Also new data standards have been developed that will affect the way KNMI data are disseminated in the near future. This highlight describes some of these developments and provides an outlook to the future.

Metadata, annotations and formats

Metadata provide a description of data. When exchanging data, it is important that the data requestor is able to quickly find the data of interest. The best way of enabling searches on data is the provision of metadata and annotations. Providing these data to registers and search engines enables 'findability' of the data and, at the same time, enhances the usability and quality of a dataset.
For metadata various, more or less extensive, standards and models are used. Below we discuss two important metadata models.
ISO 19115[3] standard for metadata defines a set of attributes. Attributes can be mandatory, conditional or optional. Only a small set is mandatory and communities like WMO[4] can expand on the core set. ISO 19115 metadata will be the backbone for emerging data infrastructures, like the WMO Information System, INSPIRE, the EUROCONTROL Weather Information Exchange Model and the National Geo-Register. In the model data can be described on 'dataset' level, where a dataset is defined as 'an identifiable collection of data'. WMO and OGC have embraced the Observation and Measurement data model, which has now become the ISO 19156 standard.

Another important metadata standard is the Climate and Forecast convention (CF)[5], primarily used in Network

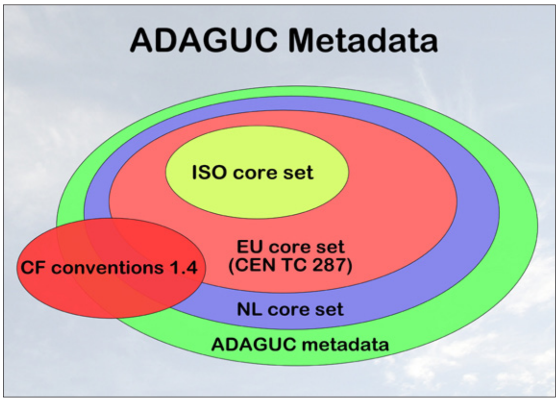

Figure 1. The ADAGUC Data format standard combines INSPIRE compliant ISO metadata and CF metadata in one netCDF4 file. ISO metadata is used to describe the dataset to which the file belongs. CF is used to describe the data contained in the file itself. The combination of both provides the data user with a well-documented, self-describing file.

Common Data Format files[6]. This community standard is widely accepted within climate modelling.
It is important to note that the above mentioned metadata standards are not in competition: all serve the same goal on a different level. Where ISO is more generic and covers descriptive metadata like points of contact, coverage and time information, CF covers domain-specific parameters within the provided dataset. Both metadata models are combined in the ADAGUC data format specification[7] (Figure 1). The ISO metadata is used for describing the dataset's metadata, the CF metadata fields are used to describe the content of the individual data product. The format specification is in use and under revision control by KNMI, the VU University Amsterdam and the SRON Netherlands Institute for Space Research.

Portals, services and networks at KNMI

KNMI has many successful data access facilities e.g. ECA&D, PROMOTE, Climate Explorer, KODAC, FTPPRO, CESAR, ADAGUC , NERIES, LVNL, and the KNMI website itself. Here we will focus on two recently developed portals: the NERIES (Network of Research Infrastructures for European Seismology) portal for seismological data and the ADAGUC (Atmospheric Data Access for the Geospatial User Community) portal for atmospheric data. Both are built using state-of–the-art services and provide and use metadata, but use different technology standards.
The NERIES portal brings together diverse distributed European seismological data to provide a single access facility from which researchers can search for and download selected data and data products (Figure 2). It also provides a framework through which new tools and processing can be included and accessed, including linkages to external processing resources and e-science infrastructures. The NERIES portal aggregates individual standardized portlets[8]. Portlets are specific targeted

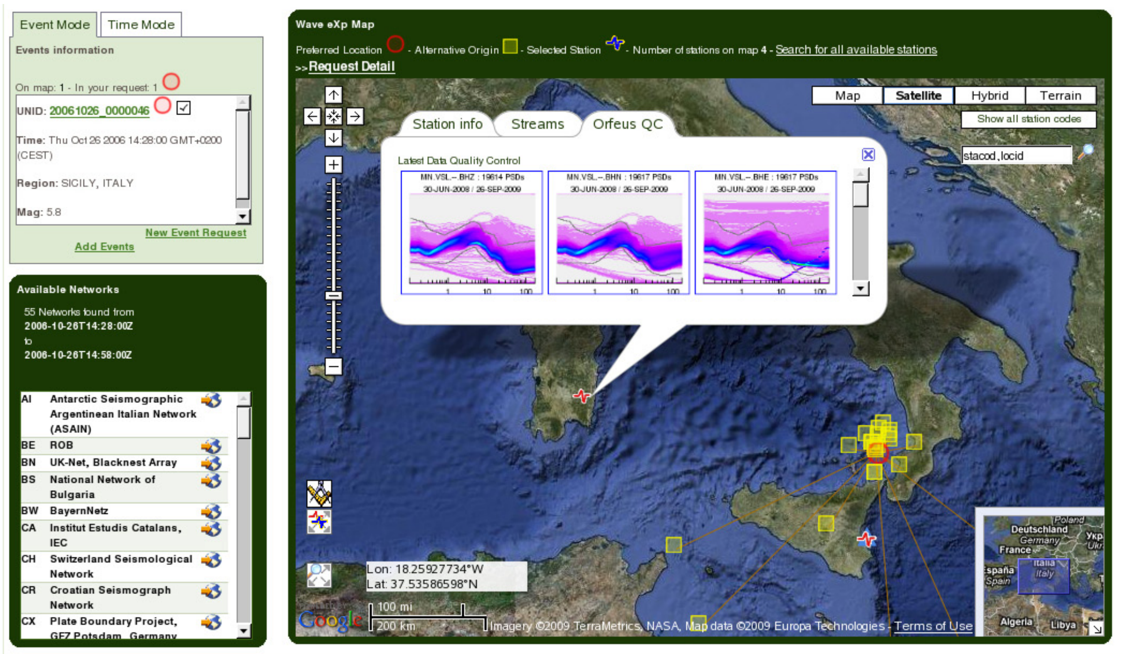

Figure 2. NERIES portal at KNMI, seismic waveform data access portlet. Screenshot of one of the portlets of the site, which allows the user to search and collect waveform data from all the European networks through an interactive map connected to the back-end web services.

web applications that conform to a standard application programming interface allowing them to be aggregated within a portlet container (runtime environment for portlets). The NERIES portlets are deployed both locally to the portal as well as remotely at participating data centres. These portlet applications access data archives through local and remote web services. These web services provide the integration points for access by other science infrastructures, such as GEMS and GEOSS.

The ADAGUC portal (Figure 3) brings together data from different OGC compliant services. The services accessible from the ADAGUC portal run both locally at KNMI and remotely at the VU. The OGC services used are Web Map Service for map display of the data and Web Coverage Service/Web Feature Standard interface for data downloading. All are accessible through the standard HTTP protocol. Others can integrate these web services into their application, which is done by e.g. the GIS software Company ESRI (Figure 4) and RIVM. The ADAGUC portal is based on ADAGUC formatted netCDF4 datasets. From these files, the services can provide the data in a large number of other formats using the Geospatial Data Abstraction Library for conversion. By implementing innovative new technologies valuable experience can be gained in terms of advantages and disadvantages of specific technologies. This experience will be used for e.g. building the next generation of the KNMI Data Centre and Satellite Data Centre.

Distributed Computing infrastructures

Distributed Computing infrastructures (DCI) are composed of services for sharing computer power and data storage capacity over the Internet, e.g. Grid services, Cloud services, High Performance Computing services. Although Earth Sciences (ES) have been active in the area

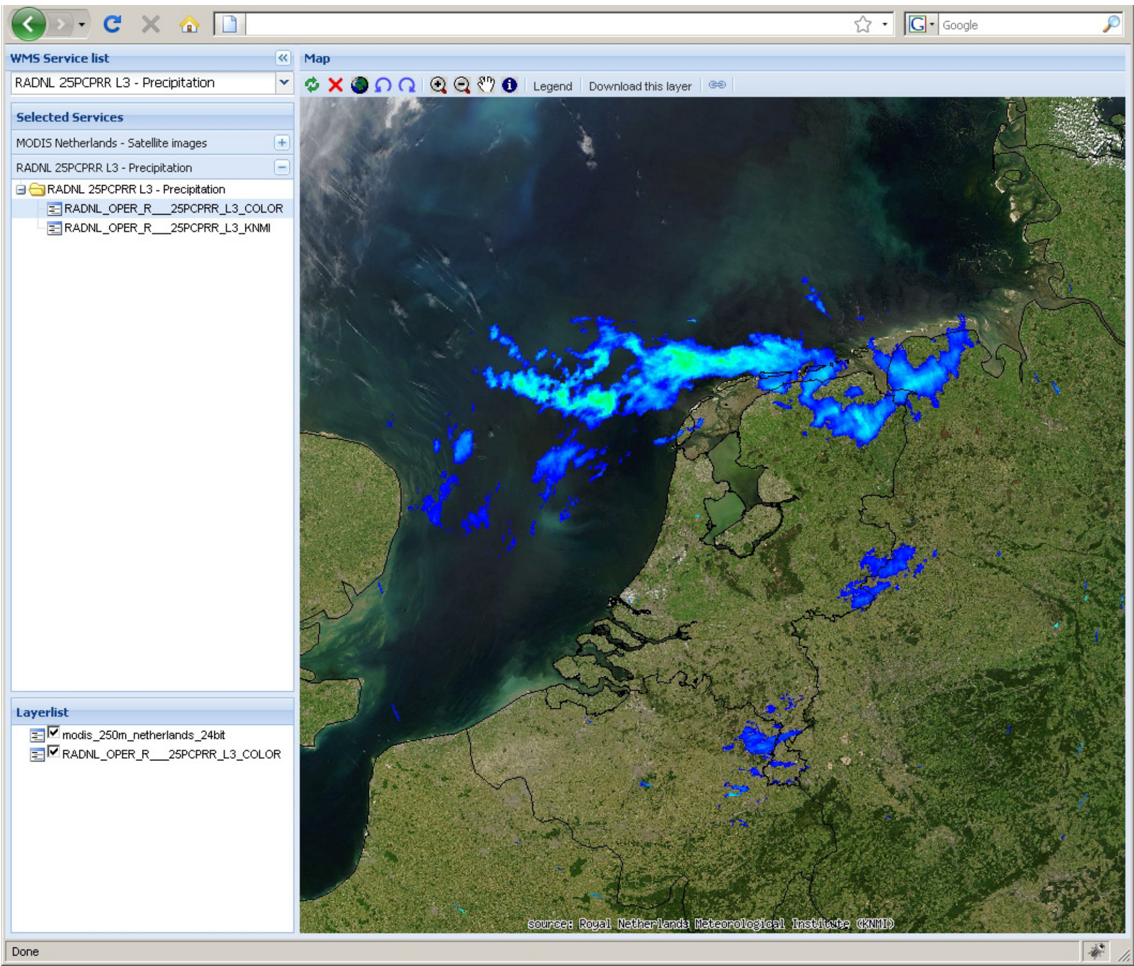

Figure 3. *The ADAGUC web portal in which real-time precipitation radar data from the KNMI radars is displayed. The portal communicates with different servers using the OGC Web Mapping service and is able to combine data from different sources. In this screenshot an image of precipitation is stacked on top of an image of the MODIS instrument. The precipitation image and the MODIS image are obtained from different services.*

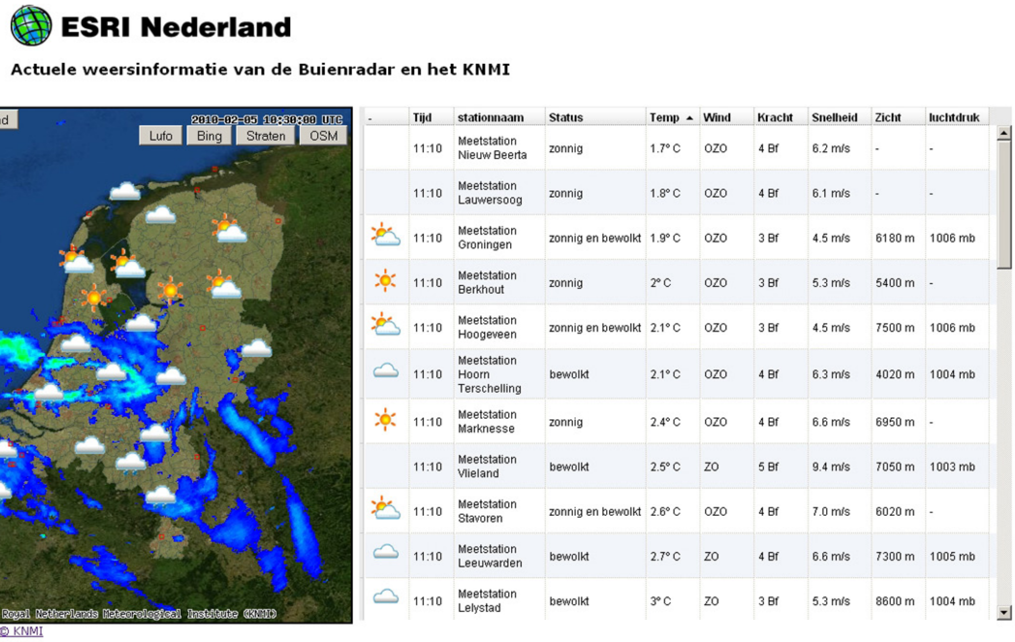

-	Tijd	stationnaam	Status	Temp ▲	Wind	Kracht	Snelheid	Zicht	luchtdruk
	11:10	Meetstation Nieuw Beerta	zonnig	1.7° C	OZO	4 Bf	6.2 m/s	-	-
	11:10	Meetstation Lauwersoog	zonnig	1.8° C	OZO	4 Bf	6.1 m/s	-	-
	11:10	Meetstation Groningen	zonnig en bewolkt	1.9° C	OZO	3 Bf	4.5 m/s	6180 m	1006 mb
	11:10	Meetstation Berkhout	zonnig	2° C	OZO	3 Bf	5.3 m/s	5400 m	-
	11:10	Meetstation Hoogeveen	zonnig en bewolkt	2.1° C	OZO	3 Bf	4.5 m/s	7500 m	1006 mb
	11:10	Meetstation Hoorn Terschelling	bewolkt	2.1° C	OZO	4 Bf	6.3 m/s	4020 m	1004 mb
	11:10	Meetstation Marknesse	zonnig	2.4° C	OZO	4 Bf	6.6 m/s	6950 m	-
	11:10	Meetstation Vlieland	bewolkt	2.5° C	ZO	5 Bf	9.4 m/s	7050 m	1003 mb
	11:10	Meetstation Stavoren	zonnig en bewolkt	2.6° C	OZO	4 Bf	7.0 m/s	6020 m	-
	11:10	Meetstation Leeuwarden	bewolkt	2.7° C	ZO	4 Bf	6.6 m/s	7300 m	1005 mb
	11:10	Meetstation Lelystad	bewolkt	3° C	ZO	3 Bf	5.3 m/s	8600 m	1004 mb

Figure 4. *ESRI portal using the KNMI radar web mapping service.*

of Grid computing since the year 2000 this has not resulted in a community-wide use of DCI platforms. The main reasons for this are the time investment for learning to use DCI platforms and the technical complexity of these platforms[9]. Moreover, in an independent development, ES communities have been engaged over recent decades in developing domain-specific data and processing infrastructures. These developments have two important drawbacks: the limited use of DCI platforms inhibits an optimal use of computing resources, while the domain-specific infrastructure development impedes interdisciplinary scientific collaboration (Figure 5a).
These issues were investigated in the FP6 project DEGREE, which proposed an ES-Grid roadmap[10,11] in order to improve Grid usage in the ES community. One of the major milestones in this roadmap is the establishment of an "Earth Science Grid platform", envisioning a collaborative environment where researchers can easily make use of the benefits of both DCI platforms and ES data. KNMI has participated in many DCI projects and experiments (DataGrid, DEGREE, SciaGrid). With this experience, KNMI has started the Earth Science Gateway (ES-G) initiative, aiming at developing a modular component framework for building ES community-specific science gateways (Figure 5b). This framework will have components for integrating ES-specific services (e.g., OGC), security, SLA and services for providing access to Grid functionality. These components will provide the crucial missing link that allows the ES community to use DCI platforms, while at the same time retaining access to existing community-based resources. Where possible, ES-G will reuse existing components. Close cooperation between all involved communities (technology providers like DCI and user communiti like Earth Science) is essential and is foreseen to be one of the main activities in this initiative. To open the development process for contributions of others, an open-source software development approach will be taken.
It is foreseen that this initiative can provide components for the ambitious National Model and Data Centre (NMDC), in which KNMI plays an important role.
The RapidSeis project (partners: NERIES, University of Liverpool and the National e-Science Centre in the UK) has proved the feasibility of the integration of computational applications within an existing data portal. RapidSeis has prototyped a scientific gateway via a web portal that allows seismologists to pick up data from Orfeus—the central repository for earthquake data in Europe hosted at KNMI —and then run several analyses on these data (on DCI infrastructures).
RapidSeis was funded by the UK Joint Information Systems Committee. JISC is an independent advisory body that works with further and higher education by providing strategic guidance, advice and opportunities to use ICT to support learning, teaching, research and administration.

Future role of data centres: curation of data

Data centres, like KNMI, are sources of information for scientists and have the important task of data preservation and curation for future research. In order to sup-

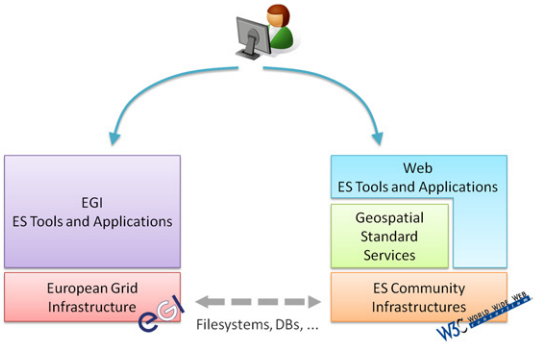

Figure 5a. *Without the Gateway.*
In the current situation, interoperability is only available on a very basic level, e.g. data resources in the ES domain are not directly accessible in the EGI domain so data needs to be copied manually to be able to use the ES data on EGI. Researchers need to have knowledge of both infrastructures.

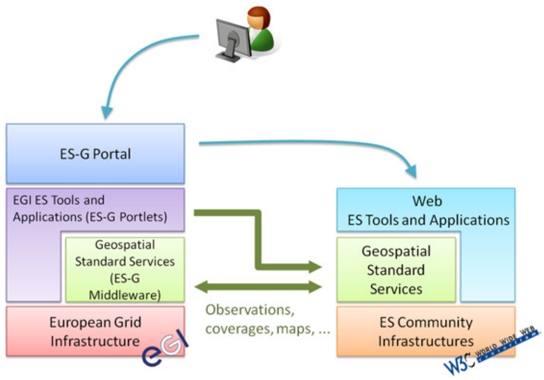

Figure 5b. *With the Earth Sciences (ES) Gateway.*
Interoperability is possible at the ES resources level. ES tools and applications built upon the ES-G middleware can access ES resources provided by ES Community Infrastructures. The portal provides a single point of access to ES tool and applications.

The increasing use of datasets in large (cross-domain) projects, and European Commission initiatives like INSPIRE, requires data centres to interconnect and harmonize their services

port researchers, data centres nowadays provide basic search, browse and download services for datasets. However, researchers often need more information and functionality than is generally provided. The increasing use of datasets in large (cross-domain) projects, and European Commission initiatives like INSPIRE, requires data centres to interconnect and harmonize their services. Such an approach is adopted in the NERIES and ADAGUC projects. This will make datasets easier accessible for scientific users but makes, at the same time, the amount of available data even more overwhelming. Therefore, the future data centres need to provide additional information in the form of annotations to assist scientists in selecting the optimal datasets for their work. By allowing the possibility to annotate datasets, the relation between scientists and data archives is developing from a one-way relation (download services) to a truly interactive relation in which scientists are offered functionality to upload information and contribute to the data archive. We aim at initiating developments towards the next generation of data archives in which an active relation exists between the archive and its users. This interactive aspect is one of the main requirements of the next generation KNMI Data Centre. The first steps involve the development of standards for data annotation and upload services and demonstrating the advantages of this new way of working to the end-users.

Conclusion

Data is one of the fundamentals for the science domains in which KNMI operates. KNMI data come from an increasing variety of sensors and models, and are used cross-domain, also in domains in which knowledge of the data is minimal. KNMI has a national role as a data centre, but is also a node in national and international data infrastructures. As a data centre, KNMI has also the responsibility for curation of its datasets. By following standards, KNMI can play this role, allowing cross-domain use of the datasets. Therefore, we actively participate and contribute to initiatives like INSPIRE, the WMO Inter-Programme Expert Team on Metadata and Date Interoperability and the Meteorology Domain Working Group of the Open Geospatial Consortium, to closely follow and influence emerging networks and standards which have a potentially high impact on the KNMI infrastructure. Research on web services, OGC standards and Grid technology enables us to play a role in these emerging international infrastructure developments but also enables us to construct the next generation KNMI Data Centre and to support increasing demands from KNMI's Climate and Seismology and Weather divisions regarding data accessibility.

References

1) The Fourth Paradigm: Data-Intensive Scientific Discovery, http://research.microsoft.com/en-us/collaboration/fourthparadigm/
2) EU ESFRI Roadmap, ftp://ftp.cordis.europa.eu/pub/esfri/docs/esfri-roadmap-report-26092006_en.pdf
3) ISO 19115 metadata standard, http://www.iso.org/iso/catalogue_detail.htm?csnumber=26020
4) WMO – IPET MDI, http://www.wmo.int/pages/prog/www/ISS/Meetings/IPET-DRC_Geneva2009/IPET-DRC_DocPlan.html
5) Gregory, J., 2003. *The CF metadata standard.* Centre for Global Atmospheric Modelling, University of Reading, UK, November 2003, http://cf-pcmdi.llnl.gov/documents/other/cf_overview_article.pdf
6) netCDF, http://www.unidata.ucar.edu/software/netcdf/
7) ADAGUC data format specification, http://adaguc.knmi.nl/contents/documents/ADAGUC_Standard.html
8) JSR-168-standard, http://developers.sun.com/portalserver/reference/techart/jsr168/
9) Som de Cerff, W.J., M. Petitdidier, A. Gemünd, L. Horstink and H. Schwichtenberg, 2009. *Earth science test suites to evaluate grid tools and middleware-examples for grid data access tools.* Earth Science Informatics, **2** (1-2), 117-131.
10) Earth Science Grid roadmap, http://www.eu-degree.eu/DEGREE/internal-section/wp6/DEGREE-D6.1.2_v2.8.pdf/view
11) Cossu, R., M. Petitdidier, J. Linford, V. Badoux, L. Fusco, B. Gotab, L. Hluchy, G. Lecca, F. Murgia, C. Plevier, P. Renard, H. Schwichtenberg, W. Som de Cerff, V. Tran and G. Vetois, 2010. *A roadmap for a dedicated Earth Science Grid platform.* ESIN Special Issue on Grid Computing, Journal Earth Science Informatics, 28 March 2010, doi: 10.1007/S12/45-010-0045-4

A monitoring and forecasting system for atmospheric composition: The GEMS project

Henk Eskes and Vincent Huijnen

Introduction

Present-day numerical weather forecasting is based on combining atmospheric models with observations from operational weather satellites and routine in-situ and surface measurements. By the 'assimilation' of measurements in weather models a detailed description of the present meteorological situation is obtained, which serves as starting point for successful weather forecasts. For the chemical composition and aerosols in the atmosphere such a comprehensive assimilation and forecast system did not exist until recently.

The GEMS consortium has built an unprecedented modelling and assimilation system to monitor and forecast the composition of the atmosphere

With the advance of satellite remote sensing of the Earth's atmospheric composition, unprecedented information is becoming available about how natural and anthropogenic emissions are influencing the greenhouse gases and aerosols, as well as near-surface air quality, which affects human health. Examples are the observation of desert dust plumes, of the Antarctic ozone hole and of nitrogen dioxide air pollution with satellite sensors like the Ozone Monitoring Instrument (OMI). The increasing availability of satellite as well as surface in-situ observations calls for global data assimilation systems, similar to numerical weather prediction, that are capable of combining the measurements of atmospheric composition and meteorology into a comprehensive global picture[1)].

The GEMS[2)] (Global and Regional Earth-System Monitoring Using Satellite and In situ Data project; 2005-2009; http://gems.ecmwf.int/) has built such a global assimilation/forecasting system for greenhouse gases, reactive gases and aerosols, as well as a regional air quality prediction system based on an ensemble of European air pollution forecasting models. GEMS was funded by the European Commission within the Global Monitoring for Environment and Security (GMES; http://www.gmes.info/) framework. GEMS is co-ordinated by ECMWF and the global assimilation and forecast system is based on the ECMWF weather model.

The KNMI Divisions Chemistry and Climate and Climate Observations have made several major contributions to GEMS:

1. The delivery of (near-real time) satellite data sets from OMI and the Scanning Imaging Absorption Spectrometer for Atmospheric Cartography (SCIAMACHY) which were used both in the assimilation and for validation. These data sets have been extensively used to produce near-real time analyses and reanalyses for the period 2003-2008.
2. The TM5 chemistry-transport model is contributed as one of the building blocks of the global atmospheric chemistry analyses.
3. OMI NO_2 data have been used for a near-real time evaluation of the European air quality forecasts.
4. The validation sub-project of GEMS was co-ordinated by KNMI.

Two example results for the second and third contribu-

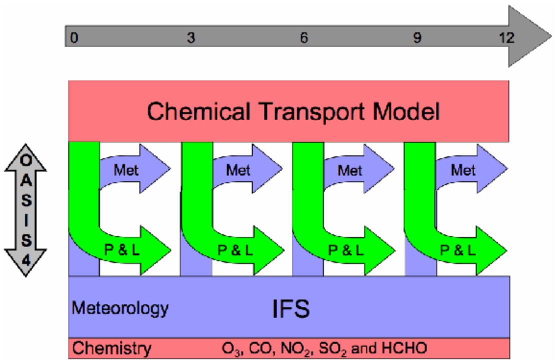

Figure 1. *Diagram showing the set-up for coupling TM5 and IFS. "Met" denotes the transfer of the meteorological fields from IFS to TM5. "P&L" denotes the transfer of the chemical production and loss terms from the CTM to IFS. Five chemical species are included and transported into the IFS assimilation system. The grey arrow de notes time.*

tion to the GEMS project are presented below, followed by a discussion of future developments and the relation with the EC-Earth model development.

Coupling the TM5 chemistry-transport model with the ECMWF Integrated Forecast System

In the reactive gases subproject three state-of-the-art atmospheric chemistry-transport models (CTMs) MOZART, MOCAGE and TM5 have been coupled to the ECMWF Integrated Forecast System (IFS)[3)]. The approach used in GEMS is shown in Figure 1. Five key chemical species have been included in the IFS model, namely ozone, carbon monoxide, nitrogen oxides, sulphur dioxide and formaldehyde. Satellite observations are available for these five gases, and have been included in the analysis. This extended IFS system is coupled to the CTMs by the coupling software OASIS version 4. This coupler passes hourly meteorological fields from IFS to the CTM. In turn, the CTM provides chemical tendencies for the five tracers to IFS. Furthermore, the assimilated spatial distribution of the five gases is passed back to the CTM to ensure consistency.

One result of the coupled IFS-CTM system is shown in Figure 2 for both IFS-MOZART and IFS-TM5 in runs with and without assimilation of ozone observed by the satellite instruments SBUV (Solar Backscatter Ultraviolet Experiment), OMI and MLS (Microwave Limb Sounder). The forecast with IFS-MOZART without assimilation predicted the start of the ozone hole at the right time. Its extent was, however, underestimated by about 40%. Stratospheric ozone in TM5 is constrained by a climatology. This climatological approach in IFS-TM5 did not capture the long duration of the 2008 ozone hole which lasted until mid-December. Hence both of these model simulations have deficiencies. In contrast to the free runs, the forecasts including the assimilation of satellite observations are very similar and also agreed very well with independent ozone observations. This means that, despite the differences in the underlying chemistry schemes of MOZART-3 and TM5, the observations were well able to constrain the GEMS modelling system and significantly improve the simulated ozone distribution during ozone-hole conditions.

Figure 3 shows a validation of the resulting ozone vertical

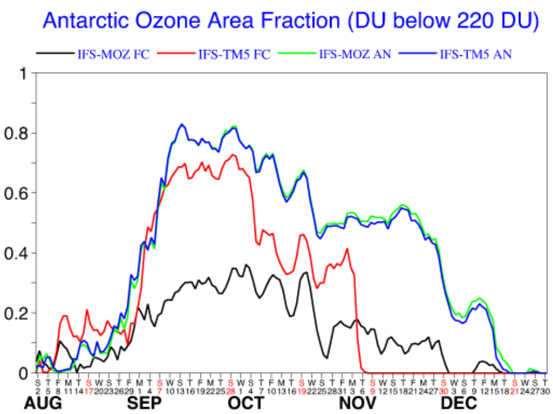

Figure 2. *Time series of the extent of the Antarctic ozone hole 2008, defined as the area fraction where the ozone column is < 220 Dobson Units (DU). Shown are the free run with the coupled system IFS-MOZART without assimilation (black), a free run with IFS-TM5 (red) and two runs with assimilation of SBUV, OMI and MLS ozone retrievals with the IFS-MOZART (green) and the IFS-TM5 (blue) set-up.*

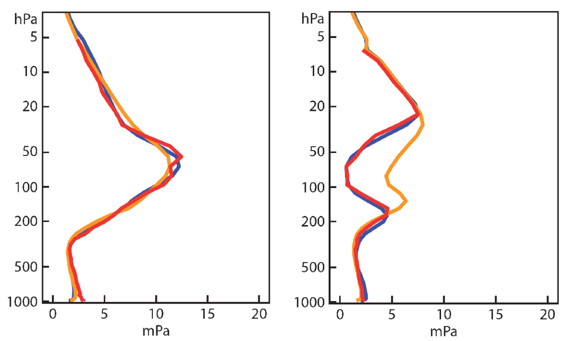

Figure 3. *Monthly averaged ozone profiles (partial pressure in mPa) forecast by IFS-TM5 with assimilation (blue), without assimilation (orange) and ozone sonde in-situ observations (red) from Neumayer Station in Antarctica for August and October 2008. The depletion of ozone inside the ozone hole is clearly visible in October. This ozone loss is not well described by the free running model, but the assimilation of multiple satellite ozone sensors with this GEMS system leads to an accurate description.*

The development of the coupled TM5-IFS system for GEMS has been instrumental for the EC-Earth climate model

profile in the TM5 forecasts with and without the analysis of satellite observations. It shows that the modelled profile resulting from the assimilation is well in line with independent ozone sonde observations. This can be attributed to the multi-sensor approach, where the microwave limb sounder (MLS) has been essential to get a good profile shape and the UV-visible sounders added important information on the total column amount of ozone. This example demonstrates the benefits of applying advanced assimilation techniques, developed in the weather community, to atmospheric chemistry.

Comparing OMI NO2 measurements with the GEMS regional and global atmospheric chemistry models

An evaluation of the model-simulated NO_2 spatial distributions was carried out using OMI observations[4)]. Figure 4 shows the comparison between OMI NO_2 measurements, three European-scale air quality models (EURAD, CHIMERE, SILAM), and two global atmospheric

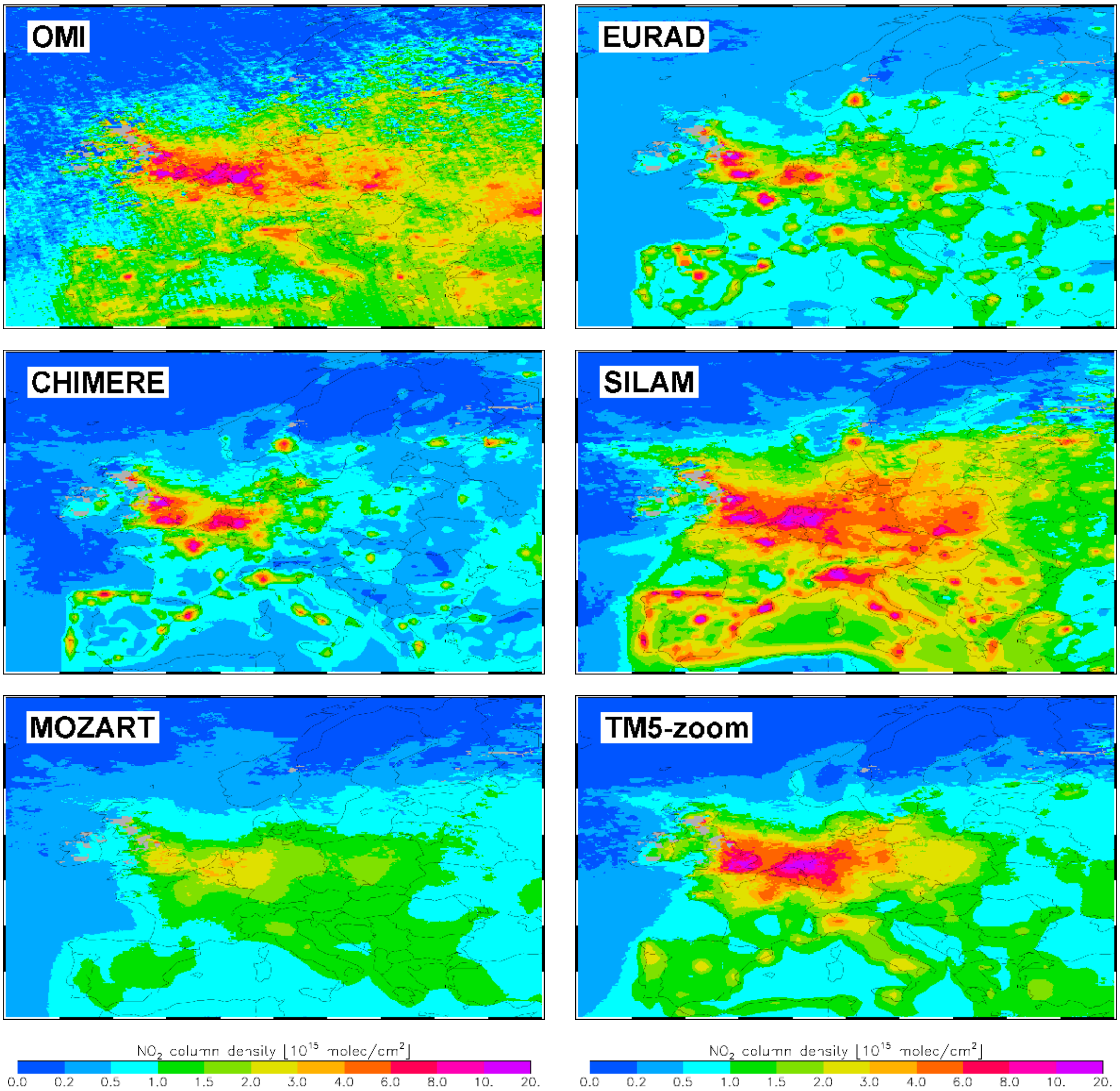

Figure 4. *Mean tropospheric NO_2 columns in August 2008 measured with the OMI satellite instrument, compared with simulations from three selected regional air quality models (EURAD, CHIMERE, SILAM), from the global MOZART model, and from the global TM5 model with a 1 degree resolution spatial zoom over Europe.*

chemistry models (TM5 and MOZART). The results show the importance of the high model resolution of the regional models (20-40 km) as compared to the global models (100-300 km) to resolve the spatial variability of air pollution concentrations. The differences between the air quality forecast results give an indication of the degree of uncertainty associated with these models. The study has helped to identify and repair shortcomings of some individual models (for instance errors in the implementation and application of emissions) as well as to quantify uncertainties in the OMI retrieval (such as an overestimate of NO_2 in summer)[4)]. Hence such an evaluation benefits both the models and the observations.

GEMS and EC-Earth

The development of the coupled TM5-IFS system for GEMS has also been useful for the parallel development of the EC-Earth climate model which is led by KNMI. In EC-Earth, TM5 is used for simulating greenhouse gases (currently ozone and methane) and various types of aerosols for simulations of climate change. The coupled systems set up for GEMS and EC-Earth necessarily differ in several respects: the version of the coupling software (OASIS4 versus OASIS3), the feedback of chemical fields (chemical tendencies in one case versus concentrations and radiative properties in the other), and the assimilation and transport of TM5 tracers in IFS which is absent in EC-Earth. However, apart from these differences, the use of online meteorological fields for driving TM5 could be done similarly in both systems. In GEMS the TM5 model has been extensively validated and model improvements have been implemented. The EC-Earth project directly benefits from these activities. The EC-Earth and GEMS activities thus resulted in a high degree of synergy.

Outlook

The European 7th framework project "Monitoring Atmospheric Composition and Climate" (MACC), co-ordinated by the ECMWF, has started at 1 June 2009 and is a direct continuation of the GEMS activity. MACC will expand the GEMS work in several respects. For instance, GEMS has focussed on building the global atmospheric composition assimilation-forecast system, while in MACC there will be more focus on the development of products for specific user communities such as environmental agencies, policy makers and the general public.
The KNMI involvement in GEMS will be continued in MACC. Two important new contributions are planned:

- Together with TNO we will contribute to the European regional air quality model ensemble forecasts with the Netherlands national air quality model LOTOS-EUROS. Because MACC includes the leading European air quality models, and by applying an ensemble approach, MACC will produce the hitherto most advanced analysis of air pollution on the European scale.
- Within MACC chemistry modules will be implemented directly in IFS for which we will supply and implement the TM5 model code. This is expected to lead to significant model performance improvements, and will ultimately replace the present version of the GEMS coupled system (Figure 1).

It is intended that MACC will evolve into the operational GMES atmosphere (core) service in the timeframe 2012-2014. The planned future TROPOMI satellite mission, for which KNMI has the scientific lead, will deliver the kind of observations that are crucial input for this GMES atmosphere service.

Conclusion

The GEMS consortium, led by ECMWF, has built an unprecedented modelling and assimilation system to analyse, monitor and forecast global atmospheric composition, in particular greenhouse gases, reactive gases and aerosols. This is achieved by applying advanced meteorological assimilation techniques to the field of atmospheric chemistry. The global GEMS system is coupled to an ensemble of forecasts from about 10 European regional air quality models, providing a detailed picture of air quality over Europe. In the GEMS system both the meteorology and the composition (gases, aerosols) are treated in a consistent way. The reanalyses provided by GEMS are a valuable source of information for air quality and climate monitoring. GEMS is the start of a long-term commitment, part of the European GMES programme, to provide up-to-date and accurate information on the atmospheric composition to environmental agencies, policy makers, scientists and the public.

KNMI has contributed substantially to the GEMS development, with the TM5 model, satellite observational data sets, contributions to the regional air quality subproject, and co-ordination activities. A major new activity in MACC will be the inclusion of the Dutch LOTOS-EUROS model in the ensemble of air quality models, in collaboration with TNO and RIVM.

References

1) IGACO, 2004. *An Integrated Global Atmospheric Chemistry Observation theme for the IGOS partnership.* GAW Report 159, 54pp. Available online at www.wmo.int/pages/prog/arep/gaw/documents/gaw159.pdf.
2) Hollingsworth, A., R.J. Engelen, C. Textor, A. Benedetti, O. Boucher, F. Chevallier, A. Dethof, H. Elbern, H. Eskes, J. Flemming, C. Granier, J.W. Kaiser, J.J. Morcrette, P. Rayner, V.H. Peuch, L. Rouil, M.G. Schultz, A.J. Simmons and the GEMS consortium, 2008. *Toward a Monitoring and Forecasting System for Atmospheric Composition: The GEMS Project.* Bull. Amer. Meteor. Soc., **89**, 1147-1164. Available online at http://ams.allenpress.com/archive/1520-0477/89/8/pdf/i1520-0477-89-8-1147.pdf.
3) Flemming, J., A. Inness, H. Flentje, V. Huijnen, P. Moinat, M.G. Schultz and O. Stein, 2009. *Coupling global chemistry transport models to ECMWF's integrated forecast system.* Geosci. Model Dev., **2**, 253-265.
4) Huijnen, V., H.J. Eskes, B. Amstrup, R. Bergstrom, K.F. Boersma, H. Elbern, J. Flemming, G. Foret, E. Friese, A. Gross, M. D'Isidoro, I. Kioutsioukis, A. Maurizi, D. Melas, V.-H. Peuch, A. Poupkou, L. Robertson, M. Sofiev, O. Stein, A. Strunk, A. Valdebenito, C. Zerefos and D. Zyryanov, 2009. *Comparison of OMI NO_2 tropospheric columns with an ensemble of global and European regional air quality models.* Atmos. Chem. Phys. Discuss., **9**, 22271-22330. Available online at http://www.atmos-chem-phys-discuss.net/9/22271/2009/acpd-9-22271-2009.pdf.

Air quality monitoring and forecasting in China

Bas Mijling and Ronald van der A

Introduction

For the last decade the industrial activity of China has been growing at rapid pace, bringing economic wealth to its 1300 million inhabitants, but also generating an unprecedented level of air pollution. This deteriorates the air quality of the densely populated and industrialized areas such as Beijing, Shanghai and the Pearl River Delta, and increases the background pollution levels world-wide[1]. The EU AMFIC project, led by KNMI, kicked off in September 2007 and aims at monitoring and forecasting the air quality in China by using satellite observations and model simulations, together with ground observations from collaborating Chinese institutes. The combination of these instruments and tools offers a unique possibility to investigate trends in air pollution and the effectiveness of air quality policy.

The EU AMFIC project, aims at monitoring and forecasting the air quality in China by using satellite observations and model simulations, together with ground observations from collaborating Chinese institutes

The following sections describe the use of satellite instruments to monitor air quality, the implementation of an operational air quality model for China, and the use of both satellite observations and model simulations to estimate the effect of the air quality measures during the 2008 Beijing Olympic Games.

Observing air quality from space

Ground measurements of air quality in China are often sparse and inaccessible, which make satellite observations the obvious tool to monitor country-wide pollution levels on a daily basis and to observe concentration trends on longer time scales. The Ozone Monitoring Instrument (OMI) is a nadir looking solar backscatter spectrometer, which measures in the ultraviolet and visible wavelength range to infer trace gases, such as ozone and nitrogen dioxide (NO_2). Since it was launched in 2004 onboard NASA's EOS-Aura satellite it observes the Earth's atmosphere at a spatial resolution of about 20 km. In October 2006 a comparable instrument, GOME-2, was launched onboard the MetOp-A satellite. GOME-2 measures at a wider spectral range, but at a lower spatial resolution of about 40 km. Both instruments have near-daily global coverage.

Trace gas columns are retrieved from the depth of typical absorption structures in the atmospheric reflectance spectrum. Radiative transfer calculations are used to relate the measured absorption to a vertical column concentration, taking into account the viewing angle and atmospheric conditions, such as clouds, surface reflectance and the vertical profile of the trace gas. For nitrogen dioxide, the main interest for air quality monitoring is its amount in the troposphere. To separate the tropospheric column from the total column a data assimilation scheme is applied that provides the stratospheric column. Subtraction from the total column provides the tropospheric column.

The satellite instruments have a fixed overpass time: GOME-2 measures in the morning (9:30 local time) and OMI measures in the afternoon (at 13:30). This allows us to probe the diurnal cycle of nitrogen dioxide (Figure 1).

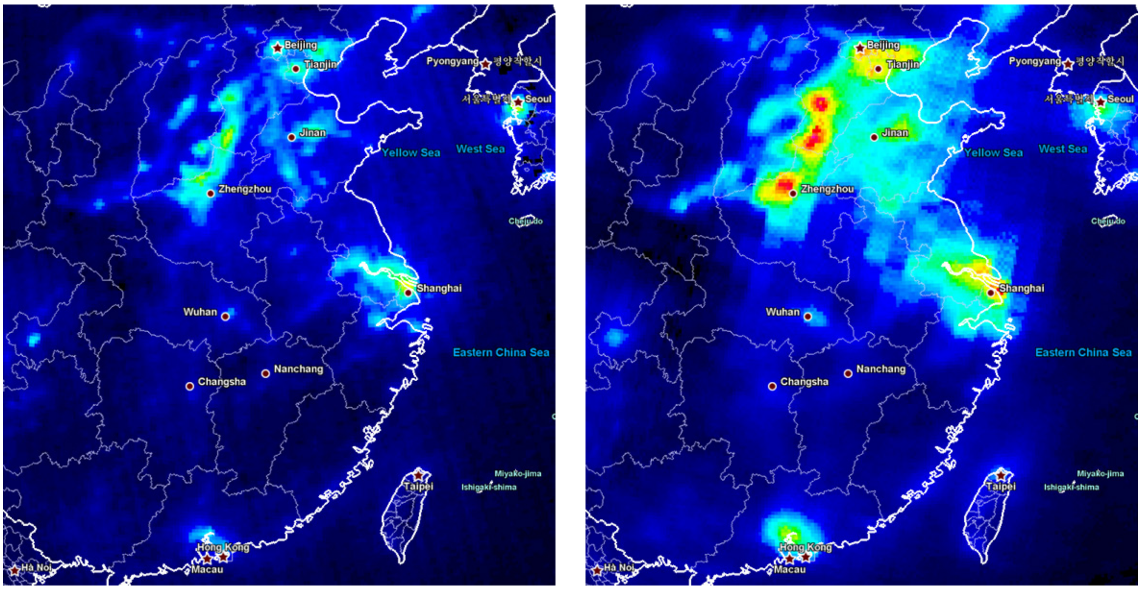

Figure 1. *Observations of the average tropospheric NO_2 over East China in May-June 2009 by OMI (left) and GOME-2 (right). Hotspots of human activity are clearly visible. Note the higher spatial resolution of the OMI instrument. Due to the diurnal cycle of NO_2, GOME-2 (local overpass time 9:30) observes a stronger signal than OMI (overpass time 13:30).*

Besides the diurnal cycle also weekly and seasonal cycles are monitored. This variability in the amount of nitrogen dioxide is due to chemical conversions depending on sunlight (photo-dissociation) and to time-dependent emissions of nitrogen dioxide and related species.

Nitrogen dioxide has significant natural sources (e.g. soil emissions, wildfires and lightning), but in populated areas NO_2 sources are predominantly anthropogenic (e.g. fuel combustion and human-induced biomass burning). By monitoring the concentration of nitrogen dioxide over several years, information on the trend of the emission sources can be determined. For the period 1996-2006, a time series has been constructed by combining the observations of GOME (launched in 1995)

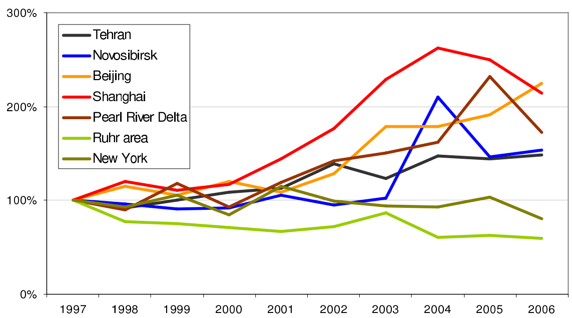

Figure 2. *Trends of tropospheric NO_2 columns for different urban areas, taken from 10 years of SCIAMACHY data. 1997 is taken as the reference year.*

with SCIAMACHY (launched in 2002; almost same overpass time) of the daily global nitrogen dioxide concentrations2). The monthly NO_2 columns for these ten years have been fitted with a linear function superposed on an annual seasonal cycle on a grid with a spatial resolution of 1x1 degree. Western-Europe and the East coast of the US show slightly negative trends due to emission regulations (Figure 2), but positive trends are found for Asian cities with a strong economical growth like Teheran (Iran), Novosibirsk (Russia) and especially for the booming cities in the East of China.

Modelling air quality in China

For a better interpretation of satellite measured air pollution and for the conversion of measured column data to emission rates, an appropriate model is required which is able to simulate pollutant concentrations. CHIMERE is a regional chemistry transport model which is successfully used in Europe for air quality forecasts on urban to continental scales. For the AMFIC project (Air quality Monitoring and Forecasting in China) we implemented CHIMERE on a 0.25x0.25 degree resolution over East China, enclosing all important populated and industrialized areas. The model simulates the evolution of 44 gaseous species and aerosols in 8 atmospheric layers in the troposphere up to 500 hPa. The meteorological data needed for calculating the transport, deposition and the chemistry of the species is taken from the European Centre for Medium-Range Weather Forecasts (ECMWF).

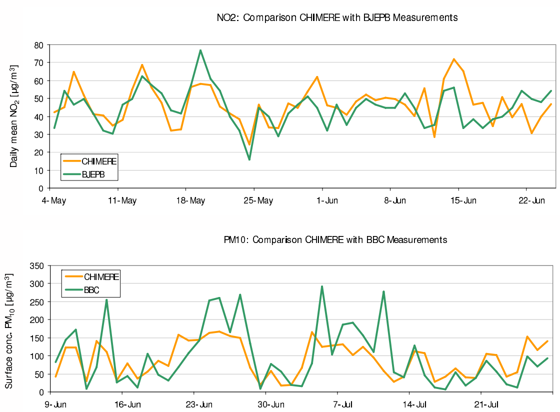

Figure 3. *(Above) Comparison of the daily-averaged surface concentrations of NO_2 from CHIMERE over Beijing with the measured concentrations published by BJEPB for the period 4 May to 30 June 2008. (Below) Comparison of the surface concentrations of PM10 from CHIMERE at 13:00 local time with measurements done by the BBC before and during the Olympic Games. Measurements were done with a handheld DustTrak instrument at midday in the city centre.*

The sparse available ground measurements from China makes model validation complicated, but not impossible[3)]. Figure 3 shows comparisons of CHIMERE simulations with daily averaged measured surface concentrations of NO_2 published by the Beijing Environmental Protection Bureau (BJEPB), and PM10 (particulate matter of 10 microns or less in diameter) surface concentrations measured by the British Broadcasting Company (BBC) at 13:00 local time. Both comparisons illustrate the capability of CHIMERE of capturing the day-to-day variability of pollutant concentrations.

By using meteorological forecast data, the model is able to generate daily air quality forecasts up to five days ahead. The result for East China and for the greater urban areas of Beijing, Shanghai, Hong Kong, Shenyang, Qingdao and Seoul are published on an English-Chinese bilingual website (see Figure 4). The daily model output is also used as boundary condition for a higher resolution model of Beijing and Shenyang by the Flemish Institute for Technical Research (VITO) and the street level model of Beijing by Cambridge Environmental Research Consultants (CERC). On request of the Dutch National Olympic Committee, during the 2008 Beijing Olympic Games a dedicated website was made available by KNMI to inform the athletes on the forecasted air quality and meteorology at all Olympic venues.

Nitrogen dioxide reduction during the 2008 Beijing Olympic Games

Heavy air pollution in Beijing, mainly originating from dense traffic, construction activities, industry, and coal-fired power plants, is a major concern for local authorities. To prevent high levels of air pollution during the Beijing Olympic Games (8-24 August 2008) and the

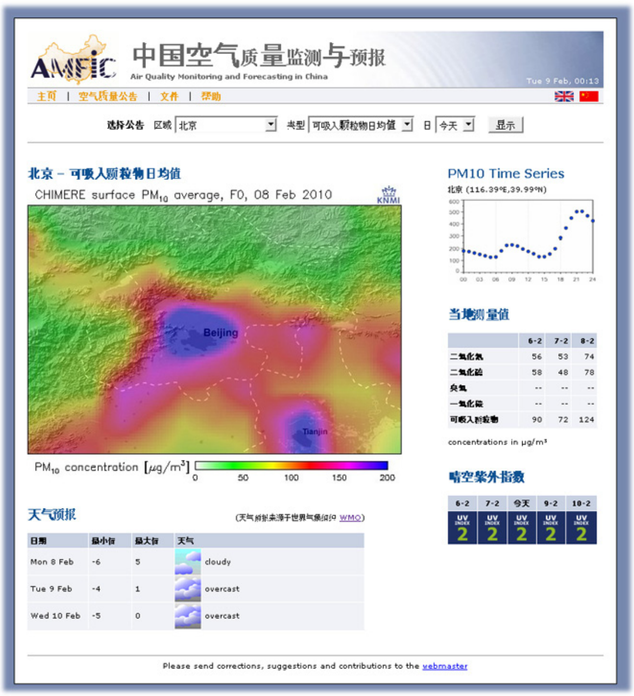

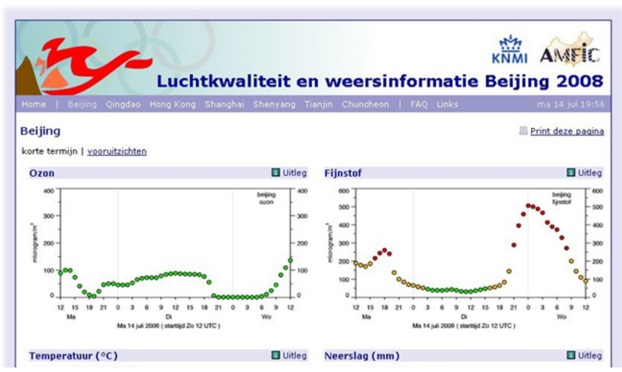

Figure 4. *Presentation of operational air quality forecasts on the internet. Left the AMFIC air quality bulletin (http://www.amfic.eu/bulletin), showing maps of forecasted concentrations of ozone, PM10, and NO_2 for urban areas in China. Right the website showing time series of ozone and particulate matter for the Olympic venues as it was active during the Olympic Games of 2008.*

Figure 5. *Morning traffic flow on the East 4th Ring Road in Beijing during the restrictions on Friday 19 September (left), and after the restrictions on Monday 22 September (right) (source: China Daily).*

Paralympics (6-17 September 2008), important measures inside and outside the city have been taken, including the temporarily shut down of polluting industry, the suspension of construction activities, and traffic restrictions. Traffic within the ring roads was restricted to cars with even number plates on even days and with odd numbers on odd days, 300.000 high-emission vehicles were banned from the city's roads, and the use of governmental and commercial vehicles was restricted (see Figure 5).

During the Beijing Olympic Games, the GOME-2 and OMI columns show a reduction of 59%–69% with respect to pre-Olympic values

To study the effect of the air quality measures on tropospheric nitrogen dioxide concentrations, we compare the NO_2 observations over the Beijing area by OMI and GOME-2 before and during the Olympic Games. We take advantage of the high spatial resolution and daily global coverage of OMI, and the stronger anthropogenic nitrogen dioxide signal (due to its earlier overpass in the day) of GOME-2[4]. As can be seen in Figure 6, the nitrogen dioxide concentration over Beijing during the Olympic Games is significantly less than before. This, however, can partly be explained by favourable meteorological conditions during this period: predominant northerly winds bring in clean air masses from the sparsely populated mountain areas, and more precipitation on more rainy days washes out the air pollution over the city. By comparing the satellite observations with CHIMERE simulations based on pre-Olympic nitrogen dioxide emission estimates, we compensate for these atypical meteorological conditions[5]. Differences between observation and simulation can only be explained by changes in anthropogenic emissions.

The model results are interpolated to the time and the footprint of the satellite observation. For the pre-Olympic reference period (2 May to 30 June 2008) we see good agreement between simulations and observations for the Beijing area. When the air quality measures are enforced, the observations drop with respect to the simulations, which are based on an unchanged emission scenario. During the Beijing Olympic Games, the GOME-2 and OMI columns show a reduction of 59%–69% with respect to pre-Olympic values. Figure 6 shows the geographic extent of the concentration reductions as observed by GOME-2. In the pre-Olympic period both satellite and model show high concentrations in the populated and industrialized areas. During the Olympic period, the satellite observes decreased nitrogen dioxide concentrations for Beijing, whereas the other cities continue to show high concentrations. Highest concentration reductions are found in and around Beijing and the industrial areas in the south and south-east (60%–70%). The surrounding cities of Tianjin and Shijiazhuang show smaller reductions of about 30% and 20%, respectively. In the two months after the Olympic Games the nitrogen dioxide concentrations are still reduced with 40%, mainly due to the prolonged air quality measures and the reduced economic activity. One year afterwards, however, nitrogen dioxide levels have returned to their high pre-Olympic values.

Conclusion

Satellite observation of tropospheric columns of nitrogen dioxide are extremely useful to analyze air pollution levels world-wide. The long-term data record

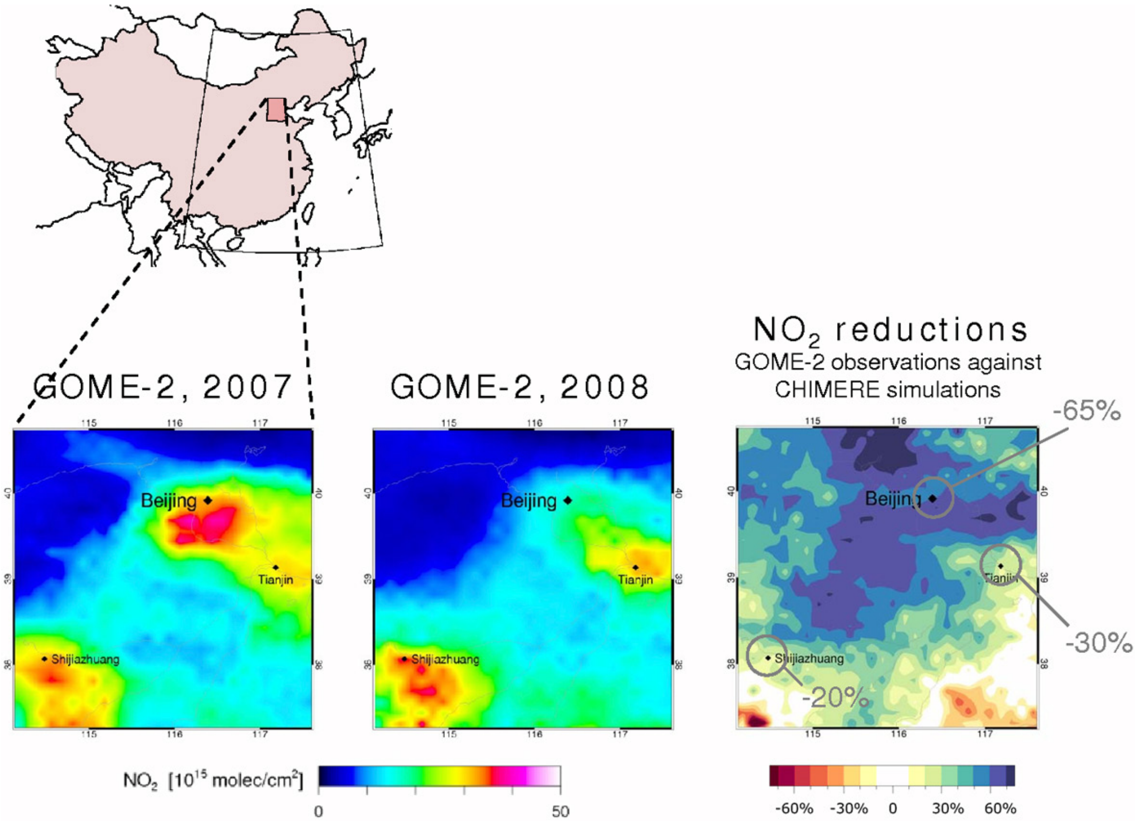

Figure 6. *Observations of the tropospheric NO2 columns by GOME-2 over the Beijing area during the Olympic period (middle panel) and the corresponding period one year before (left panel). The right panel shows the associated concentration reduction, when compared with the model results: the air quality measures were especially effective in the area around Beijing; the cities of Tianjin and Shijiazhuang showed smaller reductions in air pollution.*

from 1995 onwards shows strongly increasing pollution levels in China and slowly decreasing levels in Western Europe and Eastern USA. Observed trends can be attributed to economic growth and emission reduction measures.

On a shorter time scale, the effect of emission reductions during the Beijing Olympic Games of 2008 has been studied. By comparing satellite observations with air quality model results, we find a reduction of approximately 65% above Beijing during the Olympic period, showing the (temporary) success of the Chinese air pollution control efforts.

Future research will concentrate on improved methods to couple tropospheric pollutant concentrations observed by satellites to their underlying emission sources[6)]. The trend and variability of emissions inferred from long-term satellite observations will give a better understanding of the effectiveness of air quality policies.

References

1) Zhang, L., D.J. Jacob, K.F. Boersma, D.A. Jaffe, J.R. Olson, K.W. Bowman, J.R. Worden, A.M. Thompson, M.A. Avery, R.C. Cohen, J.E. Dibb, F.M. Flocke, H.E. Fuelberg, L.G. Huey, W.W. McMillan, H.B. Singh and A. J. Weinheimer, 2008. *Transpacific transport of ozone pollution and the effect of recent Asian emission increases on air quality in North America: an integrated analysis using satellite, aircraft, ozonesonde, and surface observations.* Atm. Chem. Phys., **8**, 6117-6136.
2) A, R.J. van der, H.J. Eskes, K.F. Boersma, T.P.C. van Noije, M. Van Roozendael, I. De Smedt, D.H.M.U. Peters, J.J.P. Kuenen and E.W. Meijer, 2008. *Identification of NO2 sources and their trends from space using seasonal variability analyses.* J. Geophys. Res., **113**, doi:10.1029/2007JD009021
3) Lampe, A., 2009. *Evaluation of the diurnal cycle of trace gases over Beijing as modelled by* CHIMERE. KNMI report / Master Thesis, University of Twente, 61pp.
4) Boersma, K.F., D.J. Jacob, H.J. Eskes, R.W. Pinder, J. Wang and R. J. van der A, 2008. *Intercomparison of SCIAMACHY and OMI tropospheric NO_2 columns: observing the diurnal evolution of chemistry and emissions from space.* J. Geophys. Res., **113**, D16S26, doi:10.1029/2007JD008816
5) Mijling, B., R.J. van der A, K.F. Boersma, M. Van Roozendael, I. De Smedt and H.M. Kelder, 2009. *Reductions of NO2 detected from space during the 2008 Beijing Olympic Games.* Geophys. Res. Lett., **36**, doi:10.1029/2009GL038943
6) Stavrakou, T., J.-F. Müller, K.F. Boersma, I. De Smedt and R.J. van der A, 2008. *Assessing the distribution and growth rates of NO_x emission sources by inverting a 10-year record of NO_2 satellite columns*. Geophys. Res. Lett., **35**, L10801, doi:10.1029/2008GL033521

Prediction and occurrence of aircraft lightning encounters around Amsterdam Airport Schiphol

Jan Hemink,
William R. Gough and Thomas H. Fahey (formerly of Northwest Airlines, now Delta Air Lines)

Introduction

Lightning strikes (Figure 1) cost airlines significant amounts of money each year through repair expenses, flight delays, and other additional costs due to the removal of aircraft from service[1]).

In this highlight a study[1)] on lightning encounters around Amsterdam Airport Schiphol is summarized. At Northwest Airlines (NWA) a study[2)] was done in 2006 with historic data from NWA aircraft lightning encounters in the USA from 1997 through early 2006. The focus of the study was to look at cold season aircraft lightning encounters in relation to the characteristics of the surrounding atmosphere. One result was the discovery that 40% of all lightning encounters occurred during the months of October through April, which is not the period of the most frequent thunderstorm activity, which is the ‘warm season’.

Next, the weather conditions surrounding aircraft lightning encounters around Amsterdam Airport Schiphol were examined for the ‘cold season’ months.

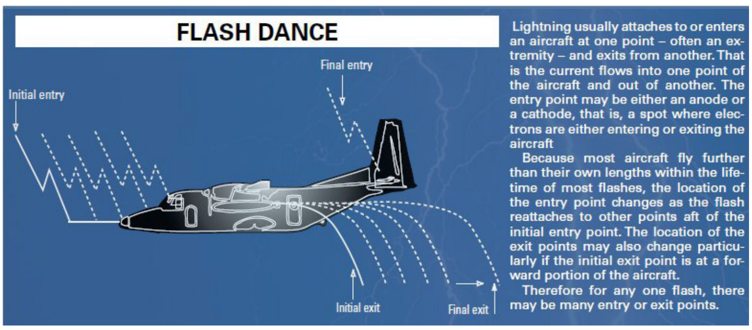

Figure 1. *Lightning strike. (source: Flight Safety Australia, July-August 2005)*

Located at about 12 km to the east of the North Sea, the climatology of Schiphol shows on average 13 days with thunderstorms in the cold season. Compared to other commercial airports like Frankfurt (5 days), Brussels and Hamburg (8), Rotterdam (9) and Paris (4) this is remarkably high. KNMI has observed that lightning originating from 10.000 to 15.000 ft cloud-tops (3-5 km) is not uncommon and aviation meteorologists have speculated that the aircraft in the vicinity frequently trigger the lightning strikes[2)]. For a better understanding an additional study was performed, based on the NWA study[2)] in the cold season (October 2003 - April 2007).

In this highlight a summary of this lightning study for Amsterdam Airport is presented first, followed by an introduction of the so-called awareness report for Aircraft Induced Lightning (AIL), a new tool to make users aware of the occurrence of this specific weather situation in the Amsterdam Flight Information Region (FIR), and by some conclusions.

The lightning study

For the study we used archived radiosonde data (twice a day, station De Bilt), METAR data (Amsterdam Airport Schiphol), radar and lightning data (from the KNMI SAFIR/FLITS network) and Pilot Reports. From the De Bilt soundings several instability indices were derived, as well as the 700 hPa (Flight Level 100) wind direction and speed and temperature. With the help of the radar data several cloud and precipitation characteristics that are used in aviation were derived and from the SAFIR/FLITS lightning data the frequency of strikes and correlation with detected precipitation echoes were derived.
As in the NWA-study[2)], a strong correlation between stability indices from the nearest sounding observation

In some cases we were able to relate a single recorded lightning strike with the reported aircraft lightning incident

and the lightning encounters was noted. If only data is considered for which radar echoes were observed, threshold values for potential convective activity were reached for all stability indices in over 80% of the cases.

In all cases, the temperatures observed at the Lifting Condensation Level (LCL) were above the –10 °C threshold criterion required for cloud-to-ground strike, but Equilibrium Level (EL) temperatures were generally not cold enough (below -20 °C) to reach the criteria of the Storm Prediction Center (SPC) of the US National Weather Service (NWS) for the prediction of cloud-to-ground lightning[3]. However, the soundings in nearly every case where EL and LCL criteria were met, showed a range of temperatures in the clouds between –10 °C and –20 °C where ice and supercooled liquid water droplets can co-exist, stimulating the separation of electrical charges during the convective process. It was observed that lightning strikes invariably were recorded from convective cells with a minimum intensity of 31dBz (in a range to over 47 dBz) on the KNMI-radar. In some cases we were able to relate a single recorded lightning strike with the reported aircraft lightning incident.

The convective region showed little change in time in intensity and coverage while passing the investigated area. Only 5% of the cases showed a decrease and 25% of the cases showed an increase in intensity and coverage. About 44% of the cases contained tops of convective clouds at only 15,000 ft or less. 68% of the lightning encounters occurred with a 700 hPa flow out of the NW (270 through 360 degrees) quadrant. 26% occurred with a wind from the SW quadrant, mainly between 250-270 degrees. Most of the cases with winds more southwesterly than 250 degrees had thunderstorms with warmseason characteristics. Significant cold season convection was often triggered over the North Sea, combining cells to form larger cells over land. However, some events seemed to be independent of this typical North Sea process.

Pattern Classification for northwest airflows

A northwesterly wind brings unstable and cool or even cold air from higher latitudes over the relative warm North Sea to the Netherlands. Figure 2 is an example of this typical airflow at 500 hPa.

The frequency of occurrence of this airflow was computed for the research period 2003 – 2006, cold season only. November to February showed the highest occurrence (29% to 35%), the lowest was in March, April and October (20% or lower). Figure 3 is a satellite image of the organized clouds over the North Sea, lined up in cloud streets or open cell structures depending on wind and instability, similar to the Lake effect over the Great Lakes in the USA.

Aircraft Induced Lightning (AIL) in the operational Meteorological Service

To test whether a forecasting tool is a) practical to produce, and b) could be beneficial for avoidance procedures, a prototype forecast for AIL in the form of an experimental awareness report, created by KNMI and issued to aviation users, was developed and tested. Given the unexpectedly high frequency of lightning in autumn and winter it is important to make dispatchers and crews aware of the presence of this specific weather scenario. Unexpected, sudden lightning strikes in small showers, sometimes

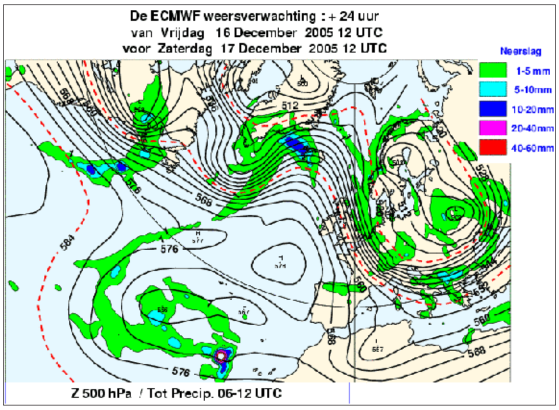

Figure 2*. Northwest flow at 500 hPa over the North Sea. Green is forecast precipitation.*

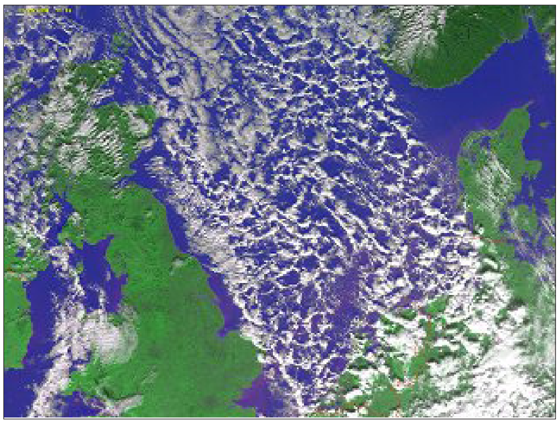

Figure 3. *NOAA AVHRR image: showers over the North Sea (13-11-2004).*

Given the unexpectedly high frequency of lightning in autumn and winter it is important to make dispatchers and crews aware of the presence of this specific weather scenario

triggered by aircraft may lead to unforeseen, additional costs. As induced lightning often occurs at low altitude on approach and descent, the Schiphol Terminal Control Area (TMA) (Figure 4) was chosen as the best area for this test. An awareness report on the specific phenomena for this area only will trigger alertness and may lead to a correct decision for a possible avoidance procedure and so to saving costs.

In the test period (7.1 - 16.4 2008) reports covering all busy hours at the airport were issued daily by the aviation meteorologist in the Central Forecasting Office of KNMI. Figure 5 shows an example of an AIL Awareness Report. By using specific colours the meteorologist can highlight specific periods of the day that have an increased lightning probability.

An evaluation of the AIL forecast, using pattern recognition and SAFIR/FLITS data in the Schiphol TMA, gave the following results. Out of 82 days, 48 (58%) days showed a reported wind at 700 hPa in the sector 250-020 degrees. 25 days (of 82) were classified as days with reported lightning, either by pilots or by the SAFIR/FLITS system, 19 of these with a northwesterly wind. Obviously not all days with northwesterly winds contribute to unstable weather. The combination of criteria on wind direction, low freezing level (<3000 ft) and cold upper air (T≤ -10 °C at 700 hPa) showed a good result: 72% of the reported lightning strikes were predicted by this method. By using instability indices only the result was 76%. With a computed Probability of Detection of 86% and a False Alarm Ratio of 24% the value of the awareness report is in par with other aviation meteorology products (Figure 6).

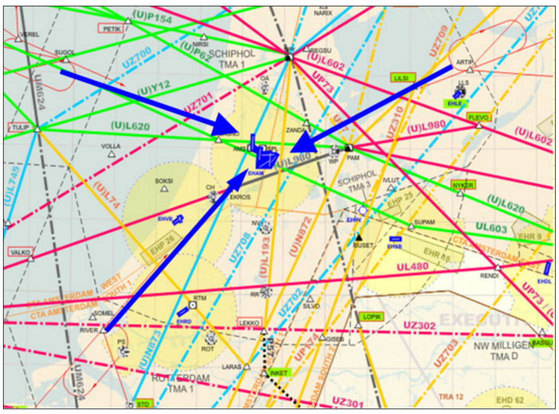

Figure 4. Part of Schiphol Terminal Control Area and 3 navigation beacons.

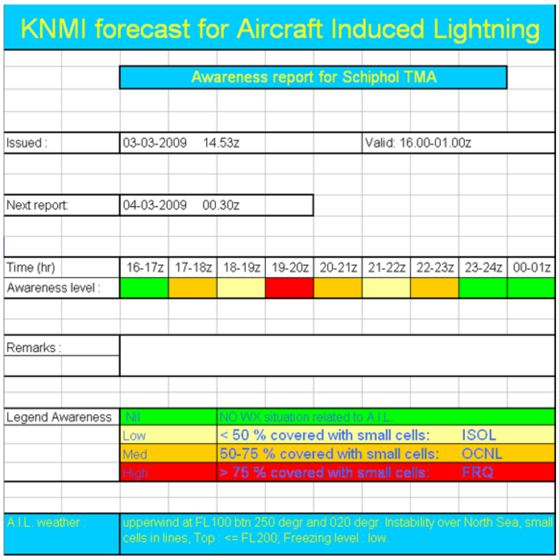
KNMI forecast for Aircraft Induced Lightning

Awareness report for Schiphol TMA

Issued :	03-03-2009 14.53z				Valid: 16.00-01.00z				
Next report:	04-03-2009 00.30z								
Time (hr)	16-17z	17-18z	18-19z	19-20z	20-21z	21-22z	22-23z	23-24z	00-01z
Awareness level :									
Remarks :									
Legend Awareness	Nil	NO WX situation related to A.I.L.							
	Low	< 50 % covered with small cells:				ISOL			
	Med	50-75 % covered with small cells:				OCNL			
	High	> 75 % covered with small cells:				FRQ			
A.I.L. weather :	upperwind at FL100 btn 250 degr and 020 degr. Instability over North Sea, small cells in lines, Top : <= FL200; Freezing level : low.								

***Figure 5**. Example AIL Awareness Report.*

A.I.L.- verification:	OBS	NO OBS
7 Jan - 16 April, all days		
FCST	31	10
NO FCST	5	69

***Figure 6.** Verification AIL-report.*

WinterKOUW

Complementary to KOUW[4], which is an operational probabilistic forecast system of (severe) thunderstorms in the warm season for the purpose of issuing a weather alarm, WinterKOUW was developed for the cold season[5]. KOUW is a Model Output Statistics (MOS) system based on a statistical relation between the occurrence of lightning discharges and a set of potential predictors calculated from the Numerical Weather Prediction models HIRLAM and ECMWF and an ensemble of advected lightning and radar data[6]. In KOUW the (conditional) probability of (severe) thunderstorms is calculated for 12 districts shown in Figure 7. As lightning is less frequent in winter, WinterKOUW presents the probability of ≥1 lightning discharge in only 4 districts around Amsterdam Airport (almost in the centre, Figure 7). Out of a large pool of potential predictors such as traditional instability indices, the most useful predictors appeared to be the HIRLAM Boyden index, the ECMWF convective precipitation, two radar advection predictors and the HIRLAM Convective Available Potential Energy (CAPE).

Figure 7 is an example of a WinterKOUW probability forecast. The forecast probabilities for this example are (much) higher than the climatological probabilities of <=7% (period 2004 – 2007) for the 4 districts. Several lightning reports were received through Air Traffic Control and detected by SAFIR/FLITS. Green area corresponds to 31% and 1 observation; yellow 58%, 3 observations; and blue 15% and 9%, no observations. The WinterKOUW forecast system turned out to have a good skill compared to the climatology.

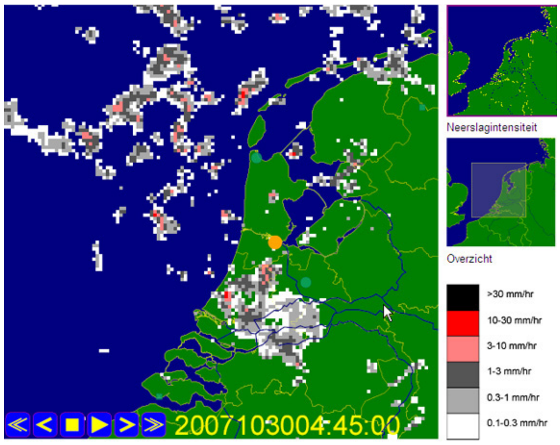

Figure 8. *Radar image with small active showers.*

Lightning reports

From the NWA-study[2)] it is known that the number of lightning reports in the USA from aircraft in flight in the cold season exceeds the number of reports in the warm season. For a comparison with the Dutch Airspace, reports of aircraft lightning encounters were obtained from Air Traffic Control for the period May 2005 – April 2008. Knowing that not all encounters are reported, the numbers must be treated as a test at random. In total 33 lightning reports were received. Only 10 were reported in the warm season, of which 8 at unknown altitude, 1 in take off and 1 in descent. For the cold season 23 reports were received, 12 at unknown altitude, 6 in take off and 5 in descent. Comparing these numbers it may be concluded that winter thunderstorms are en route more difficult to detect or recognize in relation to summer storms.

In practice

A weather radar image with small, convective, pink and red coloured cells in a weather situation for which an AIL report was issued, is displayed in Figure 8. In fact three lightning strike reports from heavy aircraft were received. SAFIR/FLITS detected no lightning in the hours before.

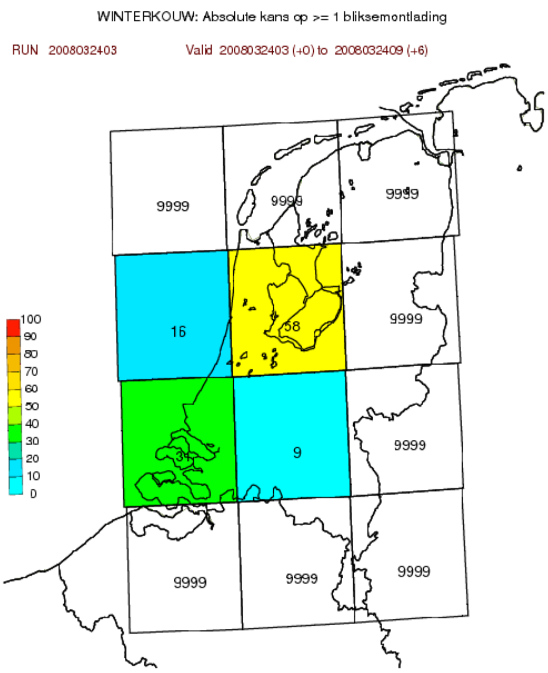

Figure 7. *WinterKOUW probability forecast (%) of >= 1 lightning discharge for March 24 2008 03-09 UTC; Colour scale indicates 0 to 100 %.*

Conclusion

A study was done on the weather conditions around aircraft during lightning encounters in the area around Amsterdam Airport Schiphol. A cold west-to-north flow over the relatively warm North Sea bringing low-level instability and development of small convective cells, sometimes embedded in larger cloud structures, has a potential for aircraft induced lightning events. Relations were found between lightning events and traditional instability indices. A tool for operational aviation weather forecasting was developed, the promising WinterKOUW probability forecast.

The Aircraft Induced Lightning awareness reporting procedure became available in October 2008 for users in the Dutch Airspace. The main purpose is to make the aviation users aware of the presence of this specific weather type, not to forecast lightning in individual cells.

Most of the lightning encounters (74%) occurred in situations with isolated lightning producing cells with at least moderate echo intensity on the radar. These cells can be detected on most airborne weather radars, helping a crew to carry out avoidance techniques, if advised and possible.

References

1) Hemink, H.J., W. Gough, S. Niemeijer and T. Fahey, 2009. *The Prediction and Occurrence of Aircraft Lightning Encounters at Amsterdam-Schiphol Airport.* Proc. 47^{th} American Institute of Aeronautics and Astronautics Meeting and Exhibit, Orlando, Florida, USA, January 2009.
2) Fahey, T., A. Stach, W. Gough and S. Niemeijer, 2007. *The Prediction and Occurrence of Aircraft Lightning Encounters in Low-Topped Convection.* Proc. 45^{th} American Institute of Aeronautics and Astronautics Meeting and Exhibit, Reno, Nevada, USA , January 2007.
3) Broecke, M.S. van den, D.M. Schultz, R.H. Johns, J.S, Evans and J.E. Hales, 2005. *Cloud-to-Ground Lightning Production in Strongly Forced, Low-Instability Convective Lines Associated with Damaging Wind.* Weather and Forecasting, **20**, 517-530.
4) Schmeits, M. J., C.J. Kok, D.H.P. Vogelezang and R.M. van Westrhenen, 2008. *Probabilistic forecasts of (severe) thunderstorms for the purpose of issuing a weather alarm in the Netherland.* Weather and Forecasting, **23**, 1253–1267.
5) Slangen, A. 2008. *Probabilistic forecasts of winter thunderstorms around Schiphol Airport using model output statistics.* KNMI Technical Report TR-300, 53pp.
6) Wilks, D. S. 2006. *Statistical Methods in the Atmospheric Sciences, 2^{nd} Edition.* Academic Press, London, 627pp.

Improved and tailored low visibility forecasts for Amsterdam Airport Schiphol

Janet Wijngaard, Nico Maat, Daan Vogelezang and Hans van Bruggen

Introduction

Accurate, reliable and unambiguous information concerning the actual and expected visibility conditions at Amsterdam Airport Schiphol is important for the available operational flow capacity. Inaccurate and unreliable visibility forecasts have a negative impact on safety and operational expenses. Under low visibility conditions the so-called 'Low Visibility Procedure' (LVP) comes in charge. Table 1 shows the different visibility categories, including ceiling, with their related capacity and flow restrictions at Schiphol. A new forecast system should enhance the quality of the decision making process under low visibility conditions at the airport.

Visibility class	Visibility / RVR (m)		Cloud base (ft)	Capacity (movements per hour)	Flow restrictions
Good	VIS ≤5000	and	CLB ≤1000	68 amhi or 74 depart. max 104/108 movements	No
Marginal	1500 ≤VIS ≤5000	or	300 ≤CLB ≤1000	As above but with independant parallel runways	No
LVP2) phase A	550 ≤RVR ≤1500	or	200 ≤CLB ≤300	56 amhi or 52 depart. max 80 movements	In general no
LVP phase B	350 ≤RVR ≤500	or	CLB ≤200	44 amhi or 52 depart. max 74 movements	Yes
LVP phase C	200 ≤RVR ≤300			30 amhi or 17 depart. max 47 movements	Yes
LVP phase D	RVR ≤200			16 amhi or 20 depart. max 36 movements	Yes

Table 1. *Relation between categories of visibility/ceiling and capacity/flow restrictions at Amsterdam Airport Schiphol (May 2007). 1) VIS: Visibility, 2) RVR: Runway Visual Range, 3) LVP: Low Visibility Procedure. Cloud base (Ceiling) gives the base height of the lowest clouds having at least a cloud cover of 5/8.*

An update of the visibility forecast system is achieved in close collaboration with the main users of the airport, i.e. Air Traffic Control, the airport authorities and KLM airlines. Next to the improved forecast system, a methodology is provided to support the user's challenge of making an economically well-founded decision based on a probability forecast.

Tailoring the visibility forecast

The existing automated system that is used to create visibility forecasts comprises HIRLAM (High Resolution Limited Area Model) output in combination with a statistical post-processing module, the TAFG (Terminal Aerodrome Forecast Guidance)[1]. Output of both is supplied to the forecaster who issues the operational probability forecast, the Schiphol Probability Forecast (in Dutch: Schipholkansverwachting; SKV). Figure 1 gives a schematic overview of the forecast cascade that leads to the SKV. To tailor the visibility forecasts for the specific needs of the Amsterdam Airport Schiphol community, we have extended the statistical post-processing module TAFG.

Accurate, reliable and unambiguous information concerning the actual and expected visibility conditions at Amsterdam Airport Schiphol is important for the available operational flow capacity

Special Visibility Definitions

The statistical post processing module TAFG has been extended with special predictands for several combinations of visibility and ceiling, fully in line with the thresholds for LVP phases used by Air Traffic Control. These thresholds include special visibility definitions, such as Runway Visual Range (RVR). RVR values are usually derived from the regularly observed visibility, the

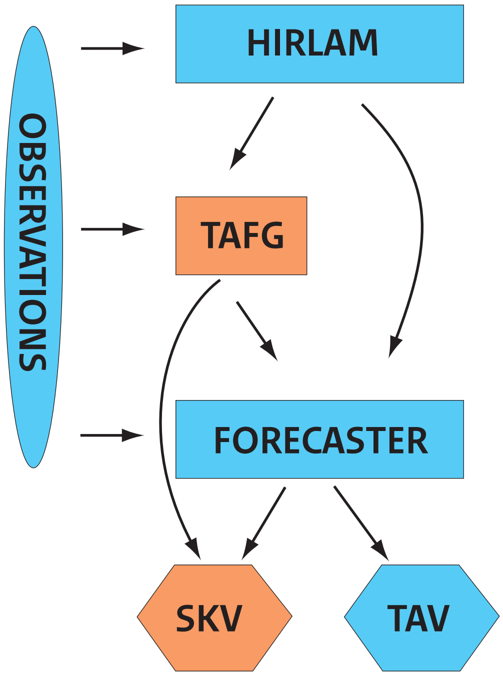

Figure 1. *Schematic overview of the forecast cascade leading to the probabilistic forecast (SKV) for Schiphol. HIRLAM is the numerical weather prediction model, which feeds the TAFG and the forecaster. Observations are necessary input for HIRLAM, the TAFG and the forecaster. Note that the TAF (Terminal Aerodrome Forecast) in the lower right of the overview is an existing internationally agreed standard forecast which is not discussed in this highlight.*

Meteorological Optical Range (MOR), and observations of the background luminance. In order to be able to provide forecasts for the RVR, forecasts of the background luminance and a probabilistic MOR forecast have to be combined. Obviously, for the background luminance astronomical parameters play the dominant role (sunrise and sunset), but use of meteorological parameters like cloud amount and cloud base height can improve the statistical skill of the background luminance forecast. To give an example of a result of the procedure, a predictand denoting the probability of MOR visibility being less than 400 m can be transformed into a probability of RVR being less than 867 m.

For determining the LVP phase, we need the probabilities of RVR at the thresholds of 200, 350, 550 and 1500 m (Table 1). The probabilities of the LVP phases are interpolated from the derived RVR probabilities.

Verification

In this paragraph the improved SKV forecasts are verified against observations to examine their performance. In addition, verification results of the old and the new TAFG are compared.

In Figure 2 a reliability diagram is presented for LVP class A or worse. For the period July 2004 to April 2007 comparison is shown between the old TAFG, the new TAFG and the Schiphol probability forecast SKV as issued by the forecaster (and based on the old TAFG). This dataset was also used to develop the new TAFG. This means that the new TAFG verification results in this figure are dependent. Ideally, all points should be on the diagonal in a reliability diagram2). The comparison between the new TAFG and the old TAFG gives a strong indication of increased reliability. The old TAFG and the SKV show overforecasting, i.e. forecast probabilities are higher than observed frequencies (data points below the diagonal). The forecaster achieves for the short term about the same reliability as the old TAFG, but has added value by making a more distinct forecast by also forecasting high probabilities. The forecaster reached up to 100% whereas both the old and new TAFG do hardly exceed 80%, in other words the forecaster adds resolution. In addition to the reliability, the skill of the forecasts is determined. The Brier Skill Score (BSS) expresses the quality of the forecast by comparing to a defined reference forecast, in this case the climatological probabilities. A BSS of 100% indicates a perfect forecast, 0% indicates the same skill as climatology and a negative percentage means that the climatological forecast is better[2)]. All forecasts show a positive BSS (Figure 2), the new TAFG provides the highest score followed by the forecaster.

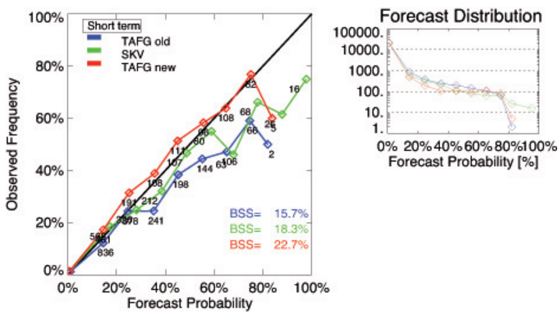

Figure 2. *Left panel: Reliability diagram for short term forecast (3, 6 and 9 hours ahead) of LVP phase A or worse (see Table 1). In the reliability diagram the observed frequency is plotted against the forecast probability. Reliability is indicated by the proximity of the plotted curve to the diagonal. Verification is shown for the old TAFG, new TAFG and the SKV as issued by the forecaster (based on the old TAFG). The number of the various forecast values is depicted below the curves and also shown in the right panel on a logarithmic scale. Brier Skill Scores are also given for these three forecasts. Verification is performed against Schiphol (AUTO)SYNOP data for the period July 2004 until April2007. This dataset was also used to develop the new TAFG.*

From June 2007 and onwards the new TAFG could be verified on an independent data set. The verification results in Figure 3 show the results for that period. Both forecaster (SKV) and TAFG show a high reliability. Again the forecaster adds resolution, whereas the BSS is somewhat higher for the TAFG. These verification results demonstrate the usefulness of the new TAFG and the Schiphol probability forecast.

Optimizing the categorical decision

Once the probability forecast is available, it is the user's challenge to use this probabilistic information to make an economically well-founded categorical decision. Ideally, the user chooses the category that corresponds to a fixed predetermined (optimal) percentile of the probability distribution. In Fig 4 a conceptual methodology is presented which shows the potential benefit that can be gained by combining: a) the quality of the probabilistic forecasts and b) the user's sensitivity to false alarms and misses in his categorical decision. The system performance over a recent period is given in the form of a contingency table of forecast versus observed categories. In a so-called expense matrix the extra 'costs' or damage due to wrong forecasts is specified. Multiplying the performance table by the expense matrix yields the user-specific costs due to wrong forecasts over the period involved. The 'optimal' percentile can be derived by calculating the extra costs for a large number of choices of the percentile and determine for which value these costs are lowest. Although based on past performance, it is plausible that also for actual forecasts this optimal percentile will be economically the best choice.
In Figure 5 an example of the above is presented; it shows the expenses as a function of the decision-percentile for a number of fictitious users with different ratio of sensitivity for false alarms and misses.

The new statistical post-processing yields a tailored and improved low visibility forecast for Amsterdam Airport Schiphol

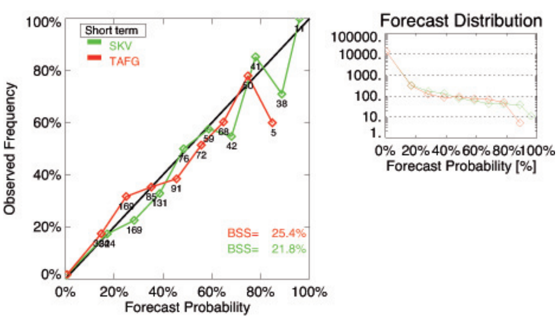

Figure 3. *Reliability diagram, similar as Figure 2, for the new TAFG and the SKV as issued by the forecaster (based on the TAFG). Data are from the period June 2007 until February 2009; from May 2008 the new TAFG became available to the forecaster.*

System performance

	CD	B	A	MG
CD	0	2	1	1
B	8	9	10	19
A	2	7	2	23
MG	3	9	21	300

X

User's "cost'

	CD	B	A	MG
CD	0	1	10	300
B	1	0	1	10
A	10	1	0	1
MG	100	10	1	0

→

Total

	CD	B	A	MG
CD	0	2	30	300
B	8	0	30	150
A	20	7	0	23
MG	300	50	21	0

Figure 4. *The system performance multiplied with the user's cost estimation delivers the total expense. The system performance is based on a threshold percentage of 25%; the category that corresponds to the 25th percentile of the probability distribution is taken. The headings CD, B, A and MG refer to the LVP classes as described in Table 1.*

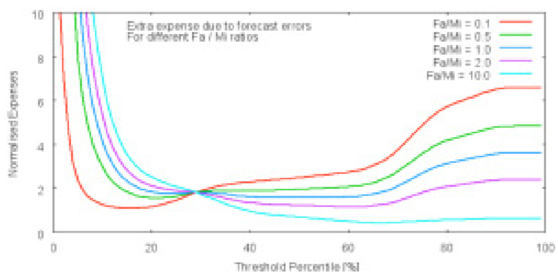

Figure 5. *Expense as a function of threshold percentage for different false alarm miss ratios (indicated by Fa/Mi). Different ratios lead to different optimal threshold percentages (at minimum of the plotted curve). The forecasts are the +4 of the new TAFG system over the period 2003-2007.*

Conclusion

The new statistical post-processing yields a tailored and improved low visibility forecast for Amsterdam Airport Schiphol. The newly developed forecast for background luminance in combination with - the already available - MOR forecast made the production of a RVR forecast possible. Verification of the RVR forecast showed a reliable and skilful product. Under low visibility conditions this runway related visibility is important in the decision making process. This improved and tailored forecast can directly benefit the operations at the airport. By taking into account the user-specific operation and optimizing the decision threshold, the benefit can be even higher. In future, accurate forecasts will continue to be important for the airport. Future research is planned to further

Figure 6. *Impression of Schiphol Airport during a fog event. Photo: Peter de Vries*

improve the low visibility forecasting and the understanding of the physical processes underlying fog. The use of high-resolution 3D models, a 1 column model for the very local physical processes and the introduction of new sensor technology for optimizing the detection of low visibility, are possibilities to be considered. The practical and meteorological feasibility for differentiating the Schiphol probability forecast, by making specific forecasts for various parts of the airport, is another issue to be investigated.

References

1) Jacobs, A.J.M. and N. Maat, 2005. *Numerical Guidance Methods for Decision Support in Aviation Meteorological Forecasting.* Weather and Forecasting, **20**, 82-100.
2) Wilks D. S, 1995. *Statistical Methods in the Atmospheric Sciences. An introduction.* Academic press, San Diego, us, 627pp.
3) KDC-LVP Project team [Hove, R. ten and J.B. Wijngaard (Eds.)], 2008. *Improved Low visibility and Ceiling Forecasts at Schiphol Airport, final report, part* 1. KNMI Publication 222.

EC-EARTH: goals, developments and scientific perspectives

Richard Bintanja, Wilco Hazeleger, Rein Haarsma, Frank Selten, Camiel Severijns, Andreas Sterl, Bart van den Hurk, Xueli Wang and Twan van Noije

Introduction

In recent years, it has become clear that the dynamic response of the Earth's global climate system is strongly affected by the interactions between its various subsystems[1]. As a result, attention has shifted to the development of Earth System Models (ESMs) that go beyond the more 'traditional' state-of-the-art coupled atmosphere-ocean general circulation models (AOGCMs). These ESMs will include additional climate components such as ocean biochemistry, dynamic vegetation, atmospheric chemistry, carbon cycle components and dynamic ice sheets. In the coming decade, ESMs will thus enable us to study the Earth's climate system and its response to perturbations in the broadest sense, with the interactions between the various subsystems most likely resulting in increased accuracy of climate predictions as well as in valuable new insights in climate variability and interactions. In addition, there is rising interest in predicting the anthropogenic climate change and natural climate variability beyond seasonal to interannual time scales.

A few years ago, it was henceforth decided by the European Centre for Medium-range Weather Forecast (ECMWF) member states that it would be imperative to initiate the development of an ESM, and the ECMWF weather prediction model was chosen as a starting point. Despite their different purposes, climate and weather forecasting are obviously based on the same physical principles. This has been recognized with the introduction of the concept 'seamless prediction'[2], which intends to address the predictability of the Earth's climate system (in its broadest sense) within one common framework.

These considerations have led a large number of ECMWF member states to commence with the development of a common ESM, coined EC-Earth (Figure 1), an initiative in which the Global Climate Division of KNMI has taken the lead. Among the various member states that participate in this initiative, three scientific and practical common goals have been identified[3]:

Figure 1. *The EC-Earth logo.*

Investigate Earth system feedbacks

Currently there is significant spread in climate sensitivity among climate models, which can be attributed to inaccurate knowledge of the main climate feedbacks such as cloud feedbacks, the lapse-rate feedback and the snow/ice albedo feedback[4]. To improve on this, such processes should be studied within the framework of a detailed ESM and validated with independent observations. Additionally, adding new components to the ESM will most likely bring to light previously unknown climate feedbacks, which will affect the modelled climate sensitivity.

Study interannual to multi-decadal climate fluctuations and predictability

This aspect of climate, and especially its interaction with projected greenhouse warming, is currently not understood very well. Large ensemble integrations with ESMs are required to usefully address the possible interactions between the dominant variability patterns (e.g. the North

A large number of ECMWF member states are involved in the development of a common Earth System Model, coined EC-Earth, an initiative in which the Global Climate Division of KNMI has taken the lead

Atlantic Oscillation (NAO), El Niño – Southern Oscillation (ENSO), the Pacific Decadal Oscillation (PDO), Atlantic Ocean meridional overturning) and climate change. These experiments are initialized using estimates from the observed state of the climate, and ocean in particular, to obtain predictions.

Develop an advanced modelling tool for making climate scenarios

There is a strong need for ESMs to accurately quantify climate change in its broadest sense and to make projections for future change. This will aid the development of mitigation policies, and will also facilitate adaptation strategies that will mostly be based on regional climate change. The latter can be obtained by coupling a global ESM such as EC-Earth to a regional model such as RACMO (Regional Atmospheric Climate Model), developed by the Regional Climate Division of KNMI[5].

Development and tuning

The development of EC-Earth within the EC-Earth consortium started with ECMWF's Integrated Forecast System (IFS) as a well-tested atmospheric module, with different components being added over time. The current version of EC-Earth is a fully coupled AOGCM, with oceanic, sea ice and land surface components having been coupled to the IFS. The model is off-line coupled to the TM5 atmospheric chemistry model.

The different demands of a climate model as opposed to a weather prediction model forced us to seek improvements to the uncoupled version of IFS (called CY31), which was initially chosen as the starting point of EC-Earth. These improvements should be reflected in the mean current climate as well as in its variability[6]. The tuning group of the EC-Earth consortium has performed several experiments to improve the skill of the model. In the following we will highlight a few changes that significantly improved the simulated climate.

The first improvement relates to problems in the simulated tropical climate in CY31, and most prominently to the underestimation of precipitation over the Pacific warm pool region (mainly the months JJA) and over Amazonia (mainly the months DJF), and to the overestimation of precipitation in the ITCZ (Inter Tropical Convergence Zone). It was noted that IFS cycle CY33 did not exhibit these problems and the changes could eventually be pinpointed to the different entrainment formulation in deep convection. Indeed, adopting the CY33 deep-convection entrainment in CY31 greatly reduced these deficiencies (Figures 2 and 3). Obviously, the agreement still is far from perfect, with e.g. somewhat degraded Asian monsoonal precipitation rates. An interesting 'side' effect is that the changed tropical convection and the associated heat transports also significantly improved the vertical distribution of temperature (Figure 3). The latter can also be inferred from a more systematic approach to assess the effect of model changes involving a performance index (PI).

We have adopted the performance index of Reichler and Kim (RK)[7], which has been used to compare the performance of various models contributing to the Coupled Model Intercomparison Project CMIP3. It is based on the squared differences of a number of simulated parameters with observations, such as 2 meter temperature (T2m), mean sea level pressure (MSLP), precipitation and vertical distributions of various quantities, scaled with the interannual variance in the observed quantity. Figure 4 graphically depicts the RK performance of some selected

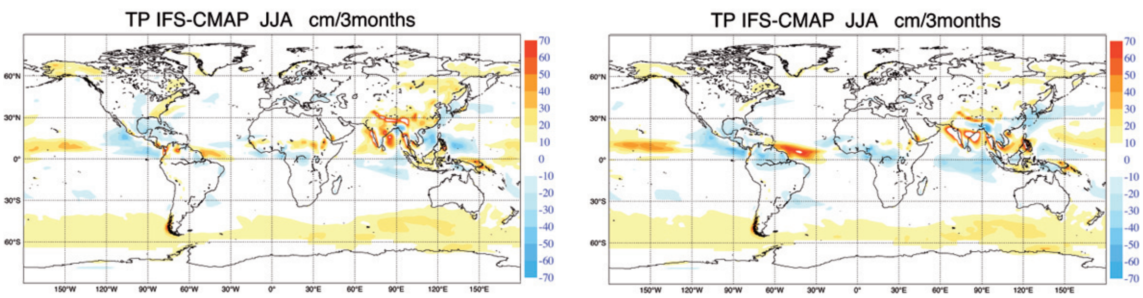

Figure 2. *Geographical distribution of June-July-August (JJA) precipitation (simulated minus observed) for a) CY31 convection, b) CY33 deep convection. The difference between a and b is indicative of the effect of including the CY33 deep convection scheme. Units are cm per 3 months.*

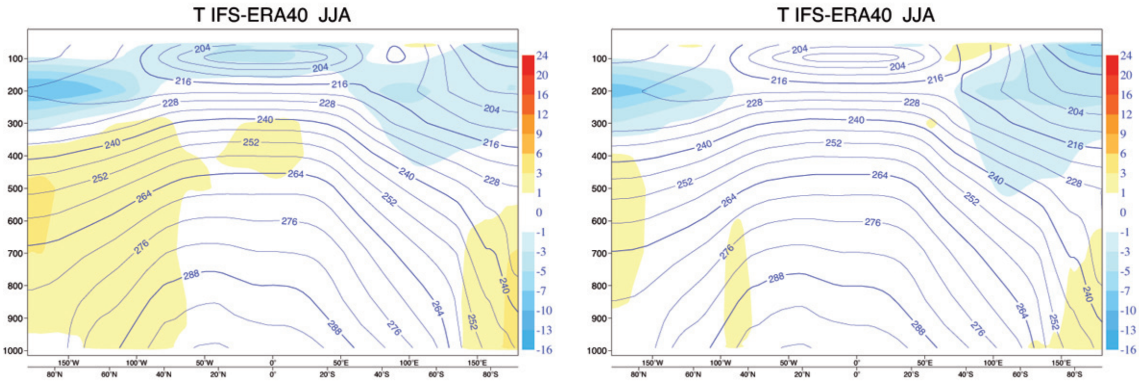

Figure 3. *As in Fig. 2 but for vertical distribution of zonal mean temperature; lines denote absolute temperature (K), colours denote differences with* ERA40 *(K).*

key model experiments. The top three entries depict the mean, best and worst CMIP3 AOGCMS, which are included for reference (being a next-generation model, one would expect that EC-Earth would generally outperform the CMIP3 models). The next four entries show the results for cumulative changes to the CY31 model version, for which is it important to note that these employ prescribed Sea Surface Temperatures (SST). The final two entries relate to the latest version of EC-Earth, which is a fully coupled AOGCM. The different colours depict four selected parameters, and the total (in black) reflects all variables (ten in total) combined. All values are scaled with the 'mean CMIP3' results to facilitate comparison between variables.

The uncoupled version CY31 in T95L40 resolution already yields results that are far better than the mean CMIP3, and are even comparable with the best CMIP3 model. While this seems reassuring, it should be noted that this is for a large part due to the fact that uncoupled models always outperform coupled models for obvious reasons. A notable result is that increasing the resolution to T159L62 significantly increases the performance of all variables. This is an expected result, but it is instructive to infer which variables benefit most from the increase in resolution (MSLP and T2m); generally it seems that variables associated with the dynamics depend stronger on model resolution than those connected to the physics. Including CY33 convection yields, as explained above, better precipitation rates and associated vertical distributions of temperature, in particular in the equatorial region. As shown by the black bar, its inclusion significantly increases the total performance. For this reason, and also because improved precipitation rates may favourably affect the climate of the model after coupling to an ocean component, this change was incorporated in the final version.

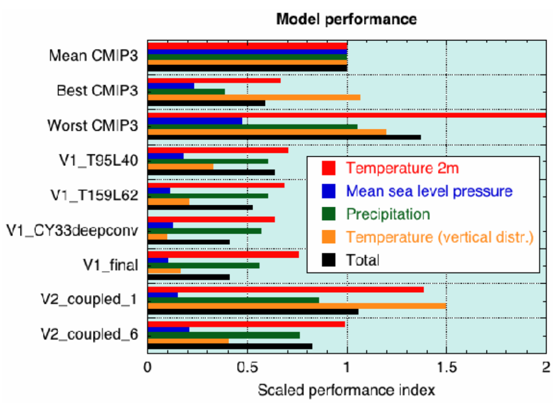

Figure 4. *Scaled performance indices (based on squared differences of model and observations) for the various model versions (including mean, best and worst* CMIP3 *models), scaled with the results from the mean* CMIP3 *models.*

The model version denoted by 'V2_coupled_1' is identical to the V1_final but for the coupling to the ocean (NEMO3) and sea ice (LIM2) components, and therefore represents the first coupled version of EC-Earth prior to tuning the coupled system. Not unexpectedly, the performance degrades significantly for all variables. Note, however, that the average performance of the first untuned coupled system of EC-Earth is only slightly worse than that of the mean CMIP3 model. Coupled model 'V2_coupled_6' represents the state after several bug fixes as well as changes to the snow albedo scheme and to the ocean. Clearly an improvement in most variables and in the total performance has been achieved. The process of development and tuning the coupled system is still ongoing, so further improvements can be expected.

An example of the state of the latest coupled model is

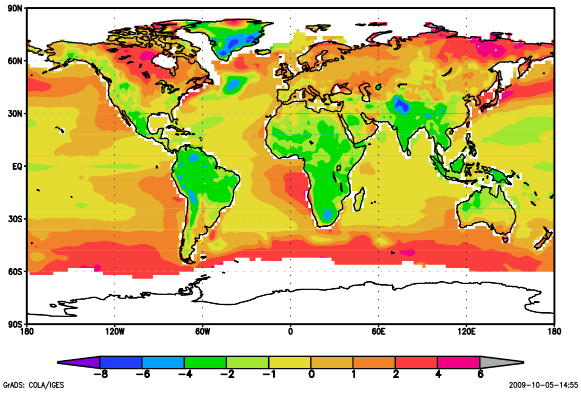

Figure 5*. Geographical distribution of annual mean 2m temperature over land, and sea surface temperature over the oceans. Plots show simulated minus observed values (K) against the respective observations. White areas indicate that observations are absent.*

The current version of EC-Earth will participate in the next CMIP5 initiative, and the model will also contribute to the next Intergovernmental Panel on Climate Change report

given in Figure 5. Annual T2m has a positive bias over the Northern Hemisphere (NH) continents, in particular in the subarctic regions (excluding regions permanently covered by land ice, such as Greenland). Analysis shows that this feature is due mainly to too warm winters, a feature present not only in the IFS model but also in many other climate models[4]. The reason for this bias may lie in the treatment of snow physics and/or the parameterization of vertical transports in the stable boundary layer. Attempts to address this issue have so far been largely unsuccessful. Another important bias is present in the sub polar sea surface temperatures (SST), in particular in the Southern Ocean. Also this bias is a fairly common feature among coupled climate models; attempts to reduce this are ongoing.

First scientific results

Even though the model has only recently been finalized, already some studies have been carried out with preliminary versions of EC-Earth. As an example of the kind of issues EC-Earth will be able to address, we will here briefly discuss the results of a recent paper by Haarsma et al.[8]. This paper focuses on possible causes of anomalously warm Western European summers under future climate change. The hypothesis is that warming of the Mediterranean region in concert with drier soils induces a large-scale heat low that causes easterly winds over Central Europe. This has been tested in the uncoupled (atmosphere only, prescribed SST) version of EC-Earth by applying an artificial net downward surface flux of energy over the Mediterranean that mimics conditions under the SRES A1B scenario for 2100. The results (Figures 6 a, b, c and d) show a strong increase in T2m, which is attributed to the depletion of soil moisture and a consequent decrease in latent heat flux. A heat low indeed develops, causing more easterlies in Western/Central Europe, as well as increased subsidence, less clouds, reduced precipitation and increased solar warming: all aspects of a more continental summer climate in Western Europe. This example nicely illustrates how EC-Earth can be used in a case-study manner to investigate specific aspects of climate in more detail, thereby bringing to light possible causes of (regional) climate change.

Conclusion

While the current version of EC-Earth is essentially a state-of-the-art AOGCM, a number of additional components are currently under development and will be added to EC-Earth in the coming years. These include dynamic vegetation, ocean biochemistry, carbon cycle components and dynamic ice sheets. We work actively with academia where there is expertise on these earth system components. As such, we provide the EC-Earth model to various research groups, in order to facilitate studying earth system feedbacks in an integrated earth system model. An important component that will probably be added already in the next version is an atmospheric chemistry module, which consists of an online version of the atmospheric chemistry and transport model TM5[9]. Being developed at KNMI's Chemistry and Climate division in collaboration with Wageningen University and Research Centre (WUR) and (inter)national partners, this module calculates the concentrations of reactive gases and various aerosol types for the meteorological conditions simulated by the atmospheric module of EC-Earth (IFS). The concentrations of the simulated greenhouse gases and the concentrations and relevant optical properties of the aerosols will be fed back into the atmospheric module to calculate the associated direct and indirect radiative forcings.

The current version of EC-Earth will participate in the next CMIP5 initiative, and the model will also contribute to the next report of the Intergovernmental Panel on Climate Change (~2013). The experiments will include traditional projections of future climate change in response to changes in greenhouse gasses, aerosols and land use, and novel decadal predictions. Obviously, this

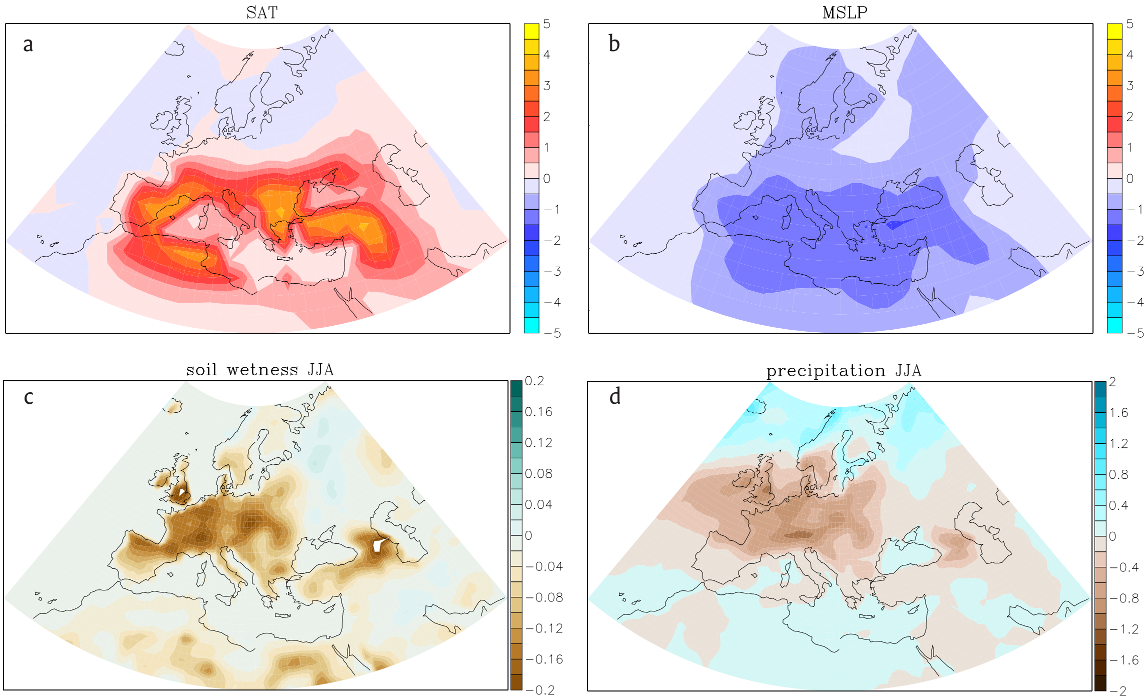

__Figure 6.__ Simulated JJA fields of a) surface air temperature (K), b) mean sea level pressure (hPa), c) soil wetness (the average moisture content of the upper meter of the soil), and d) precipitation (mm day^{-1}), for the experiment with an enhanced surface flux in the Mediterranean[8]. Plots depict the difference between the model runs with and without the artificial energy flux.

fits with the goals to address future climate change and contribute to climate scenarios as specified above. Preparations for this are already under way, as quite a number of (long) model runs are required for this purpose. To address regional (e.g. Western European) climate change, also in the framework of the climate scenarios, the output of EC-Earth simulations will most likely also be used as boundary conditions for regional climate models such as RACMO.

To conclude, we anticipate that EC-Earth will be used extensively in the near-future for all kinds of climate (change) applications, and will as such provide KNMI's climate activities a strong strategic position, both nationally and internationally.

References

1) Lenton, T.M., 2003. *Land and ocean carbon cycle feedback effects on global warming in a simple Earth system model.* Tellus, **52B**, 1159-1188.
2) Palmer, T.N., F.J. Doblas-Reyes, A. Weisheimer and M.J. Rodwell, 2008. *Toward Seamless Prediction: Calibration of Climate Change Projections Using Seasonal Forecasts.* Bull. Amer. Meteor. Soc., **89**, 459–470.
3) Hazeleger, W., 2007. *EC-Earth, science and implementation plan.* Internal document, 22pp. (to be obtained from http://ecearth.knmi.nl/index.php?n=PmWiki.Background).
4) Randall, D.A., R.A. Wood, S. Bony, R. Colman, T. Fichefet, J. Fyfe, V. Kattsov, A. Pitman, J. Shukla, J. Srinivasan, R.J. Stouffer, A. Sumi and K.E. Taylor, 2007. *Climate Models and Their Evaluation.* In: Climate Change 2007, The Physical Science Basis. Contribution of Working Group I to the Fourth Assessment Report of the Intergovernmental Panel on Climate Change (Solomon, S., D. Qin, M. Manning, Z. Chen, M. Marquis, K.B. Averyt, M.Tignor and H.L. Miller (Eds.)). Cambridge University Press, Cambridge, United Kingdom and New York, NY, USA, 589-662.
5) Lenderink, G., B.J.J.M. van den Hurk, E. van Meijgaard, A.P. van Ulden and H. Cuijpers, 2003. *Simulation of present-day climate in RACMO2: first results and model developments.* KNMI Technical Report TR-252, 24pp.
6) Räisänen, J., 2007. *How reliable are climate models?* Tellus, **59A**, 2-29.
7) Reichler, T. and J. Kim, 2008. *How Well do Coupled Models Simulate Today's Climate?* Bull. Amer. Meteor. Soc, **89**, 303-311.
8) Haarsma, R.J., F. Selten, B. van den Hurk and W. Hazeleger, 2009. *Drier Mediterranean soils due to greenhouse warming bring easterly winds over summertime central Europe.* Geophys. Res. Lett., **36**, L04705, doi:10.1029/2008GL036617
9) Krol, M., S. Houweling, B. Bregman, M van den Broek, A. Segers, P. van Velthoven, W. Peters, F. Dentener and P. Bergamaschi. *The two-way nested global chemistry-transport zoom model TM5: algorithm and applications.* Atmos. Chem. Phys., **5**(2), 417-432.

High-end climate change scenarios for flood protection of the Netherlands

Caroline Katsman, Andreas Sterl, Jules Beersma and Wilco Hazeleger

Introduction

Sea level rise, especially combined with possible changes in storm surges and increased river discharge resulting from climate change, poses a major threat for a low-lying delta like the Netherlands. Future flood protection strategies need to take these possible changes into account. Therefore, high-impact, low-probability climate change scenarios for the Netherlands were developed[1] at the request of the second Delta Committee[2]. In this study, local sea level rise, changes in storm surge height and peak discharges of the river Rhine were considered. Such detailed information goes beyond the KNMI'06 climate change scenarios[3] that span the range of most probable outcomes. The newly-developed high-end scenarios are discussed one-by-one below. The complex flood risk implied by the combination of these scenarios is illustrated by considering the situation near Rotterdam in the final section.

Sea level rise along the Dutch coast

The high-end scenario for local sea level rise is constructed using the methodology developed for the KNMI'06 scenarios[4]. First, separate high-end contributions for the processes that dominate the global mean changes were estimated: thermal expansion of the ocean, and mass changes of small continental glaciers and ice caps, the Antarctic Ice Sheet (AIS) and the Greenland Ice Sheet (GIS). Next, local effects are considered.

We assume that all contributions except that of AIS depend (partly) on the rise in global mean temperature, as for KNMI'06[4]. A global mean rise of 2 to 6 °C in 2100 was assumed, akin to the range projected for the most severe emission scenario (A1FI) of the Intergovernmental Panel on Climate Change (IPCC)[5].

The contributions from global mean thermal expansion and from small glaciers were estimated by exploiting simple scaling laws for their relationship with atmospheric temperature rise derived from climate model results[1,4], as well as conceptual models and observations[5] (Figure 1).

Ice sheets

The contributions from AIS and GIS are the most uncertain components[1,6]. The mass of ice stored on land in the ice sheets can change as a result of changes in surface mass balance (the net effect of snow accumulation, runoff and evaporation / sublimation) or by the flux of ice leaving the grounded ice sheet and entering the ocean (either as floating ice or melt water). The former is largely a response to changes in the atmosphere, while the latter is a complex response to atmospheric and oceanographic forcing and internal changes in the ice sheet of which we have limited understanding. Therefore, there is little confidence that the present generation of ice sheet models correctly

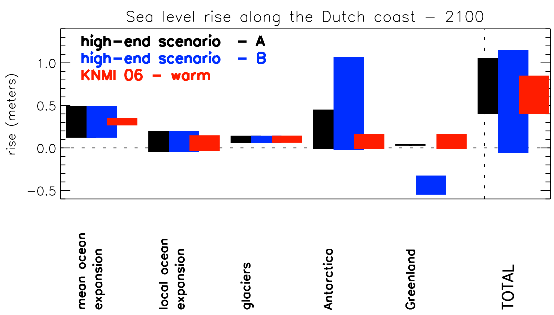

***Figure 1.** Individual contributions and total projected local sea level rise along the Dutch coast for 2100, for high-end scenarios A and B (black/ blue)[1] and the KNMI'06 warm scenario[3].*

simulates changes in ice flux in response to changing climate conditions. We therefore rely on recent observations and expert judgement to assess the possible contributions of GIS and AIS[1].

The most vulnerable parts of ice sheets are the so-called marine ice sheets (ice sheets that rest on bed rock that is below sea level and slopes downwards from the continental margin inland). Positive feedbacks in a marine ice sheet system can lead to a runaway collapse of the ice sheet, which would stop only where the retreat encountered a rising bed slope. The timescale over which such a collapse might occur is not well understood, but for large sections of an ice sheet it would probably be longer than a century. The largest marine ice sheet that exists today covers the majority of West Antarctica. The strongest inland bed slope, and hence the strongest tendency to instability, exists in that portion of the West-Antarctic Ice Sheet which drains into the Amundsen Sea (Pacific sector, near 100-110 W). In Greenland, only Jacobshavn Isbrae (on the west coast) contains a similar prominent inland slope, so that it could potentially display a sustained retreat[6].
The estimated contributions of AIS and GIS in the high-end scenario for sea level rise (Figure 1) combine the model-based assessment of surface mass balance changes[5] with a contribution due to fast ice dynamics, estimated from observations focusing on the vulnerable marine parts of the ice sheets[1,6].

Fresh water released by land ice melt is not distributed evenly over the oceans

Local effects on sea level
To arrive at a local sea level rise scenario, the ocean circulation changes in the North East Atlantic Ocean and their effect on local sea level[4,1] are assessed by analyzing climate model simulations. In addition, we take into account that fresh water released by land ice melt is not distributed evenly over the oceans. Large land-based ice masses exert a gravitational pull on the surrounding ocean, yielding higher relative sea levels in the vicinity of the ice mass (Figure 2, black line). When the ice mass shrinks, global mean sea level rises (blue line). In addition, the gravitational pull decreases, so that the actual sea level (red line) will drop in the vicinity of the ice sheet (region A) as water is redistributed away from it. Farther away from the ice mass (region B in Figure 2), sea level

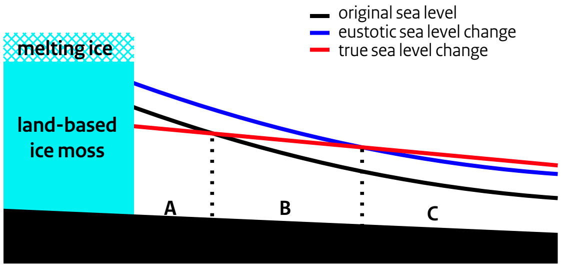

Figure 2. *Schematic illustration of gravity effects on local sea level changes induced by land-ice melt (black line: original sea level, blue: sea level after ice melt assuming equal distribution of the melt water; red: true sea level after ice melt).*

does rise, but this rise is smaller than the global mean rise that would result from equal distribution of the melt water. At even greater distances (region C), local sea level rise becomes larger than the global mean rise. Moreover, the solid Earth deforms under the shifting loads of ice and water and this deformation affects the gravity field and hence local sea level as well. As a result of these local gravitational and elastic changes, a
shrinking land ice mass yields a distinct pattern of local sea level rise sometimes referred to as its fingerprint[1,6]. These effects can be incorporated by multiplying each of the global mean contributions from land ice melt by their respective relative fingerprint ratios. For GIS and AIS, there appear to be large (poorly understood) differences in the fingerprints published by various authors[1,6]. To cover the extremes, two scenarios were developed.

After summing the various components, we arrive at a plausible high-end scenario for sea level rise along the Dutch coast of 0.40 to 1.05 meters for 2100 (excluding local land movement) when quantifying the gravity-elastic effects for the one extreme (scenario A in Figure 1). Using the other extreme (scenario B), the range becomes -0.05 to +1.15 meters. Not surprisingly, this high-end scenario is substantially higher than the KNMI'06 scenario for local sea level rise of 0.35 to 0.85 meters for 2100. The main causes for the difference are the more extreme global mean temperature range that is used as the starting-point and the larger contributions of GIS and AIS due to fast ice dynamics that are included[7].

Storm surges
The height of extreme storm surges is also important for flood protection of the Netherlands. Hence, it needs to be assessed whether and how climate change affects the heights of extreme surges, and in particular the statutory once-in-10,000 years storm surge height. To this end, the

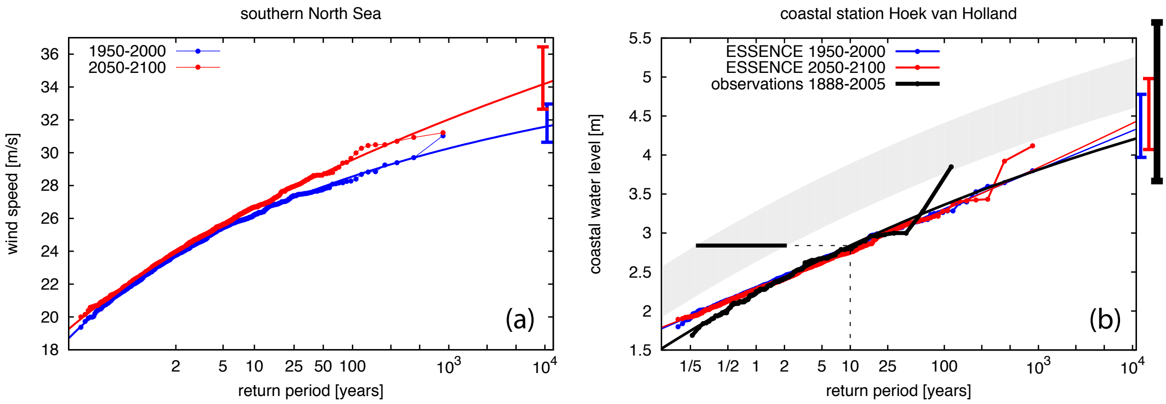

Figure 3*. Present (blue, 1950-2000) and future (red, 2050-2100) wind speed in the southern North Sea (a) and water level at coastal station Hoek van Holland (b), as a function of the return period. In (b), also the observed values for the period 1888-2005 are shown (black). Adding the high-end scenario for sea level rise to the surge height yields a coastal water level indicated by the grey band by 2100. It implies that the Maeslant barrier (Figure 5) will need to be closed five to fifty times more often than at present.*

wind fields from a 17-member ensemble climate-change simulation, in combination with an operationally-used surge model for the North Sea area were used to analyze[8] surge heights at the Dutch coast for two periods (1950-2000 and 2050-2100). Wind speeds in the southern North Sea are projected to increase (Figure 3a), due to an increase in south-westerly winds. However, the highest surges along the Dutch coast are caused by north-westerly winds because of their long fetch and the geometry of the coastline. As a result, local extreme surge heights are expected to be largely unaffected by the increase in wind speed (Figure 3b), as was found in earlier climate model studies[1].

Peak river discharge

The Netherlands also faces possible flooding from the river Rhine. Several studies using climate models in combination with hydrological models indicate that the peak discharge with a 1250-years return period (statutory safety level for the major rivers) may increase by about 5 to 40% over the twenty-first century[1]. In most studies, the increase in peak discharge is caused by an increase in mean winter precipitation combined with a shift from snowfall to rainfall in the Alps. In addition, some studies project a considerable change in the multi-day precipitation variability in winter (decreases as well as increases have been reported), which in turn has a substantial effect on the peak discharge.

Another relevant factor is that the flood defence guidelines in Germany are currently less strict than in the Netherlands, and probably will remain so in the near future. As a consequence, uncontrolled flooding in Germany is anticipated in case of extreme discharges, preventing these extreme discharges to reach the Dutch part of the Rhine delta (Figure 4). Taking this constraint into account, the high-end scenario for the 1250-year peak discharge for the Netherlands for 2100 is estimated to increase by about 10%[1,6].

Possible combined impacts: Rotterdam

The possible consequences of the combined impacts of

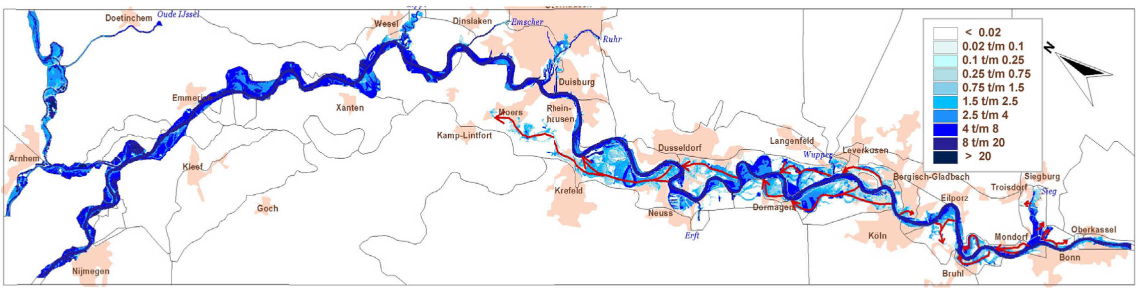

Figure 4. *Example of a simulation of flooding along the lower Rhine (dike situation 2020). Given are maximum water depths [m, in blue] and main streams behind the dikes[6].*

Figure 5. *The Maeslant storm surge barrier near Rotterdam during a test closure (source: www.BeeldbankVenW.nl).*

The possible consequences of the combined impacts of local sea level rise, storm surges, and peak river discharge become apparent when considering the situation near Rotterdam

local sea level rise, storm surges, and peak river discharge become apparent when considering the situation near Rotterdam. Its harbour is protected by the Maeslant storm surge barrier (Figure 5), which closes automatically when the local water level reaches a prescribed criterion; an event that nowadays is expected to occur on average every 10 years. If the high-end projection for sea level rise presented here becomes reality, the storm surge barrier is expected to close five to fifty times more often (Figure 3b). This would severely hamper the accessibility of Rotterdam harbour, resulting in large economic losses[2)]. In addition, the projected increases in sea level and peak river discharge will significantly enhance the probability that the storm surge barrier needs to be closed while the river discharge is large. During closure, the river system behind the barrier rapidly fills, increasing the local flood risk. It remains to be quantified exactly how large this risk will become.
It depends among other things on the duration of the closure (which in turn depends on the duration of the storm and its timing with the tidal phase) and on the temporal storage or re-routing of the river discharge through the interacting distributaries in the lower Rhine-Meuse delta.

Conclusion

The plausible high-impact, low-probability scenarios[1)] described here form the basis for updated flood protection strategies for the twenty-first century recently proposed by the Dutch Delta Committee[2)]. While such high-end scenarios inevitably have rather large uncertainties, the example of Rotterdam shows that evaluation of the complex, combined risks of sea level rise, storm surges and peak river discharge is crucial to updating flood management strategies.

References

1) Katsman, C.A., A. Sterl, J.J. Beersma, H.W. van den Brink, J.A. Church, W. Hazeleger, R.E. Kopp, D. Kroon, J. Kwadijk, R. Lammersen, J. Lowe, M. Oppenheimer, H-P. Plag, J. Ridley, H. von Storch, D.G. Vaughan, P. Vellinga, L.L.J. Vermeersen, R.S.W. van de Wal and R. Weisse, 2009. *Exploring high-end scenarios for local sea level rise to develop flood protection for a low-lying delta. Submitted to Climatic Change*.
2) Kabat, P., L.O. Fresco, M.J.F. Stive, C.P. Veerman, J.S.L.J. van Alphen, B.W.A.H. Parmet, W. Hazeleger and C.A. Katsman, 2009. *Dutch coasts in transition.* Nature Geoscience **2**, 450-452, doi:10.1038/ngeo572.
3) Hurk, B.J.J.M. van den, A.M.G. Klein Tank, G. Lenderink, A.P. van Ulden, G.J. van Oldenborgh, C.A. Katsman, H.W. van den Brink, F. Keller, J.J.F. Bessembinder, G. Burgers, G.J. Komen, W. Hazeleger and S.S. Drijfhout, 2006. *KNMI Climate Change Scenarios 2006 for the Netherlands.* KNMI Scientific Report WR-2006-01, 82 pp.
4) Katsman, C.A., W. Hazeleger, S.S. Drijfhout, G.J. van Oldenborgh and G.J.H. Burgers, 2008. *Climate scenarios of sea level rise for the northeast Atlantic Ocean: a study including the effects of ocean dynamics and gravity changes induced by ice melt.* Climatic Change, doi:10.1007/s10584-008-9442-9.
5) Meehl, G.A., T.F. Stocker, W.D. Collins, P. Friedlingstein, A.T. Gaye, J.M. Gregory, A. Kitoh, R. Knutti, J.M. Murphy, A. Noda, S.C.B. Raper, I.G. Watterson, A.J. Weaver and Z.-C. Zhao, 2007. *Global Climate Projections.* In: Climate Change 2007: The Physical Science Basis. Contribution of Working Group 1 to the Fourth Assessment Report of the Intergovernmental Panel on Climate Change, Solomon, S. et al. (Eds.), Cambridge University Press, Cambridge, United Kingdom and New York, NY, USA.
6) Vellinga, P., C.A. Katsman, A. Sterl, J.J. Beersma, J.A. Church, W. Hazeleger, R.E. Kopp, D. Kroon, J. Kwadijk, R. Lammersen, J. Lowe, N. Marinova, M. Oppenheimer, H.P. Plag, S. Rahmstorf, J. Ridley, H. von Storch, D.G. Vaughan, R.S.W. van der Wal and R. Weisse, 2008. *Exploring high-end climate change scenarios for flood protection of the Netherlands.* International Scientific Assessment carried out at request of the Delta Committee. KNMI Scientific Report WR-2009-05, KNMI / Alterra, the Netherlands, available from http://www.knmi.nl/bibliotheek/knmipubWR/WR2009-05.pdf
7) See also http://www.knmi.nl/klimaatscenarios/aanvullend/DC/index.php.
8) Sterl, A., H. van den Brink, H. de Vries, R. Haarsma and E. van Meijgaard, 2009. *An ensemble study of extreme North Sea storm surges in a changing climate.* Ocean Science, **5**, 369-378.

Appendices

Organisation chart

The organization of KNMI has, next to supplying staff, two business area departments (Weather Service and Climate and Seismology), and one department supplying these business areas with ICT and observation services. The divisions in these departments that perform (only or for a part) research, are marked red in the chart below. In the following appendices the publications are listed per division.

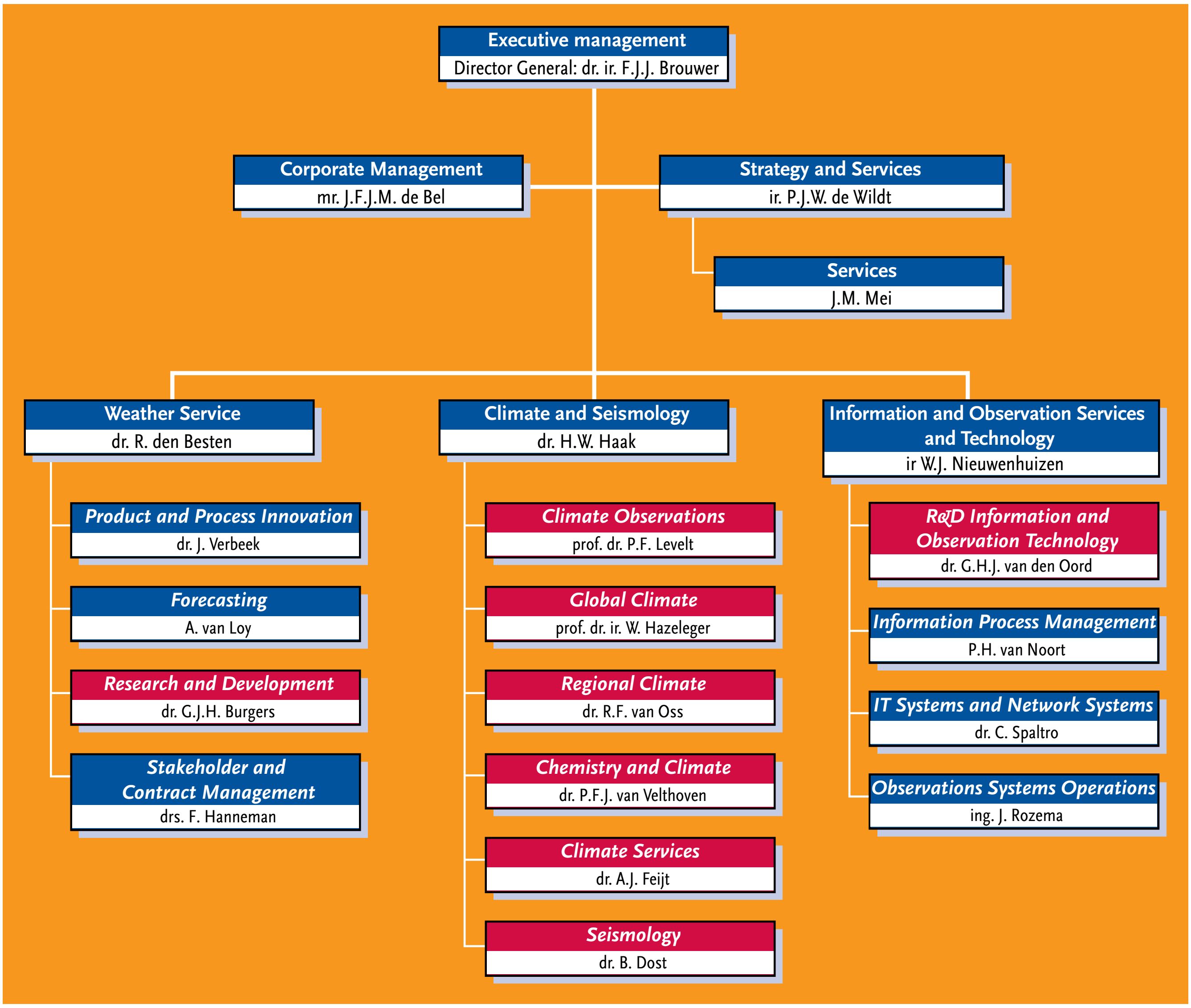

Publications Weather Research and Development

The Weather Research and Development division is aimed at improving the quality and efficiency of the weather service in meeting the requirements of our users. An important focus is on more precise severe weather forecasts and providing better severe weather warnings. To this end, KNMI weather research ranges from observations to meteorological processes to models, applying innovative techniques and systems that fit our user needs best.

Reviewed Publications

2007

Hersbach, H., A. Stoffelen and S. de Haan, 2007. *An Improved C-band scatterometer ocean geophysical model function: CMOD5.* J. Geophys. Res., **112**.

Holleman, I., 2007. *Bias adjustment and long-term verification of radar-based precipitation estimates.* Meteorological Applications (Royal Met. Society), **14**, 195-203.

Hooghoudt, J.O. and J. Barkmeijer, 2007. *The interaction between the stratosphere and the troposphere as revealed by singular vectors.* Meteor. Z., **16**, 6, 723-739.

Huuskonen, A. and I. Holleman, 2007. *Determining weather radar antenna pointing using signals detected from the sun at low antenna elevations.* J. Atm. Oceanic Technol., **24**, 3, 476-483.

Jarvinen, H., R. Eresmaa, H. Vedel, K. Salonen, S. Niemela and J. de Vries, 2007. *A variational data assimilation system for ground-based GPS slant delays.* Quart. J. Royal Meteor. Soc., **133**.

Kent, E., S. Woodruff, N. Rayner, T. Arbetter, C. Folland, F.B. Koek, D. Parker, R. Reynolds, R. Saunders, V. Smolyanitsky, S. Worley and T. Yoshida, 2007. *Advances in the Use of Historical Marine Climate Data.* Bull. Amer. Meteor. Soc.

Kudryavtsev, V.N. and V.K. Makin, 2007. *Aerodynamic roughness of the sea surface at high winds.* Bound.-Layer Meteorol., **125**.

Makin, V.K., H. Branger, W.L. Peirson and J.P. Giovanangeli, 2007. *Stress above wind-plus-paddle waves: modeling of a laboratory experiment.* J. Phys. Oceanogr., **37**.

Manders, A.M.M., W.T.M. Verkley, J.J. Diepeveen and A.R. Moene, 2007. *Application of a potential vorticity modification method to a case of rapid cyclogenesis over the Atlantic Ocean.* Quart. J. Royal Meteor. Soc., **133**.

Wheeler, D., R. García Herrera, F.B. Koek, C. Wilkinson, G.P. Können, M. del Rosario Prieto, P.D. Jones and R. Casale, 2007. *CLIWOC, Climatological database for the world's oceans: 1750 to 1850; Results of a research project EVK1-CT-2000-00090.* 2007, Brussels, European Commission, ISBN 92-894-8279-6, 190p.

2008

Babanin, A.V. and V.K. Makin, 2008. *Effect of wind trend and gustiness on the sea drag: Lake George study.* J. Geophys. Res., **113**

Caulliez, G., V. Makin and V. Kudryavtsev, 2008. *Drag at the water surface at limited fetches:observations and modelling.* J. Phys. Oceanogr., **38**.

Delgado, G., P. de Valk, A. Redano, S. van der Veen and J. Lorente, 2008. *Verification of a MSG Image Forecast Model: METCAST.* Weather and Forecasting, **23**.

Gasteren, H. van, I. Holleman, W. Bouten and E. van Loon, 2008. *Extracting bird migration information from C-band Doppler weather radars.* Ibis, **150**.

Geertsema, G.T., 2008. *Re-analysis of meteorology for the 1994 European Tracer Experiment using present day modeling techniques.* ANS 2008 EP&R and R&RS Topical meeting,, 9/3/2008-12/3/2008, 2008, Albuquerque, ANS, ISBN 0-89448-060-X, 155-161.

Haan, S. de, 2008. *Meteorological applications of a surface network of Global Positioning System receivers.* Thesis, Wageningen University, 2008, Wageningen, 157p.

Holleman, I., H. van Gasteren and W. Bouten, 2008. *Quality Assessment of Weather Radar Wind Profiles during Bird Migration.* J. Atm. Oceanic Technol., **25**.

Iversen, T., J. Kristiansen, T. Jung and J. Barkmeijer, 2008. *Optimal atmospheric forcing perturbations for the cold-ocean warm-land pattern.* Tellus, **60A**.

Kok, K., B. Wichers Schreur and D. Vogelezang, 2008. *Valuing information from mesoscale forecasts.* Meteorological Applications (Royal Met. Society), **15**.

Makin, V.K., 2008. *On the possible impact of a following-swell on the atmospheric boundary layer.* Bound.-Layer Meteorol., **129**.

Marseille, G.J., A. Stoffelen and J. Barkmeijer, 2008. *Sensitivity Observing System Experiment (SOSE) - A New Effective NWP-based Tool in Designing the Global Observing System.* Tellus, A, **60**.

Marseille, G.J., A. Stoffelen and J. Barkmeijer, 2008. *A cycled sensitivity observing systeme experiment on simulated Doppler wind lidar data duren the 1999 christmas storm.* Tellus, A, **60**.

Marseille, G.J., A. Stoffelen and J. Barkmeijer, 2008. *Impact assessment of prospective space borne Doppler wind lidar observations scenarios.* Tellus, A, **60**.

Meulen, J.P. van der and T. Brandsma, 2008. *Thermometer Screen Intercomparison in De Bilt (the Netherlands), Part I: Understanding the weather-dependent temperature differences.* Int. J. Climatology, 1, **28**.

Overeem, A., T.A. Buishand and I. Holleman, 2008. *Rainfall depth-duration-frequency curves and their uncertainties.* J. Hydrol., **348**.

Roebeling, R.A., H.M. Deneke and A.J. Feijt, 2008. *Validation of cloud liquid water path retrievals from SEVIRI using one year of CLOUDNET observations.* J. Appl. Meteor., 1, **47**.

Roebeling, R.A., S. Placidi, D.P. Donovan, H.W.J. Russchenberg and A.J. Feijt, 2008. *Validation of liquid cloud property retrievals from SEVIRI using ground-based observations.* Geophys. Res. Lett., **35**.

Roebeling, R.A., 2008. *Cloud physical properties retrieval for climate studies using SEVIRI and AVHRR data.* Thesis, Wageningen Universiteit, 2008, Wageningen, 158p.

Roebeling, R.A., A.J. Feijt and E. van Meijgaard, 2008. *Evaluation of the diurnal cycle of model predicted cloud properties using MSG-SEVIRI observations.* International Radiation Symposium (IRS2008), 3/8/2008-8/8/2008, 2008, Iguacu Falls, Brazil, IRS.

Rooy, W.C. de and A.P. Siebesma, 2008. *A simple parameterization for detrainment in shallow cumulus.* Mon. Wea. Rev., **136**.

Schmeits, M.J., C.J. Kok, D.H.P. Vogelezang and R.M. van Westrhenen, 2008. *Probabilistic forecasts of (severe) thunderstorms for the purpose of issuing a weather alarm in the Netherlands.* Weather and Forecasting, **23**.

Schutgens, N.A.J., W. Greuell and R.A. Roebeling, 2008. *Effect of inhomogeneity on the validation of SEVIRI LWP.* International Radiation Symposium (IRS2008), 3/8/2008-8/8/2008, 2008, Iguacu Falls, Brazil, IRS.

Steeneveld, G.J., T. Mauritsen, E.I.F. de Bruijn, J. Vila-Guerau de Arellano, G. Svensson and A.M.M. Holtslag, 2008. *Evaluation of limited area models for the representation of the diurnal cycle and contrasting nights in CASES99.* J. Appl. Meteor., **47**.

Sterl, A., C. Severijns, H. Dijkstra, W. Hazeleger, G.J. van Oldenborgh, M. van den Broeke, G. Burgers, B. van den Hurk, P.J. van Leeuwen and P. van Velthoven, 2008. *When can we expect extremely high surface temperatures?* Geophys. Res. Lett., **35**.

Tan, D.G.H., E. Andersson, J. de Kloe, G.J. Marseille, A. Stoffelen and et al., 2008. *The ADM-Aeolus wind retrieval algorithms.* Tellus, A, **60**.

Vu, V. Thieu, G.J. Cats and A. Wolters, 2008. *Asynchronous Communication in the HIRLAM weather Forecast.* ASCI, 2008.

Zagar, N., A. Stoffelen, G.J. Marseille, C. Accadia and P. Schlussel, 2008. *Impact Assessment of Simulated Wind Lidars with a Multivariate Variational Assimilation in the Tropics.* Mon. Wea. Rev., **136**.

2009

Bourassa, M., A. Stoffelen and et al., 2009. *Remotely sensed winds and wind stresses for marine forecasting and ocean modeling.* OceanObs'09, 21/9/2009-25/9/2009, M bourassa (Ed.), 2009, Venice, Italy, IGBP/GCOS/CLIVAR. Geertsema, G.T. and B.G.J. Wichers Schreur, 2009. *The effect of improved nowcasting of precipitation on air quality modeling.* Atmos. Environm., **43**.

Greuell, W. and R.A. Roebeling, 2009. *Towards a standard procedure for validation of satellite-derived cloud liquid water path: a study with SEVIRI data.* J. Appl. Meteor., **48**.
Haan, S. de, I. Holleman and A.A.M. Holtslag, 2009. *Real-Time Water Vapor Maps from a GPS Surface Network: Construction, Validation, and Applications.* J. Appl. Meteor., **48**.
Kudryavtsev, V.N. and V.K. Makin, 2009. *Model of the spume sea spray generation.* Geophys. Res. Lett., **36**.
Overeem, A., I. Holleman and T.A. Buishand, 2009. *Derivation of a 10-year radar-based climatology of rainfall.* J. Appl. Meteor., **48**.
Overeem, A., T.A. Buishand and I. Holleman, 2009. *Extreme rainfall analysis and estimation of depth-duration-frequency curves using weather radar.* Water Resour. Res., **45**.
Overeem, A., 2009. *Climatology of extreme rainfall from rain gauges and weather radar.* Thesis, Wageningen University, 2009, Wageningen, 144p.
Portabella, M. and A.C.M. Stoffelen, 2009. *On Scatterometer Ocean Stress.* J. Atm. Oceanic Technol., **26**.
Roebeling, R.A. and E. van Meijgaard, 2009. *Evaluation of the daylight cycle of model predicted cloud amount and condensed water path over Europe with observations from MSG-SEVIRI.* J. Climate, **22**.
Roebeling, R.A. and I. Holleman, 2009. *SEVIRI rainfall retrieval and validation using weather radar observations.* J. Geophys. Res., D2120, **114**.
Rontu, L., F. Obleitner, S. Gollvik, C. Zingerle and A.B.C. Tijm, 2009. *HIRLAM experiments on surface energy balance across Vatnajokull, Iceland.* Meteor. Atmos. Phys., **103**.
Schulz, J., H. Deneke, R. Roebeling, E. Wolters and et al., 2009. *Operational climate monitoring from space: the EUMETSAT satellite application facility on climate monitoring (CM-SAF).* Atm. Chem. Phys.
Schutgens, N.A.J. and R.A. Roebeling, 2009. *Validating the validation: the influence of liquid water distribution in clouds on the intercomparison of satellite and surface observations.* J. Atm. Oceanic Technol., **26**.
Slangen, A.B.A. and M.J. Schmeits, 2009. *Probabilistic forecasts of winter thunderstorms around Amsterdam Airport Schiphol.* Advances in Science and Research, **3**.
Verkley, W.T.M., 2009. *A balanced approximation of the one-layer shallow-water equations on a sphere.* J. Atmos. Sci., **66**.
Verkley, W.T.M. and P. Lynch, 2009. *Energy and enstrophy spectra of geostrophic turbulent flows derived from a maximum entropy principle.* J. Atmos. Sci., **66**.
Vogelzang, J., A. Stoffelen, A. Verhoef, J. de Vries and H. Bonekamp, 2009. *Validation of two-dimensional variational ambiguity removal on SeaWinds scatterometer data.* J. Atm. Oceanic Technol., 7, **26**.
Vries, J.W. de, 2009. *Probability Forecasts for Water Levels at the Coast of The Netherlands.* Marine Geodesy, **32**.
Vu, V.T., G.J. Cats and A.A. Wolters, 2009. *Automatic Code Generation For Finite Element Methods Applied To The Shallow-Water Equations*. 2009 International Conference on Scientific Computing (CSC 2009), 7/2009-7/2009, 2009, CSC, CSREA Press, 101-107.
Vu, V.T., G.J. Cats and A.A. Wolters, 2009. *Automatic Code Generation for Finite Element Methods Applied to the Shallow-Water Equations.* 15th annual conference of the Advanced School for Computing and Imaging, 3/6/2009-5/6/2009, 2009, Zeewolde.

Other publications

2007

Dabas, A., P. Poli, D. Tan, E. Andersson, A. Stoffelen, J. de Kloe and G.J. Marseille, 2007. *ADM-Aeolus Rayleigh-Brillouin Correction Look-up Tables Generator IODD.* ADM-Aeolus Level-2B/2C Processor development, ESA.
Gabarró, C., M. Portabella, M. Talone and J. Font, 2007. *Analysis of the SMOS ocean salinity inversion algorithm.* International Geoscience and Remote Sensing Symposium (IGARSS), 23/7/2007-27/7/2007, 2007, Barcelona, Spain, IEEE.
Holleman, I. and F. Kroonenberg, 2007. *Verificatie van de SODAR bij Kerncentrale Borssele.* KNMI Internal Report IR-2007-06, pp18.
Kloe, J. de, A. Stoffelen, K. Houchi, G.J. Marseille, E. Andersson, P. Poli, M.L. Denneulin, A. Dabas, D. Huber, O. Reitebuch, P. Flamant, O. Le Rille and H. Nett, 2007. *Development of ADM-Aeolus portable level 2B wind retrieval software.* EUMETSAT Meteorological Satellite Conference, 24/9/2007-28/9/2007, 2007, Amsterdam, EUMETSAT.
Kloe, J. de, D. Tan and D. Huber, 2007. *Aeolus Level 2b Processor Software Verification & Validation Plan.* ADM-Aeolus Level-2B/2C Processor development, ESA.
Koek, F.B. and M. Stam, 2007. *Van Turbo2 naar TurboWin (From Turbo2 to TurboWin).* Meteorologisch Informatiebulletin Maritiem, pp4.

Kudryavtsev, V.N. and V.K. Makin, 2007. *Aerodynamic roughness of the sea surface at high winds.* In Atmosheric Boundary Layers, Baklanov and Grisogono (Eds.), 2007, Springer, ISBN 978-0-387-74318-9, p133-148.

Marseille, G.J., 2007. *The added value of prospective spaceborne Doppler wind lidar for extreme weather events.* 29th EWGLAM and 14th SRNWP Meetings, 8/10/2007-11/10/2007, 2007, Dubrovnik.

Marseille, G.J., 2007. *Scheepswaarnemingen voor numerieke weersverwachting - zinvol of achterhaald?* Meteorologisch Informatiebulletin Maritiem, 73, 6-11.

Marseille, G.J., 2007. *Ship observations for numerical weather prediction - useful or redundant?* Meteorologisch Informatiebulletin Maritiem, 73, 6-11.

Masutani, M., A. Stoffelen, G.J. Marseille and et al., 2007. *Progress in Joint OSSES.* AMS 18th conference on Numerical Weather Prediction, 25/6/2007-29/6/2007, 2007, Parkcity UT, USA, AMS.

Meulen, J.P. van der, 2007. *The Challenge to Increase the Perfomance of an AWS.* Proceedings of the 4th ICEAWS, Lisboa, 24-26 May 2.

Meulen, J.P. van der, 2007. *Mistdetectie en signalering (Programma Gevaarlijk Weer, Project Verwachtingen voor mist en lage stratus).* KNMI Internal Report IR-2007-04, pp28.

North, S. and F.B. Koek, 2007. *Het Maritieme Waarnemers Logbook.* Meteorologisch Informatiebulletin Maritiem, pp3.

Portabella, M., A. Stoffelen, J. Vogelzang, A. Verhoef and J. Verspeek, 2007. *Towards a high-resolution ASCAT scatterometer wind product.* 19/11/2007, International Geoscience and Remote Sensing Symposium (IGARSS) (Ed.), 2007, Barcelona, Spain, IEEE.

Portabella, M., A. Stoffelen, A. Verhoef, J. Verspeek and J. Vogelzang, 2007. *Towards a high-resolution gridded ocean forcing.* EUMETSAT/AMS conference, 24/9/2007-28/9/2007, 2007, Amsterdam, The Netherlands, EUMETSAT .

Portabella, M., A. Stoffelen, J. Verspeek, A. Verhoef and J. Vogelzang, 2007. *ASCAT scatterometer ocean calibration.* International Geoscience and Remote Sensing Symposium (IGARSS), 23/7/2007-23/7/2007, 2007, Barcelona, Spain, IEEE.

Roebeling, R.A., A.J. Feijt and E. van Meijgaard, 2007. *Evaluation of the diurnal cycle of model predicted cloud liquid water path with MSG-SEVIRI observations.* EUMETSAT/AMS Met. Sat. Conference, 24/9/2007-28/9/2007, 2007, Amsterdam, Eumetsat.

Schmeits, M.J., C.J. Kok, D.H.P. Vogelezang and R.M. van Westrhenen, 2007. *Probabilistic 0-12 h forecasts of (severe) thunderstorms for the purpose of issuing a weather alarm.* In: KNMI Biennial scientific report 2005-2006, 2007.

Schmeits, M.J., C.J. Kok, D.H.P. Vogelezang and R.M. van Westrhenen, 2007. *Kansverwachtingen voor onweer ten behoeve van uitgifte Weeralarm (KOUW).* KNMI Internal Report IR-2007-03.

Stappers, R. and J. Barkmeijer, 2007. *Hirlam singular vectors.* Hirlam Newsletter, **52**, 79-83.

Stoffelen, A., 2007. *OSI SAF: Contributions to the analysis fo the ASCAT 3-dimensional measurement space (which inclusdes ASCAT CA/VAL Activities.* Draft report.

Stoffelen, A., 2007. *OSI SAF: Development of a global scatterometer validation and monitoring.* Final Report.

Stoffelen, A., G.J. van Oldenborgh, J. de Kloe, M. Portabella and A. Verhoef, 2007. *SOS - Development of a scatterometer ocean stress product.* CM SAF report.

Tan, D.G.H., E. Andersson, J. de Kloe, G.J. Marseille, A. Stoffelen, P. Poli, M.L. Denneulin, A. Dabas, D. Huber, O. Reitebuch, P. Flamant, O. Le Rille, A.G. Straume and H. Nett, 2007. *ADM-Aeolus Level-2B Wind Retrieval Algorithms.* 14th Bi-Annual Coherent Laser Radar Conference (CLRC), 9/7/2007-13/7/2007, 2007, Snowmass, Colorado USA, Universities Space Research Association (USRA).

Tan, D.G.H., E. Andersson, J. de Kloe, G.J. Marseille, A. Stoffelen, P. Poli, M.L. Denneulin, A. Dabas, D. Huber, O. Reitebuch, P. Flamant, O. Le Rille and H. Nett, 2007. *The ADM-Aeolus wind retrieval algorithms.* 2007, ECMWF, Technical Memorandum, 27p.

Verhoef, A., A. Stoffelen, M. Portabella, J. Verspeek and J. Vogelzang, 2007. *EUMETSAT SAF and EARS scatterometer wind services at KNMI.* EUMETSAT/AMS conference, 24/9/2007-28/9/2007, 2007, Amsterdam, The Netherlands, EUMETSAT.

Verhoef, A. and A. Stoffelen, 2007. *ERS Scatterometer Product User Manual version 1.3.* KNMI-publicatie ; 212c, EUMETSAT.

Verhoef, A. and A. Stoffelen, 2007. *ASCAT Wind Product User Manual version 1.0.* SAF/OSI/CDOP/KNMI/TEC/MA/126, EUMETSAT.

Verhoef, A. and A. Stoffelen, 2007. *ERS Scatterometer Product User Manual version 1.4.* KNMI-publicatie ; 212d, EUMETSAT.

Verhoef, A. and A. Stoffelen, 2007. *ASCAT Wind Product User Manual version 1.1.* SAF/OSI/CDOP/KNMI/TEC/MA/126, EUMETSAT.

Verhoef, A. and A. Stoffelen, 2007. *ERS Scatterometer Product User Manual version 1.5.* KNMI-publicatie ; 212e, EUMETSAT.

Verhoef, A. and A. Stoffelen, 2007. *SeaWinds Product Manual version 1.4.* SAF/OSI/CDOP/KNMI/TEC/MA/134, EUMETSAT.

Verhoef, A. and A. Stoffelen, 2007. *ASCAT Wind Product User Manual version 1.2.* SAF/OSI/CDOP/KNMI/TEC/MA/126, EUMETSAT.

Verhoef, A. and A. Stoffelen, 2007. *ASCAT Wind Product User Manual version 1.3.* SAF/OSI/CDOP/KNMI/TEC/MA/126, EUMETSAT.

Verhoef, A., J. Vogelzang and A. Stoffelen, 2007. *AWDP User Manual and Reference Guide version 1.0k.* NWPSAF-KN-UD, EUMETSAT.

Verspeek, J., A. Stoffelen, M. Portabella, A. Verhoef and J. Vogelzang, 2007. *ASCAT scatterometer cal/val and winds.* EUMETSAT/AMS conference, 24/9/2007-28/9/2007, 2007, Amsterdam, The Netherlands, EUMETSAT.

Vitart, J.F. and J. Barkmeijer, 2007. *Organized convection and weather prediction on sub-seasonal time-scales.* BAMS.

Vogelzang, J., A. Stoffelen, M. Portabella, A. Verhoef and J. Verspeek, 2007. Mesoscale winds over the oceans. EUMETSAT/AMS conference, 24/9/2007-28/9/2007, 2007, Amsterdam, The Netherlands, EUMETSAT.

Vogelzang, J., 2007. *Two dimensional variational ambiguity removal (2DVAR).* Technical report NWPSAF-KN-TR-004, EUMETSAT.

Vogelzang, J., 2007. *Validation of 2DVAR on SeaWinds data.* Technical Report NWPSAF-KN-TR-005, EUMETSAT.

Wijngaard, J.B., D.H.P. Vogelezang, J. van Bruggen and N. Maat, 2007. *Low visibility and ceiling forecasts at Schiphol; Part 1-assessment of the current system.* pp30. (Wijngaard is a staff member of the Product and Process Innovation Division, for which in this report no separate list of publications is presented).

2008

Barkmeijer, J., F. Vitart, M. Leutbecher, T. Jung and J.O. Hooghoudt, 2008. *The Stratosphere-Troposphere connection in ensemble forecasting.* Workshop on Ensemble Prediction, 7/11/2007-9/11/2007, 2008, Reading, ECMWF.

Bruijn, E.I.F. de and A.B.C. Tijm, 2008. *Overall tuning of the turbulence scheme of HIRLAM with the focus on the stable boundary layer.* HIRLAM Newsletter, 53, 32-36.

Burgers, G., F. Koek, J.W. de Vries and M. Stam, 2008. *Searching for Factors that Limit Observed Extreme Maximum Wave Height Distributions in the North Sea.* In Extreme Ocean Waves, E. Pelinovksy, C. Kharif (Eds.), 2008, Springer.

Cats, G.J., 2008. *Numerieke weersverwachtingen.* Eureka!, 21, 4-7.

Cats, G.J., 2008. *24 More Years of Numerical Weather Prediction: A Model Performance Model.* KNMI Scientific Report WR-2008-1.

Dekker, A., H. van Gasteren, W. Bouten, J. Shamoun-Baranes, A. Borst, I. Holleman, A. Dokter, A. Ginati and G. Garofalo, 2008. *The European Space Agency's FlySafe project, looking at the bird strike problem from another perspective.* 28th Meeting of International Bird Strike Committee, 10/2008, 2008, Brazilie, IBSC.

Geertsema, G.T., S. Calabretta-Jongen and H. Eskes, 2008. *Daily air quality forecasts, experiences with CHIMERE interfacing to HIRLAM data.* HIRLAM Newsletter, 53, 79-86.

Holleman, I., L. Delobbe and A. Zgonc, 2008. *Update on the European Weather Radar Network (OPERA).* WMO Technical Conference (TECO 2008), 11/2008, 2008, St. Petersburg, WMO.

Holleman, I., L. Delobbe and A. Zgonc, 2008. *The European Weather Radar Network (OPERA): An opportunity for hydrology!.* Weather Radar and Hydrology 2008, 10/3/2008, 2008, Grenoble.

Holleman, I., L. Delobbe and A. Zgonc, 2008. *Update on the European Weather Radar Network (OPERA).* ERAD 5, 30/6/2008-4/7/2008, 2008, Helsinki.

Holleman, I., 2008. *Wind observations with Doppler weather radar.* ERAD 5, 30/6/2008-4/7/2008, 2008, Helsinki.

Holleman, I., A. Huuskonen, M. Kurri and H. Beekhuis, 2008. *Monitoring of weather radar receivers using solar signals detected in operational scan data.* WMO Technical Conference (TECO 2008), 11/2008, 2008, St. Petersburg, WMO.

Hove, R. ten and J.B. Wijngaard (Eds.), Improved Low visibility and Ceiling Forecasts at Schiphol Airport, KNMI-publicatie: KDC/2008/0089 - KNMI publication 222, 7/2008.

Holleman, I., 2008. *Wind observations with Doppler weather radar.* WMO Technical Conference (TECO 2008), 11/2008, 2008, St. Petersburg, WMO.

Holleman, I., 2008. *Dopplerwaarnemingen met buienradar.* Nederlands Tijdschrift voor Natuurkunde, **9**, 304-308.

Holleman, I., 2008. *Echotops for annotation on radar imagery*. KNMI Technical Report TR-299, pp28.

Kloe, J. de, G.J. Marseille and A. Stoffelen, 2008. *Vertical Aeolus Measurement Positioning,Technical note TN1, v.1.0.* Vertical Aeolus Measurement Positioning, TN1, V1.0, KNMI.

Kloe, J. de, A. Stoffelen and P. Poli, 2008. *Aeolus Level 2b Processor Product Specification.* SAF documentation on ADM-Aeolus L2Bp development, KNMI.

Kloe, J. de, 2008. *The ADM Atmospheric database.* ADM-Aeolus Level-2B/2C Processor development, ESA.

Kloe, J. de, P. Poli and D. Tan, 2008. *Aeolus Level 2b Processor Top Level Design.* SAF documentation on ADM-Aeolus L2Bp development, KNMI.

Kloe, J. de and A. Stoffelen, 2008. *ADM-Aeolus, Ocean albedo, v.1.0.* Technical note on Ocean Albedo as a function of local wind and wave conditions and its effect on the zero-wind calibration., KNMI.

Kloe, J. de, 2008. *Aeolus Level 2b Processor Users Guide.* L2BP Users Guide, ESA.

Kloe, J. de and A. Stoffelen, 2008. *ADM-Aeolus Mission, Guide on applying L2B processed winds.* SAF documentation on ADM-Aeolus L2Bp development, KNMI.

Leijnse, H., R. Uijlenhoet and I. Holleman, 2008. *Sources of error in microwave link rainfall estimation.* Weather Radar and Hydrology 2008, 6/2/2008, 2008.

Liechti, F., A. Dokter, J. Shamoun-Baranes, H. van Gasteren and I. Holleman, 2008. *Combining radar systems to get a 3D – picture of the bird migration.* 28th Meeting of International Bird Strike Committee, 10/2008, 2008, Brazilie, IBSC.

Masutani, M., A. Stoffelen, G.J. Marseille and et al., 2008. *Progress in Joint OSSEs - Three Joint OSSE nature runs and simulation of observation.* 12th Conference on IOAS - AOLS, 20/1/2008-24/1/2008, 2008, New Orleans, LA, USA, AMS, AMS.

Masutani, M., A. Stoffelen, G.J. Marseille and et al., 2008. *Progress in Joint OSSEs - Three Joint OSSE nature runs and simulation of observation.* 88th AMS annual meeting 2008, 20/1/2008-24/1/2008, 2008, New Orleans, AMS.

Overeem, A., I. Holleman and A. Buishand, 2008. *A 10-year Radar-based Climatology of Rainfall.* ERAD 5, 30/6/2008-4/7/2008, 2008, Helsinki.

Poli, P., A. Dabas, D. Tan, E. Andersson, J. de Kloe and G.J. Marseille, 2008. *ADM-Aeolus Level-2b Processor Test Plan.* ADM-Aeolus Level-2b Processor Test Plan, ESA.

Poli, P., J. de Kloe and D. Tan, 2008. *ADM-Aeolus Level-2B processor Input/Output Fortran structures description.* SAF documentation on ADM-Aeolus L2Bp development, KNMI.

Roebeling, R. and I. Holleman, 2008. *Validation of Rain Rate Retrievals from SEVIRI using Weather Radar Observations.* EUMETSAT Meteorological Satellite Conference, 9/2008, 2008, Darmstadt, EUMETSAT.

Slangen, A., 2008. *Probabilistic forecasts of winter thunderstorms around Schiphol Airport using Model Output Statistics.* KNMI Technical Report TR-300, pp55.

Stappers, R.J.J. and J. Barkmeijer, 2008. *Hirlam CAPE singular vectors.* Hirlam Newsletter, 54.

Stappers, R.J.J., 2008. *De voorspelbaarheid van diepe convectie.* Meteorologica, **17**, 4.

Stoffelen Ad, 2008. *ON IMPROVED MESOSCALE FORCING*. EuroGOOS, 20/5/2008-22/5/2008, 2008, Exeter, UK, EuroGOOS,.

Stoffelen Ad, Marcos Portabella, Anton Verhoef, Jeroen Verspeek and Jur Vogelzang, 2008. *Advancements in Scatterometer Wind Processing.* 9th International Winds Workshop, 14/4/2008-18/4/2008, 2008, Annapolis, Maryland, USA, NOAA, EUMETSAT.

Stoffelen Ad, Marcos Portabella, Anton Verhoef and Jur Vogelzang, 2008. *ON HIGH RESOLUTION COASTAL WINDS.* EuroGOOS, 20/5/2008-22/5/2008, 2008, Exeter, UK, EuroGOOS,.

Stoffelen, A., M. Portabella, A. Verhoef, J. Verspeek and J. Vogelzang, 2008. *HIGH-RESOLUTION ASCAT SCATTEROMETER WINDS NEAR THE COAST.* International Geoscience and Remote Sensing Symposium (IGARSS), 6/7/2008-11/7/2008, 2008, Boston, USA, IEEE.

Stoffelen, A.C.M., G.J. Marseille, J. de Kloe, K. Houchi, H. Körnich and N. Žagar, 2008. *SCIENTIFIC PREPARATIONS FOR AEOLUS AND AEOLUS FOLLOW-ON.* 9th International Winds Workshop, 14/4/2008-18/4/2008, 2008, Annapolis, maryland, USA, NOAA, EUMETSAT.

Stoffelen, A. and J. de Kloe, 2008. *Science Plan, improved wind profile assimilation procedure for ADM-Aeolus.* SAF documentation on ADM-Aeolus L2Bp development, KNMI.

Stoffelen, A., G.J. Marseille, J. de Kloe, A. Dabas, D. Huber, O. Reitebuch, P. Flamant and D. Tan, 2008. *Comparison of Aeolus burst and continuous mode concepts.* TN 5.1, burst vs. continuous, ESA.

Tan, D.G.H., E. Andersson, J. de Kloe, G.J. Marseille, A. Stoffelen, P. Poli, A. Dabas, D. Huber, O. Reitebuch, P. Flamant, A.G. Straume, O. Le Rille and H. Nett, 2008. *ADM-AEOLUS WIND RETRIEVAL ALGORITHMS FOR NWP.* 9th International Winds Workshop (9IWW), 14/4/2008-18/4/2008, 2008, Annapolis, Maryland, USA, NOAA/NESDIS/EUMETSAT/CIMSS.

Tan, D., E. Andersson, A. Dabas, P. Poli, A. Stoffelen, J. de Kloe and D. Huber, 2008. *ADM-Aeolus Level-2B/2C Processor Input/Output Data Definitions Interface Control Document.* L2BP IODD, ESA.

Tijm, A.B.C., 2008. *Intercomparison of STRACO and KF-RK.* HIRLAM Newsletter, 53, 13-24.

Tijm, A.B.C., 2008. *HIRLAM physics changes and importance for ACT modelling.* Summer school on ACT modelling, 6/7/2008-10/7/2008, 2008, Zelenogorsk, NetFAM, COST 728.

Tijm, A.B.C., 2008. *Vertical diffusion*. In NetFAM, COST 728 summer school on HIRLAM and ACT, Baklanov & Mahura (Eds.), 2008.

Tijm, A.B.C., 2008. *Overview of contents HIRLAM system.* In NetFAM, COST 728 summer school on HIRLAM and ACT, Baklanov & Mahura (Eds.), 2008.

Tijm, A.B.C., 2008. *HIRLAM strategy on ACT modelling.* NetFAM, COST 728 summer school on HIRLAM and ACT, 6/7/2008-10/7/2008, Baklanov & Mahura (Eds.), 2008.

Tijm, A.B.C., 2008. *Strategy on HARMONIE physics developments.* Beschrijving van strategie voor mesoschaal fysica ontwikkeling HARMONIE.

Verhoef, A. and A. Stoffelen, 2008. SeaWinds Product Manual version 1.5. SAF/OSI/KNMI/TEC/MA/134, EUMETSAT.

Verhoef, A., J. Vogelzang and A. Stoffelen, 2008. Validation of SeaWinds 25 km winds. SAF/OSI/CDOP/KNMI/TEC/RP/143, EUMETSAT.

Verhoef, A. and A. Stoffelen, 2008. ASCAT Wind Product User Manual version 1.4. SAF/OSI/KNMI/TEC/MA/126, EUMETSAT.

Verhoef, A., M. Portabella, A. Stoffelen and H. Hersbach, 2008. *CMOD5.n - the CMOD5 GMF for neutral winds.* SAF/OSI/CDOP/KNMI/TEC/TN/165, EUMETSAT.

Verhoef, A., J. Vogelzang, J. Verspeek and A. Stoffelen, 2008. *AWDP Test Report, version 1.0.14.* NWPSAF-KN-TV-005, EUMETSAT.

Verhoef, A. and A. Stoffelen, 2008. *ASCAT Wind Product User Manual version 1.5.* SAF/OSI/CDOP/KNMI/TEC/MA/126, EUMETSAT.

Verhoef, A. and A. Stoffelen, 2008. *ERS Scatterometer Product User Manual version 1.6.* KNMI-publicatie ; 212f, EUMETSAT.

Verhoef, A., J. Vogelzang, J. Verspeek and A. Stoffelen, 2008. AWDP User Manual and Reference Guide, version 1.0.16. NWPSAF-KN-UD-005, EUMETSAT.

Verspeek, J., A. Stoffelen, M. Portabella, A. Verhoef and J. Vogelzang, 2008. *Ascat scatterometer ocean calibration.* International Geoscience and Remote Sensing Symposium (IGARSS), 6/7/2008-11/7/2008, 2008, Boston, USA, IEEE.

Verspeek, J., M. Portabella, A. Stoffelen and A. Verhoef, 2008. *Calibration and Validation of ASCAT Winds, version 4.0.* SAF/OSI/KNMI/TEC/TN/163, EUMETSAT.

Vogelezang, D. and K. Kok, 2008. *Kansen in de weersverwachting.* Euclides, **83**, 4, 204-207.

Vogelzang, J., 2008. *SDP 2.0 validation.* NWPSAF-KN-TR-006, EUMETSAT.

Vogelzang, J., A. Verhoef and A. Stoffelen, 2008. *AWDP 1.0 validation, version 1.0.* NWPSAF-KN-TR-020, EUMETSAT.

Vries, J.W. de, 2008. *Probability forecasts for water levels at the coast of the Netherlands.* ECMWF Newsletter, **114**, 23-29.

Wichers Schreur, B. and G. Geertsema, 2008. *Theory for a TKE based parameterization of wind gusts.* HIRLAM newsletter, 54, 177-188.

Zweers, N.C., 2008. *Atmosfeer-oceaan interactie bij extreem weer.* Meteorologica, **17**, 4.

2009

Barkmeijer, J., 2009. *Adjoint diagnostics for the atmosphere and ocean.* Diagnosis of Forecasting and Data Assimilation Systems, 20/11/2009, 2009, Reading (UK), ECMWF.

Barkmeijer, J., 2009. Adjoint diagnostics for the atmosphere and ocean. Diagnosis of Forecasting and Data Assimilation Systems, 7/9/2009-10/9/2009, 2009, Reading (UK), ECMWF.

Carbajal Henken, C.K., M.J. Schmeits, E.L.A. Wolters and R.A. Roebeling, 2009. Detection of Cb and TCu clouds using MSG-SEVIRI cloud physical properties and weather radar observations. KNMI Scientific Report WR-2009-04.

Dabas, A., A. Stoffelen, G.J. Marseille, J. de Kloe and D. Huber, 2009. *TN3.1b, Test results for the L2B processor, v0.1.* ADM-Aeolus simulation and processing test results, v0.1, ESA.

Egger, G. and M. Belmonte Rivas, 2009. *Post-EPS Competing Scatterometer Designs: ASCAT versus RFSCAT.* ARSI - Advanced RF Sensors and Remote Sensing Instruments, 16/11/2009-18/11/2009, 2009, Noordwijk (The Netherlands), European Space Agency.

Geertsema, G.T. and B.G.L. Wichers Schreur, 2009. *Evaluation of diabatic initialization improvements in the numerical weather prediction model Hirlam.* AQ7: 7th international conference on Air Quality, 24/3/2009-27/3/2009, 2009, Istanbul, AQ7, ISBN 978-1-905313-64-8, 747-750.

Kloe, J. de, A. Stoffelen, G.J. Marseille, D. Tan, L. Isaksen, C. Desportes, C. Payan, A. Dabas, D. Huber, O. Reitebuch, P. Flamant, H. Nett, O. le Rille and A.G. Straume, 2009. *ADM-Aeolus Ocean Surface Calibration and Level-2B Wind-Retrieval Processing.* International Symposium on Tropospheric Profiling (ISTP2009), 19/10/2009-23/10/2009, 2009, Delft, RIVM, KNMI, TU-Delft, only published online (www.istp2009.nl), not on paper.

Kloe, J. de, G.J. Marseille and A. Stoffelen, 2009. *ADM-Aeolus, VAMP, Vertical Aeolus Measurement Positioning, TN3, v0.3.* ADM-Aeolus VAMP quality control possibilities, ESA.

Kloe, J. de and A. Stoffelen, 2009. *A SPONTANEOUS RAYLEIGH-BRILLOUIN SCATTERING EXPERIMENT FOR THE CHARACTERIZATION OF ATMOSPHERIC LIDAR BACKSCATTER (TN4 part 3).* ADM-Aeolus Brillouin project, TN4, part 3, ESA.

Kloe, J. de, G.J. Marseille and A. Stoffelen, 2009. *ADM-Aeolus, VAMP, Task 4:Quantification of L2B HLOS wind accuracies for typical wind shear, aerosol and cloud conditions.* VAMP TN3, ESA.

Kok, K. and D. Vogelezang, 2009. *Warning system of extreme precipitation for the Dutch water boards.* Proceedings of the Joint MAP D-PHASE Scientific Meeting - COST731 mid-term seminar. Challenges in hydromeorological forecasting in complex terrain, 19/5/2008-22/5/2008, Andrea Montani et al. (Eds.), 2009, Bologna, ARPA-SIM en COST, 22-27.

Marseille, G.J., A. Stoffelen, J. de Kloe, K. Houchi, H. Kornich, H. Schyberg, A.G. Straume and O. LeRille, 2009. *ADM-Aeolus vertical sampling scenarios.* International Symposium on Tropospheric Profiling (ISTP), 19/10/2009-23/10/2009, 2009, Delft, KNMI - TU Delft - RIVM.

Marseille, G.J., A. Stoffelen, J. de kloe, H. Schyberg, H. Kornich, A.G. Straume-Lindner, O. LeRille and K. Houchi, 2009. *ADM-Aeolus vertical sampling scenarios.* ISTP - International Symposium on Troposheric Profiling, 19/10/2009-23/10/2009, 2009, Delft, KNMI/RIVM/TU-Delft.

Masutani, M., Ad Stoffelen, G.-J. Marseille and et al., 2009. *Expa nding collaboration in Joint OSSES.* AMS 13th Conference on Integrated Observing and Assimilation Systems for the Atmosphere, Oceans, and Land Surface, 11/1/2009-15/1/2009, 2009, Phoenix AZ, AMS, 13.

Placidi, S., D.P. Donovan, R. Roebling and H.W.J. Russchenberg, 2009. *Organizing Committee of the 8th International Symposium on Tropospheric Profiling.* 8th ISTP, 19/10/2009, A. Apituley, H.W.J. Russchenberg, W.A.A. Monna (Eds.), 2009, Delft, Delft/KNMI/RIVM, Organizing Committee of the 8th International Symposium on Tropospheric Profiling, ISBN 978-90-6960-2.

Overeem, A., I. Holleman and T.A. Buishand, 2009. *Neerslagklimatologie uit weerradar.* H_2O, **42**, 8, 31-33.

Roebeling, R.A., H. Deneke, W. Greuell and N.A.J. Schutgens, 2009. *Towards a Standard Procedure for Validation of Satellite Derived Cloud Properties with Ground-Based Observations.* Hyperspectral Imaging and Sounding of the Environment (HISE) Topical Meeting, 27/4/2009-30/4/2009, 2009, Vancouver, Canada, OSA.

Stoffelen, A., 2009. *ADM-Aeolus Quasi Real-Time and Near Real-Time Wind Profiles.* 2009, EUMETSAT, EUMETSAT STG-SWG, 8p.

Tan, D., E. Andersson, P. Poli, A. Dabas, J. de Kloe, G.J. Marseille and A. Stoffelen, 2009. *ADM-AEOLUS Level-2B Algorithm Theoretical Baseline Document, v2.2.* ADM-Aeolus Level-2B/2C Processor ATBD, v2.2, ESA.

Verhoef, A. and A. Stoffelen, 2009. *Validation of ASCAT 12.5-km winds, version 1.1.* SAF/OSI/CDOP/KNMI/TEC/RP/147, EUMETSAT.

Verhoef, A. and A. Stoffelen, 2009. *ASCAT Wind Product User Manual version 1.6.* SAF/OSI/CDOP/KNMI/TEC/MA/126, EUMETSAT.

Verhoef, A. and A. Stoffelen, 2009. *Validation of ASCAT 12.5-km winds, version 1.2.* SAF/OSI/CDOP/KNMI/TEC/RP/147, EUMETSAT.

Verhoef, A. and A. Stoffelen, 2009. *ASCAT Wind Product User Manual version 1.7.* SAF/OSI/CDOP/KNMI/TEC/MA/126, EUMETSAT.

Verhoef, A. and A. Stoffelen, 2009. *SeaWinds Product User Manual version 1.6.* SAF/OSI/KNMI/TEC/MA/134, EUMETSAT.

Verspeek, J.A. and A. Stoffelen, 2009. *ASCAT tandem coverage.* OSISAF, KNMI.

Vogelzang, J., A. Stoffelen, M. Belmonte rivas, A. Verhoef and J. Verspeek, 2009. *The quality of the ASCAT 12.5 km wind product.* EUMETSAT Meteorological Satellite Conference, 14/9/2009-18/9/2009, 2009, Bath, UK, EUMETSAT, EUMETSAT.

Vu, V.T., G.J. Cats and A.A. Wolters, 2009. *Overlapping Communications With Calculations.* International Conference on Parallel and Distributed Processing Techniques and Applications Distributed Processing Techniques and Applications487-4, 7/2009-7/2009, 2009, PDPTA 2009, CSREA Press, 487-493.

Wallbrink, H. and F.B. Koek, 2009. *Historical Maritime Wind Scales until 1947.* 2009, KNMI, HISKLIM, 20p.

Wallbrink, H. and F.B. Koek, 2009. *Historical wind speed equivalents of the Beaufort scale, 1850-1950. 2009,* KNMI, HISKLIM, 29p.

Wallbrink, H. and F.B. Koek, 2009. *HISKLIM-COADS, final report..* KNMI Publication PUBL-210, ISBN 90-369-2269-0, pp22.

Wallbrink, H., F.B. Koek and T. Brandsma, 2009. *The US Maury Collection Metadata 1796-1861.* KNMI Publication PUBL-225, pp59.

Woodruff, S.D., E. Freeman, C. Wilkinson, R. Allan, H. Anderson, P. Brohan, G. Compo, S. Claesson, F.B. Koek, S. Lubker, C. Marzin, T. Ross, M. Seiderman, D. Wheeler and S. Worley, 2009. *ICOADS Marine Data Rescue: Status and Future CDMP Priorities.*

Publications Climate Observations

The Climate Observations division employs satellite observations to study the earth system. Current research topics are atmospheric composition in relation to climate, air quality and stratospheric ozone.

Reviewed publications

2007

Balis, D., M. Kroon, M. Koukouli, E.J. Brinksma, G. Labow, J.P. Veefkind and R. McPeters, 2007. *Validation of Ozone Monitoring Instrument total ozone column measurements using Brewer and Dobson spectrophotometer groundbased observations.* J. Geophys. Res., **112**.

Boersma, K.F., H.J. Eskes, J.P. Veefkind, E.J. Brinksma, R.J. van der A, M. Sneep, G.H.J. van den Oord, P.F. Levelt, P. Stammes, J.F. Gleason and E.J. Bucsela, 2007. *Near-real time retrieval of tropospheric NO_2 from OMI.* Atm. Chem. Phys., 2013-2118,.

Carn, S.A., A.J. Krueger, N.A. Krotkov, K. Yang and P.F. Levelt, 2007. *Sulfur dioxide emissions from Peruvian copper smelters detected by the Ozone Monitoring Instrument.* Geophys. Res. Lett., **34**.

Hilsenrath, E., M.R. Schoeberl, A.R. Douglass, P.K. Bhartia, J. Barnett, R. Beer, J. Waters, M. Gunson, L. Froidevaux, J. Gille and P.F. Levelt, 2007. *Early data from Aura and continuity from UARS and TOMS. 2007*, Solar Variability and Planetary Climates; Space science series of ISSI, Springer, ISBN 978-0-387-48339-9.

Kroon, M., M.R. Dobber, R. Dirksen, J.P. Veefkind, G.H.J. van den Oord and P.F. Levelt, 2007. *Ozone Monitoring Instrument Geolocation Verification*. J. Geophys. Res..

Kroon, M., J.P. Veefkind, M. Sneep, R.D. McPeters, P.K. Bhartia and P.F. Levelt, 2007. *Comparing OMI-TOMS and OMI-DOAS total ozone column data.* J. Geophys. Res.

Laat, A.T.J. de, 2007. *Mixing Politics and Science in Testing the Hypothesis that Greenhouse Warming is Causing a Global Increase in Hurricane Intensity.* Bull. Amer. Meteor. Soc., **88**, 2, 251-252.

Laat, A.T.J. de, J. Landgraf, O. Hasekamp, I. Aben and B. Bregman, 2007. *Validation of GOME ozone profiles and evaluation of stratospheric transport in a global chemistry-transport model.* J. Geophys. Res., **112**.

Laat, A.T.J. de, A.M.S. Gloudemans, I. Aben, J.F. Meirink, M. Krol, G. van der Werf and H. Schrijver, 2007. *SCIAMACHY carbon monoxide total columns: Statistical evaluation and comparison with CTM results.* J. Geophys. Res., **112**.

Laat, A.T.J. de et al., 2007. *correction to SCIAMACHY Carbon Monoxide total columns: Statistical evaluation and comparison with CTM results.* J. Geophys. Res., **112**.

Schoeberl, M.R., J.R. Ziemke, B. Bojkov, N. Livesey, P.F. Levelt, M. Allaart and H.M. Kelder, 2007. *A trajectory-based estimate of the tropospheric ozone column using the residual method.* J. Geophys. Res., **112**.

Shavrina, A.V., Y.V. Pavlenko, A. Veles, I. Syniavskyi and M. Kroon, 2007. *Ozone columns obtained by ground-based remote sensing in Kiev for Aura Ozone Measuring Instrument validation.* J. Geophys. Res.

Teyssèdre, H., M. Michou, H.L. Clark, B. Josse, F. Karcher, D. Olivié, V.H. Peuch, D. Saint-Martin, D. Cariolle, J.L. Attié, P. Nédélec, P. Ricaud, V. Thouret, R.J. van der A and A. Volz-Thomas, 2007. *A new tropospheric and stratospheric Chemistry* *and Transport Model* MOCAGE*-Climat for multi-year studies: evaluation of the present-day climatology and sensitivity to surface processes*. Atm. Chem. Phys., **7**, 22, 5815-5860.

Tilstra, L.G. and P. Stammes, 2007. *Earth reflectance and polarization intercomparison between* SCIAMACHY *on Envisat and* POLDER *on* ADEOS*-2*. J. Geophys. Res., **112**.

Wang, Y., M.B. McElroy, K.F. Boersma, H.J. Eskes and J.P. Veefkind, 2007. *Traffic restrictions associated with the Sino-African summit: Reductions of NO_x detected from space.* Geophys. Res. Lett., **34**, L08814.

2008

A, R.J. van der, H.J. Eskes, K.F. Boersma, T.P.C. van Noije, M. Van Roozendael, I. De Smedt, D.H.M.U. Peters, J.J.P. Kuenen and E.W. Meijer, 2008. *Identification of NO_2 sources and their trends from space using seasonal variability analyses.* J. Geophys. Res., **113**.

Boersma, K.F., D.J. Jacob, E.J. Bucsela, A.E. Perring, R. Dirksen, R.J. van der A, R.M. Yantosca, R.J. Park, M.O. Wenig, T.H. Bertram and R.C. Cohen, 2008. *Validation of* OMI *tropospheric NO2 observations during* INTEX*-B and application to constrain NO_x emissions over the eastern United States and Mexico.* Atmos. Environm., **42**, 4480-4497.

Boersma, K.F., D.J. Jacob, H.J. Eskes, R.W. Pinder, J. Wang and R.J. van der A, 2008. *Intercomparison of* SCIAMACHY *and* OMI *tropospheric NO_2 columns: observing the diurnal evolution of chemistry and emissions from space.* J. Geophys. Res., **113**, 1-14.

Boesche, E., P. Stammes, R. Preusker, R. Bennartz, W. Knap and J. Fischer, 2008. *Polarization of skylight in the O2A band: effects of aerosol properties.* Appl. Optics, **47**, 3467-3480.

Boesche, E., P. Stammes and R. Bennartz, 2008. *Aerosol Influence on Polarization and Intensity in Near-Infrared O_2 and CO_2 Absorption Bands Observed from Space.* J. Quant. Spectros. Rad. Transf.

Brinksma, E.J., G.J. Pinardi, R. Braak, H. Volten, A. Richter, R.J. Dirksen, T. Vlemmix, D.P.J. Swart, W.H. Knap, J.P. Veefkind, H.J. Eskes, M. Allaart, R. Rothe, A.J.M. Piters and P.F. Levelt, 2008. *The 2005 and 2006* DANDELIONS *NO_2 and Aerosol Intercomparison Campaigns.* J. Geophys. Res.

Bucsela, E.J., A.E. Perring, R.C. Cohen, K.F. Boersma, E.A. Celarier, J.F. Gleason, M.O. Wenig, T.H. Bertram, P.J. Wooldridge, R. Dirksen and J.P. Veefkind, 2008. *Comparison of tropospheric NO_2 from in situ aircraft measurements with near-real-time and standard product data from* OMI*.* J. Geophys. Res., **113**.

Celarier, E., E.J. Brinksma, J.P. Veefkind, D.P.J. Swart, H. Volten, M. Kroon and P.F. Levelt, 2008. *Validation of Ozone Monitoring Instrument Nitrogen Dioxide Columns.* J. Geophys. Res., **113**.

Dobber, M., Q. Kleipool, R. Dirksen, P.F. Levelt, G. Jaross, S. Taylor, T. Kelly, L. Flynn, G. Leppelmeier and N. Rozemeijer, 2008. *Validation of Ozone Monitoring Instrument level 1b data products.* J. Geophys. Res., **113**.

Dobber, M., R. Voors, R. Dirksen, Q. Kleipool and P. Levelt, 2008. *The high-resolution solar reference spectrum between 250 and 550 nm and its application to measurements with the Ozone Monitoring Instrument.* Solar Physics, **249**, 281-291.

Frankenberg, C., P. Bergamaschi, A. Butz, S. Houweling, J.F. Meirink, J. Notholt, A.K. Petersen, H. Schrijver, T. Warneke and I. Aben, 2008. *Tropical methane emissions: A revised view from* SCIAMACHY *onboard* ENVISAT*.* Geophys. Res. Lett., **35**.

Ghude, S.D., S. Fadnavis, G. Beig, Y.K. Tiwari, R.J. van der A, S.D. Polade and S. Shau, 2008. *Detection of surface emission hotspots, trends and seasonal cycle from satellite-retrieved NO_2 over India.* J. Geophys. Res., **113**.

Hassinen, S., J. Tamminen, A. Tanskanen, G. Leppelmeier, A. Mälkki, T. Koskela, J.M. Karhu, K. Lakkala, P. Veefkind, N. Krotkov and O. Aulamo, 2008. *Description and validation of the* OMI *very fast delivery products.* J. Geophys. Res., **113**.

Ionov, D., Y.M. Timofeyev, V.P. Sinyakov, V.K. Semenov, F. Goutail, J.P. Pommereau, E.J. Bucsela, E.A. Celarier and M. Kroon, 2008. *Ground-based validation of* EOS*-Aura* OMI *NO_2 vertical column data in the midlatitude mountain ranges of Tien Shan (Kyrgyzstan) and Alps (France).* J. Geophys. Res., **113**.

Kleipool, Q.L., M.R. Dobber, J.F. de Haan and P.F. Levelt, 2008. *Earth surface reflectance climatology from 3 years of* OMI *data.* J. Geophys. Res., **113**.

Krol, M.C., J.F. Meirink, P. Bergamaschi, J.E. Mak, D. Lowe, P. Joeckel, S. Houweling and T. Roeckmann, 2008. *What can 14CO measurements tell us about OH?.* Atm. Chem. Phys., **8**, 5033-5044.

Kroon, M., M.R. Dobber, R. Dirksen, J.P. Veefkind, G.H.J. van den Oord and P.F. Levelt, 2008. *Ozone Monitoring Instrument Geolocation Verification.* J. Geophys. Res., **113**.

Kroon, M., J.P. Veefkind, M. Sneep, R.D. McPeters, P.K. Bhartia and P.F. Levelt, 2008. *Comparing* OMI*-*TOMS *and* OMI*-*DOAS *total ozone column data.* J. Geophys. Res., **113**.

Kroon, M., I. Petropavlovskikh, R. Shetter, S. Hall, K. Ullman, J.P. Veefkind, R.D. McPeters and P.F. Levelt, 2008. OMI *total Ozone Column Validation with Aura-*AVE CAFS *Observations.* J. Geophys. Res., **113**.

Krotkov, N.A., B. McClure, R.R. Dickerson, S.A. Carn, C. Li, P.K. Bhartia, K. Yang, A.J. Krueger, Z. Li, P.F. Levelt, H. Chen, P. Wang and D. Lu, 2008. *Validation of SO_2 retrievals from the Ozone Monitoring Instrument over NE China.* J. Geophys. Res., **113**.

Kuipers Munneke, P., C.H. Reijmer, M.R. van den Broeke, G. Koenig-Langlo, P. Stammes and W.H. Knap, 2008. *Analysis of clear-sky Antarctic snow albedo using observations and radiative transfer modeling.* J. Geophys. Res., D1711, **113**.

Laat, A.T.J. de, 2008. *Current climate impact of heating from energy usage.* EOS Transactions, **89**.

McPeters, R.D., M. Kroon, G. Labow, E.J. Brinksma, D. Balis, I. Petropavlovskikh, J.P. Veefkind, P.K. Bhartia and P.F. Levelt, 2008. *Validation of the Aura Ozone Monitoring Instrument Total Column Ozone Product.* J. Geophys. Res., **113**.

Meirink, J.F., P. Bergamaschi, C. Frankenberg, M.T.S. d'Amelio, E.J. Dlugokencky, L.V. Gatti, S. Houweling, J.B. Miller, T. Roeckmann, M.G. Villani and M.C. Krol, 2008. *Four-dimensional variational data assimilation for inverse modelling of atmospheric methane emissions: Analysis of SCIAMACHY observations.* J. Geophys. Res., **113**.

Meirink, J.F., P. Bergamaschi and M.C. Krol, 2008. *Four-dimensional variational data assimilation for inverse modelling of atmospheric methane emissions: Method and comparison with synthesis inversion.* Atm. Chem. Phys., **8**, 6341-6353.

Migliorini, S., R. Brugge, A. O'Neill, M. Dobber, V. Fioletov, P.F. Levelt and R. McPeters, 2008. *Evaluation of ozone total column measurements by the Ozone Monitoring Instrument using a data assimilation system.* J. Geophys. Res., **113**.

Petropavlovskikh, I., L. Froidevaux, R. shetter, S. Hall, K. Ullmann, P.K. Bhartia, M. Kroon and P.F. Levelt, 2008. *In-flight validation of Aura MLS ozone with CAFS partial ozone columns.* J. Geophys. Res., **113**.

Schutgens, N.A.J., W. Greuell and R.A. Roebeling, 2008. *Effect of inhomogeneity on the validation of SEVIRI LWP.* International Radiation Symposium (IRS2008), 3/8/2008-8/8/2008, 2008, Iguacu Falls, Brazil, IRS.

Smedt, I. De, J.F. Muller, T. Stavrakou, R.J. van der A, H. Eskes and M. Van Roozendael, 2008. *Twelve years of global observation of formaldehyde in the troposphere using GOME and SCIAMACHY sensors.* Atm. Chem. Phys., **8**, 16, 4947-4963.

Sneep, M., J.F. de Haan, P. Stammes, P. Wang, C. Vanbauce, J. Joiner, A.P. Vasilkov and P.F. Levelt, 2008. *Three-way comparison between OMI and PARASOL cloud pressure products.* J. Geophys. Res., **113**.

Spurr, R., J.F. de Haan, R. van Oss and A. Vasilkov, 2008. *Discrete Ordinate Radiative Transfer in a Stratified Medium with First Order Rotational Raman Scattering.* J. Quant. Spectros. Rad. Transf., **109**, 3, 404-425.

Stajner, I., K. Wargan, S. Pawson, H. Hayashi, L. Chang, R.C. Hudman, L. Froidevaux, N. Livesey, P.F. Levelt, A.M. Thompson, D.W. Tarasick, R. Stübi and S.B. Andersen, 2008. *Assimilated ozone from EOS-Aura: Evaluation of the tropopause region and tropospheric columns.* J. Geophys. Res., **113**.

Stammes, P., M. Sneep, J.F. de Haan, J.P. Veefkind, P. Wang and P. Levelt, 2008. *Effective cloud fractions from the Ozone Monitoring Instrument: Theoretical framework and validation.* J. Geophys. Res., **113**.

Stavrakou, T., J.F. Muller, K.F. Boersma, I. De Smedt and R.J. van der A, 2008. *Assessing the distribution and growth rates of NOx emission sources by inverting a 10-year record of NO_2 satellite columns.* Geophys. Res. Lett., **35**.

Vassilkov, A., J. Joiner, R. Spurr, P.K. Bhartia, P.F. Levelt and G. Stephens, 2008. *Evaluation of the OMI Cloud Pressures Derived from Rotational Raman Scattering by Comparisons with Other Satellite Data and Radiative Transfer Simulations.* J. Geophys. Res., **113**.

Wang, P., P. Stammes, R. van der A, G. Pinardi and M. van Roozendael, 2008. *FRESCO+: an improved O_2 A-band cloud retrieval algorithm for tropospheric trace gas retrievals.* Atm. Chem. Phys., **8**, 9697-9729.

Wenig, M.O., A.M. Cede, E.J. Bucsela, E.A. Celarier, K.F. Boersma, J.P. Veefkind, E.J. Brinksma, J.F. Gleason and J.R. Herman, 2008. *Validation of OMI tropospheric NO_2 column densities using direct-sun mode Brewer measurements at NASA Goddard Space Flight Center.* J. Geophys. Res., **113**.

Wolters, E.L.A., R.A. Roebeling and A.J. Feijt, 2008. *Evaluation of cloud phase retrieval methods for SEVIRI onboard METEOSAT-8 using ground-based lidar and cloud radar data.* J. Appl. Meteor., **47**, 6, 1723-1738.

2009

Anton, M., M. Lopez, J.M. Vilaplana, M. Kroon, R.D. McPeters, M. Banon and A. Serrano, 2009. *Validation of OMI-TOMS and OMI-DOAS total ozone column using five Brewer spectroradiometers at the Iberian peninsula.* J. Geophys. Res., **114**, 14307.

Bergamaschi, P., C. Frankenberg, J.F. Meirink, M. Krol, M.G. Villani, S. Houweling, F. Dentener, E.J. Dlugokencky, J.B. Miller, L.V. Gatti, A. Engel and I. Levin, 2009. *Inverse modeling of global and regional CH_4 emissions using SCIAMACHY satellite retrievals.* J. Geophys. Res., **114**, D22301.

Boersma, K.F., D.J. Jacob, M. Trainic, Y. Rudich, I. DeSmedt, R.J. Dirksen and H.J. Eskes, 2009. *Validation of urban NO_2 concentrations and their diurnal and seasonal variations observed from space (SCIAMACHY and OMI sensors) using in situ measurements in Israeli cities.* Atm. Chem. Phys., **9**, 3867-3879.

Boesche, E., P. Stammes and R. Bennartz, 2009. *Aerosol Influence on Polarization and Intensity in Near-Infrared O_2 and CO_2 Absorption Bands Observed from Space.* J. Quant. Spectros. Rad. Transf., **110**, 3, 223-239.

Bowman, K.W., D.B.A. Jones, J.A. Logan, H. Worden, K.F. Boersma and et al., 2009. *The zonal structure of tropical O_3 and CO as observed by the Tropospheric Emission Spectrometer in November 2004 - Part 2: Impact of surface emissions on O3 and its precursors.* Atm. Chem. Phys., **9**, 3563-3582.

Dirksen, R., F. Boersma, A.T.J. de Laat, P. Stammes, G. van der Werf and H. Kelder, 2009. *An aerosol boomerang: rapid around-the-world transport of smoke from December 2006 Australia forest fires observed from space.* J. Geophys. Res., **114**.

Ghude, S.D., R.J. van der A, G. Beig, S. Fadnavis and S.D. Polade, 2009. *Satellite derived trends in NO_2 over the major global hotspot regions during the past decade and their inter-comparison.* Environmental Pollution, **157**, 6, 1873-1878.

Gloudemans, A.M.S., A.T.J. de Laat, H. Schrijver, I. Aben, J.F. Meirink and G.R. van der Werf, 2009. *SCIAMACHY CO over land and oceans: 2003-2007 interannual variability.* Atm. Chem. Phys., **9**, 3799-3813.

Greuell, W. and R.A. Roebeling, 2009. *Towards a standard procedure for validation of satellite-derived cloud liquid water path: a study with SEVIRI data.* J. Appl. Meteor., **48**, 8, 1575-1590.

Laat, A.T.J. de, R.J. van der A and M. van Weele, 2009. *Evaluation of tropospheric ozone columns derived from assimilated GOME ozone profile observations.* Atm. Chem. Phys., **9**, 8105-8120.

Laat, A.T.J. de et al., 2009. *Global evaluation of SCIAMACHY and MOPITT carbon monoxide column differences for 2004-2005.* J. Geophys. Res.

Marmer, E., F. Dentener, J. van Aardenne, F. Cavalli, E. Vignati, K. Velchev, J. Hjorth, K.F. Boersma, G. Vinken, N. Mihalopoulos and F. Raes, 2009. *What can we learn about ship emission inventories from measurements of air pollutants over the Mediterranean Sea?* Atm. Chem. Phys., **9**, 6815-6831.

Mijling, B., R.J. van der A, K.F. Boersma, M. Van Roozendael, I. De Smedt and H.M. Kelder, 2009. *Reduction of NO_2 detected from space during the 2008 Beijing Olympic Games.* Geophys. Res. Lett., **36**.

Peet, J.C.A. van, R.J. van der A, A.T.J. de Laat, O.N.E. Tuinder, G. Koenig-Langlo and J. Wittig, 2009. *Height resolved ozone hole structure as observed by the Global Ozone Monitoring Experiment–2.* Geophys. Res. Lett., **36**.

Schulz, J., H. Deneke, R. Roebeling, E. Wolters and et al., 2009. *Operational climate monitoring from space: the EUMETSAT satellite application facility on climate monitoring (CM-SAF).* Atm. Chem. Phys., **9**, 1-23.

Stammes, P., L.G. Tilstra, R. Braak, M. de Graaf and I. Aben, 2009. *Estimate of solar radiative forcing by polluted clouds using OMI and SCIAMACHY satellite data.* International Radiation Symposium IRS2008, 3/8/2008-8/8/2008, T. Nakajima and M.A. Yamasoe (Ed), 2009, IRC/IAMAS, American Institute of Physics, ISBN 978-0-7354-0635-3, 577-580.

Verma, S., J. Worden, B. Pierce, D.B.A. Jones, J. Al-Saadi, K.F. Boersma, K. Bowman, A. Eldering, B. Fisher, L. Jourdain, S. Kulawik and H. Worden, 2009. *Ozone production in boreal fire smoke plumes using observations from the Tropospheric Emission Spectrometer and the Ozone Monitoring Instrument.* J. Geophys. Res., **114**.

Wang, P., W.H. Knap, P. Kuipers Munneke and P. Stammes, 2009. *Clear-sky shortwave radiative closure for the Cabauw Baseline Surface Radiation Network site, the Netherlands.* J. Geophys. Res., **114**.

Wang, P., W.H. Knap, P. Kuipers Munneke and P. Stammes, 2009. *Clear sky atmospheric radiative transfer: a model intercomparison of shortwave irradiances.* International Radiation Symposium IRS2008, 3/8/2008-8/8/2008, T. Nakajima and M.A. Yamasoe (Ed), 2009, IRC/IAMAS, American Institute of Physics, ISBN 978-0-7354-0635-3, 125-128.

Zyrichidou, I., M.E. Koukouli, D.S. Balis, E. Katragkou, D. Melas, A. Poupkou, I. Kioutsioukis, R.J. van der A, K.F. Boersma, M. Van Roozendael and A. Richter, 2009. *Satellite observations and model simulations of tropospheric NO2 columns over south-eastern Europe.* Atm. Chem. Phys., **9**, 6119-6134.

Other Publications

2007

Brinksma, E.J., T. Vlemmix and P.F. Levelt, 2007. *Satellietvalidatie door scholieren.* Nederlands Tijdschrift voor Natuurkunde, maart, 73, 77.

Claas, J.J., 2007. *PL-OMIE-KNMI-870, Test Plan Reprocessing Readiness Test.* 2007, KNMI.

Claas, J.J., 2007. *TN-OMIE-KNMI-872 OMI Reprocessing Status.* 2007, KNMI.

Deneke, H., R.A. Roebeling, E.L.A. Wolters and A.J. Feijt, 2007. *Globale stralingsmeting vanuit de ruimte.* Meteorologica, **16**, 3, 21-25.

Gloudemans, A.M.S., A.T.J. de Laat, M. Krol, J.F. Meirink, I. Aben, G. van der Werf and J. Schrijver, 2007. *Evidence for long-range transport of carbon monoxide in the southern hemisphere from SCIAMACHY observations.* ESA ENVISAT symposium, 22/4/2007-27/4/2007, 2007, Montreux, Zwitserland.

Kroon, M., E.J. Brinksma, J.P. Veefkind, R. McPeters, G. Labow, P.F. Levelt and P.K. Bhartia, 2007. *Validation from more than one year of data from the Ozone Monitoring Instrument.* Measuring Tropospheric Trace Species from Space - AT2 in 2005 -6, ACCENT-Troposat.

Levelt, P.F., J.P. Veefkind, M . Kroon, E.J. Brinksma, R.D. McPeters, G. Labow, N. Krotkov, D. Ionov, E. Hilsenrath, A. Tanskanen, G.H.J. van den Oord and P.K. Bhartia, 2007. *Several First Year's Results of the Ozone Monitoring Instrument.* Conference Proceedings.

Snoeij, P., A. Piters, H. Fischer, Y. Meijer, J.C. Lambert and T. Fehr, 2007. *Summary of the atmospheric chemistry instrument validation results as presented at the ACVE-3 workshop.* Third Workshop on Atmospheric Chemistry Validation of Envisat (ACVE-3), 4/12/2006-7/12/2006, 2007.

Tilstra, L.G., M. de Graaf, I. Aben and P. Stammes, 2007. *Analysis of 5 years SCIAMACHY Absorbing Aerosol Index data.* Envisat Symposium, 23/4/2007-27/4/2007, 2007, Montreux (CH), ESA SP-636, ESA/ESTEC.

Tilstra, L.G., M. de Graaf, S. Noel, E.A.A. Aben and P. Stammes, 2007. *SCIAMACHY's Absorbing Aerosol Index and the consequences of instrument degradation.* Third Workshop on the Atmospheric Chemistry Validation of ENVISAT (ACVE-3), 4/12/2006-7/12/2006, 2007.

Vlemmix, T., E.J. Brinksma, J.P. de Vroom and P.F. Levelt, 2007. *Dutch Students Contribute to OMI Aerosol Validation.* The Earth Observer, **19**, 5, 7-9.

Wang, P., P. Stammes and R. van der A, 2007. *The FRESCO+ cloud algorithm for GOME and SCIAMACHY: improvement and validation.* ENVISAT Symposium, 23/4/2007-27/4/2007, 2007, Montreux, Switzerland.

Wang, P., P. Stammes and R. van der A, 2007. *The FRESCO+ cloud algorithm for GOME and SCIAMACHY: improvement and validation.* ENVISAT Symposium, 23/4/2007-27/4/2007, 2007, Montreux, Switzerland.

Weele, M. van and R. van der A, 2007. *Spaceborne surface UV radiation products as available from TEMIS.* 18/9/2007-20/9/2007, J. Groebner (Ed), 2007, Davos, Zwitserland, PMOD, 175-176.

Zhang, Y., P. Zhang, J. Kuenen, X. Zhang, X. Li, H. Qiu and W. Wang, 2007. *Variations of Carbon Monoxide and Nitrogen Dioxide column concentrations of China in 2003 using the TM_5 simulation results.* Remote Sensing Information, 6.

2008

Claas, J.J., 2008. *Deriving attitude and ephemeris data: GBAD versus OMI ancillary data.* TN-OMIE-KNMI-908.

Claas, J.J., 2008. *Impact of the AURA re-phasing on OMI.* TN-OMIE-KNMI-910.

Claas, J.J., 2008. *Input NRB FMU Anomaly.* TN-OMIE-KNMI-905.

Claas, J.J., 2008. *Minutes NRB FMU Anomaly.* TN-OMIE-KNMI-906.

Claas, J.J., 2008. *OMI hardware vervanging.* LE-OMIE-KNMI-914.

Claas, J.J., 2008. *Operational Remarks on OMI White Light Source (WLS).* TN-OMIE-KNMI-912.

Hoek, M. van, 2008. *Extension of Solar measurements.* TN-OMIE-909.

Hoek, M. van, 2008. *Monitoring AURA Re-phasing.* KNMI Preprint PR, TN-OMIE-907.

Piters, A., F. Wittrock, A. Richter, M. van Roozendael and F. Goutail, 2008. *First demonstration of satellite validation for tropospheric NO_2.* GEOMON Project deliverable M18.

Piters, A.J.M., 2008. *The Development of Validation Strategies for Tropospheric Satellite Data Products using Existing Data; Activity Report: March 2006 to March 2007*. Annual Report ACCENT-Troposat 2.

Wang, P., W.H. Knap, P. Kuipers Munneke and P. Stammes, 2008. *Clear-sky Atmospheric Radiative Transfer: A Model Inter-comparison for Shortwave Irradiances.* International Radiation Symposium (IRS-2008), 3/8/2008-8/8/2008, 2008, Brazil.

Wolters, E.L.A., H.M. Deneke, J.F. Meirink and R.A. Roebeling, 2008. *Impact of broken and inhomogeneous clouds in satellite cloud-phase retrieval.* EUMETSAT Meteorological Satellite Conference, 8/9/2008-12/9/2008, 2008, Darmstadt, Germany, EUMETSAT.

2009

Aben, I. and P.F. Levelt, 2009. *De Aardatmosfeer gezien vanuit de ruimte.* Nederlands Tijdschrift voor Natuurkunde, **75**, 6, 193-198.

Carbajal Henken, C.K., M.J. Schmeits, E.L.A. Wolters and R.A. Roebeling, 2009. *Detection of Cb and TCu clouds using MSG-SEVIRI cloud physical properties and weather radar observations.* KNMI Scientific Report WR-2009-04.

Claas, J.J., 2009. *Overview OMI row anomaly.* TN-OMIE-KNMI-924.

Claas, J.J., 2009. *Timing dark current measurements.* TN-OMIE-KNMI-920.

Dirksen, R.J., K.F. Boersma, A.T.J. de Laat and P. Stammes, 2009. *Three dimensional OMI observations of rapid around the world transport of an aerosol plume released from the Australian forest fires on 14 December 2006.* 8th International Symposium on Tropospheric Profiling Registration, 19/10/2009-23/10/2009, A. Apituley, H.W.J. Russchenberg and W.A.A. Monna (Eds.), 2009, Delft, KNMI, RIVM, TU Delft, ISBN 978-90-6960-2.

Hoexum, A.M., A. Apituley, M.A.F. Allaart and A.J.M. Piters, 2009. *Tropospheric Ozone Lidar for OMI validation.* ISTP 8, 19/10/2009-23/10/2009, 2009, Delft.

Marmer, E., F. Dentener, J. van Aardenne, F. Cavalli, E. Vignati, K. Velchev, J. Hjorth, K.F. Boersma, G.C.M. Vinken, N. Milahopoulos and F. Raes, 2009. *What can we learn about ship emission inventories from measurements of air pollutants over the Mediterranean Sea?* Atm. Chem. Phys. Disc., **9**, 7155-7211.

Meirink, J.F., R.A. Roebeling and P. Stammes, 2009. *Atmospheric correction for the KNMI Cloud Physical Properties retrieval algorithm.* KNMI Technical Report TR-304, pp22.

Piters, A.J.M., B. Buchmann, D. Brunner, R.C. Cohen, J.C. Lambert, G. de Leeuw, P. Stammes, M. van Weele and F. Wittrock, 2009. *Data quality and validation of satellite measurements of tropospheric composition.* In The Remote Sensing of Trop. Composition from Space, 2009, Springer.

Sluis, W.W., M.A.F. Allaart and A.J.M. Piters, 2009. *Development of a Nitrogen Dioxide Sonde.* ISTP 8, 19/10/2009-23/10/2009, 2009, Delft.

Veefkind, J.P., P.F. Levelt, B.J. Kerridge, R. Siddans, G. de Leeuw, J. Remedios and P.F. Coheur, 2009. *CAMELOT Final Report.* Final Report CAMELOT Study (ESA contract no: 21533/07/NL/HE), KNMI.

Vlemmix, T., A.J.M. Piters, P. Stammes, P. Wang and P.F. Levelt, 2009. *MAX-DOAS AEROSOL CORRECTED TROPOSPHERIC VERTICAL COLUMNS OF NITROGEN DIOXIDE.* ISTP 8, 19/10/2009-23/10/2009, 2009, Delft.

Wang, P. and W.H. Knap, 2009. *Energy redistribution due to the cloud layer.* 8th International Symposium of Tropospheric Profiling, 19/10/2009-23/10/2009, 2009, Delft.

Wolters, E.L.A., R.A. Roebeling, P. Stammes, P. Wang, A. Ali and G. Brissebrat, 2009. *Evaluation of SEVIRI-derived rain rates and accumulated rainfall with TRMM-TMI and rain gauge data over West-Africa.* Earth Observations and Water Cycle Science conference, 18/11/2009-20/11/2009, 2009, Frascati, Italie, ESA.

Zhou, Y., D. Brunner, K.F. Boersma, R.J. Dirksen and P. Wang, 2009. *An improved tropospheric NO_2 retrieval for satellite observations in the vicinity of mountainous terrain.* Atmos. Meas. Tech. Discuss., **2**, 781-824.

Zyrichidou, I., M.E. Koukouli, D.S. Balis, E. Katragkou, D. Melas, A. Poupkou, I. Kioutsioukis, R.J. van der A, K.F. Boersma, M. Van Roozendael and A. Richter, 2009. *Satellite NO2 observations and model simulations of tropospheric columns over South-eastern Europe.* Atm. Chem. Phys., **9**, 16, 6119-6134.

Publications
Global Climate

In the Global Climate division, large-scale climate variability is studied, including the effects of climate change. The research activities in the group focus on quantifying decadal to centennial climate variability, studying feedbacks in the earth system, development of global climate scenarios and development of monthly, seasonal and decadal predictions. The group maintains global climate models of intermediate complexity and develops a state-of-the-art earth system model (EC-EARTH) as research tool and as tool for developing climate scenarios. The group is internationally recognized in the fields of climate extremes, thermohaline circulation, tropical variability, atmospheric dynamics and land processes.

Reviewed Publications

2007

Almeida, R.A.F. de, P. Nobre, R.J. Haarsma and E.J.D. Campos, 2007. *Negative ocean-atmosphere feedback in the South Atlantic Convergence Zone.* Geophys. Res. Lett., **34**.

Bierkens, M.P. and B.J.J.M. van den Hurk, 2007. *Groundwater convergence as a possible mechanism for multi-year persistence in rainfall.* Geophys. Res. Lett., **34**.

Bracco, A., F. Kucharski, F. Molteni, W. Hazeleger and C. Severijns, 2007. *A recipe for simulating the interannual variability of the Asian Summer Monsoon and its relation with ENSO.* Clim. Dyn., **28**, 441-460.

Breugem, W.P., W. Hazeleger and R.J. Haarsma, 2007. *Mechanisms of northern tropical Atlantic variability and response to CO_2 doubling.* J. Climate, **20**, 11, 2691-2705.

Breugem, W.P., 2007. *The effective viscosity of a channel-type porous medium.* Physics of Fluids, **19**, 10.

Drijfhout, S.S. and W. Hazeleger, 2007. *Detecting Atlantic MOC changes in an ensemble of climate change simulations.* J. Climate, **20**, 8, 1571-1582.

Drijfhout, S.S. and L.R.M. Maas, 2007. *Impact of channel geometry and rotation on the trapping of internal tides.* J. Phys. Oceanogr., **37**, 11, 2740-2763.

Friocourt, Y., B. Levier, S. Speich, B. Blanke and S.S. Drijfhout, 2007. *A regional numerical ocean model of the circulation in the Bay of Biscay.* J. Geophys. Res., **112**, 9.

Haarsma, R.J. and W. Hazeleger, 2007. *Extra-tropical atmospheric response to equatorial Atlantic cold tongue anomalies.* J. Climate, **20**, 10, 2076-2091.

Hurk, B.J.J.M. van den, A.M.G. Klein Tank, G. Lenderink, A. van Ulden, G.J. van Oldenborgh, C. Katsman, H. van den Brink, F. Keller, J. Bessembinder, G. Burgers, G. Komen, W. Hazeleger and S. Drijfhout, 2007. *New climate change scenarios for the Netherlands.* Water Science and Technology, **56**, 4, 27-33.

Hurk, B.J.J.M. van den, 2007. *Interactie tussen Hemel en Aarde.* 2007, ISBN 978-90-393-4618-1, 24p.

Jia, Y., A.C. Coward, B.A. de Cuevas, D.J. Webb and S.S. Drijfhout, 2007. *A model analysis of the behaviour of the Mediterranean water in the North Atlantic.* J. Phys. Oceanogr., **37**, 3, 764-786.

Leeuwenburgh, O., 2007. *Validation of an EnKF System for OGCM Initialization Assimilating Temperature, Salinity, and Surface Height Measurements.* Mon. Wea. Rev., **135**, 125-139.

Marsh, R., W. Hazeleger, A. Yool and E. Rohling, 2007. *Stability of the Thermohaline Circulation under Millennial CO-2 Forcing and Two Alternative Controls on Atlantic Salinity.* Geophys. Res. Lett., **34**.

McDougall, T.J., P.R. Gent and S.S. Drijfhout, 2007. *Comment on two papers by Canuto and Dubovikov.* Ocean Mod., **17**, 163-171.

Mohamed, Y., B.J.J.M. van den Hurk and H.H.G. Savenije, 2007. *Moisture recycling over the Nile basin.* IAHS Red Book Series 317, **317**, 18-23.

Moolenaar, H.E., J. Grasman, F.M. Selten and M. de Gee, 2007. *Testing a method for analyzing the effect of parameter change in climate driven ecological systems.* Boreal Environment Research.

Oldenborgh, G.J. van, 2007. *How unusual was autumn 2006 in Europe?* Climate of the Past, **3**, 659-668.

Schrier, G. van der, S.S. Drijfhout, W. Hazeleger and L. Noulin, 2007. *Increasing the Atlantic subtropical jet cools the circum-North Atlantic.* Meteor. Z., **16**, 6, 675-684.

Shongwe, M.E., C.A.T. Ferro, C.A.S. Coelho and G.J. van Oldenborgh, 2007. *Predictability of cold spring seasons in Europe.* Mon. Wea. Rev., **135**, 4185-4201.

Sterl, A., G.J. van Oldenborgh, W. Hazeleger and G. Burgers, 2007. *On the robustness of ENSO teleconnections.* Clim. Dyn.

Stone, D.A., M.R. Allen, F.M. Selten, M. Kliphuis and P.A. Stott, 2007. *The detection and attribution of climate change using an ensemble of opportunity.* J. Climate, **20**, 504-516.

Swaluw, E. van der, S.S. Drijfhout and W. Hazeleger, 2007. *Bjerknes compensation at high Northern latitudes: The ocean forcing the atmosphere.* J. Climate, **20**, 24, 6023-6032.

Wit, M.J.M. de, B. van den Hurk, P.M.M. Warmerdam, P.J.J.F. Torfs, E. Roulin and W.P.A. van Deursen, 2007. *Impact of climate change on low flows in the river Meuse.* Climatic Change.

2008

Balsamo, G., P. Viterbo, A. Beljaars, B.J.J.M. van den Hurk, A. Betts and K. Scipal, 2008. *A revised hydrology for the ECMWF model: Verification from field site to terrestrial water storage and impact in the Integrated Forecast System.* J. Hydrometeor..

Breugem, W.P., P. Chang, C.J. Jang, J. Mignot and W. Hazeleger, 2008. *Barrier layers and tropical Atlantic SST biases in coupled GCMs.* Tellus, 60, **5**.

Chang, P., R. Zhang, W. Hazeleger, C. Wen, X. Wan, L. Ji, R. Haarsma, W.P. Breugem and H. Seidel, 2008. *An Oceanic Bridge Between Abrupt Changes in North Atlantic Climate and the African Monsoon.* Nature Geoscience, **1**, 444-448.

Drijfhout, S.S., W. Hazeleger, F. Selten and R. Haarsma, 2008. *Future changes in internal Atlantic Meridional Overturning Circulation variability.* Clim. Dyn., **30**, 4, 407-419.

Drijfhout, S.S. and A. Naveira Garabato, 2008. *The Zonal Dimension of the Indian Ocean Meridional Overturning Circulation.* J. Phys. Oceanogr., **38**, 2, 359-379.

Friocourt, Y., B. Blanke, S.S. Drijfhout and S. Speich, 2008. *On the dynamics of the Slope Current system along the west European margin. Part II: Analytical calculations and numerical simulations with seasonal forcing.* J. Phys. Oceanogr., **38**, 12, 2619-2638.

Friocourt, Y., S.S. Drijfhout and B. Blanke, 2008. *On the dynamics of the slope current system along the West European margin. Part I: Steady-state analytical and numerical circulations.* J. Phys. Oceanogr., **38**, 12, 2597-2618.

Haarsma, R.J., E.J.D. Campos, W. Hazeleger and C.A. Severijns, 2008. *Influence of the Meridional Overturning Circulation on Tropical Atlantic Climate and Variability.* J. Climate, **21**, 1403-1416.

Hurk, B.J.J.M. van den, J. Ettema and P. Viterbo, 2008. *Analysis of soil moisture changes in Europe during a single growing season in a new ECMWF soil moisture assimilation system.* J. Hydrometeor., **9**, 116-131.

Jacobs, C.M.J., E.J. Moors, H. ter Maat, A.J. Teuling, G. Balsamo, K. Bergaoui, J. Ettema, M. Lange, B.J.J.M. van den Hurk, P. Viterbo and W. Wergen, 2008. *Validation of European Land Data Assimilation System (ELDAS) products using in situ observations.* Tellus, **60A**, 1023-1037.

Katsman, C.A., W. Hazeleger, S.S. Drijfhout, G.J. van Oldenborgh and G.J.H. Burgers, 2008. *Climate scenarios of sea level rise for the northeast Atlantic Ocean: a study including the effects of ocean dynamics and gravity changes induced by ice melt.* Climatic Change.

Leander, R., T.A. Buishand, B.J.J.M. van den Hurk and M.J.M. de Wit, 2008. *Estimated changes in flood quantiles of the river Meuse from resampling of regional climate model output.* J. Hydrol., **351**, 331-343.

McDougall, T.J., P.R. Gent and S.S. Drijfhout, 2008. *Comment on 2 papers by Dubovikov and Canuto.* Geophys. and Astrophys. Fluid Dyn., **102**, 3, 249-256.

Pasmanter, R.A. and H.W. Capel, 2008. *Mixing and coherent structures in two-dimensional viscous flows.* Phys. Rev. E., **237**, 1993-1997.

Sterl, A., C. Severijns, H. Dijkstra, W. Hazeleger, G.J. van Oldenborgh, M. van den Broeke, G. Burgers, B. van den Hurk, P.J. van Leeuwen and P. van Velthoven, 2008. *When can we expect extremely high surface temperatures?* Geophys. Res. Lett., **35**, 14, L14703.

Van den Brink, H.W. and G.P. Konnen, 2008. *The statistical distribution of meteorological outliers.* Geophys. Res. Lett., L2370, **35**, 1-5.

2009

Balsamo, G., P. Viterbo, A. Beljaars, B.J.J.M. van den Hurk, A. Betts and K. Scipal, 2009. *A revised hydrology for the ECMWF model: Verification from field site to terrestrial water storage and impact in the Integrated Forecast System.* J. Hydrometeor., **10**, 623-643.

Bencivenga, F., A. Cimatoribus, A. Gessini, M.G. Izzo and C. Masciovecchio, 2009. *Temperature and density dependence of the structural relaxation time in water by inelastic ultraviolet scattering.* J. Chem. Phys., **131**, 144502.

Branstator, G. and F.M. Selten, 2009. *Modes of variability and climate change.* J. Climate, **22**, 2639-2658.

Broeke, M. van den, J. Bamber, J. Ettema, E. Rignot, E. Schrama, W.J. van den Berg, E. van Meijgaard, I. Velicogna and B. Wouters, 2009. *Partitioning Recent Greenland Mass Loss.* Science, **326**, 5955, 984-986.

Graversen, R.G. and M. Wang, 2009. *Polar amplification in a coupled climate model with locked albedo.* Clim. Dyn., **33**, 629-643.

Griffies, S., W. Hazeleger, C. Severijns et al., 2009. *Coordinated Ocean-Ice Reference Experiments (CORES).* Ocean Mod., **26**, 1-2.

Guilyardi, E., A. Wittenberg, A. Fedorov, M. Collins, C. Wang, A. Capotondi and G.J. van Oldenborgh, 2009. *Understanding El Niño in Ocean-Atmosphere General Circulation Models: progress and challenges.* Bull. Amer. Meteor. Soc., **90**, 325-340.

Haarsma, R.J., F.M. Selten, B.J.J.M. van den Hurk, W. Hazeleger and X. Wang, 2009. *Drier Mediterranean Soils due to Greenhouse Warming bring easterly Winds over Summertime Central Europe.* Geophys. Res. Lett., **36**, L04705.

Jong, F. de, S.S. Drijfhout, W. Hazeleger, H.M. van Aken and C.A. Severijns, 2009. *Simulations of hydrographic properties in the north western North Atlantic Ocean in Coupled Climate Models.* J. Climate, **22**, 7, 1767-1786.

Koehler, P. and R. Bintanja, 2009. *The carbon cycle during the mid Pleistocene transition: the Southern Ocean decoupling hypothesis.* Climate of the Past, **4**, 311-332.

Laurian, A., S. S Drijfhout, W. Hazeleger and R. van Dorland, 2009. *Global surface cooling: the atmospheric fast feedback response to a collapse of the thermohaline circulation.* Geophys. Res. Lett., **36**.

Oldenborgh, G.J. van, S.S. Drijfhout, A. van Ulden, R. Haarsma, A. Sterl, C. Severijns, W. Hazeleger and H. Dijkstra, 2009. *Western Europe is warming much faster than expected.* Climate of the Past, **5**, 1, 1-12.

Oldenborgh, G.J. van, L.A. te Raa, H.A. Dijkstra and S.Y. Philip, 2009. *Frequency- or amplitude-dependent effects of the Atlantic meridional overturning on the tropical Pacific Ocean.* Ocean Science, **5**, 293-301.

Pasmanter, R.A. and F.M. Selten, 2009. *Decomposing data sets into skewness modes.* Physica D.

Pelt, S. van, P. Kabat, H. ter Maat, B.J.J.M. van den Hurk and A. Weerts, 2009. *Discharge simulations performed with a hydrological model using bias corrected regional climate model input.* Hydrology and Earth System Sciences, **13**, 2387-2397.

Philip, S.Y. and G.J. van Oldenborgh, 2009. *Atmospheric properties and the ENSO cycle: models versus observations.* Clim. Dyn.

Philip, S.Y. and G.J. van Oldenborgh, 2009. *Significant atmospheric nonlinearities in the ENSO cycle.* J. Climate, **22**, 14, 4014-4028.

Philip, S.Y., 2009. *Exploring El Niño mechanisms in climate models.* Thesis, Universiteit Utrecht, 2009, De Bilt, 166p.

Pitman, A.J., N. de Noblet, F.T. Cruz, E.L. Davin, G.B. Bonan, V. Brovkin, M. Claussen, C. Delire, V. Gayler, B.J.J.M. van den Hurk, P.J. Lawrence, M.K. van der Molen, C. Mueller, C.H. Reick and 3 co-authors, 2009. *Land use and climate via the LUCID intercomparison study: implications for experimental design in AR5.* Geophys. Res. Lett., **36**, L14814.

Selten, F.M. and R.A. Pasmanter, 2009. *Skewness modes in Northern Hemisphere winter.* J. Climate.

Shongwe, M.E., G.J. van Oldenborgh, B.J.J.M. van den Hurk, B. de Boer, C.A.S. Coelho and M.K. van Aalst, 2009. *Projected changes in extreme precipitation in Africa under global warming. Part 1: Southern Africa.* J. Climate, **22**, 3819-3837.

Shongwe, M.E., R.G. Graversen, G.J. van Oldenborgh, B.J.J.M. van den Hurk and F.J. Doblas-Reyes, 2009. *Energy budget of the extreme Autumn 2006 in Europe.* Clim. Dyn.

Sterl, A., H. van den Brink, H. de Vries, R. Haarsma and E. van Meijgaard, 2009. *An ensemble study of extreme North Sea storm surges in a changing climate.* Ocean Science, **5**, 369-378.

Teuling, R., R. Uijlenhoet, B. van den Hurk and S. Seneviratne, 2009. *Parameter Sensitivity in LSMS: An Analysis Using Stochastic Soil Moisture Models and ELDAS Soil Parameters.* J. Hydrometeor., **10**, 751-765.

Vautard, R., P. Yiou and G.J. van Oldenborgh, 2009. *The decline of fog, mist and haze in Europe during the last 30 years: a warming amplifier?* Nature Geoscience, **2**, 115-119.

Other publications

2007

Boer, B. de, 2007. *The impact of climate change on rainfall extremes over Northeast Africa.* WR Scientific Report WR-2007-03, pp46.

Boscolo, R. and W. Hazeleger, 2007. *CLIVAR Implementation Panel: 8th session.* Clivar Exchanges, **12**, 26-27.

Dijkstra, H., W. Hazeleger, A. Sterl and G.J. van Oldenborgh, 2007. *Gevolgen versterkte broeikaseffect in 2030 overal in Europa merkbaar.* Weer Magazine, **3**, 26-29.

Endalew, G., 2007. *Changes in the frequency and intensity of extremes over Northeast Africa.* KNMI Scientific Report WR-2007, pp46.

Hazeleger, W. and EC-EARTH consortium, 2007. *EC-EARTH Science and Implementation Plan.* -217, pp22.

Hurk, B.J.J.M. van den and G. Komen, 2007. *Droge zomers in zicht.* Geografie, 1, **16**, 9-12.

Katsman, C.A., R. van Dorland, W. Hazeleger, B. Strengers, T. Kram, W. Ligtvoet and B. Eickhout, 2007. *Zeespiegel rijst, maar niet de pan uit.* NRC Handelsblad opiniepagina 19 januari.

Oldenborgh, G.J. van, 2007. *De zachte winter van 2007.* WR Kenniscentrum.

Oldenborgh, G.J. van, 2007. *Extraordinarily mild Europe autumn 2006 due to global warming?* IGBP Newletter, **67**, 18-20.

Oldenborgh, G.J. van, 2007. *How unusual was autumn 2006 in Europe?* Climate of the Past Disc., **3**, 811-837.

Oldenborgh, G.J. van, 2007. *Lente 2007: al weer een temperatuurrecord.* KNMI Kenniscentrum.

Oldenborgh, G.J. van, 2007. *Summer in April - a very unlikely event?* KNMI Kenniscentrum.

Oldenborgh, G.J. van, 2007. *The mild winter of 2007: what were the causes?* KNMI Kenniscentrum.

Oldenborgh, G.J. van, 2007. *Zomer in april: hoe zeldzaam is dit?* KNMI Kenniscentrum.

Pasmanter, R.A. and H.W. Capel, 2007. *Mixing and coherent structures in two-dimensional viscous flows.* Euler Equation 250, 18/6/2007-22/6/2007, U. Frisch (Ed.), 2007, Aussois, Frankrijk, CNRS, Academie des Sciences, Observatoire de la Cote d'Azur, Elsevier, Physica D.

Pater, F. de and C.A. Katsman, 2007. *Zeespiegelstijging Nederland 'slechts' twee meter als Groenland smelt.* H_2O, **40**, 4-5.

Sterl, A., 2007. *Het Argo-programma / The Argo Program.* Meteorologisch Informatiebulletin Maritiem, 12-14.

Sterl, A., R. Haarsma, F. Selten and H. Dijkstra, 2007. *The ESSENCE project – the power of a large model ensemble.* In Biennial Scientific Report 2005-2006, W. Monna (Ed), 2007, De Bilt, KNMI, p114-118.

The DRAKKAR Group, W. Hazeleger and C. Severijns, 2007. *Eddy-permitting Ocean Circulation Hindcasts of Past Decades.* Clivar Exchanges, **12**, 3, 8-10.

2008

Bessembinder, J., C. Katsman, W. Hazeleger, S. Drijfhout, H. van den Brink, G. Lenderink, E. Meijgaard, M. de Wit, H. Buiteveld and W. van Deursen, 2008. *Extreme klimaatverandering en waterveiligheid in Nederland.* KNMI Publication.

Drijfhout, S.S., 2008. *Changes in the Atlantic Meridional Overturning Circulation.* KNMI Biennial Report 2005-2006.

Drijfhout, S.S., 2008. *Veranderingen in de Warme Golfstroom.* Meteorologisch Informatiebulletin Maritiem, **Jan**., 6-12.

Hazeleger, W., 2008. *Ocean and Climate Studies: Linking Physical, Biogeochemical and Ecosystems Research.* Eos, **89**, 25, 227-227.

Hurk, B.J.J.M. van den and D. Jacob, 2008. *The art of predicting climate variability and change.* In Climate Change and Adaptation in the Water sector, P. Kabat and H. v Schaik (Eds.), 2008, Earthscan.

Hurk, B.J.J.M. van den and E.M. Blyth, 2008. *WATCH/LoCo workshop report.* Gewex newsletter, 12-14.

Hurk, B.J.J.M. van den, R. Haarsma, F. Selten and S. Seneviratne, 2008. *Soil moisture influence on European Atmospheric circulation.* ECMWF Seminar Physical Parameterizations, 1/9/2008-5/9/2008, 2008, Reading, ECMWF.

Jacob, D. and B.J.J.M. van den Hurk, 2008. *Climate Change Scenarios at the global and local scale.* In Climate Change and Adaptation in the Water sector, P. Kabat and H. v Schaik (Ed.), 2008, Earthscan.

Kabat (Red.), P., W. Hazeleger, C. Katsman, A. Sterl, J. Beersma, A. Klein Tank, P. Vellinga, R. Hutjes and R. Swart, 2008. *Toelichting op door de Deltacommissie gebruikte klimaatscenario's - Bijlage 3 van 'Samen werken met water'.* In: Samen werken met water, Deltacommissie 2008 (Ed), 2008, ISBN 978-90-9023484-7, p106-117.

Katsman, C.A., 2008. *Noordpool in 2013 ijsvrij?* Weer Magazine, **1**, 17.

Meijgaard, E. van, L.H. van Ulft, W.J. van de Berg, F.C. Bosveld, B.J.J.M. van den Hurk, G. Lenderink and A.P. Siebesma, 2008. *The KNMI regional atmospheric climate model RACMO, version 2.1.* KNMI Technical Report TR-302, pp43.

Oldenborgh, G.J. van and R. Haarsma, 2008. *Stijging wereldgemiddelde temperatuur - de langjarige trend gaat door.* KNMI Kenniscentrum.

Oldenborgh, G.J. van, 2008. *How unusual was autumn 2006 in Europe?* PAGES News, **16**, 26-28.

Oldenborgh, G.J. van, 2008. *Wereldgemiddelde temperatuur januari 2008.* KNMI Kenniscentrum.

Oldenborgh, G.J. van, C.A.S. Coelho and F.J. Doblas-Reyes, 2008. *Exploratory analysis and verification of seasonal forecasts with the KNMI Climate Explorer.* ECMWF Newsletter, **116**, 4-5.

Oldenborgh, G.J. van, S.S. Drijfhout, A. Sterl and A. van Ulden, 2008. *Nederland warmt sneller op dan verwacht.* De toestand van het klimaat in Nederland 2008, 16-23.

Sterl, A., G.J. van Oldenborgh, W. Hazeleger and H. Dijkstra, 2008. *Extreme maximumtemperaturen in de toekomst.* Meteorologica, **17**, 3, 4-7.

Vellinga, P., C.A. Katsman, A. Sterl and J.J. Beersma (Eds.), 2008. *Onderzoek naar bovengrensscenario's voor klimaatverandering voor overstromingsbescherming van Nederland: een internationale wetenschappelijke beoordeling.* Publicatie van KNMI en Wageningen UR (Alterra, Earth System Science and Climate Change Group), pp178.

Wallbrink, H. and T. Brandsma, 2008. *DIGISTAD: Disclosure of the hourly meteorological observations of the Amsterdam City Water Office 1784-1963.* KNMI Preprint PR-220, Hisklim 9, pp26.

Wallbrink, H. and T. Brandsma, 2008. *DIGISTAD: Disclosure of the hourly meteorological observations of the Amsterdam City Water Office 1784-1963.* KNMI Publication PUBL-220, pp26.

2009

Bintanja, R., 2009. *IJstijden: hoe, wat, waar en waarom.* Zenit.

Gelderloos, R., C.A. Katsman and S.S. Drijfhout, 2009. *De rol van drie soorten wervels in het restratificeren van het Labrador Zee.* Meteorologica.

Hazeleger, W., 2009. *EC-Earth: a seamless prediction approach to earth system modelling.* SOLAS Newsletter, **9**, 12-12.

Hurk, B. van den, 2009. *SMOS satelliet gelanceerd.* Meteorologica, **4**, 13-14.

Hurk, B. van den, E. Dutra, B. Smith, M. Brandt, M. Weiss, R. Haarsma, W. Hazeleger, G. Balsamo and M. van der Molen, 2009. *The EC-Earth modelling challenges.* ECMAF/GLASS workshop, 9/11/2009-12/11/2009, Beljaars (Ed.), 2009, Reading, ECMWF.

Hurk, B. van den, E. van Meijgaard and G. Lenderink, 2009. *Climate Research Netherlands - Research Highlights.* KvR international newsletter, 6-12.

Hurk, B.J.J.M. van den, 2009. *De feiten liegen niet, de zee stijgt.* Volkskrant 7 jan, 11.

Kabat, P., L.O. Fresco, M.J.F. Stive, C.P. Veerman, J.S.L.J. van Alphen, B.W.A.H. Parmet, W. Hazeleger and C.A. Katsman, 2009. *Dutch coasts in transition.* Nature Geoscience, **2**, 7, 450-452.

Koehler, P. and R. Bintanja, 2009. *The carbon cycle during the Mid Pleistocene Transition: the Southern Ocean decoupling hypothesis.* Climate of the Past Discussions, **4**, 809-858.

Oldenborgh, G.J. van, R. Vautard and P. Yiou, 2009. *Mist en nevel zijn de afgelopen 30 jaar sterk afgenomen.* Weer Magazine, **2**, 39-41.

Roemmich, D., the Argo Steering Team, among others: and A. Sterl, 2009. *Argo - The challenge of continuing 10 years of progress.* Oceanography, **22**, 46-55.

Sterl, A. and C. Severijns, 2009. *NEMO + LIM + IFS + OASIS = EC-Earth.* OASIS user meeting 2009, 25/5/2009-26/5/2009, S. Valcke (Ed.), 2009, Toulouse, France, CERFACS.

Sterl, A., 2009. *Float of the month - March 2009: Caught in the Agulhas Current.* http://wo.jcommops.org/.

Sterl, A., H. van den Brink, H. de Vries, R. Haarsma and E. van Meijgaard, 2009. *An ensemble study of extreme North Sea storm surges in a changing climate.* Ocean Science Disc., **6**, 1131-1159.

Sterl, A., H. van den Brink, R. Haarsma, H. de Vries and E. van Meijgaard, 2009. *Stormklimaat en hoogwaters.* Meteorologica, **18**, 2, 10-11.

Vellinga, P., C.A. Katsman, A. Sterl and J.J. Beersma (Eds.), 2009. *Exploring high-end climate change scenarios for flood protection of the Netherlands.* International Scientific Assessment carried out at the request of the Delta Committee. KNMI Scientific Report WR-2009-05.

Wallbrink, H., F.B. Koek and T. Brandsma, 2009. *The US Maury Collection Metadata 1796-1861.* KNMI Publication PUBL-225, pp59.

Publications Regional Climate

The Regional Climate division combines model development, observations and fundamental research to address current issues in climate research on the regional scale. Current model development and application centres around the regional climate model RACMO-2, which is used for the national climate scenarios, IPCC Assessments and various research projects. An extensive groundbased observation programme is carried-out at the Cabauw Experimental Site for Atmospheric Research (CESAR), serving atmospheric research, model validation and climate monitoring. The main research topics of the division are clouds, radiation, aerosols and boundary layer physics.

Reviewed Publications

2007

Ekström, M., P.D. Jones, H.J. Fowler, G. Lenderink, T.A. Buishand and D. Conway, 2007. *Regional climate model data used within the SWURVE project 1: projected changes in seasonal patterns and estimation of PET.* Hydrology and Earth System Sciences, **11**, 3, 1069-1083.

Graaf, M. de, P. Stammes and E.A.A. Aben, 2007. *Analysis of reflectance spectra of UV-absorbing aerosol scenes measured by SCIAMACHY.* J. Geophys. Res., **112**.

Held, A., R. Niessner, F. Bosveld, T. Wrzesinsky and O. Klemm, 2007. *Evaluation and Application of an ElectricalLow Pressure Impactor in Disjunct Eddy Covariance Aerosol Flux Measurements.* Aerosol Science and Technology, **41**, 510-519.

Heymsfield, A.J., G.J. van Zadelhoff, D.P. Donovan, F. Fabry, R.J. Hogan and A.J. Illingworth, 2007. *Refinements to Ice Particle Mass Dimensional and Terminal Velocity Relationships for Ice Clouds. Part II: Evaluation and Parameterizations of Ensemble Ice Particle Sedimentation Velocities.* J. Atmos. Sci., **64**, 4, 1068-1088.

Hinssen, Y.B.L. and W.H. Knap, 2007. *Comparison of pyranometric and pyrheliometric methods for the determination of sunshine duration.* J. Atm. Oceanic Technol., **24**, 5, 835-846.

Illingworth, A.J., R.J. Hogan, E.J. O'Connor, D. Bouniol, M.E. Brooks, J. Delanoe, D.P. Donovan, N. Gaussiat, J.W.F. Goddard, M. Haeffelin, H. Klein Baltink, O.A. Krasnov, J. Pelon, J.M. Piriou and G.J. van Zadelhoff, 2007. *Cloudnet - continuous evaluation of cloud profiles in seven operational models using ground-based observations.* Bull. Amer. Meteor. Soc., **88**, 6, 883-898.

Jacob, D., L. Barring, O.B. Christensen, J.H. Christensen, M. de Castro, M. Deque, F. Giorgi, S. Hagemann, M. Hirschi, R. Jones, E. Kjellstrom, G. Lenderink, B. Rockel, A.P. van Ulden and B.J.J.M. van den Hurk, 2007. *An inter-comparison of regional climate models for Europe: model performance in present-day climate.* Climatic Change.

Jacobs, C.M.J., A.F.G. Jacobs, F.C. Bosveld, D.M.D. Hendriks, A. Hensen, P.S. Kroon, E.J. Moors, L. Nol, A. Schrier-Uijl and E.M. Veenendaal, 2007. *Variability of annual CO_2 Exchange from Dutch Grasslands.* Biogeosciences, **4**, 803-816.

Kjellström, E., L. Bärring, D. Jacob, R.J. Jones, G. Lenderink and C. Schär, 2007. *Modelling daily temperature extremes: Recent climate and future changes over Europe.* Climatic Change,.

Kohsiek, W., C. Liebethal, T. Foken, R. Vogt, S.P. Oncley, C. Bernhofer and H.A.R. de Bruin, 2007. *The energy balance experiment EBEX-2000. Part III: Behaviour and quality of the radiation measurements.* Bound.-Layer Meteorol., **123**, 55-75.

Löhnert, U., E. van Meijgaard, H. Klein Baltink, S. Groß and R. Boers, 2007. *Accuracy assessment of an integrated profiling technique for operationally deriving profiles of temperature, humidity and cloud liquid water.* J. Geophys. Res., **112**.

Lenderink, G., A. van Ulden, B. van den Hurk and E. van Meijgaard, 2007. *Summertime inter-annual temperature variability in an ensemble of regional model simulations: analysis of the surface energy budget.* Climatic Change.

Lenderink, G., T.A. Buishand and W.P.A. van Deursen, 2007. *Estimates of future discharges of the river Rhine using two climate scenario methodologies: direct versus delta approach.* Hydrology and Earth System Sciences, **11**, 3, 1145-1159.

Lenderink, G., A. van Ulden, B. van den Hurk and F. Keller, 2007. *A study on combining global and regional climate model results for generating climate scenarios of temperature and precipitation for the Netherlands.* Clim. Dyn., **29**, 2, 157-176.

Rauber, R.M., B. Stevens, H.T. Ochs III and A.P. Siebesma, 2007. *Rain in Shallow Cumulus over the Ocean; The RICO Campaign.* Bull. Amer. Meteor. Soc., 12, **88**, 1912-1937.

Roode, S.R. de, 2007. *The role of eddy diffusivity profiles on stratocumulus liquid water path biases.* Mon. Wea. Rev., **135**, 7, 2786-2793.

Roode, S.R. de and Q. Wang, 2007. *Do stratocumulus clouds detrain?* FIRE I data revisited.. Bound.-Layer Meteorol., **122**, 479-491.

Siebesma, A.P., P.M.M. Soares and J. Teixeira, 2007. *A Combined Eddy-Diffusivity Mass-Flux Approach for the Convective Boundary Layer.* J. Atmos. Sci., **64**, 1230-1248.

Ulden, A.P. van, G. Lenderink, B. van den Hurk and E. van Meijgaard, 2007. *Circulation statistics and climate change in Central Europe: PRUDENCE simulations and observations.* Climatic Change, **81**, 179-192.

Wyant, M.C., C.S. Bretherton, A. Chlond, B.M. Griffin, H. Kitagawa, C.L. Lappen, V.E. Larson, A. Lock, S. Park, S.R. de Roode, M. Zhao and A.S. Ackerman, 2007. *A single-column model intercomparison of a heavily drizzling stratocumulus topped boundary layer.* J. Geophys. Res., **112**.

Zadelhoff, G.J. van, E. van Meijgaard, D.P. Donovan, W.H. Knap and R. Boers, 2007. *Sensitivity of the shortwave radiative budget to the parameterization of ice crystal effective radius.* J. Geophys. Res., **112**, 1-11.

Zadelhoff, G.J. van, A.J. Heymsfield, D.P. Donovan and M.J. McGill, 2007. *Evaluating lidar-radar microphysics retrieval using in-situ measurements.* J. Geophys. Res., **112**.

2008

Baas, P., S.R. de Roode and G. Lenderink, 2008. *The Sclaing Behaviour of a Turbulent Kinetic Energy Closure Model for Stably Stratified Conditions.* Bound.-Layer Meteorol.

Boesche, E., P. Stammes, R. Preusker, R. Bennartz, W. Knap and J. Fischer, 2008. *Polarization of skylight in the O_2A band: effects of aerosol properties.* Appl. Optics, **47**, 3467-3480.

Boesche, E., P. Stammes and R. Bennartz, 2008. *Aerosol Influence on Polarization and Intensity in Near-Infrared O_2 and CO_2 Absorption Bands Observed from Space.* J. Quant. Spectros. Rad. Transf., **110**, 223-239.

Brinksma, E.J., G.J. Pinardi, R. Braak, H. Volten, A. Richter, R.J. Dirksen, T. Vlemmix, D.P.J. Swart, W.H. Knap, J.P. Veefkind,
H.J. Eskes, M. Allaart, R. Rothe, A.J.M. Piters and P.F. Levelt, 2008. *The 2005 and 2006 DANDELIONS NO_2 and Aerosol Intercomparison Campaigns.* J. Geophys. Res.

Casso-Torralba, P., J. Vila`-Guerau de Arellano, F.C. Bosveld, M.R. Soler, A. Vermeulen, C. Werner and E. Moors, 2008. *Diurnal and vertical variability of the sensible heat and carbon dioxide budgets in the atmospheric surface layer.* J. Geophys. Res., **113**.

Deneke, H.M., A.J. Feijt and R.A. Roebeling, 2008. *Estimating surface solar irradiance from METEOSAT SEVIRI-derived cloud properties.* Remote Sens. Environ., **112**, 3131-3141.

Deneke, H., R.A. Roebeling, E. Wolters, A. Feijt and C. Simmer, 2008. *On the Sensitivity of Satellite-Derived Cloud Properties to Sensor Resolution and Broken Clouds.* International Radiation Symposium (IRS2008), 3/8/2008-8/8/2008, 2008, Iguacu Falls, Brazil, IRS.

Helsen, M.M., M.R. van den Broeke, R.S.W. van de Wal, W.J. van de Berg, E. van Meijgaard, C.H. Davis, Y. Li and I. Goodwin, 2008. *Elevation Changes in Antarctica Mainly Determined b y Accumulation Variability.* Science, **320**, 1626-1629.

Heus, T., G. van Dijk, H.J.J. Jonker and H.E.A. van den Akker, 2008. *Mixing in shallow cumulus clouds studied by Lagrangian particle tracking.* J. Atmos. Sci., **65**, 2581-2597.

Heus, T., H.J.J. Jonker, H.E.A. van den Akker, E.J. Griffith, M. Koutek and F.H. Post, 2008. *A statistical approach to the life-cycle analysis of cumulus clouds selected in a Virtual Reality Environment.* J. Geophys. Res.

Heus, T., 2008. *On the edge of a cloud.* Thesis, TU Delft, 2008, Delft, 141p.

Hurk, B.J.J.M. van den, J. Ettema and P. Viterbo, 2008. *Analysis of soil moisture changes in Europe during a single growing season in a new ECMWF soil moisture assimilation system.* J. Hydrometeor., **9**, 116-131.

Jacobs, C.M.J., E.J. Moors, H. ter Maat, A.J. Teuling, G. Balsamo, K. Bergaoui, J. Ettema, M. Lange, B.J.J.M. van den Hurk, P. Viterbo and W. Wergen, 2008. *Validation of European Land Data Assimilation System (ELDAS) products using in situ observations.* Tellus, **60A**, 1023-1037.

Kuipers Munneke, P., C.H. Reijmer, M.R. van den Broeke, G. Koenig-Langlo, P. Stammes and W.H. Knap, 2008. *Analysis of clear-sky Antarctic snow albedo using observations and radiative transfer modeling.* J. Geophys. Res., D1711, **113**.

Lenderink, G. and E. van Meijgaard, 2008. *Increase in hourly precipitation extremes beyond expectations from temperature changes.* Nature Geoscience, **1**, 8, 511-514.

Rignot, E., J.L. Bamber, M.R. van den Broeke, C. Davis, Y. Li, W.J. van de Berg and E. van Meijgaard, 2008. *Recent Antarctic ice mass loss from radar interferometry and regional climate modelling.* Nature Geoscience, **1**, 2, 106-110.

Teixeira, J., B. Stevens, C.S. Bretherton, R. Cederwall, J.D. Doyle, J.C. Golaz, A.A.M. Holtslag, S.A. Klein, J.K. Lundquist, D.A. Randall, A.P. Siebesma and P.M.M. Soares, 2008. *Parameterization of the Atmospheric Boundary Layer: A view from just above the inversion.* Bull. Amer. Meteor. Soc., **89**, 4, 453-458.

2009

Apituley, A., K.M. Wilson, C. Potma, H. Volten and M. de Graaf, 2009. *Performance Assessment and Application of Caeli - A high-performance Raman lidar for diurnal profiling of Water Vapour, Aerosols and Clouds.* 8th International Symposium on Tropospheric Profiling, 19/10/2009-23/10/2009, A. Apituley, H.W.J. Russchenberg, W.A.A. Monna (Eds.), 2009, Delft, Proceedings of the 8th International Symposium on Tropospheric Profiling, ISBN 978-90-6960-233-2.

Baas, P., 2009. *Turbulence and Low-Level Jets in the Stable Boundary Layer.* Thesis, Wageningen University, 2009, Wageningen, 152p.

Baas, P., F.C. Bosveld, H. Klein Baltink and A.A.M. Holtslag, 2009. *A climatology of nocturnal low-level jets at Cabauw.* J. Appl. Meteor., **48**, 8, 1627-1642.

Boesche, E., G.J. van Zadelhoff and D.P. Donovan, 2009. *Microphysical properties of cirrus clouds as derived from CloudSat/CALIPSO.* 8th ISTP, 19/10/2009-23/10/2009, A. Apituley, H.W.J. Russchenberg, W.A.A. Monna (Ed.), 2009, Delft, Delft/KNMI/RIVM, Organizing Committee of the 8th International Symposium on Tropospheric Profiling, ISBN 978-90-6960-233-2.

Boesche, E., P. Stammes and R. Bennartz, 2009. *Aerosol Influence on Polarization and Intensity in Near-Infrared O_2 and CO_2 Absorption Bands Observed from Space.* J. Quant. Spectros. Rad. Transf., **110**, 3, 223-239.

Broeke, M. van den, J. Bamber, J. Ettema, E. Rignot, E. Schrama, W.J. van den Berg, E. van Meijgaard, I. Velicogna and B. Wouters, 2009. *Partitioning Recent Greenland Mass Loss.* Science, **326**, 5955, 984-986.

Cheinet, S. and A.P. Siebesma, 2009. *Variability of Local Structure Parameters in the Convective Boundary Layer.* J. Atmos. Sci., **66**, 1002-1017.

Deneke, H.M., W.H. Knap and C. Simmer, 2009. *Multiresolution Analysis of the Temporal Variance and Correlation of Transmittance and Reflectance of an Atmospheric Column.* J. Geophys. Res.

Donovan, D.P. and G.J. van Zadelhoff, 2009. *An Optimal-Estimation based hybrid Rayleigh-Mie Extinction and Backscatter retrieval Method for HSRL lidars.* 8th ISTP, 16/10/2009, 2009, Delft, Delft/KNMI/RIVM, The Organizing Committee of the 8th International Symposium on Tropospheric Profiling, ISBN 978-90-6960-233-2.

Ettema, J., M.R. van den Broeke, E. van Meijgaard, W.J. van de Berg, J.L. Bamber, J.E. Box and R.C. Bales, 2009. *Higher surface mass balance of the Greenland ice sheet revealed by high-resolution climate modeling.* Geophys. Res. Lett., **36**.

Graaf, M. De, D.P. Donovan and A. Apituley, 2009. *Aerosol microphysical properties from inversion of tropospheric optical Raman lidar data.* 8th International Symposium on Tropospheric Profiling, 19/10/2009, Edited by A. Apituley, H.W.J. Russchenberg, W.A.A. Monna (Eds.), 2009, Delft, The Netherlands, Delft/RIVM/KNMI, Organizing Committee of the 8th International Symposium on Tropospheric Profiling, ISBN ISBN 978-90-6960-2.

Klein, S.A. et al., 2009. *Intercomparison of model simulations of mixed-phase clouds observed during the ARM Mixed-Phase Arctic Cloud Experiment.* I: Single-layer cloud. Quart. J. Royal Meteor. Soc., **135**, 979-1002.

Lenderink, G. and E. van Meijgaard, 2009. *Reply: Unexpected rise in extreme precipitation caused by a shift in rain type?* Nature Geoscience, **2**, 6, 373.

Lenderink, G., E. van Meijgaard and F. Selten, 2009. *Intense coastal rainfall in the Netherlands in response to high sea surface temperatures: analysis of the event of August 2006 from the perspective of a changing climate.* Clim. Dyn., **32**, 19-33.

Neggers, R.A.J., 2009. *A dual mass flux framework for boundary layer convection. Part II: Clouds.* J. Atmos. Sci., **66**, 6, 1489-1506.

Neggers, R.A.J., M. Koehler and A.C.M. Beljaars, 2009. *A dual mass flux framework for boundary layer convection. Part I: Transport.* J. Atmos. Sci., **66**, 1465-1487.

Nuijens, L., B. Stevens and A.P. Siebesma, 2009. *The Environment of Precipitating Shallow Cumulus Convection.* J. Atmos. Sci., **66**, 1962-1979.

Ronda, R.J. and F.C. Bosveld, 2009. *Deriving the surface soil heat flux from observed soil temperature and soil heat flux profiles using a variational data-assimilation approach.*. J. Appl. Meteor., **48**, 3, 644-656.
Schulz, J., H. Deneke, R. Roebeling, E. Wolters and et al., 2009. *Operational climate monitoring from space: the EUMETSAT satellite application facility on climate monitoring (CM-SAF).* Atm. Chem. Phys., 9, 1-23.
Siebesma, A.P., 2009. *Cloud-Controlling Factors.* In Clouds in the Perturbed Climate System, Heintzenberg and Charlson (Eds.), 2009, Cambridge Massachusetts, MIT Press, ISBN 978-0-262-01287-4, p269-290.
Stammes, P., L.G. Tilstra, R. Braak, M. de Graaf and I. Aben, 2009. *Estimate of solar radiative forcing by polluted clouds using OMI and SCIAMACHY satellite data.* International Radiation Symposium IRS2008, 3/8/2008-8/8/2008, T. Nakajima and M.A. Yamasoe (Eds.), 2009, IRC/IAMAS, American Institute of Physics, ISBN 978-0-7354-0635-3, 577-580.
Sterl, A., H. van den Brink, H. de Vries, R. Haarsma and E. van Meijgaard, 2009. *An ensemble study of extreme North Sea storm surges in a changing climate.* Ocean Science, **5**, 369-378.
Su, Z., F.C. Bosveld, H. Klein Baltink, R. Rothe and et al., 2009. *EAGLE 2006 – multi-purpose, multi-angle and multi-sensor in-situ, airborne and space borne campaigns over grassland and forest.* Hydrology and Earth System Sciences, 13, 833-845.
Wang, P., W.H. Knap, P. Kuipers Munneke and P. Stammes, 2009. *Clear-sky shortwave radiative closure for the Cabauw Baseline Surface Radiation Network site, the Netherlands.* J. Geophys. Res., **114**.
Wang, P., W.H. Knap, P. Kuipers Munneke and P. Stammes, 2009. *Clear sky atmospheric radiative transfer: a model intercomparison of shortwave irradiances.* International Radiation Symposium IRS2008, 3/8/2008-8/8/2008, T. Nakajima and M.A. Yamasoe (Eds.), 2009, IRC/IAMAS, American Institute of Physics, ISBN 978-0-7354-0635-3, 125-128.
Zadelhoff, G.J. van and D.P. Donovan, 2009. *A potential FeatureMask algorithm for the EarthCARE lidar.* 8th ISTP, 19/10/2009, A. Apituley, H.W.J. Russchenberg, W.A.A. Monna (Eds.), 2009, Delft, Delft/KNMI/RIVM, Organizing Committee of the 8th International Symposium on Tropospheric Profiling, ISBN 978-90-6960-233-2.

Other publications

2007

Beyrich, F., W. Adam, F.C. Bosveld, J. Poutiainen and T. Savunen, 2007. *The contribution of the BALTEX In-situ reference sites to CEOP.* Fith Study Conference on BALTEX, 4/6/2007-8/6/2007, H.-J. Isemer (Ed.), 2007, Kuressaare, Estonia, International BALTEX Secretariat.
de Haij, M.J., W.M.F. Wauben and H. Klein Baltink, 2007. *Continuous mixing layer height determination using the LD-40 ceilometer: a feasibility study.* KNMI Scientific Report WR-2007-01.
Deneke, H.M., S. Johnston, M. Reuter, R.A. Roebeling, A. Tetzlaff, W. Thomas, E.L.A. Wolters and K.G. Karlsson, 2007. *Final validation of CM-SAF cloud products derived from MSG/SEVIRI data.* Validatierapportage voor CM-SAF wolkenproducten afgeleid uit SEVIRI-data, EUMETSAT.
Roode, S.R. de, 2007. *Thermodynamics of cumulus clouds.* In monographical issue Fisica de la Tierra, C. Yague (Ed.), 2007.
Tilstra, L.G., M. de Graaf, I. Aben and P. Stammes, 2007. *Analysis of 5 years SCIAMACHY Absorbing Aerosol Index data.* Envisat Symposium, 23/4/2007-27/4/2007, 2007, Montreux (CH), ESA SP-636, ESA/ESTEC.
Tilstra, L.G., M. de Graaf, S. Noel, E.A.A. Aben and P. Stammes, 2007. *SCIAMACHY's Absorbing Aerosol Index and the consequences of instrument degradation.* Third Workshop on the Atmospheric Chemistry Validation of ENVISAT (ACVE-3), 4/12/2006-7/12/2006, 2007.
Wolters, E.L.A., H.M. Deneke, R.A. Roebeling and A.J. Feijt, 2007. *Comparison of seviri and modis cloud phase determination over mid-latitude regions.* Joint 2007 EUMETSAT Meteorological Satellite Conference and the 15th AMS Satellite Meteorology and Oceanography Conference, 24/9/2007-28/9/2007, 2007.

2008

Apituley, A., H. Russchenberg, R. Boers, F. Bosveld, H. ten Brink and G. de Leeuw, 2008. *Fijn stof ook een klimaatprobleem.* Tijdschrift Lucht, **6**, 19-22.
Baas, P., F.C. Bosveld and H. Klein Baltink, 2008. *Low-level jets boven Cabauw.* Meteorologica.
Bessembinder, J., C. Katsman, W. Hazeleger, S. Drijfhout, H. van den Brink, G. Lenderink, E. Meijgaard, M. de Wit, H. Buiteveld and W. van Deursen, 2008. *Extreme klimaatverandering en waterveiligheid in Nederland.* KNMI Publication.
Boers, R. and G. van Zadelhoff, 2008. *IMPACT: Intensive Observation Period at CESAR Tower.* EUCAARI 2007 Annual Meeting, 19/11/2007-23/11/2007, Prof. Markku Kulmala (Ed.), 2008, Helsinki, University of Helsinki.
Boesche, E., 2008. *Influence of aerosols on polarization of skylight in gaseous absorption bands.* KNMI Scientific Report WR-2008-04.

Braam, M., 2008. *Determination of the surface sensible heat flux from the structure parameter of temperature at 60 m height.* KNMI Technical Report TR-303.

Brandau, C., H.W.J. Russchenberg and W.H. Knap, 2008. *Retrieval of water cloud properties using ground-based remote sensing measurements.* International Conference on Clouds and Precipitation ICCP-2008, 7/7/2008-11/7/2008, 2008, Cancun, Mexico.

De Martino, G., B. van Ulft, H. ten Brink, M. Schaap, E. van Meijgaard and R. Boers, 2008. *An aerosol-cloud module for inclusion in the KNMI regional climate model RACMO2.* KNMI Scientific Report WR-2008-05.

Donovan, D.P., 2008. *ALGORITHM THEORETICAL BASIS DOCUMENT (ATBD) FOR A-Extinction-KNMI.* Lidar extinction retrieval ATBD for the Casper project, Deimos Space S.L..

Donovan, D.P., G.J. van Zadelhoff and et al., 2008. *CASPER Products and Algorithms Requirements Document (PARD).* Products and Algorithms Requirements Document Casper project, Deimos Space S.L.

Donovan, D.P., G.J. van Zadelhoff and et al., 2008. *CASPER Product Definition Document (PDD).* The Product Definition Document for the Casper project, Deimos Space S.L.

Donovan, D.P., J.R. Acaretta, J.J. Ramos and G.J. van Zadelhoff, 2008. *End-to-END Mission/System Performance Simulation.* ECSIM Simulator Interface Control Document. EarthCARE simulator interface document, Deimos Space S.L.

Donovan, D.P., R.H. Voors, G.J. van Zadelhoff and J.R. Acaretta, 2008. *ECSIM Model and Algorithms Document.* Technisch Rapport EarthCare Simulator, Deimos Space S.L.

Graaf, M. de, D.P. Donovan and A. Apituley, 2008. *Refractive index and integral aerosol properties retrieval from Raman lidar data using principle component analysis.* 24th International Laser Radar Conference, 23/6/2008-27/6/2008, 2008, Boulder, Co., Organizing Committee of the 24th International Laser Radar Conference, ISBN 978-0-615-21489-4, 11-14.

Leijnse, H., R. Uijlenhoet, J. Bokhorst, H. Stricker, H. Russchenberg, F.C. Bosveld, W. Knap, R. Boers, H. ten Brink, G. de Leeuw and A. Apituley, 2008. *Klimaat Observaties in Cabauw.* Geografie.

Lenderink, G. and J. Beersma, 2008. *Kustneerslag en zomerdroogte.* De toestand van het klimaat in Nederland 2008.

Meijgaard, E. van, L.H. van Ulft, W.J. van de Berg, F.C. Bosveld, B.J.J.M. van den Hurk, G. Lenderink and A.P. Siebesma, 2008. *The KNMI regional atmospheric climate model RACMO, version 2.1.* KNMI Technical Report TR-302, pp43.

Oldenborgh, G.J. van, S.S. Drijfhout, A. Sterl and A. van Ulden, 2008. *Nederland warmt sneller op dan verwacht.* De toestand van het klimaat in Nederland 2008, 16-23.

Ramos, J.J., J.R. Acaretta and D.P. Donovan, 2008. *End-to-END Mission/System Performance Simulation.* ECSIM SYSTEM USER'S Manual. 2008, Deimos Space S.L., 121p.

Siebesma, A.P., 2008. *Advences in modelling and Observing Clouds and Convection Highlighted at the 4th PAN-GCSS meeting.* GEWEX News Letter, **18**, 4, 8-10.

Teixeira, J., S. Cardoso and A.P. Siebesma, 2008. *Results from the first 2 years of the GCSS Pacific Cross Section Intercomparison.* GEWEX News Letter, **18**, 1-4.

Zadelhoff, G.J. van, 2008. ALGORITHM THEORETICAL BASIS DOCUMENT (ATBD) FOR A-FeatureMask-KNMI. Lidar featuremask ATBD for the Casper project, Deimos Space S.L.

2009

Christensen, J.H., M. Rummukainen and G. Lenderink, 2009. *Formulation of very-high-resolution regional climate model ensembles for Europe.* Chapter in Summary of research and results from the ENSEMBLES project, Met Office Hadley Centre.

Engelbart, D.A.M., W.A.A. Monna, J. Nash and C. Mätzler, (Eds.) 2009. *Integrated Ground-Based Remote-Sensing Stations for Atmospheric Profiling.* Final Report COST Action 720, Publication Office of the European Union, Luxemburg, ISBN 978-92-898-0050-1, doi: 10.2831/10752.

Graaf, M. de, D.P. Donovan and A. Apituley, 2009. *Aerosol microphysical properties from inversion of tropospheric optical Raman lidar data.* 8th International Symposium on Tropospheric Profiling, 19/10/2009-23/10/2009, A. Apituley, H.W.J. Russchenberg, W.A.A. Monna (Eds.), 2009, Delft, Proceedings of the 8th International Symposium on Tropospheric Profiling, ISBN 978-90-6960-233-2.

Klein Baltink, H., B. Wilkens, M. Savenije and F.C. Bosveld, 2009. *Webaccess to the CESAR data: the CESAR DATBASE SYSTEM portal.* 8th International Symposium on Tropospheric Profiling, 19/10/2009-23/10/2009, A. Apituley, H.W.J. Russchenberg, W.A.A. Monna (Eds.), 2009, Delft, ISBN 978-90-6960-233-2.

Klein Tank, A., G. Lenderink, B. Overbeek and J. Bessembinder, 2009. *Klimaat Nederland verandert sterk.* Weer Magazine, **5**, 20-23.

Meijgaard, E. van, L. Wipfler, B.J.J.M. van den Hurk, K. Metselaar, J. van Dam, R. Feddes, L.H. van Ulft, S. Zwart and W. Bastiaanssen, 2009. *Evaluation of the land surface scheme HTESSEL with satellite derived surface energy fluxes at the seasonal* *time scale.* 2nd International Lund RCM Workshop, 4/5/2009-8/5/2009, 2009, Lund, Zweden, Lund University, Zweden; Baltex Secretariat, Geeshacht, Germany, Int. Baltex Secretariat Publication, ISBN ISSN 1681-6471, 105-106.

Monna, W.A.A. et al., 2009. *Climate Change Monitoring in the Netherlands; A proposal based on the GCOS Implementation Plan in Support of the UNFCCC.* Rapport van WAB project 500102011. WAB 500102011, Netherlands Environmental Assessment Agency PBL, PO Box 303, 3720 AH Bilthoven, NL.

Ulden, A. van, G.J. van Oldenborgh and G. van der Schrier, 2009. *The Construction of a Central Netherlands Temperature.* KNMI Scientific Report WR-2009-03, pp15.

Wang, P. and W.H. Knap, 2009. *Energy redistribution due to the cloud layer.* 8th International Symposium of Tropospheric Profiling, 19/10/2009-23/10/2009, 2009, Delft.

Williams, J.E., G.J. van Zadelhoff and M.P. Scheele, 2009. *The effect of updating scavenging and conversion rates on cloud droplets and ice particles in the TM global chemistry transport model.* KNMI Technical Report TR-308, pp45.

Publications
Chemistry and Climate

The mission of the Chemistry and Climate division is to quantify, understand and predict anthropogenic and natural changes in atmospheric composition and their consequences for climate, air quality and ultraviolet radiation. The main activity is the improvement of models of the life cycles of non-CO2 greenhouse gases, air pollutants, aerosols and their precursors in order to produce accurate short-term air quality forecasts, long-term scenarios for the future and reconstructions of palaeoclimates.

Reviewed Publications

2007

Blond, N., K.F. Boersma, H.J. Eskes, R.J. van der A, M. Van Roozendael, I. De Smedt, G. Bergametti and R. Vautard, 2007. *Intercomparison of SCIAMACHY nitrogen dioxide observations, in situ measurements and air quality modeling results over Western Europe.* J. Geophys. Res., **112**.

Denman, K.L., G. Brasseur, T. van Noije (contributing author) and co-authors, 2007. *Couplings between changes in the climate system and biogeochemistry.* In Climate Change 2007: The Physical Science Basis, S. Solomon, D. Qin, et al. (Ed), 2007, Cambridge, United Kingdom and New York, NY, USA, Cambridge University Press, p499-587.

Driesschaert, E., T. Fichefet, H. Goosse, P. Huybrechts, I. Janssens, A. Mouchet, V. Brovkin, G. Munhoven and S.L. Weber, 2007. *Modeling the influence of the Greenland ice sheet melting on the Atlantic MOC during the next millennia.* Geophys. Res. Lett., **34**.

Ebinghaus, R., F. Slemr, C.A.M. Brenninkmeijer, P. van Velthoven, A. Zahn, M. Hermann, D.A. O' Sullivan and D.E. Oram, 2007. *Emissions of gaseous mercury from biomass burning in South America in 2005 observed during CARIBIC flights.* Geophys. Res. Lett., **34**, L08813.

Eyring, V., D.S. Stevenson, A. Lauer, F.J. Dentener, T.P.C. van Noije and co-authors, 2007. *Multi-model simulations of the impact of international shipping on Atmospheric Chemistry and Climate in 2000 and 2030.* Atm. Chem. Phys., **7**, 757-780.

Fortuin, J.P.F., C.R. Becker, M. Fujiwara, F. Immler, H.M. Kelder, M.P. Scheele, O. Schrems and G.H.L. Verver, 2007. *Origin and transport of tropical cirrus clouds observed over Paramaribo, Suriname (5.8 N, 55.2 W).* J. Geophys. Res., **112**.

Guillaume, B., C. Liousse, R. Rosset, H. Cachier, P. van Velthoven, B. Bessagnet and N. Poisson, 2007. *ORISAM-TM4 : a new global sectional multi-component aerosol model including SOA formation - Focus on carbonaceous BC and OC aerosols.* Tellus, B, **59**, 2, 283-302.

Haklander, A.J., P.C. Siegmund and H.M. Kelder, 2007. *Interannual variability of the stratospheric wave driving during northern winter.* Atm. Chem. Phys., **7**, 2575-2584.

Juckes, M.N., M.R. Allen, K.R. Briffa, J. Esper, G.C. Hegerl, A. Moberg, T.J. Osborn and S.L. Weber, 2007. *Millennial temperature reconstruction intercomparison and evaluation.* Climate of the Past, **3**, 591-609.

Krijger, J.M., M. van Weele, I. Aben and R. Frey, 2007. *Technical Note: The effect of sensor resolution on the number of cloud-free observations from space.* Atm. Chem. Phys., **7**, 2881-2891.

Otto-Bliesner, B.L., C.D. Hewitt, T.M. Marchitto, E. rady, A. Abe-Ouchi, M. Crucifix, S. Murakami and S.L. Weber, 2007. *Last Glacial Maximum ocean thermohaline circulation: PMIP2 model intercomparisons and data constraints.* Geophys. Res. Lett., **34**.

Roche, D.M., H. Renssen, S.L. Weber and H. Goosse, 2007. *Could meltwater pulses have been sneaked unnoticed into the deep ocean during the last glacial?* Geophys. Res. Lett., **34**.

Roche, D.M., T.M. Dokken, H. Goosse, H. Renssen and S.L. Weber, 2007. *Climate of the Last Glacial Maximum: sensitivity studies amd model-data comparison with the LOVECLIM coupled model.* Climate of the Past, **3**, 205-224.

Tuenter, E., S.L. Weber, F.J. Hilgen and L.J. Lourens, 2007. *Simulating sub-Milankovitch climate variations associated with vegetation dynamics.* Climate of the Past, **3**, 169-180.

Wang, Y., M.B. McElroy, K.F. Boersma, H.J. Eskes and J.P. Veefkind, 2007. *Traffic restrictions associated with the Sino-African summit: Reductions of NO_x detected from space.* Geophys. Res. Lett., **34**, L08814.

Weber, S.L., S.S. Drijfhout, A. Abe-Ouchi, M. Curcifix, M. Eby, A. Ganopolski, S. Murakami, B. Otto-Bliesner and W.R. Peltier, 2007. *The modern and glacial overturning circulation in the Atlantic ocean in PMIP coupled model simulations.* Climate of the Past, **3**, 51-64.

Weber, S.L. and S.S. Drijfhout, 2007. *Stability of the Atlantic meridional Overturning Circulation in the Last Glacial maximum climate.* Geophys. Res. Lett., **34**.

2008

A, R.J. van der, H.J. Eskes, K.F. Boersma, T.P.C. van Noije, M. Van Roozendael, I. De Smedt, D.H.M.U. Peters, J.J.P. Kuenen and E.W. Meijer, 2008. *Identification of NO_2 sources and their trends from space using seasonal variability analyses.* J. Geophys. Res., **113**.

Bintanja, R. and R.S.W. van de Wal, 2008. *North American ice-sheet dynamics and the onset of the 100,000-year glacial cycles.* Nature, **454**, 869-872.

Bonisch, H., P. Hoor, C. Gurk, W. Feng, M. Chipperfield, A. Engel and B. Bregman, 2008. *Model evaluation of CO_2 and SF_6 in the extratropical UT/LS region.* J. Geophys. Res., **113**.

Engvall, A.-C., R. Krejci, J. Ström, R. Treffeisen, R. Scheele, O. Hermansen and J. Paatero, 2008. *Changes in aerosol properties during spring-summer period in the Arctic troposphere.* Atm. Chem. Phys., **8**, 3, 445-462.

Haklander, A.J., P.C. Siegmund, M. Sigmond and H.M. Kelder, 2008. *How does the northern-winter wave driving of the Brewer-Dobson circulation increase in an enhanced-CO_2 climate simulation?* Geophys. Res. Lett., **35**.

Haklander, A., 2008. *The Brewer-Dobson circulation: Interannual variability and climate change.* Thesis, Technische Universiteit Eindhoven, 2008, Eindhoven, 97p.

Hermann, M., C.A.M. Brenninkmeijer, F. Slemr, J. Heintzenberg, B.G. Martinsson, H. Schlager, P.F.J. van Velthoven, A. Wiedensohler, A. Zahn and H. Ziereis, 2008. *Submicrometer aerosol particle distributions in the upper troposphere over the mid-latitude North Atlantic results from the third route of CARIBIC.* Tellus, 60, **1**, 106-117.

Nguyen, H.N., B.G. Martinsson, J.B. Wagner, E. Carlemalm, M. Ebert, C.A.M. Brenninkmeijer, J. Heintzenberg, M. Hermann, P.F.J. van Velthoven and A. Zahn, 2008. *Chemical Composition and Morphology of Individual Aerosol Particles from a CARIBIC Flight at 10 km Altitude between 50 N and 30 S.* J. Geophys. Res., **113**.

Slemr, F., R. Ebinghaus, C.A.M. Brenninkmeijer, M. Hermann, H.H. Kock, B. Martinsson, T. Schuck, D. Sprung, P.F.J. van Velthoven, A. Zahn and H. Ziereis, 2008. *Gaseous mercury distribution in the upper troposphere and lower stratosp here observed onboard the CARIBIC passenger aircraft.* Atm. Chem. Phys., Disc., **8**, 18651-18688.

Smedt, I. De, J.F. Muller, T. Stavrakou, R.J. van der A, H. Eskes and M. Van Roozendael, 2008. *Twelve years of global observation of formaldehyde in the troposphere using GOME and SCIAMACHY sensors.* Atm. Chem. Phys., **8**, 16, 4947-4963.

Weber, S.L., 2008. *Can you step twice into the same river?* Climate change through time. Netherlands Journal of Geosciences, **87**, 3, 231-239.

Wohlfahrt, J., S.P. Harrison, P. Braconnot, C.D. Hewitt, A. Kitoh, U. Mikolajewicz, B. Otto-Bliesner and S.L. Weber, 2008. *Evaluation of coupled ocean-atmosphere simulations of the mid-Holocene using palaeovegetation data from the northern hemisphere extratropics.* Clim. Dyn., **31**, 871-890.

2009

Brunner, D. and P. Siegmund, 2009. *The SCOUT-O3 Darwin Aircraft Campaign: rationale and meteorology.* Atm. Chem. Phys., **9**, 93-117.

Flemming, J., A. Inness, H. Flentje, V. Huijnen, P. Moinat, M.G. Schultz and O. Stein, 2009. *Coupling global chemistry transport models to ECMWF's integrated forecast system.* Geoscientific Model Development, 2, 253-265.

Hoor, P., J. Borken-Kleefeld, D. Caro, O. Dessens, O. Endresen, M. Gauss, V. Grewe, D. Hauglustaine, I.S.A. Isaksen, P. Jockel,

J. Lelieveld, E. Meijer, D. Olivie, P.F.J. van Velthoven and et al., 2009. *The impact of traffic emissions on atmospheric ozone and OH: results from QUANTIFY.* Atm. Chem. Phys., **9**, 3113-3136.
Koppe, M., M. Hermann, C.A.M. Brenninkmeijer, J. Heintzenberg, H. Schlager, T. Schuck, F. Slemr, D. Sprung, P.F.J. van Velthoven, A. Wiedensohler, A. Zahn and H. Ziereis, 2009. *Origin of aerosol particles in the mid-latitude and subtropical upper troposphere and lowermost stratosphere from cluster analysis of CARIBIC data.* Atm. Chem. Phys., **9**, 8413-8430.
Martinsson, B.G., C.A.M. Brenninkmeijer, S.A. Carn, M. Hermann, K.P. Heue, P.F.J. van Velthoven and A. Zahn, 2009. *Influence of the 2008 Kasatochi Volcanic Eruption on Sulfurous and Carbonaceous Aerosol Constituents in the Lower Stratosphere.* Geophys. Res. Lett., **36**, 1-5.
Otto-Bliesner, B., R. Schneider, E. Brady, ...and S.L. Weber, 2009. *A comparison of PMIP2 model simulations and the MARGO proxy reconstruction for tropical sea surface temperatures at last glacial maximum.* Clim. Dyn., **32**, 799-815.
Schnadt Poberaj, C., J. Staehelin, R. Bintanja, P.F.J. van Velthoven, O. Dessens, M. Gauss, I.S.A. Isaksen, V. Grewe, P. Jockel, P. Hoor, B. Koffi, D. Hauglustaine and D. Olivie, 2009. *QUANTIFY model evaluation of global chemistry models: carbon monoxide.* Transport, Atmosphere and Climate Confernece (TAC-2), 10/6/2009-25/6/2009, R. Sausen (Ed.), 2009, Aken-Maastricht, DLR, KNMI.
Slemr, F., R. Ebinghaus, C.A.M. Brenninkmeijer, M. Hermann, H.H. Kock, B. Martinsson, T. Schuck, D. Sprung, P.F.J. van Velthoven, A. Zahn and H. Ziereis, 2009. *Gaseous mercury distribution in the upper troposphere and lower stratosphere observed onboard the CARIBIC passenger aircraft.* Atm. Chem. Phys., **9**, 6, 1957-1969.
Weigelt, A., M. Hermann, P.F.J. van Velthoven, C.A.M. Brenninkmeijer,, G. Schlaf, A. Zahn and A. Wiedensohler, 2009. *Influence of clouds on aerosol particle number concentrations in the upper troposphere.* J. Geophys. Res., **114**.
Williams, J.E., M.P. Scheele, P.F.J. van Velthoven, J.P. Cammas, V. Thouret, C. Gacy-Lacaux and A. Volz-Thomas, 2009. *The influence of biogenic emissions from Africa on tropical tropospheric ozone during 2006: a global modeling study.* Atm. Chem. Phys., **9**, 10367-10427.

Other publications

2007

Bintanja, R., 2007. *Ice-atmosphere interactions and near-surface processes.* In Encyclopedia Antarctica, B. Riffenburgh (Ed.), 2007, New York, Routledge, p498-500.
Brenninkmeijer, C.A.M., P.F.J. van Velthoven and et al., 2007. *The CARIBIC aircraft system for detailed, long-term, global-scale measurement of trace gases and aerosol in a changing atmosphere.* IGActivities Newsletter, **37**, 2-9.
Dalsoren, S.B., T. Pulles, D. Panasiuk, M. Schultz, S. Rast, S. Schroder, T. van Noije and S. Szopa, 2007. *RETRO report on analysis of past and present policy response to trends in European air pollution.*
Hilaire, J., 2007. *Modelling of Birch pollen concentrations using an atmospheric transport model.* 2007, KNMI, 77p.
Noije, T. van, 2007. *Interactive comment on "Medium-range mid-tropospheric transport of ozone and precursors over Africa: two numerical case-studies in dry and wet seasons" by B. Sauvage et al.* Atm. Chem. Phys. Disc., **7**, S1463-S1471.
Polavarapu, S., H.J. Eskes and T.G. Shepherd, 2007. *Report on the SPARC Data Assimilation Workshop.* SPARC/WCRP Newsletter, **28**, 1285-19.
Schultz, M.G., T. van Noije, P. van Velthoven and co-authors, 2007. *REanalysis of the TROpospheric chemical composition over the past 40 years (RETRO) - A long-term global modeling study of tropospheric chemistry.* Final Report, Forschungszentrum Jülich GmbH.
Siegmund, P., 2007. *Wat beweegt de atmosfeer?* Nederlands Tijdschrift voor Natuurkunde, **73**, 7, 240-242.
Siegmund, P., H. Slaper, G. Velders, H. De Backer, R. van der A, M. van Weele, P. Veefkind, M. Allaart, D. Swart and P. den Outer, 2007. *Bescherming ozonlaag: 20 jaar effectief beleid - een welkome waarheid.* Folder.
Siegmund, P.C., 2007. *IPCC AR4, WG1, Chapter 3: Observations: Surface and atmospheric climate change (contributing author).* In Climate Change: The Physical Science Basis, 2007, Cambridge University Press.
Siegmund, P.C., 2007. *Waarom zijn de tropen zo koud en de polen zo warm?* Nederlands Tijdschrift voor Natuurkunde, **73**, 5, 153.
Siegmund, P.C., H. Slaper and G. Velders, 2007. *Bescherming ozonlaag: 20 jaar effectief beleid - een welkome waarheid.* Weer Magazine, 5, **38**.
Szopa, S., D.A. Hauglustaine, M. Schultz, T. van Noije, S. Rast, N.H. Savage and S. Dalsoren, 2007. *RETRO report on analysis of sensitivity of model trends and interannual variability to emissions, chemistry and dynamics.*
Szopa, S., M.G. Schultz, D.A. Hauglustaine, S. Dalsoren, T. van Noije, S. Rast and N.H. Savage, 2007. *RETRO report on the reanalysis simulations.*

Velthoven, P.F.J. van and M. van Weele, 2007. HYMN *First Periodic Activity Report.* HYMN First Periodic Activity Report, KNMI.

Velthoven, P.F.J. van and P. Bousquet, 2007. HYMN: *HYdrogen, Me thane and Nitrous oxide.* Workshop on Atmospheric monitoring and inverse modelling for verification of national and EU bottom-up GHG inventories, 8/3/2007-9/3/2007, P.Bergamaschi (Ed.), 2007, Ispra, Italy, Climate Change Committee Working Group I, EC-JRC, ISBN ISSN 1018-5593, 33-34.

Verver, G.H.L., 2007. *The role of the tropics in climate.* tijdschrift 'Interactie', AdeK Univ. Suriname, **8**.

Verver, G.H.L., J.P.F. Fortuin, F. Immler, C. Becker, M. DeMaziere, B. Dix, J. Notholt, S. Naipal, O. Schrems and M. Fujiwara, 2007. *Recent tropical field campaigns in Paramaribo, Suriname.* International symposium on the Tropical Stratosphere - Upper Troposphere, 5/11/2007-9/11/2007, 2007, Saint Gilles, Ile de la Reunion, SPARC - SCOUT- NDACC - CNRS.

Weber, S.L., L.J. Lourens and W.Z. Hoek, 2007. *Het klimaat en de mens.* Geo Brief (Nieuwsbrief KNGMG, ALW en KTFG), 2, 20-21.

Weele, M. van and R. van der A, 2007. *Spaceborne surface UV radiation products as available from TEMIS.* 18/9/2007-20/9/2007, J. Groebner (Ed.), 2007, Davos, Zwitserland, PMOD, 175-176.

Weele, M. van, 2007. CAMELOT *Preparation of Geophysical Scenarios for Simulations: Trace Gas Concentration Fields (Task 1.5).* Eind(deel-)rapport CAMELOT: Trace gas concentration scenarios, KNMI.

2008

Huijnen, V., 2008. *Model Documentation of TM5, with focus on GEMS settings.* GEMS-GRG project.

Huijnen, V., H. Eskes, J. Marshall, D. Ceburnis, A. Gross, M. Schulz, P. Agnew, S. Kinne and A. Ghelli, 2008. *Scoring approaches for the GEMS project.* Document on scoring approaches in GEMS.

Leeuw, G. de, M. van Weele, H. Jaervinen and T. Mielonen, 2008. CAMELOT *Geophysical scenarios for simulations.* CAMELOT Geophysical scenarios for simulations.

Noije, T. van, 2008. *Ozon, luchtkwaliteit en klimaatverandering.* Tijdschrift Lucht, **6**, 12-15.

Noije, T. van, H. Eskes, G. Verver and R. van der A, 2008. *Troposferisch ozon en het klimaat.* De toestand van het klimaat in Nederland 2008, pp47.

Velthoven, P.F.J. van, 2008. HYMN *Second Periodic Management Report.* Report to EU.

Weber, S.L., 2008. *Kan men twee keer in dezelfde rivier stappen?* klimaatverandering door de tijd. Oratie, Universiteit Utrecht, 1-25.

Weber, S.L., 2008. *Kan men twee keer in dezelfde rivier stappen?* Meteorologica, **17**, 3, 7-11.

Weber, S.L., 2008. *The discovery of global warming.* Geobrief, **5**, 14-15.

Weber, S.L., 2008. *Ups en downs van het klimaat sinds 1000 AD*. Stator, 4-9.

Williams, J.E. and T.P.C. van Noije, 2008. *On the upgrading of the modified Carbon Bond Mechanism IV for use in global Chemistry Transport Models.* KNMI Scientific Report WR-2008-02, pp64.

2009

Aarssen, S. and N. Weber, 2009. *1000 jaar vulkaanuitbarstingen en de temperatuur in de lage landen.* Meteorologica, **18**, 3, 11-15.

Eskes, H., 2009. *Luchtkwaliteitsverwachtingen (LuKwa): Productspecificatie en datastomen.* 2009, KNMI.

Huijnen, V., 2009. *Consistency of reactive trace gases in the integrated reanalysis and forecast run within the GEMS system.* GEMS report.

Piters, A.J.M., B. Buchmann, D. Brunner, R.C. Cohen, J.C. Lambert, G. de Leeuw, P. Stammes, M. van Weele and F. Wittrock, 2009. *Data quality and validation of satellite measurements of tropospheric composition.* In The Remote Sensing of Trop. Composition from Space, 2009, Springer.

Ruyter de Wildt, M.S. de, H.J. Eskes and P.F.J. van Velthoven, 2009. *Lotos-Euros versie 1.4: bias-correctie voor PM10*. 2009, KNMI, 4p.

Ruyter de Wildt, M.S. de, H.J. Eskes and P.F.J. van Velthoven, 2009. *Lotos-euros verwachting van fijn stof: vergelijking met metingen en optimalisatie.* 2009, KNMI, 11p.

Williams, J.E., G.J. van Zadelhoff and M.P. Scheele, 2009. *The effect of updating scavenging and conversion rates on cloud droplets and ice particles in the TM global chemistry transport model.* KNMI Technical Report TR-308, pp45.

Publications Climate Services

The Climate Services division provides knowledge and information on past, current and future climate to professional users and the general public.

Reviewed Publications

2007

Beersma, J.J. and T.A. Buishand, 2007. *Drought in the Netherlands - Regional frequency analysis versus time series simulation.* J. Hydrol., **347**, 332-346.

Beersma, J.J., 2007. *Extreme hydro-meteorological events and their probabilities.* Thesis, Wageningen Universiteit, 2007, Wageningen, 157p.

Buishand, T.A., 2007. *Estimation of a large quantile of the distribution of multi-day seasonal maximum rainfall: the value of stochastic simulation of long-duration sequences.* Climate Research, **34**, 3, 185-194.

Hingray, B., A. Mezghani and T.A. Buishand, 2007. *Development of probability distributions for regional climate change from uncertain global mean warming and an uncertain scaling relationship.* Hydrology and Earth System Sciences, **11**, 3, 1097-1114.

Leander, R. and T.A. Buishand, 2007. *Resampling of regional climate model output for the simulation of extreme river flows.* J. Hydrol., **332**, 487-496.

Mölg, T., D.R. Hardy, G. Kaser, E.J. Klok and N.J. Cullen, 2007. *Mass balance of a slope glacier on Kilimanjaro and its sensitivity to climate.* Int. J. Climatology.

Trenberth, K.E., P.D. Jones, P. Ambenje, R. Bojariu, D. Easterling, A. Klein Tank, D. Parker, F. Rahimzadeh, J.A. Renwick, M. Rusticucci, B. Soden and P. Zhai, 2007. *Observations: Surface and Atmospheric Climate Change.* In Climate Change 2007: The Physical Science Basis, Solomon, S. et al. (Eds.), 2007, Cambridge, Cambridge University Press, ISBN 978 0521 88009-1, p235-336.

2008

Begert, M., E. Zenkusen, C. Haeberli, C. Appenzeller and L. Klok, 2008. *An automated homogenization procedure; performance assessment and application to a large European climate dataset.* Meteor. Z., **17**, 5, 663-672.

Brandsma, T. and J.P. van der Meulen, 2008. *Thermometer Screen Intercomparison in De Bilt (the Nether-lands), Part II: Description and modeling of mean temperature differences and extremes.* Int. J. Climatology, 1, **28**, 3, 389-400.

Buishand, T.A., L. de Haan and C. Zhou, 2008. *On spatial extremes: with application to a rainfall problem.* Ann. Applied Statistics, **2**, 2, 624-642.

Deneke, H.M., A.J. Feijt and R.A. Roebeling, 2008. *Estimating surface solar irradiance from METEOSAT SEVIRI-derived cloud properties.* Remote Sens. Environ., **112**, 3131-3141.

Deneke, H., R.A. Roebeling, E. Wolters, A. Feijt and C. Simmer, 2008. *On the Sensitivity of Satellite-Derived Cloud Properties To Sensor Resolution and Broken Clouds.* International Radiation Symposium (IRS2008), 3/8/2008-8/8/2008, 2008, Iguacu Falls, Brazil, IRS.

Dorland, R. van, B. Jansen and W. Dubelaar-Versluis, 2008. *De Staat van het Klimaat 2007*. 2008, De Bilt/Wageningen, PCCC.

Haylock, M.R., N. Hofstra, A.M.G. Klein Tank, E.J. Klok, P.D. Jones and M. New, 2008. *A European daily high-resolution gridded dataset of surface temperature and precipitation for 1950-2006*. J. Geophys. Res., **113**.

Klok, E.J. and A.M.G. Klein Tank, 2008. *Updated and extended European dataset of daily climate observations.* Int. J. Climatology.

Leander, R., T.A. Buishand, B.J.J.M. van den Hurk and M.J.M. de Wit, 2008. *Estimated changes in flood quantiles of the river Meuse from resampling of regional climate model output.* J. Hydrol., **351**, 331-343.

Schrier, G. van der and P.D. Jones, 2008. *Storminess and Cold Air Outbreaks in NE America during* AD *1790-1820*. Geophys. Res. Lett., **35**, L02713.

Schrier, G. van der and P.D. Jones, 2008. *Daily temperature and pressure series for Salem, Massachusetts (1786-1829).* Climatic Change, **87**, 3, 499-515.

Wolters, E.L.A., R.A. Roebeling and A.J. Feijt, 2008. *Evaluation of cloud phase retrieval methods for SEVIRI onboard METEOSAT-8 using ground-based lidar and cloud radar data.* J. Appl. Meteor., **47**, 6, 1723-1738.

2009

Briffa, K.R., G. van der Schrier and P.D. Jones, 2009. *Wet and sry summers in Europe since 1750: evidence of increasing drought.* Int. J. Climatology, **29**, 1894-1905.

Hanel, M., T.A. Buishand and C.A.T. Ferro, 2009. *A non-stationary index-flood model for precipitation extremes in transient Regional Climate Model simulations.* J. Geophys. Res., **114**, D15107.

Wever, N., M. Lehning, A. Clifton, J.D. Ruedi, K. Nishimura, M. Nemoto, S. Yamaguchi and A. Sato, 2009. *Verification of moisture budgets during drifting snow conditions in a cold wind tunnel.* Water Resour. Res., **45**, W07423.

Zaiki, M., G.P. Können, K. Kimura, T. Mikami and T. Tsukahara, 2009. *Reconstruction of historical pressure patterns over Japan using two-point pressure–temperature datasets since the 19th century.* Climatic Change, **95**, 231-248.

Van den Brink, H.W. and G.P. Können, 2009. *Estimating 10000-year return values from short time series.* Int. J. Climatology.

Other publications

2007

Bakker, A. and J. Bessembinder, 2007. *Neerslagreeksen voor de KNMI'06 scenario's.* H_2O, **22**, 45-47.

Bakker, A.M.R., 2007. *Gevolgen klimaatverandering voor windenergie.* Meteorologica, **4**, 26-27.

Bessembinder, J. et al., 2007. *Klimaateffectschetsboek Zuid-Holland.* DHV.

Brandsma, T., 2007. *Vergelijking van thermometerhutten.* Meteorologica, **16**, 2, 21-25.

Buishand, T.A. and J.B. Wijngaard, 2007. *Statistiek van extreme neerslag voor korte neerslagduren.* KNMI Technical Report TR-295, pp19.

Deneke, H., R.A. Roebeling, E.L.A. Wolters and A.J. Feijt, 2007. *Globale stralingsmeting vanuit de ruimte.* Meteorologica, **16**, 3, 21-25.

Kattenberg, A., 2007. *De menselijke invloed op het klimaat is onmiskenbaar.* Brochure i.s.m. WEERmagazine.

Monna, W.A.A., 2007. *GCOS National Report: the Netherlands.* GCOS Steering Committee, fifteenth Session, 16/10/2007-19/10/2007, 2007, Parijs, Frankrijk, GCOS.

Schrier, G. van der and R. Groenland, 2007. *De zomerstorm van 1674.* Meteorologica, **2**, 4-9.

Schrier, G. van der, H. Wallbrink and C. Wilkinson, 2007. *Major James Rennell's current charts digitally available.* History of Oceanography Newsletter, **19**.

Sluijter, R.J.C.F., 2007. *De Bosatlas van Nederland.* In De Bosatlas van Nederland, 2007, Groningen, Wolters Noordhoff.

Sluijter, R.J.C.F., 2007. *Seizoensoverzicht lente 2007*. Weer Magazine.

Sluijter, R.J.C.F., 2007. *Seizoensoverzicht zomer 2007*. Weer Magazine.

Stuyt, L., J. Bessembinder and A. Idenburg, 2007. *Klimaatschetsboeken en eerste generatie geodatabank in de provinciale planvorming.* H_2O, **22**, 30-32.

Wit, M. de and T.A. Buishand, 2007. *Generator of Rainfall And Discharge Extremes (GRADE) for the Rhine and Meuse basins.* 2007, Rijkswaterstaat RIZA, Report 2007.027, ISBN 9789036914062, 76p.

Wolters, E.L.A., H.M. Deneke, R.A. Roebeling and A.J. Feijt, 2007. *COMPARISON OF SEVIRI AND MODIS CLOUD PHASE DETERMINATION OVER MID-LATITUDE REGIONS.* Joint 2007 EUMETSAT Meteorological Satellite Conference and the 15th AMS Satellite Meteorology and Oceanography Conference, 24/9/2007-28/9/2007, 2007.

2008

Arts, I., A. Klein Tank and G. van der Schrier, 2008. *Structural time series analysis of meteorological data: in search of weekly cycles in Europe.* KNMI Preprint PR, afstudeerverslag.

Bakker, A.M.R. and A. te Linde, 2008. *Scenario voor de piekafvoeren van de Rijn bij Lobith.* Geografie, 12-14.

Besselaar, E.J.M. van den, 2008. *ENSEMBLES gridded observational dataset (E-Obs).* Baltex Newsletter, **12**, 16-17.

Bessembinder, J., C. Katsman, W. Hazeleger, S. Drijfhout, H. van den Brink, G. Lenderink, E. Meijgaard, M. de Wit, H. Buiteveld and W. van Deursen, 2008. Extreme klimaatverandering en waterveiligheid in Nederland. KNMI Publication.

Bessembinder, J.J.E., 2008. *Aandacht voor veiligheid.* KNMI Publication PUBL-221.

Brandsma, T. and A. van Ulden, 2008. *Temperatuurreeksen.* KNMI Preprint PR, De toestand van het klimaat in Nederland, pp47.

Brandsma, T., 2008. *Data rescue and digitization: tips and tricks resulting from the Dutch experience.* International Workshop on Rescue and Digitization of Climate Records in the Mediterranean Basin, 28/11/2007-30/11/2007, Manola Brunet and Franz Kuglitsch (Eds.), 2008, Geneva, Switzerland, World Meteorological Organization, WMO, WCDMP No. 67, WMO-TD No.1432, 47-54.

Buishand, T.A. and J.B. Wijngaard, 2008. *Statistiek van extreme neerslag voor het stedelijk waterbeheer.* H_2O, **41**, 8, 28-30.

Buishand, T.A., J.J. Beersma, R. Sluiter and T. Kroon, 2008. *Definitiestudie raterdata meteorologie.* rapport, KNMI en RWS Waterdienst.

Dorland, R. van, 2008. *Maandelijkse weerpagina.* Zenit.

Dorland, R. van, 2008. *Waarom is Poznan belangrijk voor het klimaat?* Trouw, 27 november 2008.

Groen, G., 2008. *Factsheet Zware storm*. KNMI Preprint PR.

Groen, G., 2008. *Meten is weten? Over mistdruppels op spinrag voor de zichtmeter.* Meteorologica, **17**, 1, 28.

Hanel, M. and T.A. Buishand, 2008. *Preliminary evaluation of precipitation extremes in RCM data for the Rhine basin.* ENSEMBLES deliverable D5.21.

Kabat (Red.), P., W. Hazeleger, C. Katsman, A. Sterl, J. Beersma, A. Klein Tank, P. Vellinga, R. Hutjes and R. Swart, 2008. *Toelichting op door de Deltacommissie gebruikte klimaatscenario's - Bijlage 3 van 'Samen werken met water'.* In Samen werken met water, Deltacommissie 2008 (Ed.), 2008, ISBN 978-90-9023484-7, p106-117.

Lablans, W. and G. van der Schrier, 2008. *De voorspelbaarheid van het weer van Lavoisier tot Lorenz. 2. Het tijdperk van de numerieke verwachtingen.* Meteorologica, **17**, 1, 9-14.

Leander, R. and T.A. Buishand, 2008. *Rainfall generator for the Meuse basin; Description of 20000-year simulations.* -196-IV, pp15.

Lubczynska, M., G. van der Schrier and A. Klein Tank, 2008. *Feedback between soil moisture and spells of warm summer weather in Europe.* KNMI Preprint PR, afstudeerverslag.

Overeem, A., I. Holleman and A. Buishand, 2008. *A 10-year Radar-based Climatology of Rainfall.* ERAD 5, 30/6/2008-4/7/2008, 2008, Helsinki.

Petersen, A., B. Eickhout, B. Strengers and R. van Dorland, 2008. *Wetenschappers te zeker over invloed van de zon: afkoeling deze eeuw is zeer onwaarschijnlijk.* Financieel Dagblad.

Vellinga, P., C.A. Katsman, A. Sterl and J.J. Beersma (Eds.), 2008. *Onderzoek naar bovengrensscenario's voor klimaatverandering voor overstromingsbescherming van Nederland: een internationale wetenschappelijke beoordeling.* Publicatie van KNMI en Wageningen UR (Alterra, Earth System Science and Climate Change Group), pp178.

Vellinga, P., R. van Dorland and P. Kabat, 2008. *Goede vragen vereisen goede antwoorden: kritiek op gangbaar klimaatonderzoek weersproken.* Spil, 2/3, 30-33.

Wever, N., 2008. *Effectieve temperatuur en graaddagen, klimatologie en klimaatscenario's.* KNMI Publication PUBL-219.

Wit, M. de, H. Buiteveld, W. van Deursen, F. Keller and J. Bessembinder, 2008. *Klimaatverandering en de afvoer van de Rijn en Maas.* Stromingen, **14**, 1, 13-24.

Wit, M.J.M. de and T.A. Buishand, 2008. *Extreme afvoeren voor Rijn en Maas gebundeld in GRADE.* H_2O, **41**, 1, 8-9.

2009

Aarssen, S. and N. Weber, 2009. *1000 jaar vulkaanuitbarstingen en de temperatuur in de lage landen.* Meteorologica, **18**, 3, 11-15.

Bakker, A.M.R., J.J.E. Bessembinder, T. Kroon and B.J.J.M. van den Hurk, 2009. *Klimatologisch standaardjaar op dagbasis voor heden en toekomst.* 2009, KNMI, 64p.

Bessembinder (ed), J. et al., 2009. *Klimaatschetsboek Nederland: het huidige en toekomstige klimaat.* KNMI Preprint, KNMI report 223, pp84.

Brandsma, T., 2009. *Understanding inter-site temperature differences at the KNMI terrain in De Bilt (the Netherlands).* Joint 6th Seminar for homogenization and qualtity control in climatological databases and the COST-HOME meeting, 26/5/2008-30/5/2008, Hungarian Met Office (Ed.), 2009.

Buishand, T.A., 2009. *Basisgegevens neerslaggenerator Maasstroomgebied.* Basisgegevens neerslaggenerator Maasstroomgebied.

Buishand, T.A., R. Jilderda and J.B. Wijngaard, 2009. *Regionale verschillen in extreme neerslag.* KNMI Scientific Report WR-2009-01, pp47.

Caires, S., H. de Waal, G. Groen, N. Wever and C. Geerse, 2009. *Assessing the uncertainties of using land-based wind observations for determining extreme open-water winds.* Deltarees 1200264-005, Deltares.

Dorland, R. van en W. Dubelaar-Versluis. *De Staat van het Klimaat 2008.* Actueel onderzoek en beleid nader verklaard, PCCC, verschenen 2009.

Dorland, R. van, B.J. Strengers, H. Dolman, R. Haarsma, C. Katsman, G.J. van Oldenborgh, A. Sluijs and R.S.W. van de Wal, 2009. *News in Climate Science since IPCC 2007, Topics of interest in the scientific basis of climate change.* KNMI Scientific Report.

Dorland, R. van. Maandelijks populair wetenschappelijk artikel in Zenit.

Groen, G., 2009. *Discussie NVBM over het rapport van de Deltacommissie.* Meteorologica, 2.

Groen, G., 2009. *Gevoelstemperatuur in de winter, invoering JAG/TI-methode.* Meteorologica.

Groen, G., 2009. *Gevoelstemperatuur in de winter, invoering JAG/TI-methode.* Meteorologica, 18-21.

Groen, G., 2009. *Maandoverzicht juli 2009.* KNMI Preprint PR, Maandoverzicht juli 2009.

Groen, G., 2009. Storm 25 januari 1990, vergelijking potentiële wind. WTI-2011, faserapport 1b Deltares, Deltares.

Groen, G., 2009. *Wind chill equivalente temperatuur (WCET), KNMI implementatie JAG/TI-methode voor de gevoelstemperatuur in de winter.* 2009, KNMI, TR, 27p.

Groen, G., 2009. *Wind chill equivalente temperatuur.* 2009, KNMI, 27p.

Groen, G., 2009. *Windchill equivalent temperature (WCET) climatology and scenarios for Schiphol Airport.* 2009, KNMI, TR, 17p.

Hanel, M., T.A. Buishand and C.A.T. Ferro, 2009. *A non-stationary index-flood model for precipitation extremes in transient Regional Climate Model simulations.* ENSEMBLES deliverable D5.22.

Klein Tank, A. and G. Lenderink, 2009. *Klimaatverandering in Nederland: Aanvullingen op de KNMI'06 scenario's.* Scenario brochure 2009, pp36.

Klein Tank, A., 2009. *IPCC report, KNMI scenarios and the Delta Committee.* Meteorologica, 2, 7-8.

Klein Tank, A., G. Lenderink, B. Overbeek and J. Bessembinder, 2009. *Klimaat Nederland verandert sterk.* Weer Magazine, 5, 20-23.

Klein Tank, A.M.G., F.W. Zwiers and X. Zhang, 2009. *Guidelines on analysis of extremes in a changing climate in support of informed decisions for adaptation.* WMO-TD No. 1500, WMO, Geneva.

Schrier, G. van der and R. Groenland, 2009. *De najaarsstorm van 1-2 oktober 1697.* Meteorologica, **1**, 4-6.

Schrier, G. van der and R. Groenland, 2009. *De najaarsstorm van 1-2 oktober 1697.* Meteorologica.

Schrier, G. van der and R. Groenland, 2009. *De najaarsstorm van 1-2 oktober 1697.* Meteorologica, 1.

Ulden, A. van, G.J. van Oldenborgh and G. van der Schrier, 2009. *The Construction of a Central Netherlands Temperature.* KNMI Scientific Report WR-2009-03, pp15.

Vellinga, P., C.A. Katsman, A. Sterl and J.J. Beersma (Eds.), 2009. *Exploring high-end climate change scenarios for flood protection of the Netherlands.* International Scientific Assessment carried out at the request of the Delta Committee. KNMI Scientific Report WR-2009-05.

Wever, N. and G. Groen, 2009. *Improving potential wind for extreme wind statistics.* 20/1/2009, 2009.

Wever, N. and G. Groen, 2009. *Improving potential wind for extreme wind statistics.* KNMI Scientific Report WR-2009-02, pp114.

Wever, N. and G. Groen, 2009. *Preliminary investigations into the curvature problem in extreme wind statistics.* Preliminary investigations into the curvature problem in extreme wind statistics SBW-Belastingen: Phase 1b of subproject, Deltares.

Wever, N., 2009. *Windstotenklimatologie Nederland.* 2009, KNMI, 49p.

Zwiers, F., A. Klein Tank and H. Cattle, 2009. *CLIVAR/CCL/JCOMM Expert Team on Climate Change Detection and Indices.* Exchanges, **14**, 2, 30-31.

Publications Seismology

The Seismology division is a knowledge-based research centre and observatory for earthquakes and related events. On the basis of seismological and other geophysical observations like infrasound, the Seismology division is active in fundamental and applied research in the field of seismology and furthermore hosts the European centre for exchange and coordination of seismological data (ORFEUS).

Reviewed Publications

2007

Dost, B. and H.W. Haak, 2007. *Natural and Induced Seismicity.* In Geology of the Netherlands, Th.E. Wong & J. de Jager ((Eds.), 2007, Amsterdam, Royal Netherlands Academy of Arts and Sciences, ISBN 978-90-6984-481-7, p223-239.

Evers, L.G., L. Ceranna, H.W. Haak, A.L. Pichon and R.W. Whitaker, 2007. *A seismoacoustic analysis of the gas-pipeline explosion near Ghislenghien in Belgium.* Bulletin of the Seismological Society of America, **97**, 2, 417-425.

Evers, L.G. and H.W. Haak, 2007. *Infrasonic forerunners: exceptionally fast acoustic phases.* Geophys. Res. Lett., **34**.

2008

Assink, J.D., L.G. Evers, I. Holleman and H. Paulssen, 2008. *Characterization of infrasound from lightning.* Geophys. Res. Lett., **35**, L15802.

Evers, L.G., 2008. *The inaudible symphony: on the detection and source identification of atmospheric infrasound.* Thesis, TU Delft, 2008, Delft, ISBN 978-90-71382-55-0, 170p.

Ottemoller, L. and L.G. Evers, 2008. *Seismo-acoustic analysis of the Buncefield oil depot explosion in the UK, 2005.* Geophys. J. Int., **172**, 3, 1123-1134.

Suarez, G., T. van Eck, D. Giardini, T. Ahern, R. Butler and S. Tsuboi, 2008. *The International Federation of Digital Seismograph Networks (FDSN): An Integrated system of Seismological Observatories.* IEEE Systems Journal, **2**, 3, 431-438.

2009

Evers, L.G. and H.W. Haak, 2009. *The characteristics of infrasound, its propagation and some early history.* In Infrasound monitoring for atmospheric studies, A. Le Pichon (Ed.), 2009, Dordrecht, Springer.

Evers, L.G. and P. Siegmund, 2009. *The infrasonic signature of the 2009 major Sudden Stratospheric Warming.* Geophys. Res. Lett., **36**.

Evers, L.G., 2009. *Imaging of the atmosphere with infrasound.* Internoise 2009, 23/8/2009-26/8/2009, 2009, Ottawa, Canada, 1-9.

Green, D., A. Le Pichon, L. Ceranna and L.G. Evers, 2009. *Ground Truth Events: Assessing the Capability of Infrasound Networks Using High Resolution Data Analysis.* In: Infrasound monitoring for atmospheric studies, A. Le Pichon (Ed.), 2009, Springer, Dordrecht .

Pichon, A. Le, J. Vergoz, E. Blanc, J. Guilbert, L. Ceranna, L.G. Evers and N. Brachet, 2009. *Assessing the performance of the International Monitoring System infrasound network: Geographical coverage and temporal variabilities.* J. Geophys. Res., **114**.

Pichon, A. Le, K. Antier, Y. Cansi, B. Hernandez, E. Minaya, B. Burgoa, D. Drob, L.G. Evers and J. Vaubaillon, 2009. *Evidence of a meteoritic origin of the September 15th, 2007 Carancas crater.* Meteoritics & Planetary Science, **43**, 11, 1797-1809.

Zon, T. van, L.G. Evers, R. van Vossen and M. Ainslie, 2009. *Direction of Arrival estimates with vector sensors: First results of an atmospheric infrasound array in the Netherlands.* Underwater acoustic measurements, Techologies & Results, 21/6/2009-26/6/2009, 2009, Nafplion, Greece, FORTH, 1-6.

Other publications

2007

Douet, V., S. Rives and A. Spinuso, 2007. *Portal and networking infrastructures.* Report NA9-D1, Neries project.

Eck, T. van et al., 2007. *NERIES project Annual Report to the EC.* period: 01 June 2006 - 31 May 2007.

Eck, T. van, 2007. *Editor*. Orfeus Electronic Newsletter, **7**, 1.

Eck, T. van, 2007. *Editor*. Orfeus Electronic Newsletter, **7**, 2.

Eck, T. van, A. Spinuso, V. Douet and R. Bossu, 2007. *Portal concept and strategy Report.* Report NA7-D1, Neries project.

Eck, T. van, F.H. Goutbeek and B. Dost, 2007. *Site specific hazard estimates for the NUON energy plant in the Eemshaven.* KNMI Internal Report IR-2007-02, pp17.

Sleeman, R., 2007. *Ambient Earth noise and insrumental noise.* Bijdrage biennial 2005-2006.

2008

Bossu, R., T. van Eck and J. Davila, 2008. *EERWEM final report.* EERWEM final report to the EC.

Eck, T. van and NERIES Consortium, 2008. *NERIES; Second Annual Report.* Annual report EC-project NERIES.

Eck, T. van, F.H. Goutbeek and B. Dost, 2008. *Site specific hazard estimates for the LNG energy plant in the Europoort area.* KNMI Internal Report IR-2008-01, pp16.

Evers, L.G., J. de Plaa and D.G. Simons, 2008. *Listening to inaudible sound: towards acoustic remote sensing with atmospheric infrasound.* Leonardo Times, **12**, 1, 12-13.

Evers, L.G., 2008. *Het hoe, wat en waarom van infrageluid metingen.* Meteorologica.

Giardini, D., T. van Eck, R. Bossu and S. Wiemer, 2008. *Networking Research Infrastructures for Earthquake Seismology.* EOS, **89**, 219.

Hazel, G.J. van den, 2008. *Detection and processing 3C signal from a small scale seismic array.* MSc thesis Utrecht University.

2009

Evers, L.G. and J. Schweitzer, 2009. *A climatology of infrasound observations at the ARCI array in Norway.* 2009, NORSAR, Scientific Report, 13p.

Evers, L.G., 2009. *Het hoe, wat en waarom van infrageluid metingen.* Meteorologica, **18**, 1, 24-26.

Evers, L.G., 2009. *De onhoorbare symfonie.* Nederlands Tijdschrift voor Natuurkunde, 75, 5, 156-159.

Publications R&D Information and Observation Technology

The Information and observation technology research aims at innovating KNMI's ICT infrastructure and observation technology.

Reviewed publications

2007

-

2008

-

2009

Som de Cerff, W.J., M. Petitdidier, A. Gemünd, L. Horstink and H. Schwichtenberg, 2009. *Earth science test suites to evaluate grid tools and middleware - examples for grid data access tools.* Earth Science Informatics, **2**, 117-131.

Other publications

2007

Haij, M.J. de, 2007. *Automated discrimination of precipitation type using the FD12P present weather sensor: evaluation and opportunities.* KNMI Technical Report TR-297, pp73.

Haij, M.J. de, W.M.F. Wauben and H. Klein Baltink, 2007. *Continuous mixing layer height determination using the LD-40 ceilometer: a feasibility study.* KNMI Scientific Report WR-2007-01.

2008

Beekhuis, H. and I. Holleman, 2008. *From Pulse to Product: Highlights of the digital-IF upgrade of the Dutch national radar network* ERAD 5. 30/6/2008-4/7/2008, Helsinki.

Haij, M.J. de, 2008. *Assessment of automated quality control of MOR measurements by the FD12P sensor.* KNMI Technical Report TR-298, 37pp.

2009

Haij, M.J. de, 2009. *Automatische validatie van druk- en windwaarnemingen op het KNMI - een verkenning.* KNMI publication IR-2009-03, 80pp.

Haij, M.J. de, W.M.F. Wauben, H. Klein Baltink and A. Apituley, 2009. *Determination of the mixing layer height by a ceilometer.* 8th International Symposium on Tropospheric Profiling, 19/10/2009-23/10/2009, A. Apituley, H.W.J. Russchenberg, W.A.A. Monna (Eds.), Delft, ISBN 978-90-6960-2.

Acronyms

ADAGUC	Atmospheric Data Access for the Geospatial User Community
AIL	Aircraft Induced Lightning
AIRS	Atmospheric Infrared Sounder (instrument on board EOS-Aqua)
AIS	Antarctic Ice Sheet
AMFIC	Air Quality Monitoring and Forecasting in China
AMSR	Advanced Microwave Scanning Radiometer
AOGCM	Atmosphere-Ocean General Circulation Model
AOT	Aerosol Optical Thickness
API	Application Programming Interface
ASAR	Advanced SAR on Envisat
ASCAT	European Advanced Scatterometer on MetOp
AVHRR	Advanced Very High Resolution Radiometer
BBC	British Broadcasting Company
BJEPB	Beijing Environmental Protection Bureau
BSRN	Baseline Surface Radiation Network
BSS	Brier Skill Score
CAPE	Convective Available Potential Energy
CERC	Cambridge Environmental Research Consultants
CESAR	Cabauw Experimental Site for Atmospheric Research
CESAR CDS	Cabauw Experimental Site for Atmospheric Research, CESAR Data System
CF	Climate and Forecasting convention
CH_4	Methane
CMIP3	Climate Model Intercomparison 3
CO	Carbon monoxide
CTBT	Comprehensive Nuclear-Test-Ban Treaty
CTM	Chemistry-Transport Model
CY31/33	Cycle 31/33
DCI	Distributed Computing Infrastructure
DDF	Depth-Duration-Frequency
DEGREE	Dissemination and Exploitation of Grids in Earth
DJF	December-January-February
DNW	German-Dutch Wind Tunnels
DWD	German Weather Service
EC	Eddy Correlation
EC	European Commission
ECA&D	European Climate Assessment & Dataset

ECMWF	European Centre for Medium-Range Weather Forecasts
ECSN	European Climate Support Network
ECV	Essential Climate Variable
EEA	European Environment Agency
EL	Equilibrium Level
ENSO	El Niño - Southern Oscillation
ENVISAT	ESA Environmental Satellite, launched 2002
E-OBS	ENSEMBLES daily gridded dataset for Europe
EOS Aqua	NASA Earth Observing Systems Aqua Mission to study water vapour and clouds
EOS Aura	NASA Earth Observing Systems Aura Mission to study atmospheric chemistry
ERS-2	Second European Remote Sensing satellite
ES	Earth Science
ESA	European Space Agency
ES-G	Earth Science Gateway
ESM	Earth System Model
ESRI	GIS software company
EU	European Union
EU-FP	European Union - Framework Project
EUMETSAT	EUropean organisation for the exploitation of METeorological SATellites
EURAD	Regional air quality model contributed by Germany
EURO4M	European Reanalysis and Observations for Monitoring
EXL	Exloo Infrasound Array
FIR	Flight Information Region
FLITS	Flash Localization by Interferometry and Time of Arrival System
FTPPRO	KNMI FTP site
GCM	Global Climate Model
GDAL	Geospatial Data Abstraction Library
GEMS	Global and Regional Earth-System Monitoring Using Satellite and In situ Data
GEMS	Global Earthquake Monitoring System
GEOSS	Global Earth Observation System of Systems
GeoTIFF	Geospatial Tagged Image File Format, geospatial file format
GEV	Generalized Extreme Value
GIS	Greenland Ice Sheet
GIS	Geospatial Information System
GMES	Global Monitoring for Environment and Security
GMF	Geophysical Model Function
GO-ESSP	Global Organization for Earth System Science Portals
GOME-1	Global Ozone Monitoring Experiment-1
GOME-2	Global Ozone Monitoring Experiment-2
GTS	Global Telecommunications System
GWP	Global Warming Potential
H2	Molecular Hydrogen
HCHO	Formaldehyde
HDIA	High Density Infrasound Array
HIRLAM	High Resolution Local Area Model
hPa	hecto Pascal
HPC	High Performance Computing
HQL	Hibernate Query Language
HRVIS	High Resolution VISible channel
HTTP	HyperText Transfer Protocol
HYMN	Hydrogen, Methane, and Nitrous Oxide.
IASI	Infrared Atmospheric Sounding Interferometer
IFS	Integrated Forecast System
INSPIRE	Infrastructure for Spatial Information in the European Community

IPCC	Intergovernmental Panel on Climate Change
IS	Infrasonic phase from the Stratosphere
ISO	International Organization for Standardization
IT	Infrasonic phase from the Thermosphere
ITCZ	Inter-Tropical Convergence Zone
JJA	June-July-August
JSR-168	Java Specification Request
KLM	Royal Dutch Airlines
KNMI	Royal Netherlands Meteorological Institute
KODAC	KNMI Operational Data Center
LAIA	Large Aperture Infrasound Array
LAMA	Large Aperture Microbarograph Array
LES	Large Eddy Simulation
LFC	Level of Free Convection
LIM2	Liouvain-La-Neuve Ice Model 2
LNB	Level of Neutral Buoyancy
LOFAR	LOw Frequency ARray
LPM	Laser Precipitation Monitor
LST	Low Speed Tunnel
LVNL	Air Traffic Control, Netherlands
LVP	Low Visibility Procedure
MACC	Monitoring Atmospheric Composition and Climate
METAR	Meteorological Aerodrome Report
MetOp	METeorological OPerational satellite
MFB	Mean-Field Bias
MFBS	Mean-Field Bias and Spatial
MLE	Maximum Likelihood Estimator
MLS	Microwave Limb Sounder
MODIS	MODerate resolution Imaging Spectro-radiometer
MOPITT	Measurements Of Pollution In The Troposphere
MOR	Meteorological Optical Range
MOS	Model Output Statistics
MSLP	Mean Sea Level Pressure
MTG	Meteosat Third Generation
N2O	Nitrous Oxide
NAO	North-Atlantic Oscillation
NASA	National Aeronautics and Space Administration
NEMO3	Nucleus for European Modelling of the Ocean 3
NERIES	Network of Research Infrastructures for European Seismology
NESC	National E-Science Centre
netCDF	Network Common Data Form
NGR	Nationaal Geo Portaal
NH	Northern Hemisphere
NIR	Near InfraRed
NLR	Dutch National Aerospace Laboratory
NMDC	Nationaal Modellen en Data Centrum
NMHS	National Meteorological and Hydrological Service
NO2	Nitrogen dioxide
NOAA	National Oceanic and Atmospheric Administration
NOx	Nitric oxide gas (NO) and nitrogen dioxide gas (NO2)
NWA	Northwest Airlines
NWP	Numerical Weather Prediction
NWS	National Weather Service
O&M Model	Observations and Measurements model

OGC	Open Geospatial Consortium
OGF	Open Grid Forum
OMI	Ozone Monitoring Instrument
OPERA	Operational Programme for the Exchange of weather Radar information
PDO	Pacific Decadal Oscillation
PI	Performance Index
PM	Particulate Matter
ppbv	parts per billion by volume
PPI	Plan Position Indicator
PROMOTE	Protocol Monitoring for the GMES service element
QPE	Quantitative Precipitation Estimation
RACMO	Regional Atmospheric Climate MOdel
RADAR	RAdio Detection And Ranging
RCC	Regional Climate Centre
RCM	Regional Climate Model
RDF	Resource Description Framework
RIVM	Rijks Instituut voor Volksgezondheid en Milieu
RVR	Runway Visual Range
SAFIR	Surveillance et d'Alerte Foudre par Interférométrie Radioélectrique
SAR	Synthetic Aperture Radar
SATREP	Satellite Report
SBUV	Solar Backscatter Ultraviolet Experiment
SciaGrid	Sciamachy Data Centre Grid (GO project)
SCIAMACHY	Scanning Imaging Absorption Spectrometer for Atmospheric Cartography
SEB	Surface Energy Budget
SEED	Standard for the Exchange of Earthquake Data
SKV	Schiphol Probability Forecast (in Dutch: Schipholkansverwachting)
SLA	Service Level Agreements
SNR	Signal-to-Noise Ratio
SPARQL	SPARQL Protocol and RDF Query
SPC	Storm Prediction Centre
SRES	Special Report on Emissions Scenarios
SRON	Netherlands Institute for Space Research
SSM/I	Special Sensor Microwave Imager
SST	Sea Surface Temperature
STOWA	Foundation for applied water research
T2m	2 meter Temperature
TAF	Terminal Aerodrome Forecast
TAFG	TAF Guidance
TeNSor	Test of Precipitation Type sensors
TM5	Transport Model version 5
TMA	Terminal Control Area
TNO	Netherlands Organisation for Applied Scientific Research
TOS	Turbulent Organized Structures
TROPOMI	Tropospheric Ozone Monitoring Instrument
TSI	Total Sky Imager
TU Delft	Delft University of Technology
UK	United Kingdom
UTC	Universal Time, Coordinated
VIS	Visibility
VITO	Flemish Institute for Technical Research
VU	Free University
W3C	World Wide Web Consortium
WCS	Web Coverage Service

WFS	Web Feature Service
WMO	World Meteorological Organization
WMO-IPET MDI	WMO Inter-Programme Expert Team on Metadata and Data Interoperability
WMS	Web Mapping Service

Colofon

Editors
Wim Monna
Peter Siegmund

Design and lay-out
Studio KNMI, Jaap Kwakkel

Photography
Ed van Rijswijk

Print
Martin Heunks

Paper
Inner pages: 4CC 100g/m²
Cover: 4CC 200g/m²

Circulation
1000 copies

© KNMI, De Bilt, September 2010